Balancing Efficacy and Selectivity of Bispecific c-METxEGFR Antibodies

TECHNISCHE UNIVERSITÄT DARMSTADT

Vom Fachbereich Chemie
der Technischen Universität Darmstadt

zur Erlangung des akademischen Grades eines
Doctor rerum naturalium (Dr. rer. nat.)

genehmigte Dissertation
vorgelegt von
M. Sc. Carolin Sellmann
aus Hildesheim

Referent: Prof. Dr. Harald Kolmar
Korreferent: Prof. Dr. Heribert Warzecha

Tag der Einreichung: 16. September 2016
Tag der mündlichen Prüfung: 11. November 2016

Darmstadt 2016

D17

Die vorliegende Arbeit wurde unter der Leitung von Herrn Prof. Dr. Harald Kolmar am Clemens-Schöpf-Institut für Organische Chemie und Biochemie der Technischen Universität Darmstadt sowie bei Merck KGaA in Darmstadt von August 2013 bis August 2016 angefertigt.

Publications or patents derived from the presented work

Parts of this work have been published or are currently under review.

Sellmann C., Doerner A., Toleikis L., Sood V. (November 13th, 2015) Bi-specific antibodies for enhanced tumor selectivity and inhibition and uses thereof. *Patent application*. Application no. EP15192851.2

Sellmann C., Doerner A., Knuehl C., Rasche N., Sood V., Krah S., Rhiel L., Messemer A., Wesolowski J., Schuette M., Becker S., Toleikis L., Kolmar H., Hock B. (2016): Balancing selectivity and efficacy of bispecific EGFR x c-MET antibodies and antibody-drug conjugates. *under review*

Contributions to conferences

Doerner A., **Sellmann C.**, Waurisch K., Giefer M., Piater B., Toleikis L. (June 30th, 2015) c-Met as therapeutic target for monospecific one-armed, bispecific and toxin-conjugation antibody approaches. *Poster at R&D Day, Merck, Darmstadt, Germany*.

Sellmann C., Doerner A., Rasche R., Toleikis L., Schütte M., Becker S., Kolmar H., Hock B. (November 4th, 2015). Keeping the balance: selectivity and efficacy of bispecific antibodies. *Poster at Protein and Antibody Engineering Europe Conference (PEGS) Europe, Lisbon, Portugal.*

Sellmann C., Doerner A., Rasche R., Toleikis L., Schütte M., Becker S., Kolmar H., Hock B. (March 31st, 2016) Keeping the balance: selectivity and efficacy of bispecific antibodies. *Poster at Mosbacher Kolloquium, Mosbach, Germany*.

Sellmann C. (July 6th 2016) Balancing selectivity and efficacy of bispecific antibodies. *Talk at European Conference on Biotechnology, Krakow, Poland*.

Publications to related projects

Könning D., Zielonka S., **Sellmann C.**, Schröter C., Grzeschik J., Becker S., Kolmar H. (2016): Isolation of a pH-sensitive IgNAR variable domain from a yeast-displayed, histidine-doped master library. *Mar. Biotechnol.* 18 (2), 161-167.

Valldorf B., Fittler H., Deweid L., Ebenig A., Dickgiesser S., **Sellmann C.**, Becker J., Zielonka S., Empting M., Avrutina O., Kolmar H. (2016): An apoptosis-inducing peptidic heptad that efficiently clusters death receptor 5. *Angew. Chem. Int. Ed. Engl.* 55 (16), 5085-5089.

Könning D., Zielonka S., Grzeschik J., Empting M., Valldorf B., Krah S., Schröter C., **Sellmann C.**, Hock B., Kolmar H. (2016): Camelid and shark single domain antibodies: Structural features and therapeutic potential. *under review*

Table of contents

1. Abstract

1.1. Zusammenfassung

Die Zulassung mehrerer bispezifischer Antikörper (bsAbs) und Antikörper-Wirkstoff-Konjugate (ADC) in den letzten Jahren unterstreicht die Chancen dieser Wirkstoffklassen auf einen verbesserten therapeutischen Nutzen für Patienten. (Diamantis & Banerji, 2016; Garber, 2014) Zumeist sind jedoch Tumor-assoziierte Antigene, die ein breites Expressionsprofil nicht nur im Tumorgewebe aufweisen, statt Tumor-spezifischer Antigene die Zielstrukturen für hochpotente ADCs. Dies macht eine frühe Sicherheitsprüfung auf schwere Nebenwirkungen der ADCs in Normalgeweben notwendig. (Diamantis & Banerji, 2016) Kürzlich konnte elegant gezeigt werden, dass mit Bindung zweier verschiedener Antigene und der Verwendung von Bindeeinheiten mit verringerter Affinität im bispezifischen Format die Tumorselektivität gesteigert werden kann. (Mazor *et al*, 2015a; Mazor *et al*, 2015b; Robinson *et al*, 2008)

In der vorliegenden Studie wurde ein bispezifischer Antikörper entwickelt und evaluiert, der simultan die zwei klinisch validierten Krebsantigene c-MET und EGFR bindet. Deren Interaktion und redundante Signalwege können zu c-MET vermittelter, erworbener Wirkstoffresistenz während einer EGFR Monotherapie führen. (Engelman *et al*, 2007; Guo *et al*, 2008; Jo *et al*, 2000) Darüber hinaus ist die Inhibition von EGFR in Normalgewebe wie der Haut mit schwerer Toxizität assoziiert (Lacouture, 2006), welches eine sorgfältige Abwägung von Wirksamkeit und Selektivität von gegen EGFR gerichteten Bindeproteinen erfordert. In dieser Arbeit wurden nach unserem Wissen zum ersten Mal Affinitäts-optimierte, bispezifische Antikörper mit der Potenz eines ADC-Ansatzes kombiniert. Dabei konnte für c-MET und EGFR bispezifische Antikörper erhöhte Selektivität durch Avidität zu Tumormodellen im Vergleich zu Normalgewebemodellen in Zellmischungsexperimenten nachgewiesen werden. Die verbesserte Selektivität war dabei proportional zu der verringerten Affinität des EGFR Binderanteils, was jedoch gleichzeitig die Inhibition von EGFR verschlechterte. Sowohl die erhöhte Selektivität als auch die Internalisierung demonstrierten die Eignung als ADC. Bispezifische ADCs zeigten neben gleichbleibend hoher Tumorselektivität auch eine hohe zytotoxische Potenz in c-MET und EGFR exprimierenden Tumorzelllinien, nicht aber in primären Keratinozyten als Normalgewebeäquivalent.

Diese Studie stellt ein illustratives Beispiel für die Kombination von Tumor-spezifischen bispezifischen Antikörpern in Verbindung mit potenter ADC-Technologie zur Erweiterung des therapeutischen Fensters dar. Das Ausbalancieren von Selektivität und Wirksamkeit bispezifischer Antikörper durch Optimierung von Affinität und Epitopen ist ein vielversprechender Ansatz für die Erweiterung der Anwendungsmöglichkeiten von ADCs gegen breit exprimierte Antigene.

1.2. Abstract

Next generation antibodies such as bispecific antibodies (bsAbs) and antibody-drug conjugates (ADC) have reached market maturity demonstrating strong therapeutic benefit for patients. (Diamantis & Banerji, 2016; Garber, 2014) However, targeting broadly expressed, tumor-associated rather than tumor-specific antigens by highly potent ADCs warrants early safety assessment due to the risk of severe on-target side effects in normal tissues. (Diamantis & Banerji, 2016) Recently, it was elegantly shown that tumor selectivity can be increased by bispecific engagement of two antigens and the application of affinity attenuated binding moieties within a bispecific format. (Mazor *et al.*, 2015a; Mazor *et al.*, 2015b; Robinson *et al.*, 2008)

In the presented study, simultaneous targeting of two clinically validated cancer antigens, c-MET and EGFR, was evaluated, as receptor cross-talk and signaling redundancies give rise to c-MET mediated resistance mechanism during anti-EGFR monotherapy. (Engelman *et al.*, 2007; Guo *et al.*, 2008; Jo *et al.*, 2000) Furthermore, EGFR inhibition in normal tissue such as skin is associated with severe toxicities (Lacouture, 2006) which require careful balancing of efficacy and selectivity for EGFR targeting and combinatorial approaches. Herein, we combined to our knowledge for the first time bispecific antibodies carrying affinity-optimized binding moieties with the potency of ADC methodologies. Increased selectivity of c-MET x EGFR bispecific antibodies towards tumor models with high expression in both antigens by avidity over normal tissue models was confirmed by mixed cell flow cytometry. Improved tumor selectivity thereby was proportional to decreased affinity of the EGFR binding moiety, but concurrently reduced EGFR inhibition. High selectivity and internalization demonstrated ADC suitability for delivery of potent cytotoxic agents. As a result, bispecific ADCs retained increased selectivity and mediated high tumor efficacy in EGFR and c-MET overexpressing cells whereas toxicity in primary keratinocytes as normal tissue equivalent was conjointly reduced.

Hence, the presented study is an illustrative example demonstrating the promising combination of affinity optimization of bispecific antibodies for improved tumor selectivity by avidity with the powerful ADC technology for potentially broadening the therapeutic window. Balancing selectivity and efficacy in bispecific ADCs by affinity and epitope optimization could be a viable route to expand the target space of ADCs to ubiquitously expressed antigens.

2. Introduction

2.1. Role of antibodies in the immune system

The immune system serves for the recognition and protection of the host against environmental threats, e.g. infectious pathogens and foreign or toxic substances, and is divided into innate and adaptive defense mechanisms. The innate immune response thereby represents the first line of defense, is fast and displays a broad specificity for common pathogen-associated molecular patterns (PAMPs) on invading microbes recognized by receptors on macrophages and neutrophils, e.g. toll-like receptors. (Medzhitov *et al*, 1997) During innate immune response, also pro-inflammatory molecules, e.g. cytokines and chemokines, are secreted and the complement system becomes activated. The acquired immunity in contrast is delayed and is characterized by adaptive mechanisms including the generation of antigen specific molecules, the antibodies or immunoglobulins (Ig), as well as the manifestation of immunological memory and thus protection of re-infection in form of memory lymphocytes. Antibodies are thereby part of the humoral (from Latin "*umor*" = fluid) immune response building the link between the adaptive immune system and the effector functions of the cellular response of innate immunology. Antibodies and the cells they are secreted from (B- lymphocytes) occur in evolution since the class of *gnathostomata* (vertebrates with jaw). (Du, 1993) These cells carry B-cell receptors (BCR) with a unique specificity. BCRs can be structurally seen as membrane bound antibodies and variability of antibodies and BCRs is genetically encoded. Naïve recirculating B-cells, which are derived from the bone marrow, become activated in spleen and lymph nodes when they get contact with their respective antigen. The antigen in turn is presented by dendritic cells which has beforehand recognized a pathogen, engulfed and subsequently fragmented it. Based on the clonal selection theory by Burnet (1950s), one progenitor B-cell gives rise to many lymphocytes with the same BCR whereas cells recognizing self-antigens are eliminated in form of a negative selection step. This ensures the crucial discrimination of self and non-self-antigens as well as the high selectivity of antibodies. After activation, B-cells enlarge to lymphoblasts, and divide repeatedly and maturate to antibody secreting plasma cells. The majority of matured B-cells are eliminated after short time, but some survive and differentiate to memory cells. These cells genetically store immunological information and increase the immune reactivity for second antigen contact. (Janeway *et al*, 2001)

The first antigen contact is made by pentameric Igs of the isotype M. In response of antigen stimulation in combination with co-stimulatory signals, antibody class switching occurs by chromosomal recombination. This mechanism is mediated by the enzyme activation-induced cytidine deaminase (AID) which catalyzes the conversion from cytosine to uracil. (Stavnezer *et al*, 2008) Different antibody isotypes display different characteristics, e.g. the ability to oligomerize or the induction of effector

functions. One of these effector functions is antibody-dependent cellular cytotoxicity (ADCC) which describes the recruitment of innate immune effector cells (e.g. monocytes, eosinophils, neutrophils, macrophages and natural killer cells) via Fcγ-receptors (FcγRs) recognizing antibodies bound to specific target cells. Activation of effector cells by FcγR crosslinking then induces cytolysis by the secretion of perforin and granzyme. Another effector function comprises the activation of the complement system via protein C1q. A complex system of simultaneously expressed receptors which are either activating or inhibitory thereby determines prevention or induction of immune responses. Another feature of antibodies is their long half-life which is mediated by the neonatal Fc receptor (FcRn). It belongs to the family of major histocompatibility complex (MHC) class I and is expressed on endothelial and myeloid cells. The main function is the recycling of immunoglobulins after internalization as well as the placental transport of IgG. (Janeway *et al.*, 2001; Roopenian & Akilesh, 2007)

2.1.1. Antibody structure and function

Around 1960, both the peptide structure of papain cleaved antibody fragments and the first complete antibody sequence were elucidated by Porter and Edelman, respectively, which was rewarded with the Nobel Prize in 1972. (Ribatti, 2015) Antibodies are Y-shaped, symmetrical, disulfide-bond linked heterotetramers with a molecular mass of 150 kDa consisting of two identical heavy and two identical light chains (**Figure 1A-C**). By papain cleavage, antibodies can be split into two identical Fabs (fragment of antibody binding) responsible for antigen recognition and one Fc (constant fragment or fragment crystalline) mediating effector functions, e.g. ADCC, CDC as well as FcRn mediated recycling and half-life extension. Fab and Fc are connected with a region of high flexibility, the hinge region. Reduction of disulfide bonds located in the hinge region separates the antibody in light and heavy chains. Within each light and heavy chain, sequence analysis revealed the presence of regions with high variability at the N-terminus, denoted as variable region VH and VL for heavy and light chain, respectively. The diversity of variable regions is encoded by combinatory design of the genetic locus of variable heavy and light chain consisting of germline encoded V for variable, D for diversity (VH only) and J for joining gene segments. Recombination of V(D)J gene segments gives rise to the antibody's variability. Additionally, introduction of somatic hypermutations mediated by the enzyme AID (activation-induced cytidine deaminase) further increases diversity. Both VH and VL contain three hypervariable regions, denoted as complementary determining regions 1 to 3 (CDR1-3), which are flanked by more conserved regions, named framework regions 1 to 4 (FR1-4). The three CDRs of the VH and the three CDRs of the VL built up six loop structures responsible for antigen recognition which are stabilized by the framework regions. The middle part of the CDR3 of the heavy chain is encoded by the D gene segment. Consequently, the CDR-H3 is thought to contain the highest variability, both in composition and length, and it might be therefore the driving force for antigen binding. (Nimmerjahn & Ravetch, 2010; Vidarsson *et al*, 2014)

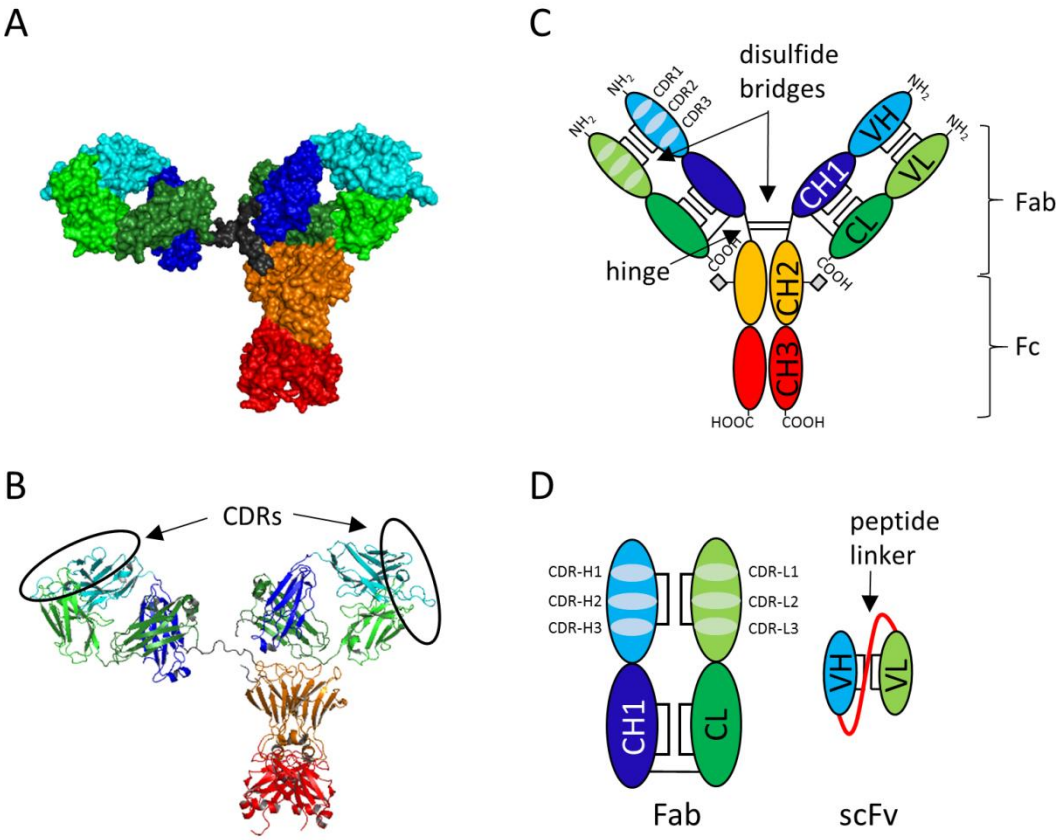

Figure 1: Antibody structure.

Crystal structure of IgG1 (from PDB: 1hzh) with sphere model **(A)** or ribbon structure **(B)** (both generated by PyMOL ver. 1.3r1) as well as schematic presentation **(C)**. Heavy chains are colored in light blue (VH), dark blue (CH1), yellow (CH2) and red (CH3). Light chains are illustrated in light green (VL) and dark green (CL). Heavy chain CH1 and CH2 are connected with a flexible region, denoted as hinge (grey) which built up two disulfide bonds between the two heavy chains. The C-termini of CL and CH1 are same wise linked with a disulfide bond. By papain cleavage, antibodies are cleaved into two Fab antibody fragments (fragment antigen binding) and one Fc (fragment crystalline). The Fab is thereby composed of the light chain and domain VH and CH1 of the heavy chain. Within the four domains of the Fab, intramolecular disulfide bonds stabilize each domain. Each variable domains contains three hypervariable domains, named complementary determining regions (CDRs) of VH and VL building up six loop structures for antigen recognition. Within the CH2 domain, glycosylation sites (squares) are located being involved in FcγR binding and complement binding. **(D)** Smaller antibody-based fragment formats are the Fab composed of light chain and VH and CH1 as well as the genetically linked scFv, e.g. by glycine serine peptide linker, consisting solely of the VH and the VL which are sufficient for antigen binding. The figure is adapted from Doerner et al. (Doerner *et al*, 2014)

C-terminal regions of both chains are highly conserved and therefore named constant regions of the heavy chain (CH) as well as of the light chain (CL). For heavy chains, five different antibody constant domain classes or isotypes can be distinguished, namely IgM, IgD, IgG, IgA and IgE. Among those, IgG is the most abundant immunoglobulin isotype in serum (up to 10 mg/ml) and is further divided into four subclasses (IgG_{1-4}). For the IgG subclasses, also genetic polymorphism based on allelic variations have been described (cf. IMGT database). Within the constant region of the heavy chains, globular domains can be recognized in the crystal structure, denoted as CH1, CH2 and CH3 (**Figure 1**). IgM and IgE contain an additional globular domain, named CH4. The constant subunit of a light chain consists of a single domain (CL) and can be discriminated by two different classes, denoted lambda (λ) and kappa (κ) with corresponding distinct gene loci. (Vidarsson *et al.*, 2014) Beside the disulfide bonds in the hinge

region, heavy chains are connect via non-covalent interactions in the CH3 domains. The C-terminus of the light chain is again linked to the CH1 domain via a disulfide bond. The hinge and the upper CH2 domain contain the overlapping epitopes for FcγR and complement binding (C1q). This region also displays the most difference among the Ig classes and even IgG subclasses resulting in different propensities to activate ADCC and CDC. Furthermore, the glycosylation pattern at the CH2-CH3 interface plays a pivotal role for the quaternary conformation of the FcγR epitope, in particular the conserved glycosylation site asparagine 297 (N297). The lack of core fucosylation of IgG-Fc for example increases binding to FcγRIIIa via glycan-glycan interactions translating into higher ADCC. (Ferrara *et al*, 2011; Shields *et al*, 2002) The FcRn binding site for antibody recycling and half-life elongation is also located in the CH2-CH3 domains of IgG. (Vidarsson *et al.*, 2014) Since the variable regions of heavy and light chain are sufficient for antigen recognition, smaller antibody formats have been developed to enable better tissue penetration in comparison to the large whole antibody with 150 kDa. These antibody fragments are for example Fab or genetically fused VH-VL domains, denoted as single chain variable fragment or scFv (**Figure 1D**). However, due to small size (50 kDa for Fab and 25 kDa for scFv) and lack of the Fc moiety, antibody fragments display shorter plasma half-life and usually lower stability. (Nimmerjahn & Ravetch, 2010; Vidarsson *et al.*, 2014)

2.2. Antibody engineering

Considering the highly diverse genetic repertoire of 10^{11} to 10^{12} different variants of the immune system *in vivo*, antibodies can be theoretically generated against every imaginable antigen. (Dübel, 2007) Due to their high target specificity, mAbs have become powerful and versatile tools for molecular biological methods as well as for diagnostic and therapeutic applications. Dependent on the usage, different antibody fragments, formats and even artificial scaffolds have therefore been engineered for optimizing binding molecule characteristics, e.g. ameliorated tissue penetration, improved pharmacokinetics and enhanced effector functions. The first approved therapeutic antibody was muromomab (Orthoclone OKT3) targeting CD3 on T-cells for suppressing the rejection of organ transplants in the year 1986. (Emmons & Hunsicker, 1987) Ten years later, the first anti-tumor antibody was approved, rituximab (Rituxan), targeting CD20 on B-cells for non-Hodgkin's lymphoma. (Anderson *et al*, 1997) By the end of 2014, 47 monoclonal antibody and antibody related products have been approved in the US and Europe for several clinical indications including cancer as well as inflammatory and infectious diseases and over 300 were in clinical development. (Ecker *et al*, 2015)

First approaches to generate antibodies against a specific target protein relied on the immunization of animals. However, not every target protein is suitable for immunization, in particular toxic agents, immune suppressive targets or proteins with high homology of human or mammalian species. Sera of

immunized animals contain a variety of different antibodies against the target protein used for immunization, denoted as polyclonal antibodies (pAb). In order to produce monoclonal antibodies (mAb), continuous culture of antibody secreting cells with desired specificity is required. For this, the hybridoma technology by Köhler and Milstein is used by fusion of isolated B cells from immunized animals with immortalized myeloma cells resulting in a hybrid cell called hybridoma. (Kohler & Milstein, 1992) However, the cell hybridization process is tedious and inefficient. Moreover, the method also struggles with the instability of aneuploid cells. Another limitation of immunization and hybridoma technology is the non-human origin of the resulting antibodies leading to immunogenicity and eventually the development of anti-drug antibodies in patients, e.g. human anti-mouse antibodies (HAMA). (Khazaeli *et al*, 1994) One approach was the humanization of for example murine antibodies by transferring either the variable domains to human constant antibody domains (Gussow & Seemann, 1991), resulting in chimeric antibodies, or by grafting the CDRs to human framework regions (Kettleborough *et al*, 1991), yielding in humanized antibodies. Another strategy to tackle the immunogenicity issue was accomplished with the generation of knock-out mice and the subsequent development of transgenic rats or mice with genetic human antibody repertoires. (Jakobovits, 1995) Fully human antibodies can also be generated by the application of recombinant antibody technologies which will be elucidated in the next chapter (2.2.1) in more detail. By use of a naïve human library, for instance an anti-TNF-α antibody was isolated, denoted adalimumab (Humira) and approved in 2002. (Ecker *et al.*, 2015)

2.2.1. Display technologies

For the *in vitro* selection of antibodies from naïve, synthetic or immune libraries, display technologies in combination with high-throughput screening technologies, e.g. fluorescence activated cell sorting (FACS) and liquid handling system, have been developed and applied. A key prerequisite within display technologies is the genotype-phenotype linkage in order to derive the genetic information of a selected binder. Display technologies can be divided into the following groups: phage, cell (prokaryotic and eukaryotic), ribosomal, mRNA, and DNA display. While the presentation of full length antibodies is mainly restricted to eukaryotic systems due to the need of the respective expression system, smaller antibody fragments, e.g. Fab and scFv, as well as single domain antibodies from other species such as single heavy chain variable domains from camelids (VHH) or sharks (vNARs), can be presented in every of the above mentioned display formats. (Doerner *et al.*, 2014)

Phage display was pioneered by Smith in 1985 using the fusion of the protein of interest, in case of antibody display a scFv or a Fab, to the pIII envelope protein of filamentous bacteriophage for screening of protein libraries. (McCafferty *et al*, 1990; Smith, 1985; Smith & Petrenko, 1997) The bacteriophage

strain M13 is a single stranded, circular DNA virus which is encompassed by a protein envelope mainly composed of the major coat protein pVIII. At one end of the rod-like bacteriophage, five copies of the minor coat protein pIII and pVI are displayed while pIII is involved in the infection of *E. coli* cells over the bacterial F-pilus. (Smith & Petrenko, 1997) After transcription and translation of phage proteins, phage particles are secreted into the periplasmatic room without inducing bacterial cell death. When using a phagemid system, *E. coli* cells are transformed with a "phagemid" encoding the antibody-fragment-pIII fusion protein and an autonomous replication signal. For phage packaging, *E. coli* cells are subsequently infected with a replication deficient M13KO7 strain (called helperphage). The use of an amber stop codon thereby allows soluble production of antibody fragments without pIII protein in *E. coli* non suppressor strains, e.g. supE. This enables analysis of antibody fragments for antigen binding, e.g. by enzyme-linked immunosorbent assay (ELISA). The panning of antibody fragment libraries on phage is an iterative process composed of binding to immobilized antigen (e.g. microtiter plates or magnetic beads), removal of non-binding phages by washing, elution of bound, antigen-specific phages by addition of trypsin, and infection of *E. coli* by detached phages in combination with helperphage enabling phage amplification and packaging. The selection of binders with slow off-rates can thereby be increased, when applying stringent washing, reducing the antigen concentration or adding soluble antigen for competition. (Dübel, 2007)

Noteworthy, cellular display systems, in particular in combination with FACS, are potent alternatives for robust and real-time adaptable selection of mAbs. Examples are the yeast surface display of antibody fragments and full IgGs by fusion to the yeast surface proteins Aga2p (Boder & Wittrup, 1997) or mammalian display technologies employing HEK293-T or CHO cells using the transmembrane domain of the human platelet-derived growth factor receptor for antibody presentation. (Ho & Pastan, 2009) Despite lower transformation rates in yeast and mammalian cells compared to phage display, the advantage of cellular display systems is the compatibility with the powerful technology of FACS for enriching binders with high affinities. (Boder & Wittrup, 1997)

2.2.2. Affinity maturation

Affinity maturation describes the process occurring in germinal centers of secondary lymphoid tissue yielding in antibodies with increased affinity and activity against pathogens in comparison to BCRs. This process involves somatic hypermutation of light and heavy chain variable genes in B-lymphocytes during antibody class switching mediated by enzymes, in particular activation-induced cytidine deaminase (AID). Martin and colleagues for example demonstrated that AID expression alone is sufficient to induce somatic hypermutation in B-cells. (Martin & Scharff, 2002) Naïve libraries, which have been built up of the highly diverse repertoire of IgM presenting B-lymphocytes, are consequently devoid of affinity

maturation with potentially comparably low affinities. Therefore, *in vitro* methods are required for affinity maturation for the introduction of random mutations. Since the 1990s, an engineering process denoted as "directed evolution" has been developed which mimics natural selection by inducing random mutations, e.g. by error-prone PCR (epPCR), in order to select for proteins with user-defined properties or functions. (Chen *et al*, 1991) In addition, several other strategies have been introduced for randomization: Using antibody chain shuffling (Kang *et al*, 1991), a new light or heavy chain is selected to a given antibody chain. Parsimonious mutagenesis describes the use of amino acids coding mixtures for a certain antibody residues which allows the reservation of the original coding amino acid to a certain percentage. (Balint & Larrick, 1993) DNA shuffling of antibody gene fragments and subsequent random assembly by PCR (Stemmer, 1994) or the use of *E. coli* mutator strains (Irving *et al*, 1996) has also been reported. Besides the application of random mutagenesis, also rational design by *in silico* engineering of antibody crystal structures can be a viable approach. (Barderas *et al*, 2008)

2.2.3. Bispecific antibodies

A bispecific antibody (bsAb) describes a molecule format enabling simultaneous and selective engagement of two antigens, either soluble or bound to the cell surface. Moreover, bsAbs can address two epitopes on the same molecule or epitopes of two – preferentially interacting – molecules displayed on the same cell surface or on two different cell surfaces of interacting cells, e.g. immune and cancer cells. There is also one case of bsAbs described in nature: Under redox conditions, disulfide bonds of IgG_4 are randomly reduced resulting in two IgG_4 half-molecules. This can give rise to the assembly of two half-molecules with different Fab arms to bispecific molecules which is also called Fab arm exchange. (van der Neut *et al*, 2007; van der Zee *et al*, 1986) This naturally occurring phenomenon is for example used in the "DuoBody" technology by introducing Fab arm exchange of IgG_1 by introducing relevant mutations in the CH3 domain of IgG_1. (Labrijn et al., 2011; Labrijn et al, 2013) In comparison to combination therapies, bsAbs offer several potential advantages such as: (a) improved efficacy due to extensive receptor crosslinking inducing internalization and degradation as well as synergistic effects in inhibiting receptor signaling via simultaneous targeting (Jarantow *et al*, 2015; Lee *et al*, 2016b), (b) increased tumor cell selectivity due to dual specificities (Mazor *et al.*, 2015b), (e) effector cell recruitment, e.g. BiTEs (Wolf *et al*, 2005), and (f) lower cost during the development and approval process of a single molecule in comparison to the marketing of a combination of two single therapeutics (Holmes, 2011). As a consequence, both pharmaceutical industry and academic research gained high interest in developing strategies for the generation of bsAbs. Amgen for example spent 1.16 billion US dollar for the acquisition of Micromet which is the developer of the BiTE format. (Garber, 2014)

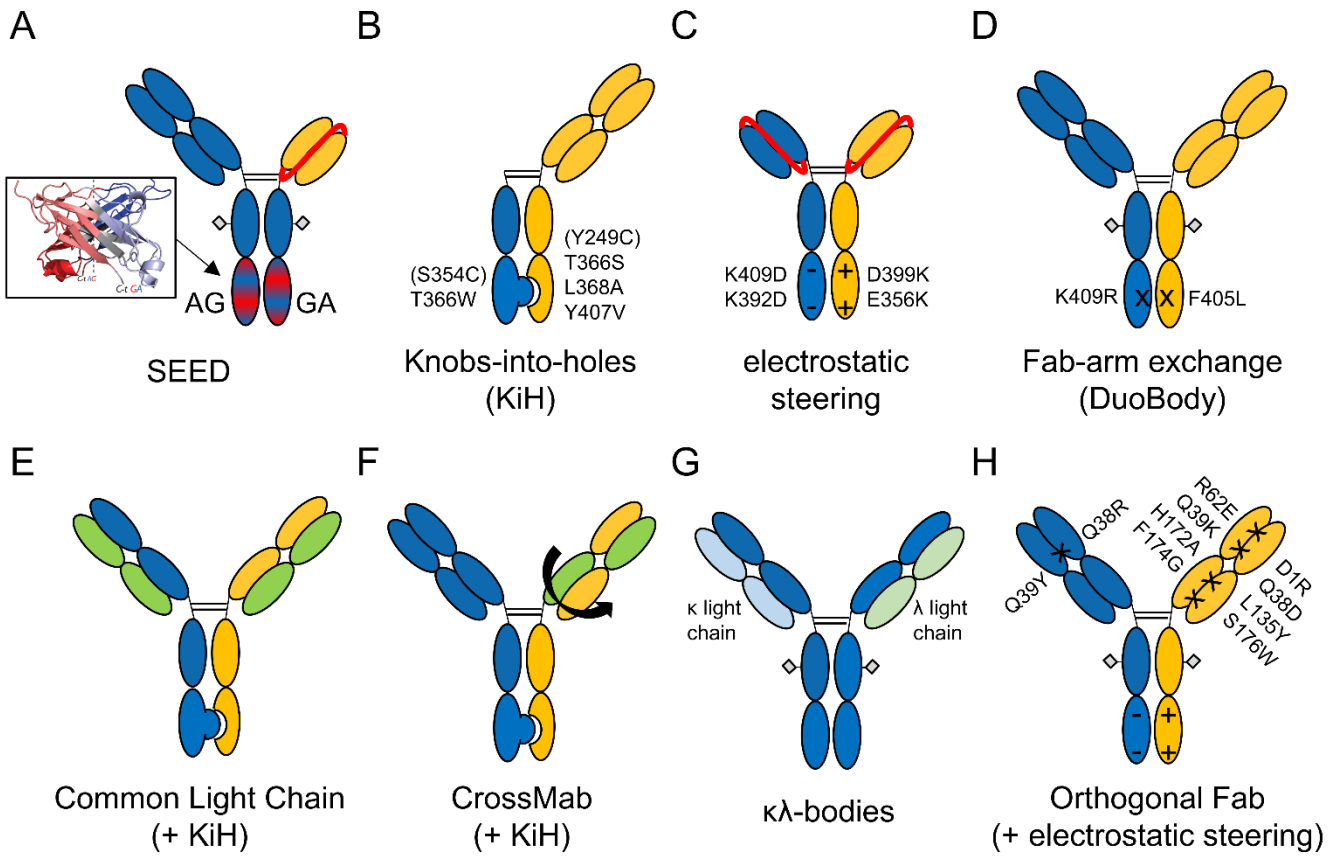

Figure 2: Technologies for correct heavy and light chain assembly in bispecific antibodies.

(A) - (D) represent exemplary technologies for heavy chain heterodimerization, while **(E) - (H)** illustrate exemplary solutions for cognate heavy-light chain pairing. **(A)** Strand-exchange engineered domain (SEED) technology (Davis *et al*, 2010) in combination with scFv-technology for one binding arm (Muda *et al*, 2011). Alternating segments of IgG and IgA were engineered in two asymmetrical chains SEED-AG and SEED-GA favoring heterodimerization. The model structure of asymmetrical CH3 chain assembly was adapted from Davis and colleagues. (Davis *et al.*, 2010) **(B)** For the knobs-into-holes technology (Ridgway et al, 1996; Spiess et al, 2015), bulky amino acid residues create a "knob" in one chain while mutations into smaller amino acids in the other chain built up a "hole". Displayed is the structure of a one-armed knobs-into-holes monovalent antibody. (Merchant et al, 2013) **(C)** Oppositely charged amino acids in both chains induce electrostatic steering favoring heterodimerization while repulsive forces prevent homodimerization. (Gunasekaran *et al*, 2010) **(D)** Based on the natural process of Fab arm exchange of IgG4, corresponding mutations were introduced in the IgG_1 format to allow controlled *in vitro* Fab arm exchange under mild reducing conditions. (Labrijn *et al*, 2011; Labrijn *et al*, 2013) **(E)** The use of common light chains in combination with engineering technologies for heavy chain heterodimerization, e.g. knobs-into-holes technology, can circumvent the light chain pairing problem. (Jackman *et al*, 2010) **(F)** Domain swapping of CH1 and CL in one Fab-antibody fragment arm can enforce cognate light to heavy chain assembly. (Schaefer *et al*, 2011b) **(G)** Fischer and colleagues introduced κλ-bodies composed of a common heavy chain in combination with one κ and one λ light chain allowing purification of bsAbs via three step affinity chromatography. (Fischer *et al*, 2015) **(H)** For the orthogonal Fab engineering, mutations were introduced at the Fab antibody fragment interface ensuring cognate light and heavy chain pairing. (Lewis *et al*, 2014) Heavy chain heterodimerization can be forced for example by electrostatic steering. (Gunasekaran *et al.*, 2010)

The first approaches for the generation of bsAbs were based on the hybridoma technology by Köhler and Milstein (1975) via fusion of two hybridoma cell lines leading to hyperploid cells, or quadroma. (Milstein & Cuello, 1983) However, co-expression of two different heavy and two different light chains results in sixteen theoretical different combinations for the antibody tetramer assembly based on stochastic calculations while only one combination consists of the desired chain pairing. Besides employing chemical coupling for the generation of bispecific antibodies with two different heavy chains (Brennan *et al*, 1985), a plethora of genetic approaches has evolved in the last years. (Kontermann & Brinkmann,

2015) In general, bsAb formats are classified into (a) lacking a Fc portion or (b) IgG-like. These can be further subdivided into symmetrical or asymmetrical. Heavy chain engineering for heterodimerization can reduce the combinatory probability of sixteen different antibody chain assemblies down to four. Consequently, the probability for the production of the desired bsAb accounts 25%. Elegant methods for heterodimerization are among others the herein used strand-exchange engineered domain (SEED) technology (Davis *et al.*, 2010) (**Figure 2A**). Davis *et al.* recognized structural similarity of immunoglobulin classes G and A. *In silico* engineering of alternating IgG and IgA segments in the CH3 domain yielded in two non-identical, antiparallel chains, designated as GA and AG chain. These two chains built up an asymmetric interface favoring heterodimerization whereas homodimerization is disfavored. (Davis *et al.*, 2010) Further methods for heavy chain heterodimerization are the knobs-into-holes technology (Ridgway *et al*, 1996; Spiess *et al*, 2015) introducing large amino acid residues in one chain while mutating to smaller residues in the other chain (**Figure 2B**), electrostatic steering by introduction of oppositely charged amino acids pairs (aspartate and lysine) on both chains (Gunasekaran *et al.*, 2010) (**Figure 2C**), and the "DuoBody" platform based on the introduction of essential amino acids responsible for the IgG_4 half-antibody exchange under mild reduced conditions into IgG_1 (Labrijn et al., 2011; Labrijn et al, 2013) (**Figure 2D**).

Cognate light and heavy chain interaction is another issue to address in order to increase the product homogeneity of bsAb. Correct light chain pairing can be achieved for example by the use of common light chains (Jackman *et al.*, 2010) (**Figure 2E**) or the application of artificial linkers as in scFv (Muda *et al.*, 2011) (**Figure 2A**). In case of common light chains, several companies developed transgenic rodents carrying the human antibody repertoire in combination with a common light chain (patent McWhirter *et al.* 2011, WO2011097603). Engineering approaches comprise the CrossMab technology (Schaefer *et al.*, 2011b) (**Figure 2F**) in which CH1 and CL domains are swapped, the development of κλ-bodies with common heavy chains (Fischer *et al.*, 2015) enabling a three step purification via κ or λ light chain specific affinity chromatography (**Figure 2G**) or the introducing of orthogonal Fab mutations via Fab interface engineering (Lewis *et al.*, 2014) (**Figure 2H**). Nevertheless, the versatility of the common light or heavy chain approach is not available when aiming at combination of existing, e.g. already approved, binding moieties. Besides, Fab interface engineering and CrossMab technology cannot be applied as generic approach but might be associated with extensive engineering efforts for individual mAbs. Facing these issues, a modular toolbox approach was chosen for this study using SEED technology for heterodimerization and scFv technology for one binding arm to assure correct light chain pairing (**Figure 2A**). (Muda *et al.*, 2011) Other mentionable engineering approaches for the generation of bispecific antibodies are the engineering of a binding site by randomization of loop structures (AB and EF loop) at the C-terminal end of the Fc-fragment denoted as Fcabs (Wozniak-Knopp *et al*, 2010) and

engineering of an additional binding specificity to the variable region of an anti-EGFR antibody yielding in “2in1 mAbs” with two specificities against EGFR and HER3, denoted as MEHD7945A (Schaefer *et al*, 2011a). Another “2in1” approach is the DutaMab-technology (Dutalys/Roche) which is based on screening synthetic libraries employing two independent paratopes within the natural human CDRs (US patent Beckmann, US2014/0206846 A1). In recent years, two bsAbs emerged to the market: catumaxomab (Removab) directed against CD3 and EpCAM, which was approved 2009, and the bispecific T-cell engager (BiTE) blinatumomab (Blincyto) directed against CD3 and CD19, approved in 2014/15. (Holmes, 2011; Kontermann & Brinkmann, 2015; Wolf *et al.*, 2005; Zeidler *et al*, 1999)

2.2.4. Antibody-drug conjugates (ADCs)

Since Paul Ehrlich envisioned the concept of tumor-selective transport of toxins as a “magic bullet” in 1913, it took eighty-seven years until the launching of the first antibody-drug conjugate (ADC) directed against CD33 (Mylotarg, gemtuzumab ozogamicin) to the market. However, due to multidrug resistance and lack of efficacy improvement in patients, it was later withdrawn. (Perez *et al*, 2014) Until today, two ADCs received approval: Adcetris (brentuximab vedotin) against CD20 and Kadcyla (trastuzumab emtansine) targeting HER2 in 2011 and 2013, respectively. (Perez *et al.*, 2014) The growing interest in this class of next generation biotherapeutics is indicated by a robust clinical pipeline with over 40 ADCs for solid and hematological tumors. (Polakis, 2016)

The concept of ADCs is to broaden the therapeutic window by increasing the maximum tolerated dose and decreasing the minimum effective dose (**Figure 3A**). This is achieved via selective delivery of the highly potent cytotoxic agent by the antibody moiety to antigen-expressing tumor cells and subsequent internalization and intracellular release of toxin. (Perez *et al.*, 2014) The safety profile of an ADC is therefore dependent on the single building blocks: the antibody, the antibody conjugation site for the linker, the linker itself, and the cytotoxic agent (**Figure 3B**). The anti-tumor selectivity of the antibody is correlated with the expression pattern of the antigen characterized by high tumor expression and low normal tissue occurrence as well as of the affinity of the antibody. So-called cancer-associated targets with normal tissue expression, e.g. EGFR and c-MET (chapter 2.3), could therefore give rise to on-target off-tumor adverse events. Furthermore, target binding of the antibody should ideally induce internalization. (Ritchie *et al*, 2013) Thus, fast internalization rates are preferred which can be dependent on the epitope of the target protein, the epitope or target specific internalization mechanisms as well as the ability to induce target clustering and the antibody’s affinity. However, strategies have been developed for non-internalizing targets utilizing triggered drug release by click reaction. (Rossin *et al*, 2016) The antibody format can also affect the ADC’s efficacy: inherent effector functions of the Fc, e.g. ADCC, CDC and FcRn recycling, could be beneficial for efficacy and half-life of the ADC on the one

hand, but could also hinder intracellular delivery of the toxin or induce off-tumor toxicity due to cellular uptake mediated by FcRn and FcγR on lymphocytes or their progenitor cells on the other hand. (McDonagh *et al*, 2008; Perez *et al.*, 2014) Intracellular toxin delivery of Kadcyla for example diminished megakaryocyte maturation via FcγRIIa. (Uppal *et al*, 2015) Silencing of FcRn binding could therefore result in a beneficial safety profile but also yield in lower pharmacokinetics.

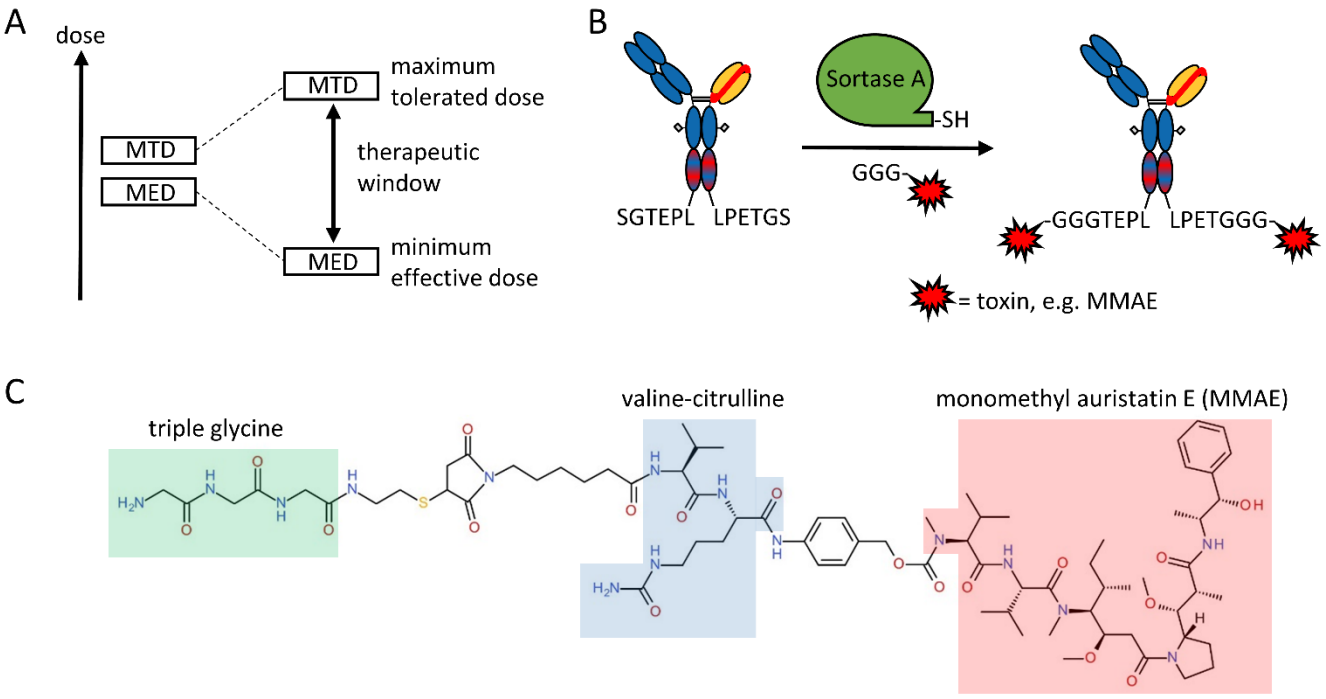

Figure 3: Definition of therapeutic window (A), antibody-toxin conjugation via sortase A (B), and structural formula of GGG-vc-MMAE (C).

(A) Definition of therapeutic window in the ADC context. Cytotoxic agents alone (left side) have a small (or even negative) difference between maximum tolerated dose (MTD) and minimal effective dose (MED). By selective delivery of the toxin mediated by the antibody, the therapeutic window between MTD and MED is theoretically increased. The figure was adapted from Panowksi *et al.*. (Panowski *et al*, 2014) **(B)** Schematic representation for the sortase A mediated conjugation of cytotoxic agents including three N-terminal glycines to the C-terminus of both antibody heavy chains containing of the sortase recognition sequence LPXTG, while X is an arbitrary amino acid. **(C)** Structural formula of the toxin conjugate triple glycine-valine-citrulline-monomethyl auristatin E (GGG-vc-MMAE). The triple glycine is highlighted in green, valine-citrulline in blue and monomethyl auristatin E in red. The three building blocks are connected via spacer.

Regarding linkers, cleavable and non-cleavable are distinguished. Ideally, linkers should have two functionalizations for efficient antibody and toxin conjugation on either side. Moreover, high stability in the blood circulation and fast intracellular toxin release are desired in order to ensure high efficacy and low toxicity in normal tissue. The most common linkers are protease cleavable, e.g. valine-citrulline (**Figure 3C**) for cleavage by lysosomal protease cathepsin B used in Adcetris. (Perez *et al.*, 2014; Ritchie *et al.*, 2013) Acid sensitive linkers, e.g. hydrazones, depend on acidification within the endosome, but suffer from instability, lower half-life and related unspecific toxicities. (Perez *et al.*, 2014) Non-cleavable linkers in contrast display high stability in serum, but are only slowly released in the process of antibody

degradation. (Perez *et al.*, 2014) For the last building block, the toxin, microtubule inhibitors and DNA alkylating agents can be discriminated. The first adds a second layer of selectivity since only fast dividing cells are targeted. Common tubulin inhibitors are auristatins, e.g. monomethyl auristatin E (MMAE) (**Figure 3C**), which are based on dolastatin 10, and maytansinoids. (Banerjee *et al*, 2008) DNA alkylators often bind within the minor groove of the DNA. Duocarmycin analogs for example alkylate adenine-N3. (Lin & Patel, 1995) Since only a small fraction of the ADC (1-2%) is proposed to be internalized in the tumor, high potencies of the payload are needed. Moreover, toxin efflux by ABC-transporters conferring to multidrug resistance, e.g. P-glycoprotein, need to be taken into consideration. (Perez *et al.*, 2014)

The selectivity and the homogeneity of the ADC product depend on the conjugation method. Since cysteine or lysine conjugation with maleimides or N-hydroxysuccinimide ester occur randomly, the stoichiometry of drug molecules per antibody moiety, denoted as drug-to-antibody ratio (DAR), and the conjugation sites have a wide and heterogeneous distribution. The DAR as well as the site of conjugation in turn can influence the biophysics of the antibody, e.g. hydrophobicity and solubility, as well as the efficacy due to varying payload. Enzyme mediated conjugation or introduction and reaction with unnatural amino acids in contrast are both site-specific methods and result in a clearly defined, homogenous DAR with defined conjugation sites. While bacterial transglutaminase catalyzes the ligation of glutamine side chains with lysine residues, sortase A mediates the hydrolysis of the threonine-glycine bond in the LPXTG motif (**Figure 3B**) followed by formation of a peptide bond between threonine and a glycine motif, e.g. triple glycine. (Perez *et al.*, 2014)

2.3. Cancer associated antigens as therapeutic targets

Due to the multifactorial nature of cancer, redundant receptor signaling, and the development of cancer resistance, monotherapies for a specific cancer target often struggle with poor efficacy. Consequently, there is the need for combinatory treatment approaches. However, many existing therapies face mild to severe adverse events as a result of basal target antigen expression in normal tissue which could be multiplied by the combination of two or more therapeutic agents. One protein family, which has been extensively studied as cancer targets, is the receptor tyrosine kinase (RTK) superfamily. Their involvement in the development and progression of tumors has been elucidated more than 30 years ago. (Downward *et al*, 1984) RTKs are membrane receptors which usually become activated by binding of growth factors and subsequent phosphorylation of tyrosine residues within the intracellular kinase domain. Endogenous functions comprise the regulation of many essential cellular processes in development, normal cell function, intercellular communication, and tissue homeostasis. (Downward *et al.*, 1984) Deregulation of ligand secretion, receptor expression as well as receptor activation and

mutational status, which are all tightly controlled in normal cells, can lead to unconstrained cellular growth.

2.3.1. The epidermal growth factor receptor (EGFR)

The epidermal growth factor receptor (EGFR, also known as: ErbB1, HER1) is part of the ErbB family of RTKs consisting of EGFR, ErbB2, ErbB3, and ErbB4 as well as c-MET among various membrane receptors. Several molecules have been identified as ligands: epidermal growth factor (EGF), transforming growth factor-α, amphiregulin, epigen, epiregulin, β-cellulin, and heparin bound-EGF. (Yarden & Sliwkowski, 2001) EGFR is expressed in cells of epithelial, mesenchymal as well as neuronal origin and is involved in cell-cell interactions in embryogenesis and adult tissue. Around 1980, EGFR signaling has been implicated with cell transformation and cancer, e.g. an aberrant from of EGFR, v-erbB, had been identified as an oncogene of avian erythroblastosis tumor virus. (Downward *et al.*, 1984) EGFR is a heavily N-glycosylated, 170 kDa protein consisting of a large extracellular domain (ECD) composed of four subdomains, a single transmembrane spanning domain, and an intracellular catalytic kinase domain (**Figure 4**). Ligand binding to domain III and I induces dramatic conformational changes from a tethered to an extended conformation of the ECD. Domain rearrangement thereby exposes a receptor dimerization interface on domain II and subsequent interaction of intracellular domains leads to transphosphorylation of tyrosine residues within the kinase domain (**Figure 4**). EGFR does not exclusively forms homodimers, but also heterodimerizes with various other receptors. Interestingly, the distinct phosphorylation pattern of tyrosine residues is dependent on the ligand. (Yewale *et al*, 2013) The phosphorylation sites within the kinase domain serve as docking sites for adaptor proteins, e.g. Gab1 and Grb2, containing Src homology domains or phospho-tyrosine binding domains. This in turn induces the activation of signaling pathways, including mitogen-activated protein kinase pathway (MAPK) and phosphaidylinositol-3-OH kinase (PI3K)-AKT-mTOR pathway, STAT3/5, PLCγ-PKC, regulating proliferation, cell survival, DNA synthesis, and migration (**Figure 4**). (Ferguson *et al*, 2003; Yarden & Sliwkowski, 2001; Yewale *et al.*, 2013)

Deregulation of EGFR signaling via constitutive activation by genetic mutations, overexpression and/or gene amplification, as well as ligand upregulation can lead to uncontrolled tumor growth and metastasis. Additionally, increased EGFR expression has been correlated with poor prognosis. (Nicholson *et al*, 2001) Consequently, EGFR has emerged to a highly evaluated anti-cancer target by small molecule tyrosine kinase inhibitors (e.g. gefitinib and erlotinib) as well as antibody entities. (Yewale *et al.*, 2013) The first anti-EGFR antibody approved was the human-murine chimeric IgG1 cetuximab for colorectal cancer and squamous cell carcinoma of the head and neck. (Li *et al*, 2005) It binds to domain III of the EGFR ECD and competes for EGF binding by steric hindrance. (Li *et al*, 2005)

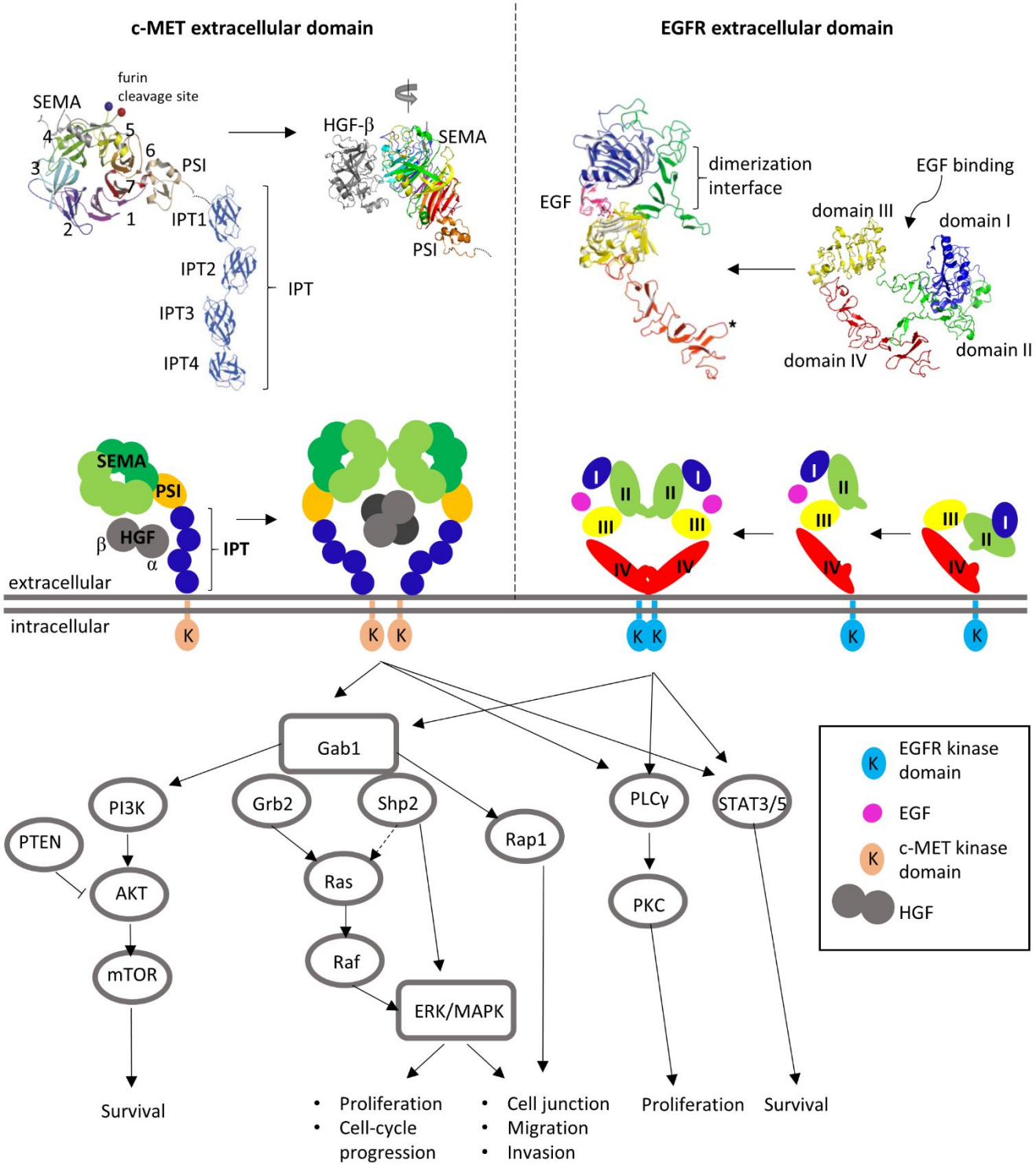

Figure 4: Redundant signaling of c-MET and EGFR.

Schematic representation of c-MET and EGFR dimerization induced by HGF and EGF binding, respectively. Crystal structures were derived from PDB (1shy for c-MET SEMA and PSI domain with HGF-β and 1nql for EGFR ECD in truncated conformation) or were adapted from Niemann *et al.*, Birchmeier *et al.* and Ferguson *et al.*. (Birchmeier *et al*, 2003; Ferguson *et al.*, 2003; Niemann, 2013) c-MET is processed from a single precursor protein by furin cleavage resulting in a disulfide linked α-chain-β-chain heterodimer. The cleavage site is located within the seven bladed β-propeller domain, called SEMA. The PSI domain is located, adjacently to the SEMA domain, standing for the homology to plexins, semaphorins, and integrins. This is followed by four immunoglobulin, plexins and transcription factor like domains (IPT 1-4), a single-spanning transmembrane domain as wells as an intracellular tyrosine-kinase domain. The only known ligand is HGF (hepatocyte growth factor or scatter factor) which is also a disulfide linked α-chain-β-chain heterodimer. Binding of HGF to c-MET induces receptor dimerization in a ligand:receptor 2:2 complex, transphosphorylation of tyrosine residues within the kinase domain, and recruitment of

intracellular signaling adaptor proteins, e.g. Gab1, Grb2 and Shp2. This is followed by activation of the PI3K-AKT-mTOR pathway stimulating cell survival as well as the Ras-Raf-MAPK/ERK signaling cascade inducing proliferation, cell-cycle progression, alterations of cell junctions, migration and invasion. PLCγ-PKC are also activated as well as STAT3/5 triggering proliferation and survival, respectively.
The epidermal growth factor receptor is composed of four extracellular domains (I-IV). Binding of EGF to domain I and III induces domain rearrangements from a tethered to an elongated conformation exposing receptor dimerization sites in domain II and IV. Receptor dimerization leads to transphosphorylation of tyrosine residues within the intracellular kinase domain activating AKT, MAPK, PLCγ, and STAT3/5 signaling. (Ferguson *et al.*, 2003; Yarden & Sliwkowski, 2001; Yewale *et al.*, 2013)
ECD = extracellular domain, ERK= extracellular signal-regulated kinase, MAPK = mitogen-activated protein kinase, PI3K = phosphatidylinositol-3-OH kinase, PKC = protein kinase C, PLCγ = phospholipase Cγ, Ras = rat sarcoma, Raf = rat fibrosarcoma, STAT = Signal transducer and activators of transcription

Therefore, cetuximab functions via the inhibition of EGFR phosphorylation and downstream signaling, receptor internalization (Mendelsohn & Baselga, 2003) as well as the initiation of ADCC (Kimura *et al*, 2007). However, good anti-tumor response mediated by cetuximab correlates with severe adverse events due to basal expression of EGFR in normal tissue, in particular the skin. (Lacouture, 2006) Acne-form skin rash, e.g. papulopustular rash, dry and itchy skin, is a characteristic adverse event during EGFR blockade by both small molecules and antibodies mediating growth arrest and the stimulation of inflammation. (Cunningham *et al*, 2004; Lacouture, 2006; Melosky *et al*, 2009) In particular, proliferating keratinocytes in the basal layer of the epidermis are predominantly affected due to high EGFR expression levels. (Lacouture, 2006) Until today, there are two other mAbs approved for anti-EGFR targeted therapy: panitumumab and nimotuzumab. Panitumumab (ABX-EGF, Vectibix), approved for colorectal cancer, is a fully human IgG2 antibody which was isolated by immunization of transgenic mice carrying human antibody repertoire ("XenoMouse") with A431 cells. (Giusti *et al*, 2007; Yang *et al*, 2001) Due to the IgG2 isotype, panitumumab is deficient of effector functions and its mode of action can be described by ligand blockade as well as the induction of internalization. (Giusti *et al.*, 2007) Similar to cetuximab, the epitope of panitumumab is located on domain III of EGFR and both antibody epitopes partially overlap with the EGF binding site. (Voigt *et al*, 2012) Nimotuzumab (h-R3, Theraloc) is a humanized IgG1 derived by mouse immunization and subsequent CDR grafting. It was approved for squamous cell carcinoma of head and neck, nasopharyngeal cancer and glioma. (Ramakrishnan *et al*, 2009) Interestingly, also nimotuzumab binds to EGFR domain III. (Tundidor *et al*, 2014) In course of this work, another humanized anti-EGFR antibody was used again targeting the domain III of EGFR, called matuzumab (425, EMD720000). (Murthy *et al*, 1987) In contrast to cetuximab, matuzumab's inhibition of EGFR signaling is ligand-independent and it acts via sterically blocking the conformation domain rearrangement required for the receptor dimerization process. (Schmiedel *et al*, 2008)

2.3.2. The hepatocyte growth factor receptor (c-MET)

The hepatocyte growth factor receptor (HGFR), also known as c-MET (for mesenchymal-epithelial transition), is a type I transmembrane protein RTK which was first identified as oncogenic TPR-MET (translocated promoter region fused to c-MET) fusion protein in chemically transformed human

osteosarcoma cells. (Cooper *et al*, 1984) Expression of c-MET and secretion of its ligand, hepatocyte growth factor (HGF, or scatter factor, SF), by mesenchymal cells are involved in cell differentiation, proliferation, survival, cytoskeleton rearrangement, cell detachment, scattering, motility and invasiveness. (Birchmeier *et al.*, 2003) The proteoglycan decorin has been also described as a ligand for c-MET. (Goldoni *et al*, 2009) On a macro-cellular level, c-MET plays a role in embryogenesis, wound healing and organ regeneration. (Birchmeier *et al.*, 2003) Tumorigenesis is characterized by morphological changes of cancer cells from epithelial to mesenchymal features enabling metastatic cell spreading. In general, higher c-MET expression can be found on metastatic lesions compared to primary tumor highlighting the involvement in metastasis. (Cipriani *et al*, 2009) c-MET is a disulfide linked α-chain-β-chain heterodimer proteolytically cleaved from a single precursor protein. It is composed of a large extracellular domain composed of a seven-bladed propeller domain called SEMA, a PSI domain related to plexins, semaphorins and integrins as well as four IPT domain repeats displaying homology to immunoglobulins, plexins and transcription factors (**Figure 4**). The furin cleavage site between α- and β-chain is located between blade 4 and 5. The single spanning transmembrane domain is followed by an intracellular tyrosine kinase domain. Ligand binding to the receptor induces its dimerization and autophosphorylation of tyrosine residues 1003, 1234 and 1235 leading to transphosphorylation of tyrosines 1349 and 1356 building up docking sites for Src homology 2 proteins (SH2). (Birchmeier *et al.*, 2003) This in turn activates intracellular signaling cascades including PI3K/AKT and Ras/MAPK pathways (**Figure 4**). The exact dimerization and receptor activation mechanism has still to be elucidated. HGF is a disulfide linked α-chain-β-chain heterodimer which is also processed from a single precursor protein. (Lokker *et al*, 1992) The HGF α-chain is composed of a N-terminal domain followed by four kringle domains, while the HGF β-chain consists only of one serine proteinase homology domain (SPH). (Lokker *et al*, 1992) It binds the proteoglycan heparin and forms HGF-homodimers in solution. (Birchmeier *et al.*, 2003) It was proposed that the ligand potentially induces dimerization of a 2:2 c-MET:HGF complex. (Niemann, 2013; Stamos *et al*, 2004) There are two proposed binding sites for HGF on c-MET: the HGF β-chain binds with low affinity to blades two and three of the SEMA domain. (Gherardi *et al*, 2003; Stamos *et al.*, 2004) The location of the high affinity binding site for the HGF α-chain is more controversially discussed: One group has described binding to IPT domains 3 and 4 by the shortened, N-terminal HGF fragment, called NK1. (Basilico *et al*, 2008) However, others suggest binding of NK1 to SEMA domain blade 5. (Niemann, 2013; Youles *et al*, 2008)

Due to the involvement of c-MET in tumorigenesis and metastasis, several HGF and c-MET directed antibodies have been developed recently and in parts have been evaluated in clinical trials. (Prat *et al*, 2014) HGF-neutralizing antibodies, e.g. rilotumumab and ficlatuzumab, only target the ligand and are therefore inefficient in cancer with constitutive c-MET activation. (Prat *et al.*, 2014) Furthermore, HGF

is stored in high abundance as an unprocessed precursor protein in the extracellular matrix of tissue hampering the efficiency of anti-HGF antibodies. (Prat *et al.*, 2014) Regarding c-MET, antibodies have been developed against several epitopes of the receptor: Onartuzumab (oa 5D5, MetMAb, RO5490258) and emibetuzumab (LY2875358) are the most advanced in clinical development with phase III and II trails, respectively. Even though the binding epitope of both antibodies is located within the c-MET SEMA domain, the monovalent onartuzumab predominantly acts via HGF-competition (Merchant *et al*, 2013) whereas the bivalent emibetuzumab induces receptor degradation besides the blockade of ligand binding (Liu *et al*, 2014). Three more anti-c-MET antibodies are currently evaluated in clinical phase I: the bivalent ABT-700 (h224G11) (Goetsch *et al*, 2010), the ADDC-enhanced ARGX-111 (WT52-E) (Basilico *et al*, 2014; Hultberg *et al*, 2015), and the bivalent c-MET degrading antibody SAIT301 (Oh *et al*, 2012). While ARGX-111 and emibetuzumab occupy an overlapping epitope, the exact binding site of SAIT301 is unknown. The latter induces c-MET degradation via LRIG1 (LRR and immunoglobulin-like domain-containing protein 1)-mediated lysosomal pathway. (Lee *et al*, 2014) This is presumably the same mode of action as described for another anti-c-MET antibody, LMH 87, binding to the top of the SEMA propeller on blade 3 and 4. (Greenall *et al*, 2012; Prat *et al.*, 2014) However, SAIT301 and LMH 87 do not display an overlapping epitope. (Lee *et al.*, 2014) Another c-MET degrading antibody is DN30 which binds to the forth IPT domain, induces degradation via the metalloprotease ADAM-10 and does not compete with ligand binding. (Vigna *et al*, 2015) Some anti-c-MET binders are prone to trigger partial or full agonism in the bivalent format (Liu *et al.*, 2014; Merchant *et al.*, 2013; Oh *et al.*, 2012; Pacchiana *et al*, 2010) requiring monovalency in parts for therapeutic application. Adverse events of the c-MET targeting antibody, e.g. onartuzumab, are mainly edema and thrombotic events being associated with the blockade of the c-MET/HGF axis regulating epithelial integrity and wound healing. (Morley *et al*, 2015)

2.3.3. Interplay of c-MET and EGFR

As described in the two former chapters, c-MET and EGFR display redundant signaling pathways, including GAB1 mediated activation of Ras-Raf-MAPK and PI3K-AKT pathways as well as induction of PLCγ-PKC and STAT3/5 signaling cascade (**Figure 4**). (Birchmeier *et al.*, 2003; Guo *et al.*, 2008; Yewale *et al.*, 2013) Due to pathway redundancies, one receptor is able to compensate for the loss of the other one upon single targeted inhibition. Furthermore, EGFR and c-MET also display interaction confirmed by co-immunoprecipitation and c-MET can also be trans-activated by the EGFR ligand TGFα. (Jo *et al.*, 2000) Beside signaling redundancies, upregulation and/or amplification of HGF and c-MET are critically involved in the development of acquired resistance in response to EGFR inhibition. Engelman and co-workers elucidated that c-MET amplification contributes to gefitinib resistance in NSCLC cells via activation of ErbB3 signaling. (Engelman *et al.*, 2007) In parts, c-MET amplification occurs in combination with the EGFR activating, drug-sensitive mutation T790M in lung cancer samples. (Bean *et*

al, 2007) HGF-secreting stromal fibroblasts in co-culture with lung cancer cells can induce insensitivity to EGFR inhibitors (Wang *et al*, 2009) and elevated HGF levels in the tumor micro-environment also contribute to innate resistance to Raf inhibitors via the activation of c-MET and subsequent MAPK as well as PI3K-AKT signaling (Straussman *et al*, 2012). In colorectal cancer, HGF and c-MET mediate intrinsic and acquired resistance in response to cetuximab. (Kammula *et al*, 2007; Liska *et al*, 2011) Beside c-MET activation, mutational status of KRAS (Kirsten rat sarcoma) negatively contributes to responsiveness to cetuximab treatment in colorectal cancer. (Knickelbein & Zhang, 2015) Due to redundant signaling and implication in resistance mechanisms, c-MET and EGFR inhibitors are currently under extensive preclinical and clinical development for both mono- and combination therapies as summarized in Prat *et al.*, Sharma and Adjei as well as Yewale *et al.*. (Prat *et al.*, 2014; Sharma & Adjei, 2011; Yewale *et al.*, 2013)

2.3.4. Bispecific antibodies directed against c-MET and EGFR

In the last three years, several bispecific antibodies targeting c-MET and EGFR have been developed which demonstrated synergistic effects in tumor proliferation and metastasis. (Castoldi *et al*, 2012; Castoldi *et al*, 2013; Garber, 2014; Jarantow *et al.*, 2015; Lee *et al*, 2016a; Lee *et al.*, 2016b; Lewis *et al.*, 2014; Spiess *et al*, 2013) In 2012, Castoldi and co-workers first described trispecific antibodies (TriMAbs, Roche) directed against c-MET, EGFR and IGF1R with a binder stoichiometry of 1:1:1 (Castoldi *et al.*, 2012) followed by a bispecific c-MET x EGFR, denoted as MetHer1 (Castoldi *et al.*, 2013). The latter was composed of a cetuximab IgG with knob-into-holes technology with a C-terminally genetically fused single chain Fab of onartuzumab to the knob-chain. The resulting molecule expressed in mammalian cells demonstrated an additive effect on the inhibition of proliferation in comparison to the treatment with the respective monospecific agents. In the same year, Genentech developed a knob-into-hole bsAb consisting of the bacterial expressed half antibodies anti-EGFR (D1.5) and onartuzumab. (Spiess *et al.*, 2013) Due to bacterial expression, this antibody lacked glycosylation and is therefore devoid of effector functions. Lewis *et al.* mentioned the generation of a bsAb targeting c-MET and EGFR by employing Fab interface engineering in order to ensure cognate light chain pairing. (Lewis *et al.*, 2014) However, the bsAb currently in clinical phase 1, LY3164530 (Eli Lilly), (Garber, 2014; Spiess *et al.*, 2015), presumably has a 2:2 stoichiometry. JNJ-61186372 (Janssen/Genmab) also recently moved to the clinic employing controlled Fab-arm exchange with a 1:1 stoichiometry. (Jarantow *et al.*, 2015; Labrijn *et al.*, 2011; Zheng *et al*, 2016) Interestingly, synergistic effects could be detected for the lower expressed target. (Jarantow *et al.*, 2015) By Samsung, Lee and colleagues introduced ME22S which induces internalization and degradation of c-MET and EGFR. (Lee *et al.*, 2016a; Lee *et al.*, 2016b) The underlying molecule is based on a 2:2 stoichiometry and the c-MET degrading antibody SAIT301. (Oh *et al.*, 2012) In summary, bsAbs with different binder stoichiometry have been developed. Stoichiometry and epitope combinations

thereby potentially influence agonistic behavior via receptor interaction and functionality via ligand competition or the induction of receptor degradation. However, tumor-selectivity has not been addressed for targeting c-MET and EGFR in a bispecific molecule.

2.4. Aim of this study

The presented work aims to evaluate the effects of bispecific targeting of two prominent tumor-associated antigens, namely c-MET and EGFR, and the application of affinity-optimized binders in order to balance high anti-tumor efficacy and reduced on-target off-tumor toxicities in normal tissue with basal expression of respective antigens (**Figure 5**). When increased tumor selectivity could be achieved by this engineering approach, the generated bsAbs could be armed with a cytotoxic agent for evaluation in an ADC context. Thus, anti-c-MET and anti-EGFR binders were selected based on their functionality, targeting of different epitopes, and distinct kinetic variants obtained by either *in vitro* affinity maturation or *in silico* screening. By combination of binders in the bispecific format in a modular toolbox approach employing SEED- and scFv-technology as well as transient transfection in mammalian cells, the appropriate affinity to retain biological function while enhancing the tumor selectivity by avidity effect should be determined. Finally, the efficacy of bsAbs could be evaluated in an ADC approach in c-MET and EGFR overexpressing cell lines in comparison to toxicity in normal tissue models, including primary keratinocytes and hepatocytes. This could lead to an *in vitro* proof of concept for enhancing the therapeutic window by application of affinity-optimized bispecific ADCs.

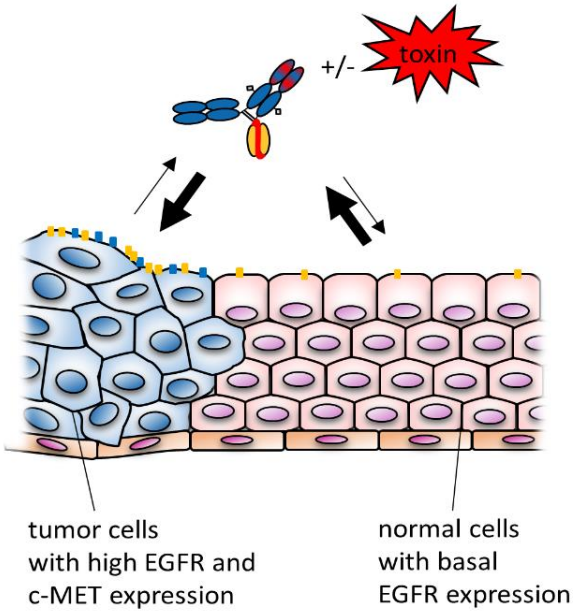

Figure 5: Strategy for bispecific anti-c-MET and anti-EGFR mAb and ADC generation.

By the combination of affinity attenuated anti-EGFR binders with anti-c-MET binders in the bispecific format in a ratio of 1:1, increased anti-tumor selectivity was aimed while retaining the efficacy for inhibiting c-MET and EGFR signaling. Receptor cross-linking by bsAbs could also lead to synergistic effects: improved efficacy due to simultaneous inhibition of both signaling pathways, increased internalization and concurrent degradation, and reduced inhibition of basally expressed EGFR in normal tissue cells which leads to attenuated EGFR-related adverse events and therefore improved tumor selectivity. Due to higher tumor selectivity, conjugation with cytotoxic agents could be considered for broadening the therapeutic window.

3. Material

3.1. Bacterial strains, bacteriophages, and human cell lines

Bacterial strains

E. coli One Shot TOP10 chemically competent cells (#C4040-10, Life Technologies, Karlsruhe, Germany); Genotype: F- *mcr*A Δ(*mrr-hsd*RMS-*mcr*BC) φ80*lac*ZΔM15 Δ*lac*X74 *rec*A1 *ara*D139 Δ (*ara-leu*) 7697 *gal*U *gal*K *rps*L (StrR) *end*A1 *nup*G

E. coli XL1 blue MRF' electrocompetent cells (#200158, Agilent Technologies, Waldbronn, Germany)

E. coli XL1 blue MRF' chemically supercompetent cells (#200230, Agilent Technologies, Waldbronn, Germany); Genotype: *(mcrA)183 (mcrCB-hsdSMR-mrr)173 endA1 supE44 thi-1 recA1 gyrA96 relA1 lac [F' proAB lacIqZM15 Tn10 (Tetr)]*

Bacteriophages

Helper phage M13K07 ('N0315S, New England BioLabs, Ipswich, MA, USA)

Mammalian cell lines

All mammalian cell lines were cultivated at 37°C, 10% CO_2. Cells were obtained from the American Type Culture Collection (ATCC®, Manassas, VA, USA), the Japanese Collection of Research Bioresources Cell Bank (JRCB), Riken Bioresource Center Cell Bank (RCB, Tsukuba, Japan), the Deutsche Sammlung von Mikroorganismen und Zellkulturen (DSMZ, Braunschweig, Germany), or companies as summarized in the following table (s. Table 1).

Table 1: List of mammalian cell lines.

Cell type and cell origin are listed for each cell line.

Cell line	Cell type	Origin
A431	human epidermoid carcinoma	ATCC® CRL 1555™
A549	human lung carcinoma	ATCC® CCL 185™
CHO-S	Chinese hamster ovary	Life Technologies, Darmstadt, Germany (R80007)
EBC-1	human lung carcinoma	JCRB0920 031496
Expi293F™	human embryonic kidney	Life Technologies, Darmstadt, Germany (A14527)
HCC-827	human lung adenocarcinoma	ATCC® CRL-2868™
HepG2	human hepatocellular carcinoma	Lipha / Merck, Darmstadt, Germany
KP-4	human pancreatic ductal cell carcinoma	RCB1005
MDA-MB-468	human breast adenocarcinoma (mammary gland)	ATCC® HTB 132™
MKN45	human gastric adenocarcinoma	DSMZ ACC 409
NCI-H1975	human NSCLC adenocarcinoma,	ATCC® CRL-5908™
NCI-H441	human lung adenocarcinoma	ATCC® HTB-174™
NCI-H596	human lung adenosquamous carcinoma	ATCC® HTB-178™
NHEK.f-c.	normal human primary keratinocytes	PromoCell, Heidelberg, Germany
Recombinant Jurkat cells	effector cells for ADCC assay	Promega, Mannheim, Germany (G701A)
SK-MEL2	human metastatic sit on skin of thigh	ATCC® HTB-68™
T47D	human metastatic site of mammary gland (pleural effusion)	ATCC® HTB-133™
U87MG	Human glioblastoma, astrocytoma	ATCC® HTB-14™

3.2. Plasmids

In the following **Figure 6** depicts the composition of the used plasmids.

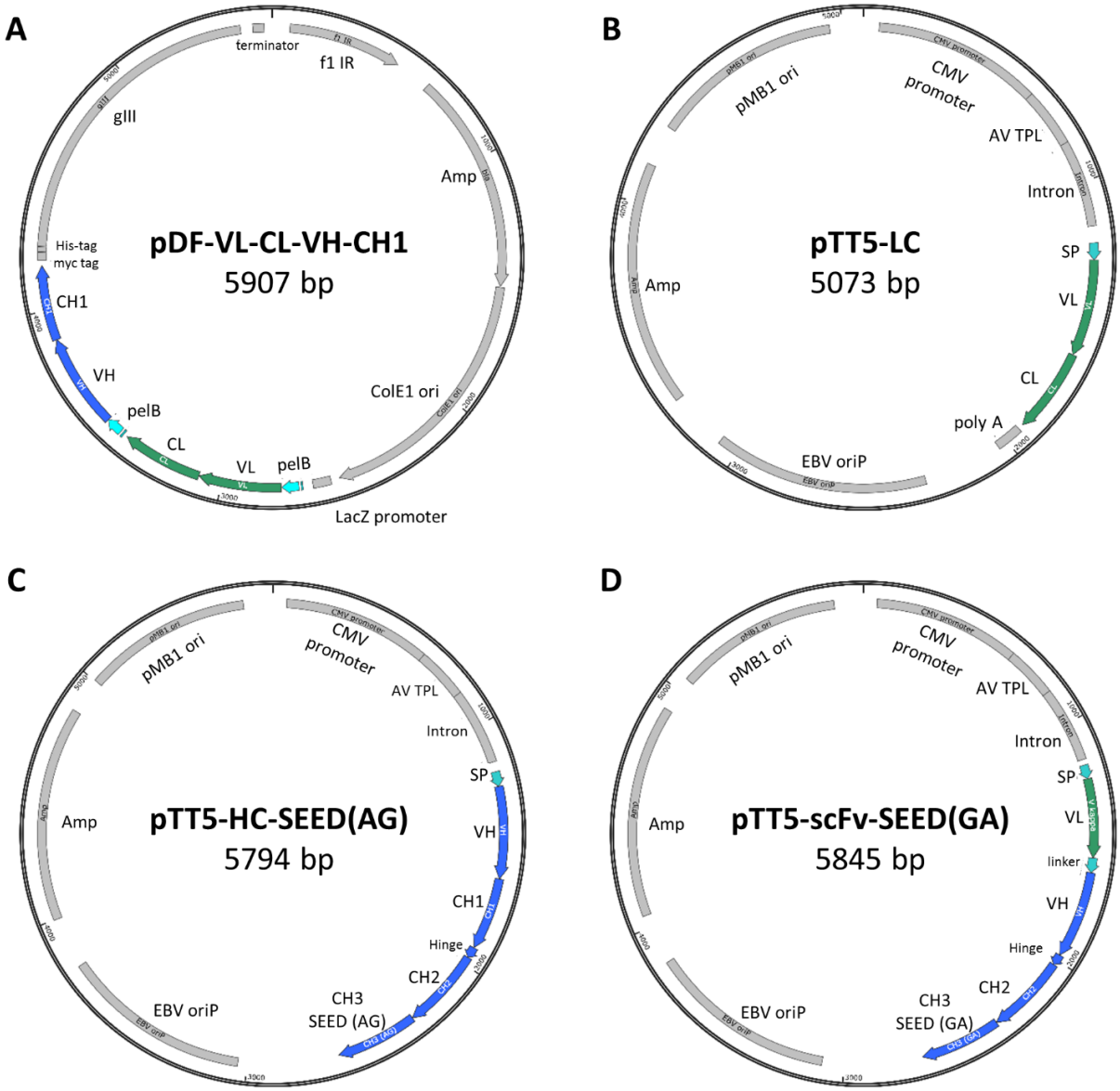

Figure 6: Schematic structure of plasmids.

(A) The pDF phagemid (kindly provided by Merck, Darmstadt, Germany) contains VL-CL and VH-CH1 sequences upstream flanked by pelB leader sequences under control of the lacZ promoter. pelB is thereby the signal sequence of the pectatlyase from *Erwinia caratovora*. (Lei *et al*, 1987) Downstream of the CH1 sequences, a myc- and His-tag are located followed by an amber stop codon and the gene for the pIII phage surface protein (gIII) and a terminator sequence. When using a supE strain with the amber stop codon, the fusion protein of Fab and pIII is expressed. The plasmid contains the ampicillin antibiotic resistance gene (Amp, β-lactamase) as selection marker for bacterial cells carrying the phagemid, Col E1 origin for bacterial replication of the phagemid, and a f1 phage origin for the synthesis of single-stranded DNA. **(B)-(D)** The pTT5 vector (National Research Council Canada) is a mammalian expression vector containing the following elements: The EBV oriP is the origin of replication in mammalian cells, again the ampicillin resistance gene (Amp, β-lactamase), the pMB1 ori as bacterial origin of replication, the pCMV stands for the cytomegalovirus immediate early promoter, AV TPL codes for the adenovirus tripartite leader, an synthetic intron including an enhancer element from the adeonivurs major late promoter enhancing protein expression (enh MLP). Downstream of the antibody sequences, the rabbit β-globin polyadenylation signal (pA) is located. (Zhang *et al*, 2009) The three vector encode the antibody light chain (VL-CL) **(B)**, the antibody heavy chain (VH-CH1-hinge-CH2-CH3) including SEED-AG sequences in the CH3 domain **(C)**, and a scFv fused to the hinge-CH2-CH3 domains **(D)** while the CH3 includes the SEED-GA sequences. The vector maps were created with SnapGene Viewer ver. 2.6.2.

3.3. Enzymes and proteins

Antarctic phosphatase, calf intestinal (CIP)	New England Biolabs, Beverly, USA
Benzonase	Novagen, Nottingham, GB
Bovine serum albumin (BSA), fraction V	Merck, Darmstadt, Germany
BSA standard solution (2 mg/ml)	Thermo Scientific, Schwerte, Germany
Gibco® Trypsin-EDTA	Life Technologies, Darmstadt, Germany
Lysozyme	Roche, Mannheim, Germany
Phosphatase inhibitor set II (#P524625)	Merck, Darmstadt, Germany (Calbiochem)
Phusion DNA polymerase	New England BioLabs, Ipswich, MA, USA
Protease inhibitor set III (#P524525)	Merck, Darmstadt, Germany (Calbiochem)
Recombinant human c-MET ECD-strepII-His	Merck, Darmstadt, Germany
Recombinant human c-MET SEMA-PSI-FLAG-His	Merck, Darmstadt, Germany
Recombinant human EGF (236-EG/CF)	R&D Systems, Minneapolis, MN, USA
Recombinant human EGFR (1-618)-His	Merck, Darmstadt, Germany
Recombinant human HGF (294-HGN/CF)	R&D Systems, Minneapolis, MN, USA
Recombinant sortase A	Merck, Darmstadt, Germany
T4 DNA ligase	New England BioLabs, Ipswich, MA, USA
Trypsin	Sigma Aldrich, Steinheim, Germany

3.3.1. Antibodies

Reference antibodies

cetuximab (Erbitux®, C225)	Merck, Darmstadt, Germany
matuzumab (C425)	Merck, Darmstadt, Germany
oa 5D5v2 g1 hinge IgG1 Fc (Knobs-into-holes)	Merck, Darmstadt, Germany
LY2875358 (LA480_vC8H241 IgG1)	Merck, Darmstadt, Germany
hu224G11 IgG1	Merck, Darmstadt, Germany
DN30 IgG1	Merck, Darmstadt, Germany
oa anti-hen egg lysozyme (HEL) SEED	Merck, Darmstadt, Germany

Anti-c-MET reference antibodies, including humanized oa 5D5 (MetMAb, onartuzumab), LY2875358 (LA480_vC8H241, emibetuzumab), hu224G11 (ABT-700), and DN30 IgG were reproduced based on VH and VL sequences derived from publicly available information (Patents no. US 6,214,344B1 (2001), US 8,398,974B2 (2013), US 8,329,173B2 (2012), EP 2500036B1 (2011)). (Liu *et al.*, 2014; Merchant *et al.*, 2013). Sequences were cloned in mammalian expression vectors (pTT5) containing constant IgG1 light

and heavy chain fragments except oa 5D5 applying knob-into-hole technology. (Ridgway *et al.*, 1996) All reference antibodies were produced in HEK293E cells using standard transfection and purification procedure (cf. chapters 4.4.1, 4.3.3 and 4.3.4) and were kindly provided by Merck, Darmstadt, Germany. Hence, the evaluated anti-c-MET reference antibodies were not derived from the respective laboratories of the original publications.

Primary antibodies for Western Blot

Rabbit anti-actin (20-30) pAb (A5060)	Sigma-Aldrich, Steinheim, Germany
Mouse anti-pIII antibody	MoBiTec, Göttingen, Germany
Rabbit anti-c-MET pAb (M3007-13A)	Biomol, Hamburg, Germany
Rabbit anti-cofilin mAb, clone D3F9 (#5175)	Cell Signaling Technologies, Cambridge GB
Rabbit anti-EGFR mAb, clone D38B1	Cell Signaling Technologies, Cambridge GB
Rabbit anti-GAPDH mAb, clone 14C10 (#2118)	Cell Signaling Technologies, Cambridge GB
Rabbit anti-p44/42 MAPK (Erk1/2) mAb, clone 137F5(#9101)	Cell Signaling Technologies, Cambridge GB
Rabbit anti-phospho p44/42 MAPK (Erk1/2) (T202/Y204) XP® mAb, clone D13.14.4E (#4370)	Cell Signaling Technologies, Cambridge GB
Rabbit anti-phospho-Akt (S473) mAb, clone D9E (#4060)	Cell Signaling Technologies, Cambridge GB
Rabbit anti-phospho-cMET mAb (Y1234/Y1235), clone D26 (#3077)	Cell Signaling Technologies, Cambridge GB
Rabbit anti-phospho-EGFR mAb (Y1173), clone E124 (ab32578)	Abcam, Cambridge,GB
Rabbit anti-Akt Ab (#9272)	Cell Signaling Technologies, Cambridge GB

Secondary antibodies for Western Blot

Goat anti-mouse IgG (H+L) peroxidase (HRP) conjugate	Jackson ImmunoResearch, Suffolk, GB
Alexa Fluor® 680 goat anti-rabbit IgG (H+L), A21076	Life Technologies, Darmstadt, Germany

Detection antibodies for flow cytometry

Anti-Alexa Fluor® 488 rabbit IgG (Quenching)	Life Technologies, Darmstadt, Germany
Goat anti-human Fc-specific Fab_2 PE conjugate	Jackson ImmunoResearch, Suffolk, GB
Goat anti-human IgG, Fc specific, FITC conjugate	Jackson ImmunoResearch, Suffolk, GB

Antibodies for receptor quantification

Mouse anti-EGFR mAb (ab187287)	Abcam, Cambridge, GB
Mouse anti-c-MET mAb (MAB3582)	R&D Systems, Minneapolis, MN, USA
Goat anti-mouse Fc $F(ab')_2$ FITC conjugate	Jackson ImmunoResearch, Suffolk, GB

Antibodies for ELISA

Anti-His6 peroxidase (HRP) conjugate	Roche, Mannheim, Germany
Mouse anti-myc	Merck, Darmstadt, Germany
Goat anti-HGF mAb, clone AF 294-NA	R&D Systems, Minneapolis, MN, USA
Goat anti-mouse IgG (H+L) peroxidase (HRP) conjugate	Jackson ImmunoResearch, Suffolk, GB
Goat anti-human IgG, Fcγ fragment specific peroxidase (HRP) conjugate	Jackson ImmunoResearch, Suffolk, GB
Rabbit anti-goat IgG (H+L) peroxidase (HRP) conjugate	Jackson ImmunoResearch, Suffolk, GB
Streptavidin-peroxidase (HRP) conjugate	Merck, Darmstadt, Germany

Capture and detection antibodies for MSD assay

Cannot be listed due to patent issues.

3.4. Oligonucleotides

Oligonucleotides were obtained from Eurofins MWG Operon, Ebersberg, Germany.

Primers for error prone PCR of c-MET binders B10 and F06:

PelB_VH_f1	GCCTACGGCAGCCGCTGG
CH1_VH_r1	GCACCAGCGGTGGCACCG
PelB_VL_f1	CTGTTGCCAACCGCTGCG
CL_VL_r1	CGCTGCTAGGCGGAAAC

Primers for site-directed mutagenesis PCR of hu225 scFv variants:

hu225_S58R_f	CGAGTGGATTGGAGTGATATGGAGAGGTGGAAACACAGAC
hu225_S58R_r	GTCTGTGTTTCCACCTCTCCATATCACTCCAATCCACTCG
hu225_N108Y_f	CTTACTACTGTCAACAAAATTATAACTGGCCAACCACGTTTGGCC
hu225_N108Y_r	GGCCAAACGTGGTTGGCCAGTTATAATTTTGTTGACAGTAGTAAG
hu225_T109D_f	GCAAGAGCCCTCGACTACTATGATTACGAGTTTGCTTACTGG
hu225_T109D_r	CCAGTAAGCAAACTCGTAATCATAGTAGTCGAGGGCTCTTGC
hu225_N109E-T112N_f	GTCAACAAAATAATGAGTGGCCAAACACGTTTGGCCAAGG
hu225_N109E-T112N_r	CCTTGGCCAAACGTGTTTGGCCACTCATTATTTTGTTGAC

Primers for sequencing:

pDFall_VL-f	GGAATTGTGAGCGGATAAC
pDFall_VH_r	CAGACAACCCAGTGCTGCG
pTT5_UP	CTGCGCTAAGATTGTCAGT
pTT5_RP	CCATATGTCCTTCCGAGTG

3.5. Chemicals

1-Step™ Ultra TMB-ELISA substrate solution	Thermo Scientific, Schwerte, Germany
Agar-agar	Merck, Darmstadt, Germany
Agarose	Life Technologies, Darmstadt, Germany
Ampicillin, sodium salt	Life Technologies, Darmstadt, Germany
Biocytin	Life Technologies, Darmstadt, Germany
Blocking solution for fluorescent Western Blot	Biomol, Hamburg, Germany
Calcium chloride ($CaCl_2$)	Merck, Darmstadt, Germany
Coomassie InstantBlue™	Expedeon Ltd, San Diego, CA, USA
Coomassie Plus - Bradford Assay™ Reagent	Thermo Scientific, Schwerte, Germany

Desocyribonucleotide triphosphates (dNTPs)	Novagen, Nottingham, GB
Disodium hydrogen phosphate (Na_2HPO_4*$2H_2O$)	Merck, Darmstadt, Germany
Eagle Minimal Essential Medium (MEM)	Sigma-Aldrich, Steinheim, Germany
EDTA (ethylenediaminetetraacetic acid)	Sigma Aldrich, Steinheim, Germany
EZ-Link-NHS-Biotin	Life Technologies, Darmstadt, Germany
Expi293™ expression medium	Life Technologies, Darmstadt, Germany
Gel filtration standards	Bio-Rad, Munich, Germany
Gel loading dye (6x)	Novagen, Nottingham, GB
GelRed™	VWR International, Darmstadt, Germany
Gibco® Dulbecco's modified eagle medium (DMEM)	Life Technologies, Darmstadt, Germany
Giboco® DMEM/F-12 (1:1)	Life Technologies, Darmstadt, Germany
Gibco® Dulbecco's PBS (DPBS, w/o $CaCl_2$, $MgCl_2$); phosphate buffered saline	Life Technologies, Darmstadt, Germany
Gibco® Fetal calf serum (FCS)	Life Technologies, Darmstadt, Germany
Gibco® L-glutamine	Life Technologies, Darmstadt, Germany
Gibco® sodium pyruvate	Life Technologies, Darmstadt, Germany
Giboc® RPMI 1640 medium	Life Technologies, Darmstadt, Germany
Glucose	Sigma-Aldrich, Steinheim, Germany
Guava instrument cleaning fluid (ICF)	Merck, Darmstadt, Germany
Glycine	Merck, Darmstadt, Germany
Hydrogen chloride (HCl)	Merck, Darmstadt, Germany
Isopropyl-β,D-thiogalactopyranosid (IPTG)	Merck, Darmstadt, Germany (Calbiochem)
Insulin	Sigma-Aldrich, Steinheim, Germany
Kanamycin sulfate	Merck, Darmstadt, Germany
Keratinocyte growth medium	PromoCell, Heidelberg, Germany
Methanol	Merck, Darmstadt, Germany
Monomethyl auristatin E (MMAE) with valine-citrulline (vc) linker and triple-glycine moiety	Merck, Darmstadt, Germany
MSD® Blocker A (R93BA-4)	Meso Scale Discovery, Gaithersburg, MD, USA
MSD® Read Buffer T (4x, R92TC-3)	Meso Scale Discovery, Gaithersburg, MD, USA
MSD® Tris Lysis Buffer (R60TX-3)	Meso Scale Discovery, Gaithersburg, MD, USA
MSD® Tris Wash Buffer (10x, R61TX-2)	Meso Scale Discovery, Gaithersburg, MD, USA
NuPAGE® LDS sample buffer (4x)	Life Technologies, Darmstadt, Germany
NuPAGE® MES SDS running buffer	Life Technologies, Darmstadt, Germany

NuPAGE® sample reducing agent	Life Technologies, Darmstadt, Germany
NuPAGE® Tris-acetate running buffer	Life Technologies, Darmstadt, Germany
Formaldehyde 37%	Merck, Darmstadt, Germany
Peptone	Merck, Darmstadt, Germany
Perfect DNA™ markers, 0.1 – 12 kbp	Merck, Darmstadt, Germany
Phusion HF buffer (5x)	New England Biolabs, Ipswich, MA, USA
Polyethylene glycol 8000	Sigma-Aldrich, Steinheim, Germany
Polyethylenimine, linear (PEI)	Polysciences Europe, Eppelheim, Germany
Potassium chloride (KCl)	Merck, Darmstadt, Germany
Potassium di-hydrogen phosphate (KH_2PO_4)	Merck, Darmstadt, Germany
Precision Plus Protein™ standards	Bio-Rad, Munich, Germany
ProCHO5 medium	Lonza, Basel, Switzerland
Propidium iodide (PI)	Life Technologies, Darmstadt, Germany
Protein standard HiMark™ pre-stained	Life Technologies, Darmstadt, Germany
Restriction enzyme buffers CutSmart or NEB1-4	New England Biolabs, Ipswich, MA, USA
RIPA cell lysis buffer (10x, #9806)	Cell Signaling Technologies, Cambridge GB
Sucrose	Merck, Darmstadt, Germany
S.O.C. medium	Life Technologies, Darmstadt, Germany
See Blue® Plus 2 prestained protein standard	Life Technologies, Darmstadt, Germany
Skim milk powder	Merck, Darmstadt, Germany
Sodium chloride (NaCl)	Merck, Darmstadt, Germany
Sodium hydroxide solution (NaOH), 2N	Merck, Darmstadt, Germany
Sodium perchlorate monohydrate ($NaClO_4*H_2O$)	Merck, Darmstadt, Germany
Sulfo-NHS-LC-Biotin	Thermo Scientific, Schwerte, Germany
Sulforic acid (H_2SO_4)	Bernd Kraft, Duisburg, Germany
SYPRO Orange	Life Technologies, Darmstadt, Germany
T4 DNA Ligation Buffer (10x)	New England BioLabs, Ipswich, MA, USA
TAE buffer	Life Technologies, Darmstadt, Germany
Tetracycline	VWR International, Darmstadt, Germany
Tris(hydrocymethyl)aminomethane (Tris)	Carl Roth, Karlsruhe, Germany
Tris-hydrochloride (Tris-HCl)	Sigma-Aldrich, Steinheim, Germany
Tween®20	Merck, Darmstadt, Germany
Ultra low IgG FCS	Life Technologies, Darmstadt, Germany
Yeast extract	Becton Dickinson, Heidelberg, Germany

3.6. Cell culture media

A431, A549, U87MG	DMEM, 10% (v/v) FCS
KP-4	DMEM/F-12 (1:1), 10% (v/v) FCS
MDA-MB-468, , HepG2, MKN45, NCI-H1975	RPMI 1640, 10% (v/v) FCS, 2 mM L-glutamine, 1 mM sodium pyruvate
HCC-827, NCI-H441, NCI-H596	RPMI 1640, 10% (v/v) FCS, 2 mM L-glutamine, 1 mM sodium pyruvate, 2.5 g/l glucose
T47D	RPMI 1640, 10% (v/v) FCS, 2 mM L-glutamine, 1 mM sodium pyruvate 10 μg/ml insulin
EBC-1	MEM Eagle, 10% (v/v) FCS, 2 mM L-glutamine
SK-MEL2	MEM Eagle, 10% (v/v) FCS, 2 mM L-glutamine, 1 mM Na-pyruvate, NEAA
CHO-S	ProCHO5, 4 mM L-glutamine
Expi293F™	Expi293™ expression medium
NHEK.f-c.	Keratinocyte growth medium (Promega)
ADCC assay medium	RPMI 1640, 4% (v/v) low IgG FCS (heat inactivated at 56°C for 30 min)

3.7. Solutions, media and buffer

Phosphate buffered saline (1xPBS)	140 mM NaCl, 3 mM KCl, 8 mM Na_2HPO_4 x $2H_2O$, 2 mM KH_2PO_4, pH 7.4
Potassium phosphate buffer	125.4 g/l K_2HPO, 23.1 g/l KH_2PO_4, pH 7.4
LB medium	10 g/l peptone, 5 g/l yeast extract, 10 g/l NaCl
LB-A medium	LB, 0.1 mg/l ampicillin
LB-A agar	LB-A, 15 g/l agar-agar,
2xTY medium	16 g/l peptone, 10 g/l yeast extract, 5 g/l NaCl, pH 7.0
2xTY-GA medium	2xTY, 20 g/l glucose, 0.1 mg/l ampicllin
2xTY-GA agar	2xTY-GA, 15 g/l agar-agar
5xTY medium	10 g/L peptone, 50 g/l yeast extract, pH 7.0
Phage dilution buffer	10 mM Tris, 20 mM NaCl, 2 mM EDTA
Polyethylenelgycol (PEG)/NaCl	200 g/l PEG6000, 2.5M NaCl ad dH_2O
Wash solution/PBS-T	0.05% (v/v) Tween® 20 in 1xPBS pH 7.4

Panning block buffer	PBS-T, 2% (w/v) BSA, 2% (w/v) milk powder
Blocking solution for peroxidase Western Blot	5% skim milk powder in PBS-T
Blocking solution for fluorescent Western Blot	1:1 Blocking solution for fluoresecent Western Blotting:1xPBS
Wash solution for fluorescent Western Blot	0.02 % Tween®20 in blocking solution for fluorescent Western Blot
FACS binding buffer	1% (w/v) BSA in DPBS
ProSepA binding buffer A	1.5 M glycine/NaOH, 3 M NaCl pH 9.0
ProSepA elution buffer B2	0.2 M glycine/HCL pH 2.5
ProSepA neutralization buffer C	1 M Tris/HCl pH 9.0
Protein A chromatography binding buffer	PBS, pH 6.8 – pH 7.0 or 10 mM Na_2HPO_4, 10 mM NaH_2PO_4, 500 mM NaCl, pH 7.0
Protein A chromatography elution buffer	0.1 M sodium citrate, pH 3.0 or 50 mM acetic acid, pH 3.0
Protein A chromatography neutralization buffer	3 M Tris/HCl, pH 8.5 or 1 M Tris/HCl, pH 9.0
Analytical size exclusion chromatography (SEC) mobile phase	PBS, pH 7.4 or 0.05 M sodium phosphate (NaH_2PO_4, Na_2HPO_4), 0.4 M sodium perchlorate, pH 6.35
Preparative SEC mobile phase	PBS, pH 7.4
Sortase reaction buffer	50 mM Tris, 150 mM NaCl, pH 7.5
Kinetics buffer (KB) for BLI	0.1% (w/v) BSA, 0.02% (v/v) Tween®20 in PBS
Low pH buffer (internalization assay for confocal microscopy)	50 mM glycine, 150 mM NaCl, pH 2.7 adjusted with HCl

3.8. Kits and laboratory materials

ADCC reporter bioassay kit	Promega, Mannheim, Germany
AirPore™ Tape Sheets, breathable sealing foil	Qiagen, Hilden, Germany
Amicon® Ultra-15 and 0.5 ml centrifugal filter units	Merck, Darmstadt, Germany
Cell culture flasks T75, T175	Greiner Bio-One, Kremsmuenster, Austria
Cell culture flat and round bottom Nucleon™ delta surface 96 well plates	Thermo Scientific, Schwerte, Germany

Cell culture 24 well plates Costar®	Thermo Scientific, Schwerte, Germany
CellTiter-Glo® luminescent cell viability assay kit	Promega, Mannheim, Germany
Gene Pulser ® electroporation cuvette, 0.1 cm	Bio-Rad, Munich, Germany
ExpiFectamine™ 293 transfection kit	Life Technologies, Darmstadt, Germany
Falcon® tumbes, 15 ml and 50 ml	VWR International, Darmstadt, Germany
FortéBio tips (AHC, streptavidin, ProteinA)	Pall ForteBio LLC, Menlo Park, CA, USA
GeneMorph II random mutagenesis kit	Agilent Technologies, Waldbronn, Germany
Gel and PCR clean-up kit NucleoSpin®	Macherey-Nagel, Dueren, Germany
HiLoad Superdex 200 pg 26/60 columns	GE Healthcare, Munich, Germany
HiTrap MabSelect SuRe columns, 5 ml	GE Healthcare, Munich, Germany
Human serum	Merck medical office, Darmstadt, Germany
iBlot® dry blotting nitrocellulose regular transfer stack (#B3010-01)	Life Technologies, Darmstadt, Germany
JETSTAR Plasmid Purification Kit (Midi and Maxi column)	Genomed, Loehne, Germany
Limulus amebocyte lysate Endosafe®-PTS™ cartriges, PTS2001F, FDA-licensed, 1-0.01 EU/ml	Charles River Laboratories, Wilmington, MA, USA
Keratinocyte detachment kit	PromoCell, Heidelberg, Germany
MaxiSorp®f flat-bottom 96 well micotiter plates	Sigma-Aldrich, Steinheim, Germany
Menzel glass coverslips	Menzel Glaser, Braunschweig, Germany
Mini-Sub® Cell GT cell gel chambers	Bio-Rad, Munich, Germany
Montage PROSEP-A spin columns (#P36486)	Merck, Darmstadt, Germany
Mouse serum (+ 0.09% soridum azide)	Bio-Rad, Munich, Germany (AbD Serotec)
NuPAGE® 3-8% Tris-Acetate gels	Life Technologies, Darmstadt, Germany
NuPAGE® 4-12% Bis-Tris gels	Life Technologies, Darmstadt, Germany
Phospho (S473)/total Akt assay whole cell lysate kit (K15100D)	Meso Scale Discovery, Gaithersburg, MD, USA
Phospho (T202/Y204;T185/Y187)/total ERK1/2 assay whole cell lysate kit (K15107D)	Meso Scale Discovery, Gaithersburg, MD, USA
PKH2 green fluorescent cell linker kit for cell membrane labeling	Sigma-Aldrich, Steinheim, Germany
Polypropylene microtiter plates, black	Greiner Bio-one, Frickenhausen, Germany

Polypropylene microtiter plates, clear	Greiner Bio-one, Frickenhausen, Germany
Polystyrene round bottom 96 well microtiter plates	Greiner Bio-one, Frickenhausen, Germany
ProLong Diamond Antifade Mountant with DAPI (4',6-diamidino-2-phenylindole)	Life Technologies, Darmstadt, Germany
Pur-A-Lyzer™ maxi dialysis kit 35100	Sigma-Aldrich, Steinheim, Germany
Qiaprep® Spin Miniprep kit	Qiagen, Hilden, Germany
Quick Ligation Kit	New England BioLabs, Ipswich, MA, USA
QFIKIT (Dako, K0078)	Agilent Technologies, Waldbronn, Germany
QuikChange II site-directed mutagenesis kit	Agilent Technologies, Waldbronn, Germany
Steriflip® filter device 0.22 μm	Merck, Darmstadt, Germany
Steritop™ bottle top filter 0.22 μm	Merck, Darmstadt, Germany
Tissue culture 24 well plates	Greiner Bio-one, Frickenhausen, Germany
TMB peroxidase substrate solution	Vector Laboratories, Burlingame, CA, USA
TSKgel SuperSW3000 column	Tosoh Bioscience, Darmstadt, Germany
Ultrafree® Centrifugal filter units	Merck, Darmstadt, Germany
Zeba Spin desalting PD-10 columns	Life Technologies, Darmstadt, Germany

3.9. Equipment

Analytical balance New Classic MF MS3002S	Mettler Toledo, Giessen, Germany
Cell counter Vi-CELL® XR	Beckmann Coulter, Brea, CA, USA
Chromatography systems ÄKTAxpress and ÄTKAexplorer 100	GE Healthcare, Munich, Germany
Confocal fluorescence microscope Leica TCS SPS, 100x objective	Leica Microsystems, Wetzlar, Germany
Electrophoresis chambers	Bio-Rad, Munich, Germany
Electroporation system Gene Pulser Xcell™	Bio-Rad, Munich, Germany
Endosafe®-PTS™ reader, PTS100	Charles River, Wilmington, MA, USA
Flow cytometer Guava easyCyte HT 2L	Merck, Darmstadt, Germany
Fluoresence reader Odyssey® CLx	LI-COR Biosciences, Bad Homburg, Germany
FortéBio Octet RED	Pall ForteBio LLC, Menlo Park, CA, USA
Gel imaging system GBOX	Syngene, Cambridge, GB
HeraSafe® Clean Bench	Thermo Scientific, Schwerte, Germany
Hot plate magnetic stirrer IKA® RCT basic	Sigma-Aldrich, Steinheim, Germany
HPLC Agilent 1200, ChemStation LC 3D	Agilent Technologies, FFM, Germany

iBlot® dry blotting system	Life Technologies, Darmstadt, Germany
Incubation shaker Minitron	Infros HT, Bottmingen, Switzerland
Incubator Heracell 150	Thermo Scientific, Schwerte, Germany
Megafuge 1.0R, rotor BS4402/A	Thermo Scientific, Schwerte, Germany
Microplate washer, ELx405™	BioTeK, Bad Friedrichshall, Germany
Microtiter plate reader BioTeK Synergy™ 4	BioTeK, Bad Friedrichshall, Germany
Microtiter plate reader SpectraMax® Paradigm®	Molecular Devices, Wals, Austria
MSD® plate reader Sector Imager 6000, Model 1200	Meso Scale Discovery, Gaithersburg, MD, USA
pH meter 744	Metrohm, Filderstadt, Germany
Power supply EC 250-90	Thermo Scientific, Schwerte, Germany
PowerPac™ basic power supply	Bio-Rad, Munich, Germany
Real-Time PCR system StepOnePlus	Life Technologies, Darmstadt, Germany
Spectrophotometer Nanodrop ND-1000	Peqlab, Erlangen, Germany
Spectrophotometer Ultrospex 3000	GE Healthcare, Munich, Germany
Table centrifuge 5415D	Eppendorf, Hamburg, Germany
Tetrad® 2 Peltier Thermal Cycler (PCR)	Bio-Rad, Munich, Germany
ThermoMixer®	Eppendorf, Hamburg, Germany
Utlracentrifuge Beckmann OptimaTM LE-80K, SW41 TI rotor	Global Medical Instrumentation, Ramsey, MN, USA
XCell SureLock™ gel electrophoresis device	Life Technologies, Darmstadt, Germany

Further equipment comprised common laboratory instrumentation.

3.10. Software

ÄKTA UNICORN software ver. 5.11 (Build 407)	GE Healthcare, Munich, Germany
Endosafe®-PTS™ data logging utility ver. 1.0	Charles River Laboratories, Wilmington, MA, USA
FortéBio octet data acquisition ver. 8.0	Pall ForteBio LLC, Menlo Park, CA, USA
FortéBio octet data analysis ver. 8.0	Pall ForteBio LLC, Menlo Park, CA, USA
Gen5™ microplate reader software ver. 1.11.5	BioTeK Instruments, Bad Friedrichshall, Germany
GraphPad Prism ver. V5.0.4	GraphPad Software, La Jolla, CA, USA
GuavaSoft ver 2.7	Merck, Darmstadt, Germany

HPLC software ChemStation	Agilent Technologies, FFM, Germany
Image Studio™ software ver. 2.1	LI-COR Biosciences, Bad Homburg, Germany
Lasergene ver. 12.3.1	DNA Star Inc., Wisconsin, WI, USA
Microsoft Office 2013	Microsoft Corp., Redmond, WA, USA
MSD Software Assay Explorer ver. 3.3	Meso Scale Discovery, Gaithersburg, MD, USA
Paradigm™ software SoftMaxPro ver. 6.3	Molecular Devices, Wals, Austria
Protein Thermal Shift™ software ver. 1.0	Life Technologies, Darmstadt, Germany
PyMOL ver. 1.3r1	Schrodinger LLC, San Diego, CA, USA
Reference Manager ver. 12	Thomson Reuters, FFM, Germany
SnapGene® Viewer ver. 2.6.2	GSL Biotech LLC, Chicago, IL, USA
Vi-CELL® XR ver. 2.04	Beckmann Coulter, Brea, CA, USA

4. Methods

4.1. Molecular biological methods

4.1.1. Determination of DNA concentration

The nucleic acid concentration in aqueous solutions was measured by a UV spectrophotometer Nanodrop ND1000 (cf. chapter 3.9) applying 1.5 µl of sample. The underlying physical principals are the law of Lambert-Beer and the absorption of aromatic nucleobases within the DNA at the wavelength 260 nm. The ratios A_{260}/A_{280} and A_{260}/A_{230} can be used as a quality criteria for the purity of the DNA and should be around 1.8 and 2.0-2.2, respectively.

4.1.2. Polymerase chain reaction

DNA can be exponentially and specifically amplified by the polymerase chain reaction (PCR) employing DNA flanking, complementary oligonucleotides or primers. (Mullis *et al*, 1986). For DNA fragment amplification prior to cloning, 10 ng of plasmid DNA were mixed with 10 µl Phusion HF buffer, 0.2 µM forward and reverse primer, 200 µM dNTPs, 0.5 µl 2 U/µl Phusion® High-Fidelity DNA polymerase, and dH_2O in a final volume of 50 µl. After initial denaturation at 95°C for 60 sec, 30 cycles of amplification were performed for each 10 sec at 95°C for denaturation, 30 sec at 55°C for annealing, and 30 sec at 72°C for extension followed by a final extension for 10 min at 72°C. The annealing temperature was adjusted to the melting temperatures of the used primer pair calculated by Seqbuilder (Lasergene).

In order to introduce nucleotide changes, QuikChangeII site-directed mutagenesis kit (Chapter 3.8) was applied according to the manufacturer's instructions. Briefly, PCR mixtures were prepared as described above except 5 µl reaction buffer and 1 µl PfuUltra HF DNA polymerase (2.5 U/µl) were used. After initial denaturation at 95°C for 30 sec, 12 to 18 cycles of amplification were used for each 30 sec at 95°C for denaturation, 1 min at 55°C for annealing, and 1 min/kb of plasmid length at 68°C for extension. After subsequent incubation for 2 min on ice, parental DNA was digested with 1 µl DpnI restriction enzyme. Then, DNA was subjected to transformation in supercompetent *E. coli* XLI blue cells.

For the randomization of variable regions of heavy and light chain, error prone PCR was conducted applying the GeneMorph II Random Mutagenesis Kit (Chapter 3.8) containing a DNA polymerase which is prone to base pair exchanges (16 mutations in 1000 bp). Briefly, 0.2 ng DNA template were added to 5 µl reaction buffer, 200 µM dNTPs, 0.2 µM forward and reverse primer, 1 µl Mutazyme II DNA polymerase (2.5 U/µl) and dH_2O in a final volume of 50 µl. After initial denaturation at 95°C for 2 min, 30 cycles of amplification were used for each 30 sec at 95°C for denaturation, 30 sec at 60°C for annealing, and 1 min at 72°C for extension.

4.1.3. Purification of DNA

DNA fragments were purified after PCR amplification or from agarose gel bands excised with a clean scalpel using the Gel and PCR clean-up kit NucleoSpin® (chapter 3.9) according to the manufacturer's instructions. DNA was eluted in 10-50 μl elution buffer from the kit or dH_2O. DNA concentration was photometrically determined (cf. chapter 4.1.1).

4.1.4. Enzymatic digestion and ligation of DNA

Type II restriction endonucleases can be used as molecular scissors for DNA fragmentation at defined sequences. For preparative digest, 5 μg DNA were digested with two restriction enzymes (each 1-2 μl) in corresponding restriction buffer for 2-3 h at the temperature optimum of the respective enzymes in a volume of 30 μl. After digestion, thermal inactivation of enzymes was carried out (in general 20 min at 65-80°C) and p.r.n. plasmid DNA was dephosphorylated by addition of 1 μl calf intestinal Antarctic phosphatase (CIP) for 1 h at 37°C. Antarctic phosphatase removes 5'-phosphate groups in linear, double strand DNA and prevents religation of plasmid DNA and the reaction was inactivated by heat (10 min, 65°C).

For ligation, three fold molar excess of insert were mixed with dephosphorylated and linearized DNA vector (50 ng for conventional ligation, 1 μg for library cloning) in ligation buffer in presence of 1 μl T4-DNA ligase in final volume of 20 or 100 μl for library generation overnight at 16°C. After ligation, DNA was purified in Amicon® centrifugal tubes and ligation mixture was subjected to transformation in *E. coli*.

4.1.5. Gel electrophoresis and gel extraction

With the help of agarose gel electrophoreses, linear DNA fragments can be separated in an electric field based on their length. In general, 1-2% (w/v) agarose gels were prepared in TAE buffer (chapter 3.5) supplemented with GelRed™ solution (1:10,000). DNA premixed with 6x loading dye were loaded on gels along with 10 μl Perfect DNA™ marker (0.1-12 kbp) for determination of size and quantity of separated DNA fragments and gels were run for 45 min at 100 V. DNA bands were visualized by UV light using the gel imaging system GBOX (chapter 3.9).

4.1.6. DNA sequencing

Isolated plasmid DNA (15 μl with 50-100 ng/μl) or alternatively transformed *E. coli* glycerol stocks in 96 well plates were transferred to Eurofins MWG Operon (Ebersberg, Germany) and sequenced using primers listed in chapter 3.4.

4.2. Microbiological methods

4.2.1. Transformation in *E. coli* and plasmid preparation

Transformation of *E. coli* XL1 blue MRF' cells with plasmid DNA was carried out by electroporation or heat shock. For library generation, 20 µl purified ligation mix was added to 30 µl electrocompetent *E. coli* cells in 0.1 cm electroporation cuvettes. After incubation on ice for 1 min, electroporation was conducted with an electric pulse of 1.7 kV for ~5 msec. Transformed cells were immediately transferred to 1 ml pre-warmed S.O.C. medium (chapter 3.5) and incubated at 37°C and 600 rpm for 1 h. Afterwards, cells were plated on 25 x 25 cm agar plates with 2xTY-GA selective agar and incubated overnight at 37°C.
For plasmid amplification (after ligation etc.), 5 µl plasmid DNA were incubated with 50 µl chemically competent *E. coli* One shot TOP10 (or alternatively 50 µl supercompetent *E. coli* XL1 blue cells for site-directed mutagenesis), which were thawed on ice, for 30 min. Heat-shock was performed for 30 sec at 42°C followed by incubation on ice for 1-2 min. Then, transformed cells were shaken in 250 µl S.O.C. medium for 1 h at 225 rpm and 37°C followed by plating on LB-A selective agar and incubation overnight at 37°C. For plasmid re-transformation, only 1 µl plasmid DNA was applied and incubation times were shortened to 10 min on ice and 30 min at 225 rpm and 37°C, respectively.

From single *E. coli* colonies, overnight *E. coli* cultures were inoculated in LB-medium. Plasmid DNA was isolated from 2 ml *E. coli* cultures using the Qiaprep® Spin Miniprep kit or from 100-200 ml *E. coli* cultures applying the JetStar plasmid preparation kits (Midi and Maxi, respectively) according to the manufacturer's information. DNA elution was carried out with 50-300 µl dH_2O depending on the size of the *E. coli* culture.

4.2.2. Sub-library generation for affinity maturation

For *in vitro* affinity maturation, three sub-libraries based on randomization of VH and –VL sequences of the anti-c-MET binder F06 were generated. F06 was derived from panning of HAL7/8 libraries (Hust *et al*, 2011) against c-MET and was kindly provided by Merck, Darmstadt, Germany.
The first two sub-libraries were generated by error-prone PCR of the F06-VH and –VL sequences using the primers PelB_VH_f1, CH1_VH_r1, PelB_VL_f1, and CL_VL_r1 (chapter 4.1.2). After PCR, amplified DNA fragments were cloned into the pDF-Fab-F06 vector with restriction enzymes (NcoI/SalI for VH and BssHII/AvrII for VL) followed by ligation and transformation in *E. coli* (cf. methods in chapters 4.1 and 4.2). For the third sub-library, a parsimonious mutagenesis approach was applied for the CDR-H3 of F06. The coding mixtures for each amino acid of the CDR-H3 was calculated so that the parental amino acid remains to a probability of 60-70% and that the generation of stop codons, methionines, and cysteins are avoided. Based on the calculated codon mixture, the sub-library was generated by GeneArt® (Life Technologies, Darmstadt, Germany) by gene synthesis. The parsimonious sub-library was cloned

with restriction enzymes NcoI/SalI into the pDF-Fab-F06 vector (chapter 3.2) followed by ligation and transformation in *E. coli* (cf. methods in chapters 4.1 and 4.2).

4.2.3. Library packaging and Fab phage production

In order to package a library, 30 ml of 2xTY-GA were inoculated with 50-200 µl *E. coli* transformed with library antigen fragment phagemid vectors (OD_{600nm}<0.1) and were grown to OD_{600nm} ~0.5 at 37°C with 250 rpm on a shaker. Then, 5 ml *E. coli* culture (~2.5x10^9 cells) were infected with 500 µl helperphage M13K07 (ratio 1:20) followed by 30 min incubation without shaking and then 30 min with 350 rpm shaking at 37°C. Due to the packaging signal coded by the phagemid and the envelope proteins coded by the phage genome, bacteriophages can be produced and secreted from *E. coli* cells. Subsequently, cells were centrifuged (3220xg, 10 min) in order to remove glucose which represses lac promoter (cf. chapter 3.2) and therefore expression of Fab-pIII fusion protein. Cells were resuspended in 30 ml 2xTY supplemented with 0.1 mg/l ampicillin and 0.03 mg/l kanamycin to produce Fab-phage overnight at 250 rpm and 30°C. Bacteria were centrifuged (3220xg, 4°C, 10 min) and bacteriophages were precipitated from the supernatant by addition of 1/5 volume PEG/NaCl (cf. chapter 3.7) for 1 h on ice followed by centrifugation. The phage pellet was resuspended in 500 µl phage dilution buffer (cf. chapter 3.7). In order to remove potential cell debris, phage solution was centrifuged once again (16,100xg, 10 min, RT) and packaged antibody phage library was stored at 4°C.

For phage titration, 50 ml 2xTY supplemented with 12.5 mg/l tetracycline were inoculated with *E. coli* XL1 blue MRF' overnight culture at 37°C and 250 rpm until reaching OD_{600nm} ~0.5. A serial dilution of the phage suspension was prepared in PBS (10^{-2} to 10^{-10} phages/ml). Afterwards, 50 µl *E. coli* culture was mixed with 10 µl of the respective dilution, incubated for 30 min at 37°C and plated on 2xTY-GA agar plates. After incubation at 37°C overnight, colony forming units (cfu) were counted and phage titer (cfu/ml) was calculated according to the dilution.

4.2.4. Selection of phage display libraries

The antibody selection was carried out in MaxiSorp® microtiter plates with immobilized c-MET ECD protein (Merck, Darmstadt, Germany). In the first panning round, 2 µg/well and in the following two rounds 1 µg/well c-MET were immobilized overnight on plates in 150 µl PBS at 4°C. After three times washing with PBS-T (300 µl) with a microplate washer ELx405™, the microtiter plate antigen-coated surface was blocked with 300 µl panning block buffer at RT for 1 h. In parallel, the Fab-antibody-fragment-phage library (first panning round: 2x10^{11}, second and third panning rounds: 5x10^{10} phages) was pre-incubated for 1 h in an empty well in 150 µl panning block in order to remove anti-plastic, anti-BSA, and anti-milk powder binders. Afterwards, the amplified Fab-antibody-fragment-phage library

(cf. chapter 4.2.3) was incubated on the surface-bound antigen at RT in a humidified chamber for 2 h. Starting in the second round, a 50 fold excess of soluble c-MET was added in the last hour of the antigen incubation in order to remove anti-c-MET binders with fast off-rates. Subsequently, stringent washing was applied (first panning round: 10x, round 2: 20x, round 3: 30x) to remove the vast excess of nonbinding antibody phages. Phages were eluted with 200 µl trypsin (10 µg/ml) at 37°C for 15 min. The phage titer after the selection was carried out as described in chapter 4.2.3. Subsequently, 20 ml of *E. coli* culture with OD_{600nm} ~0.5 was infected with phage eluate and incubated for 30 min without shaking and 30 min at 250 rpm at 37°C. After centrifugation (3220xg, 10 min), the cell pellet was resuspended and plated on 2xTY-GA agar plates overnight. The next day, agar plates were floated-off with 5 ml 2xTY-GA and either glycerol stocks were prepared (800 µl bacteria solution + 200 µl 80% (v/v) glycerol, storage at -80°C) or phages were amplified from phagemid carrying bacteria according to chapter 4.2.3 and a new selection round was started.

4.2.5. Production of soluble Fab-fragments in microtiter plates

From the selective agar plates of the respective round, single colonies were picked with sterile tips and inoculated in 96 well polypropylene microtiter plates with 150 µl TY-GA. The plates were sealed with breathable sealing film and incubated overnight at 37°C, 800 rpm, and 70% humidity. For soluble Fab-fragment production, 10 µl of each single culture was added to 180 µl 2xTY-GA in a new polypropylene microtiter plate and incubated for 2 h at 37°C, 800 rpm, and 70% humidity. To the residual culture, 100 µl/well 50% glycerol were added and stored at -80°C. After 2 h, the new culture was centrifuged (3220xg, 4°C, 10 min) and resuspended in 200 µl 5xTY medium supplemented with 1x potassium phosphate buffer, 50 mM saccharose, 0.1 mg/l ampicillin, and 100 µM isopropyl-β,D-thiogalactopyranosid (IPTG). The production of soluble Fabs was carried out overnight at 30°C, 800 rpm, and 70% humidity. After centrifugation (3220xg, 4°C, 10 min), soluble Fab-antibody fragment-containing supernatants were subjected to further analysis.

4.3. Biochemical methods

4.3.1. Determination of protein concentration

Protein concentration were photometrically determined either by absorption at 280 nm (A_{280}) according to the law of Lambert-Beer's, by Bradford assay using the Coomassie Plus - Bradford Assay™ reagent (Bradford, 1976) or applying the UV spectrophotometer Nanodrop ND1000 (cf. chapter 3.9) while the concentration was calculated to the respective molecular weight (in kDa) and molar extinction coefficient (M-1 cm-1; Protean Software, Lasergene DNASTAR, chapter 3.10) of the protein. For the Bradford assay, a serial dilution of BSA (0.1-1 mg/ml) served as a reference protein standard curve. The sample was diluted (1:2 to 1:10 depending on the concentration). 5 µl of each sample or standard

dilution were added to a microtiter plate well together with 150 µl Bradford reagent. After shaking and incubation for 10 min in the dark, adsorption at 595 nm was performed. Comparison of samples with the calibration curve was used for calculation of the protein concentration.

4.3.2. Protein biotinylation

Biotinylation was performed with the EZ-Link™ Sulfo-NHS (N-Hydroxysuccinimide)-Biotinylation Kit (chapter 3.8) according to the manufacturer's instructions incubating 50-200 µg protein with a 50-fold molar excess of EZ-Link™ Sulfo-NHS reagent in 200-700 µl PBS. Residual reagent was removed by Zeba™ Desalt Spin columns (chapter 3.8).

4.3.3. Protein A affinity chromatography

For purification of antibodies from supernatants of small-scale productions (25 ml, chapter 4.4.2) purification was carried out with PROSEP® A centrifugal Protein A columns (chapter 3.8) according to manufacturer's instructions using recommended buffers binding buffer A, elution buffer B2 and neutralization buffer C (chapter 3.7) as well as centrifugation (150xg, 5-20 min per step). Briefly, PROSEP® A columns were equilibrated with binding buffer A and supernatants mixed in a ratio of 1:1 (v/v) with binding buffer A were applied on the columns followed by two washing steps à 10 ml binding buffer A. Elution was carried out with 10 ml elution buffer B2 in tubes containing 1.3 ml neutralization buffer C. Eluates were concentrated with Amicon® Ultra-15 centrifugal filter device with 10,000 molecular weight cut-off (MWCO; 3000xg, ~10 min) and subsequently dialyzed to PBS pH 7.4 using Pur-A-Lyzer™ Dialysis Kit (both chapter 3.8).

For purification of antibodies from supernatants of large scale productions (200 ml, chapter 4.4.2) affinity chromatography using 5 ml HiTrap MabSelect SuRe (chapter 3.8) on an ÄKTAxplorer 100 or ÄKTAxpress system (chapter 3.9) was applied using binding, elution and neutralization buffer described in chapter 3.7. Briefly, the column was equilibrated with 5 column volumes (CV) of binding buffer at 2.5 ml/min. Subsequently, supernatants were applied (2.5 ml/min) with active air sensor and washed with 10 CV of binding buffer. Elution was carried out with 5 CV elution buffer. 1 ml fractions were collected in 96 deep well plates (chapter 3.8) with 200 µl neutralization buffer. Fractions from the protein peak were pooled, concentrated with Amicon® Ultra-15 centrifugal filter device with 10,000 MWCO (3000xg, ~10 min) and subjected to size exclusion chromatography (SEC, chapter 4.3.4).

4.3.4. Size exclusion chromatography

4.3.4.1. Preparative size exclusion chromatography

To separate desired antibody monomer from high molecular weight protein aggregates and in case of bsAbs also from GA-GA-SEED homodimers, preparative size exclusion chromatography (SEC) was performed using the HiLoad 26/60 Superdex 200 pg (cf. chapter 3.8) with PBS pH 7.4 or other desired buffer as mobile phase. Columns were equilibrated with 2 CV buffer at 2.5 ml/min, before 2 ml concentrated protein was loaded with a sample loop. 1 ml fractions were collected and selected fractions were pooled. Antibodies were again concentrated with Amicon® Ultra-15 centrifugal filter device (10 kDa MWCO) resulting final concentrations of 1-2 mg/ml protein. Protein concentrations and purity were determined by A_{280} spectroscopy, gel electrophoreses and analytical SEC (chapters 4.3.2, 4.3.5, 4.3.6 and 4.3.8.1). Endotoxin levels were assessed by Limulus amebocyte lysate (LAL) Endosafe® PTS cartridges and Endosafe® PTS reader (chapter 3.8, 3.9 and 3.10) according to the manufacturer's instructions.

4.3.4.2. Analytical size exclusion chromatography

For evaluation of protein purity, molecular size and presence of high molecular weight protein aggregates or SEED-homodimers for bsAbs, analytical size exclusion high performance liquid chromatography (SE-HPLC) was performed using TSK Super SW3000 column (Tosoh, chapter 3.8) and the HPLC Agilent 1200 (ChemStation LC 3D, chapter 3.9 and 3.10). Briefly, columns were equilibrated with mobile phase buffer (chapter 3.7) at 0.35 ml/min until obtaining stable baseline (~45 min). As molecular weight standard reference proteins from the gel filtration standard (Bio-Rad, chapter 3.8) were prepared and applied according to the manufacturer's instructions (diluted 1:20 in PBS). Protein samples were diluted to a final concentration of 0.5 mg/ml in PBS. The injection volume was 15 μl per run and the following sequence was injected: mobile phase, gel filtration standard, duplicates of protein samples, gel filtration standard, mobile phase. Chromatograms recorded at 280 nm (or alternatively 214 and 254 nm) were analyzed by the ChemStation software (chapter 3.10) by integration of peaks.

4.3.5. SDS-PAGE

In order to determine protein purity or analyze cell lysates, sodium dodecyl sulfate polyacrylamide gel electrophoresis (SDS-PAGE) was conducted for protein separation by molecular weight in an electric field according to Laemmli. (Laemmli, 1970) SDS (or lithium dodecyl sulfate, LDS) thereby serves as anionic detergent which attaches to proteins resulting in a total negative net charge. For this, protein samples or cell lysates were mixed with 4 x LDS sample buffer and 10 x sample reducing agent (when reduction of disulfide bonds was aimed), followed by incubation for 10 min at 70°C for protein denaturation. Samples were subjected to either NuPAGE® Bis-Tris gels (4-12%) or Tris-Acetate gels (3-

8%) using the appropriate volume according to the size of the wells which were installed in gel electrophoresis chambers with MES (2-(N-morpholino)ethanesulfonic acid) or Tris-Acetate SDS running buffer, respectively (chapter 3.8). As protein standard for antibody samples, the See Blue® Plus 2 prestained protein standard and for cell lysates or the HiMark™ pre-stained protein standard were used (chapter 3.8). Bis-Tris gels were run for 30 min at 200 V and Tris-Acetate gels for 1 h at 150 V. Next, gels were subjected to coomassie staining (chapter 4.3.6.) or Western blotting (chapter 4.3.7.).

4.3.6. Coomassie staining

Coomassie staining was performed for direct visualization of proteins separated by SDS-PAGE using Coomassie InstantBlue™ (chapter 3.5). Gels were incubated for 10-30 min and destained in dH_2O according to the manufacturer's instructions.

4.3.7. Western blotting

Western blotting for protein visualization mediated by detection antibodies conjugated to either enzymes (e.g. HRP, horse reddish peroxidase) or fluorescent dyes was carried out with the dry blotting system iBlot according to the manufacturer's instructions (chapters 3.8 and 3.9). Briefly, proteins from SDS-PAGE gels were transferred to polyvinylidene difluoride (PVDF) membranes (program 3, 7 min, 20 V) and proteins were detected with antibodies listed in chapter 3.3.1.

4.3.7.1. Peroxidase-labeled secondary antibodies

After transfer of proteins to PVDF membrane, membranes were blocked in blocking solution (chapter 3.7, 5% skim milk powder in PBS-T) for 1 h at RT. Then, membranes were incubated with primary antibodies in PBS-T for 1 h at RT. After washing three times with PBS-T, membranes were incubated with peroxidase-labeled secondary antibody for 1 h at RT. After washing, antibody binding was revealed by addition of peroxidase substrate, 3,3',5,5'-tetramethylbenzidine (TMB) within the TMB substrate kit (chapter 3.8) following the manufacturer's instructions.

4.3.7.2. Fluorescently labeled secondary antibodies

For fluorescent western blotting, PVDF membranes were blocked in 1:1 dilution of Fluorescent Western Blot Solution in PBS (chapter 3.7) for 1 h at RT. Afterwards, membranes were cut if necessary and incubated with primary antibodies in 1:1 dilution of Fluorescent Western Blot Solution in PBS (chapter 3.7) supplemented with 0.2% Tween®20 overnight at 4°C. After washing three times with 1:1 dilution of Fluorescent Western Blot Solution in PBS (chapter 3.7) supplemented with 0.05% Tween®20, detection was carried out with AlexaFluor 680 labeled secondary antibody (usually goat-anti-rabbit IgG, chapter 3.3.1) diluted 1:10,000 in washing buffer. After additional washing and drying of membranes,

fluorescent bands were visualized using the Fluorescence reader Odyssey® CLx and corresponding software Image Studio™ software (chapters 3.9 and 3.10).

4.3.8. Enzyme-linked immunosorbent assay

Determination of specific protein-protein interactions was determined by enzyme-linked immunosorbent assay (ELISA) in 96 well MaxiSorp® polystyrene microtiter plates (Engvall *et al*, 1971). All steps were carried out at room temperature in a volume of 100 µl with exception of blocking and washing which were conducted in 300 µl 2% BSA in PBS-T overnight at 4°C and 300 µl PBS-T, respectively. Washing was performed with a microplate washer ELx405™ (chapter 3.9). The peroxidase was detected by addition of 100 µl 1 step Ultra TMB ELISA substrate solution and the reaction was terminated with 100 µl 2 N sulfuric acid. Absorbance was measured at 450 nm using the Paradigm™ microtiter plate reader and respective software (chapter 3.9 and 3.10).

4.3.8.1 Binding of soluble Fab-fragments to c-MET

For the determination of soluble Fab-antibody fragments binding to c-MET, ELISA was performed with 100 ng immobilized c-MET ECD in microtiter plates which was carried out overnight at 4°C. After three times washing, plates were blocked at RT for 1 h. After a subsequent washing step, Fab-antibody fragments were added diluted in the ratio 1:2 in 100 µl 2% BSA in PBS-T. After removal of Fabs by washing, the detection was carried out with mouse anti-myc (IgG9E10, 1:1000) and peroxidase labeled goat anti-mouse IgG (H+L, 1:5000). A non-related Fab-fragment binding hen egg lysozyme (HEL) served as a negative control.

4.3.8.2 HGF competition ELISA

Competition of recombinant human HGF with antibody binding to recombinant human c-MET ECD was detected by ELISA using HGF in solid phase. For this, 1.25 pmol HGF were immobilized on 96 well MaxiSorp® plates overnight at 4°C. After blocking plates with 2% BSA in PBS-T, 1.13 pmol biotinylated c-MET ECD pre-incubated with serial dilutions of antibodies (0.2-200 nM) were added to plates. Binding was revealed using HRP-conjugated streptavidin followed by addition of 1 step Ultra TMB ELISA substrate solution and sulfuric acid. Resulting absorbance for c-MET ECD binding to HGF without addition of anti-c-MET directed antibody was defined as 100% HGF binding. Anti-HEL SEED was used as an unrelated isotype control antibody. Data were plotted as % HGF binding against the logarithm of the antibody concentration and fitted to a sigmoidal dose-response curve with variable slope (4PL) using GraphPad Prism 5 (chapter 3.10).

4.3.8.3 Serum stability ELISA

For determination of long-term stability of bsAbs in human or mouse serum, bridging ELISA was applied. Prior to the main assay, antibodies were titrated for determining the linear range for the concentration dependent reduction in ELISA signal in order to prevent signal saturation for the assay antibody concentration. 100 ng human recombinant EGFR ECD were immobilized on MaxiSorp® plates overnight at 4°C. After blocking, bsAbs were incubated in plates (B10v5x225-H and CSx225-H 1:60 dilution, B10v5x225-M and CS06x225-M 1:6 dilution) at RT for 1 h. After washing, 100 ng biotinylated human recombinant c-MET ECD were added and were detected with streptavidin-HRP conjugate (1:200 diluted, chapter 3.3.1).

Cetuximab samples were subjected to plates with immobilized EGFR ECD (100 ng) and detected with HRP-conjugated goat-anti-human IgG, Fcγ specific (1:5000 diluted, chapter 3.3.1). For the verification for immobilized EGFR-ECD, HRP-conjugated anti-His6 antibody was applied (1:500 diluted, chapter 3.3.1). The zero time point control served for each antibody as 100% control and based on this, reduction in protein functionality was determined.

4.3.8.4 Electrochemiluminescence ELISA (MSD-assay)

MSD assays (Meso Scale Discover) or electrochemiluminescence (ECL) ELISAs were performed to detect phosphorylated and total levels of c-MET, EGFR, and AKT of cell lysates which were treated with antibodies and/or stimulated prior to lysis (cf. chapter 4.4.4).

High bind 96-well plates including electrodes (L11XB-3) were coated with capture anti-total c-MET (Cell Signaling Technologies) or anti-total EGFR antibodies followed by blocking with 3% Block A (R93Ba-4) in PBS supplemented with 0.05% Tween®20. After washing three times with PBS-T, cell lysates were added (25 μl/well, 1h at RT) and detection was carried out with anti-phospho-c-MET, anti-phospho-tyrosine and by the supplier recommended detection reagents. The measurement was performed in Read Buffer T (R92TC-1) with the SECTOR® Imager 6000 (Meso Scale Discovery).

For quantification of phospho-AKT levels, the Phospho(Ser473)/Total AKT Assay Whole Cell Lyate Kit (Meso Scale Discovery, K15100D) was used according to the manufacturer's instruction. Dose response curves were plotted as the logarithm of antibody concentration versus ECL signal. IC_{50} values were calculated by a 3PL fitting model using GraphPad Prism 5 (cf. chapter 3.10). Data from at least two experiments were used to calculate mean IC_{50} ± standard deviation (s.d.).

4.3.9. Sortase A mediated toxin conjugation

Sortase mediated site-directed conjugation of valine-citrulline (vc)-monomethyl auristatin E (MMAE, chapter 3.5) to antibody Fc was performed as described elsewhere. (Chen *et al*, 2011; Dickgiesser *et al*, 2015) Briefly, antibodies carrying the enzyme recognition site (LPETG) C-terminally on both heavy chains were generated, transfected and purified by affinity chromatography. Then, one equivalent of antibody was incubated with 11 equivalents of substrate-vc-MMAE conjugate in the presence of 5 μM sortase and 5 mM $CaCl_2$ in sortase reaction buffer (50 mM Tris, 150 mM NaCl, pH 7.5) for 30 min at 22 °C. The reaction was stopped with 10 mM EDTA as calcium ion chelator. The resulting ADC was purified by SEC as described before.

4.4. Cell biological methods

4.4.1. Cultivation of mammalian cells

All mammalian cell lines (chapter 3.1) were cultivated in tissue culture flasks of appropriate sizes (chapter 3.8, T75-T175 or alternatively Erlenmeyer flask) using the recommended media formulations (chapter 3.6) under sterile conditions at 37°C, 5% CO_2 under humidified atmosphere. Cells were certified mycoplasma-free and never exceeded passage 20.

Adherent cells were detached by trypsin-EDTA (chapter 3.3) for 2-3 min at 37°C after washing with DPBS to remove residual serum components. For primary keratinocytes, the recommended DetachKit was used (chapter 3.6 and 3.8). Cell number and viability of detached adherent cells or unprocessed suspension cells were measured by the cell counting device Vi-CELL® XR (chapter 3.9) by calculating the average of 20 images of trypan blue treated cells. Alternatively, standard cell counting using Neubauer cell chamber was applied. After cell pelleting (250xg, 10 min, RT), supernatants were discarded and cells were diluted in pre-warmed medium yielding appropriate cell numbers (dependent on cell line). Cell lines were testified mycoplasma free and cell culture conditions were standardized since cell handling is known to influence receptor cell surface expression. (Panke *et al*, 2013)

4.4.2. Transfection of mammalian cells and antibody expression

Antibodies were expressed by transient co-transfection of antibody chains in Expi293F™ cells (chapter 3.1) using the corresponding transfection kit and media (chapter 3.6 and 3.8) according to the manufacturer's instruction. Briefly, Expi293F™ cells were cultivated in 200 ml in Erlenmeyer flasks at 37°C, 5% CO_2 and 180 rpm orbital shaking. For passaging, cells were counted and pelleted (250xg, 10 min) and added to fresh medium resulting in final cell number of 0.5 x 10^6 viable cells per ml. On day of transfection, cells were seeded with a final density of 2.5 x 10^6 viable cells per ml in Expi293F™ medium.

For small scale expression, 25 μg DNA (plasmid ratio: 1:1 HC:LC for mAbs or 3:2:1 for HC-AG:LC:scFv-GA for bsAbs) and 81 μl ExpiFectamine™293 were preincubated each in 1.25 ml OptiMEM® (chapter 3.8) and subsequently mixed. After 20-30 min incubation, the DNA-transfection mix was added to 21 ml cells. 16-18 h post transfection, enhancers were added. Supernatants were harvested 5 days post transfection by centrifugation (1500xg, 10 min) and sterile filtration through 0.22 μm Steriflip devices. For mid scale expression, the transfection volume was adjusted to 200 ml and the transfection mix was scaled to 200 μg DNA and 540 μl ExpiFectamine™293. The overall procedure was analog to the description above. Supernatants were harvested by centrifugation (4000xg, 20 min, 4°C) and sterile filtration using Stericup devices.

4.4.3. Flow cytometry

Flow cytometric analysis was carried out at a Guava easyCyte HT cytometer (chapter 3.9) using corresponding software Guava ExpressPro (chapter 3.10). Adherent human cell lines were detached at 70-80% confluency with trypsin-EDTA and suspension cells were directly subjected to assays. Cells were counted with the Vi-CELL® XR (chapter 3.9). All washing and sample incubation steps were carried out in FACS binding buffer (chapter 3.7) on ice for each 1 h except stated otherwise. Cells were pelleted at 250xg (4°C, 10 min). Incubation steps were performed in volume of 100 μl, washing with 300 μl.

4.4.3.1 Cellular binding

For the determination of antibody binding to cellular targets by flow cytometry, 1x10^5 vc/well were incubated with serial dilutions of bsAbs (0.02-200 nM). After washing with FACS binding buffer (3 times), antibody binding was detected via FITC conjugated goat anti-human Fcγ specific pAb. Addition of propidium iodide enabled dead cell staining. 5,000 events were detected per sample. For geometric mean fluorescence intensity (MFI) values, background autofluorescence values of cells treated with medium only were subtracted. Means of triplicate normalized MFI values were plotted versus logarithm of mAb concentration and fitted by a 3PL model using GraphPad Prism 5 (chapter 3.10).

4.4.3.2 Receptor cell surface quantification

Receptor surface expression levels on selected cell lines were determined using the QFIKIT (Dako). Briefly, five populations of calibration beads presenting different numbers of mouse mAb molecules on their surfaces were used as a calibration standard. 1.5x10^5 viable cells per well were labeled with primary mouse anti-EGFR (ab187287) or mouse anti-c-MET antibodies (MAB3582) at saturating doses (5 μg/ml). After washing with FACS buffer (3x 300 μl), beads and cells were stained with 10 μg/ml secondary goat anti-mouse Fc (Fab')$_2$ FITC conjugate and were subjected to flow cytometry

measurement. Beads and cells were measured on the same day using the same settings. Based on a calibration line for fluorescence of beads versus bead surface density, antigen cell surface densities for c-MET and EGFR were calculated.

4.4.3.3 Selectivity

The selectivity of bsAbs was assessed by analyzing binding of antibodies to a cell mixture composed of a tumor model cell line (e.g. EBC-1) with high expression in both EGFR and c-MET in presence of an excess of an epithelial model cell line (e.g. T47D) with low EGFR expression and no c-MET expression. In order to discriminate the two cell lines during flow cytometry, tumor model cells were stained with the PKH2 green fluorescent cell linker kit (chapter 3.8) according to the manufacturer's instructions using $2x10^7$ cells with 4 μl dye. Unstained epithelial model cells and stained tumor model cells were mixed in a ratio of 1:30, $1.3x10^5$ viable cells per well were added in 96 well round bottom plates and incubated with either 3 or 30 nM antibody. After washing, binding of antibodies was detected with PE-conjugated goat anti-human Fc-specific Fab_2. The samples were subjected to flow cytometric analysis with 30,000 counts collected per sample. The membrane dye PKH2 was detected in the green channel, antibody binding in the PE-channel (yellow). Due to crosstalk between green and yellow channel, green emission was compensated in the yellow channel.

4.4.3.4 Internalization

Internalization was either determined by flow cytometry using an anti-Alexa Fluor 488 quenching antibody (Gostring *et al*, 2010) or confocal fluorescence microscopy (chapter 4.5.3). For flow cytometry, $1x10^5$ viable cells were incubated with 100 nM bsAbs followed by detection with AlexaFluor 488 conjugated anti-human Fcγ specific pAb. After washing, cells were incubated at either 37°C allowing internalization or at 4°C preventing internalization for 1 h. Afterwards, residual surface binding of bsAb was quenched by anti-AlexaFluor 488 IgG or not quenched. Afterwards, cells were fixated with 4% (w/v) formaldehyde and subjected to flow cytometric analysis. Internalization was calculated as following:

$$rel.interalization\ [\%] = \frac{\left(37\ °C\ with\ quench\right) - (4\ °C\ with\ quench)}{\left(37\ °C\ without\ quench\right)} x100$$

4.4.4. Phosphorylation assay

4.4.4.1. Western blot analysis

For fluorescent Western blot analysis of antibody treated and/or stimulated cell lysates, cells were seeded into tissue culture 24-well plates on day 1 with $1\text{-}3x10^5$ viable cells per well in the respective medium of the cell line. The next day, cells were starved for 16-18 h with medium lacking FCS. On day 3, cells were treated with antibodies (300 nM in 200 μl) for 1-4 h at 37°C, followed by stimulation with 100 ng/ml

EGF or HGF for 10 min at 37°C. Then plates were transferred to ice, medium was aspirated and cells were lysed with 50 µl ice-cold RIPA buffer supplemented with protease (1:1000) and phosphatase inhibitors (1:100) as well as benzonase (1:1000) per well(chapters 3.3 and 3.8). Protein amounts of cell lysates were quantified by Bradford assay (chapter 4.3.1) and subjected to SDS-PAGE and Western blot analysis (chapters 4.3.5 and 4.3.7).

4.4.4.2. Electrochemiluminescence ELISA analysis

Phosphorylation levels were determined by c-MET or EGFR capture electrochemiluminescence (ECL) ELISA (MSD assay). Briefly, cells were plated in Nunc-Immuno 96-microwell tissue culture plates (chapter 3.8) with 12,500 viable cells per well (A549, MDA-MB-468) or 30,000 viable cells per well (MKN45, NCI-H596, NCI-H441, A431, and NHEK.f-c.) one day before treatment using recommended cell media formulations (chapter 3.1 and 3.6). On the day of treatment, cells were starved with medium lacking FCS for 1 h and serial dilution of antibodies (0 – 167 nM in 80 µl starvation medium) were added for 1 h at 37°C, 5% CO2. Upon stimulation with either 100 ng/ml HGF and/or EGF (both R&D Systems) for 5 min at 37°C, cells were lysed with 40 µl/well ice-cold lysis buffer (MSD, chapter 3.8) supplemented with protease and phosphatase inhibitors and subjected to ECL ELISA assay analysis (MSD assay) (cf. chapter 4.3.8.4).

4.4.5. Antibody dependent cellular cytotoxicity

Antibody dependent cellular cytotoxicity (ADCC) assays were performed using the ADCC Reporter Bioassay Core Kit (Promega, chapter 3.8) according to the manufacturer's instruction. Briefly, target cells (e.g. A431 or EBC-1 cells) were detached and seeded into the inner wells of opaque white tissue culture treated 96 well plates with 12,500 viable cells per well in ADCC buffer (chapter 3.7) and allowed to attach overnight in a humidified chamber at 37°C, 5% CO_2. The next day, cells were treated with 5 to 0.0016 nM of mAbs diluted in ADCC buffer and 75,000 recombinant Jurkat cells (chapter 3.1) per well as effector cells were added. After 6 h of incubation, 75 µl per well Bio Glo Luciferase substrate equilibrated at RT were added and incubated for 10 min at RT avoiding light. Luminescence was measured at a Synergy 4 plate reader with a read time of 0.5 seconds per well (sensitivity: 170, chapter 3.9 and 3.10) using the Gen5 software. Background luminescence in only medium wells was subtracted. Mean relative luminescence units (in triplicates) were plotted against the logarithm of antibody concentration and dose response curves were fitted using 3PL model by GraphPad Prism 5 (chapter 3.10).

4.4.6. Cytotoxicity or cell viability assay

Cell viability was quantified using the ATP-based luminescence CellTiter-Glo® assay (chapter 3.8) and was performed according to the manufacturer's instructions. Briefly, cells were detached and seeded in the inner wells of opaque white tissue culture treated 96 well plates. The seeding cell number ranged from 8,000 to 15,000 viable cells per well depending on the cell line in 80 μl cell line specific medium. Cells were allowed to attach at least 3 h in a humidified chamber at 37°C, 5% CO_2 before ADC treatment (ranging from 50 to 0.01 nM final) in duplicates in cell line specific medium. After 72 h, viability of cells was detected by adding 100 μl per well of CellTiter-Glo® reagent with subsequent mixing on a plate shaker for 2 min at 350 rpm and 10 min incubation in the dark at RT. Luminescence was measured at a Synergy 4 plate reader (chapter 3.9 and 3.10) with a read time of 0.5 seconds per well (sensitivity: 170). Background luminescence in wells with only medium plus the CellTiter-Glo® reagent was subtracted. Data were plotted as percentage of untreated cell viability versus the logarithm of antibody concentration and fitted with 3PL model using GraphPad Prism 5 (chapter 3.10). Data from at least three independent experiments with duplicates were used to calculate mean IC_{50} ± standard deviation (s.d.).

4.5. Biophysical methods

4.5.1. Biolayer interferometry

Biosensor experiments using biolayer interferometry were performed on an Octet Red96 platform using Octet Data Acquisition and Analysis software (cf. chapter 3.9 and 3.10) at 30°C using 1000 rpm orbital sensor agitation in a volume of 200 μl in black 96-well microplates. The physical principal of biolayer interferometry is based on the optical detection of changes within the layer thickness on biosensor tips by association and dissociation of molecules resulting in a shift in the interference pattern of reflected light. White light is thereby directed through the biosensor and is reflected once by a reference layer within the biosensor tip and secondly by the tip surface. (Rich & Myszka, 2007)

4.5.1.1. Antibody quantification

For determining the concentration of produced Fab-fragments and antibodies, anti-human Fab-CH1 and protein A biosensor tips (chapter 3.8) were used, respectively. Biosensors were equilibrated in the medium or buffer, in which the Fab-fragment or mAb is present, for 10 min at RT. Then, association of Fab-fragments or mAbs is evaluated for 300 sec at 1000 rpm. Based on standard curves of Fab-fragments or mAbs of known concentration in the respective medium, the concentration can be calculated. For this, binding rates were calculated with the analysis software based on five parameter fitting (5PL unweighted) and using either the initial slope after 120 sec or the "R equilibrium" after 300 sec.

4.5.1.2. Determination of kinetic parameters

Anti-human IgG Fc capture biosensor tips were equilibrated 30 sec in DPBS. Then, 5 μg/ml antibodies diluted in DPBS were immobilized on biosensor tips for 120 sec, a baseline was recorded for 60 sec in kinetics buffer (KB) followed by stepwise association and dissociation of the analyte (serial dilution in KB) for 600 sec and 1200 sec, respectively. Buffer controls were subtracted as background and binding parameters were calculated assuming a 1:1 Langmuir binding model performing global fitting algorithm provided by the Octet data analysis software.

4.5.1.3. Simultaneous binding

For evaluating simultaneous binding, 5 μg/ml biotinylated c-MET ECD were captured on streptavidin biosensor tips for 40 sec. Then, biosensors were first blocked with 1% milk powder, 1% BSA, 0.1% Tween®20 and 10 μg/ml biocytin for 60 sec and then stepwise subjected to 50 nM bsAbs and 50 nM EGFR-ECD for 300 sec each. As controls, the non-related isotype control anti-hen egg lysozyme (anti-HEL) or buffer controls were implemented to exclude unspecific binding.

4.5.1.4. Epitope binning

An epitope binning experiment was carried out analyzing competing binding of antibodies to c-MET ECD. (Estep *et al*, 2013) For this, binding of generated antibodies to c-MET ECD was compared to reproduced reference antibodies from the literature (oa 5D5, LY2875358, hu224G11, DN30). Anti-human Fc biosensor tips were equilibrated 30 sec in DPBS followed by capture of 25 nM bivalent mAbs or 50 nM monovalent one-armed antibodies in DPBS for 200 sec. Then, biosensors were quenched with 400 nM of a non-related control antibody (anti-HEL SEED, diluted in DPBS) to minimize subsequent binding of secondary antibodies to biosensor tips. After performing a baseline in KB for 60 sec, human c-MET-ECD was subjected to immobilized primary antibodies for 600 sec. Afterwards, interactions of secondary anti-c-MET antibodies to c-MET-ECD bound to immobilized primary antibodies was analyzed for 600 sec. Binding of secondary antibody was analyzed visually by distinguishing simultaneous binding by a higher binding rate [nm] compared to a non-related isotype control (anti-HEL SEED).

4.5.2. Determination of thermal stability

4.5.2.1. Thermal shift assay

Thermal stability of antibodies was measured using a StepOnePlus Real-Time PCR System (cf. chapter 3.9) according to the manufacturer's instruction. The method is described as differential scanning fluorimetry (DSF, thermal shift assay). (Lo *et al*, 2004) Briefly, 1 μM of protein was mixed with a 20 fold excess of SYPRO Orange in PBS pH 7.4. Melting curves were recorded from 25°C to 99°C with

an increment of 1°C/60 sec. Data were analyzed with the Protein Thermal Shift™ Software (Life Technologies) by calculating the maximum of the second derivative curve.

4.5.2.2. Long-term stability in serum

For assessment of long-term stability of bsAbs and mAbs in human and mouse serum, antibodies were incubated in triplicates at 5 μg/ml concentration in 50 μl aliquots at 37°C with 750 rpm shaking. Human sera were obtained from the Merck medical office (from female and male blood samples, Darmstadt, Germany) subsequently supplemented with 0.09% sodium azide or from AbD Serotec (Bio-Rad, chapter 3.8) for mouse serum. The zero time point sample were immediately frozen at -80°C after antibody dilution, the other samples were frozen every 3-4 days up to 24 days. Frozen samples were subjected to bridging ELISA (chapter 4.3.8.3).

4.5.3. Confocal microscopy

For fluorescence microscopy, 3x10^5 viable cells were grown on glass coverslips (chapter 3.8) placed in 6-well plates. Two days later, cells were placed on ice and treated with 100 nM bsAbs or mAbs followed by detection with Alexa Fluor 488 conjugated anti human Fc Fab-fragment. After washing with 1% BSA in PBS, cells were incubated in respective medium at either 37°C allowing internalization or 4°C preventing internalization for 1 h. By addition of ice-cold low pH buffer (chapter 3.7), residual bsAbs on the cell surface were removed. Finally, cells were fixed with 4% (w/v) formaldehyde and mounted on object slides with ProLong Diamond Antifade Mountant supplemented with DAPI (4',6-diamidino-2-phenylindole; chapter 3.8). Analysis was carried out with a Leica TCS SPS confocal microscope equipped with a 100x objective (chapter 3.9).

5. Results

5.1. Quality control of target proteins and characterization of cellular target expression

Both for selection and biophysical analysis of antibodies, high protein quality plays a pivotal role. In respect two membrane bound target, cellular receptor densities can influence binding, selectivity and pharmacodynamics of both mAbs and bsAbs. (Jarantow *et al.*, 2015)

Protein purity of recombinant EGFR and c-MET extracellular domains (ECDs) had been determined by analytical SE-HPLC and gel electrophoresis under reduced and non-reduced conditions (**Figure 7**). As expected, band sizes of 69 kDa for EGFR-ECD, 66 kDa for c-MET SEMA domain, and 104 kDa for c-MET ECD wt and N375S could be observed under non-reduced conditions. Since c-MET is a disulfide-linked heterodimer which is processed from a single precursor-protein by furin cleavage within the SEMA-domain, protein reduction resulted in two protein chains: the SEMA α-chain (~45 kDa) and the SEMA β-chain for the total SEMA domain or the c-MET ECD β-chain for c-MET ECD. The protein purity based on SDS-PAGE analysis was assessed as sufficient for all following assays.

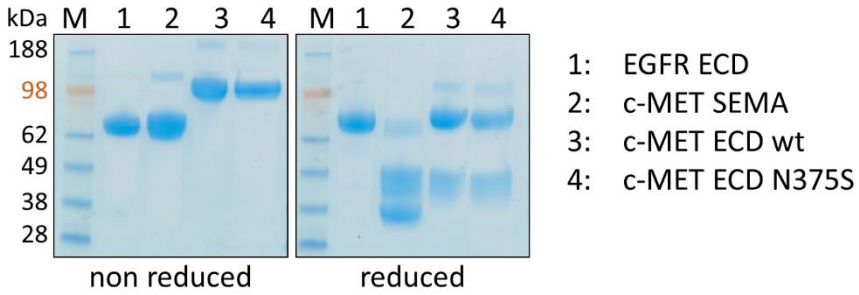

Figure 7: SDS-PAGE of EGFR ECD, c-MET SEMA domain, ECD wt, and N375S.

Protein purity was accessed by gel electrophoresis and coomassie staining of non-reduced and reduced recombinant human protein samples. For EGFR, the ECD (1-618) with His-tag was used in the following experiments (MW: 69 kDa). For c-MET, three different recombinant human proteins were evaluated: the SEMA-PSI domain (1-562) with FLAG and His-tag (MW: 66 kDa) and the c-MET ECD (1-932) with strepII- and His-tag wild type and with SNP N375S (both 104 kDa). c-MET is a disulfide-linked heterodimer and the disulfide bridge is located within the SEMA domain. Under reduced conditions, this results in two visible bands of which one is the SEMA α-chain (~45 kDa) and the second band is the SEMA β-chain (lane 2) or the ECD β-chain (lane 3+4). M = protein marker.

For later functional analysis of the generated mAbs and evaluation of the tumor selectivity of bsAbs, receptor surface expression levels of several cancer cell lines from various indications (chapter 3.1) and additionally of primary keratinocytes (NHEK.f-c.) were determined via flow cytometry (chapter 4.4.3). Within the QFKIT (chapter 3.8), five bead populations decorated with distinct numbers of mouse mAb molecules served as a standard. Concurrently, cell lines were incubated with either mouse anti-EGFR or mouse anti-c-MET antibodies with subsequent detection via anti-mouse FITC conjugates. Based on the calibration curve, EGFR and c-MET surface levels were calculated and summarized in **Table 2** (parts of

this data was kindly provided by Merck, Darmstadt). The presented data confirmed high receptor levels of EGFR on A431 and MDA-MB-468 cells, while high c-MET densities were assessed on EBC-1 and MKN45 cells (both c-MET amplified), and moderate EGFR levels were measured on primary keratinocytes in accordance with previously published data. (Hyatt & Ceresa, 2008; Jarantow *et al.*, 2015) Taken together, several c-MET and EGFR double positive cancer cell lines could be confirmed.

Table 2: c-MET and EGFR quantification on cancer cell lines.

c-MET and EGFR cell surface expression levels on several cancer cell lines as well as primary keratinocytes (NHEK.f-c.) were measured via flow cytometry employing the QFIKIT. Values are indicated as mean of antigens per cell from triplicates based on the calibration curve which was measured by five bead populations with distinct molecules per bead. Standard deviations (s.d.) are given in percent. Additionally, cell line origin, dependence on HGF, and KRAS mutational status are listed. Legend: ACA = adenocarcinoma, CA = carcinoma, n.a. = not accessible.

Cell line	Origin	HGF dependence	c-MET density [x 10^3 ± s.d %]	EGFR density [x 10^3 ± s.d %]	KRAS mutation
A431	epidermoid CA	n.a.	14.7 ± 0.2	661.0 ± 1.4	
A549	lung ACA	yes	18.0 ± 0.6	39.3 ± 0.6	G12S
EBC-1	lung SCC	no	261.6 ± 1.1	62.2 ± 1.1	
HepG2	hepatocellular CA	n.a.	11.1 ± 1.4	1.3 ± 4.7	
KP-4	pancreatic CA	yes	7.7 ± 0.5	50.8 ± 0.9	
MDA-MB-468	breast ACA	n.a.	14.2 ± 1.0	1825.5 ± 0.1	
MKN45	gastric ACA	no	171.7 ± 1.0	45.4 ± 0.3	
NCI-H1975	lung ACA	yes	35.5 ± 0.7	37.8 ± 0.7	
NCI-H441	lung ACA	yes	52.2 ± 0.8	46.6 ± 3.7	G12V
NCI-H596	lung ACA	yes	6.7 ± 1.0	148.5 ± 1.4	
NHEK.f-c.	keratinocytes	n.a.	7.1 ± 8.9	128.7 ± 8.7	
T47D	breast ACA	n.a.	0.0	13.2 ± 0.9	

5.2. Selection and characterization of c-MET binders

To evaluate the influence of kinetic variants in c-MET x EGFR bsAbs on the tumor selectivity, a broad panel of c-MET binders with distinct affinities was generated by affinity maturation. Two low affinity anti-c-MET binders, B10 and F06, isolated by phage display (Hust *et al*, 2007; Hust *et al.*, 2011) as well as one affinity matured anti-c-MET binder, B10v5, isolated by yeast surface display (Benatuil *et al*, 2010; Rakestraw *et al*, 2009), were kindly provided by Merck, Darmstadt, Germany. For the affinity maturation of Fab-fragment F06, sub-libraries were generated by (1) randomization of variable heavy chain of parental clone F06 by error prone PCR (epPCR, theoretical diversity $2.4x10^6$) and (2) parsimonious mutagenesis of the CDR-H3 (theoretical diversity $4.1x10^6$, cf. Appendix **Table 12**). Due to fast dissociation rate of F06, an off-rate screening strategy was applied using stringent washing conditions (10 or 20 times washing with panning buffer), and competition with an excess of soluble c-MET ECD during panning (cf. chapter 4.2.4). After two rounds of panning, 96 clones were analyzed by Sanger sequencing for each approach and unique clones (in terms of identical amino acid sequence) were analyzed by ELISA (cf. Appendix **Table 12** and data not shown). Binding of *E. coli* expressed soluble Fab-fragment F06v1 from sub-library 1 to c-MET ECD was confirmed by ELISA and displayed an improved affinity with slower off-rate confirmed by biolayer interferometry (BLI). Fab-fragment F06v1 contained four mutations in the VH region (**Figure 8**).

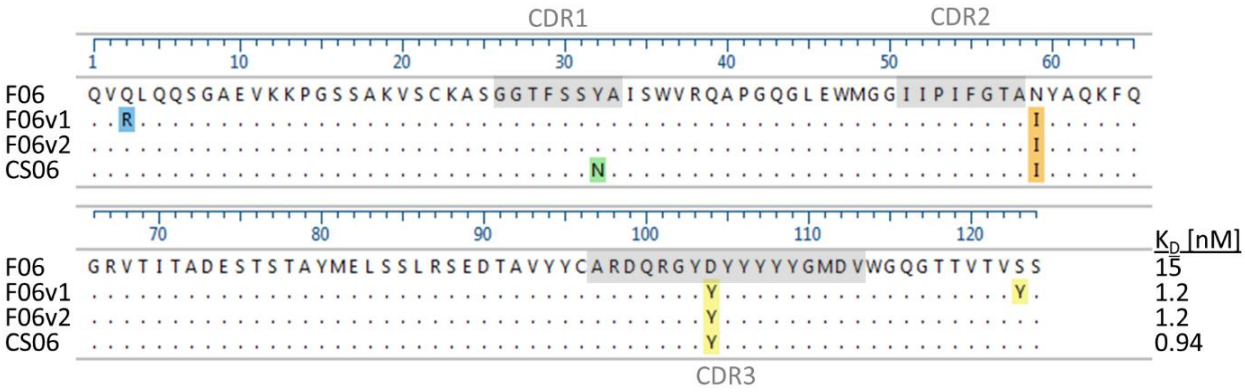

Figure 8: Sequence alignment of affinity matured variants to the parental VH sequence of Fab-fragment F06.

Sequence analysis revealed four mutations of variant F06v1 compared to parental Fab-fragment F06 within the VH region. This clone was derived from the epPCR sub-library approach. Combinatory analysis of mutations indicated that only two mutations were responsible for affinity increase from equilibrium dissociation constant values K_D = 15 nM to K_D = 1.2 nM. Rational combination with an additional mutation, which was abundant in the epPCR sequence analysis and is located in the CDR-H1, further slightly increased affinity to c-MET (K_D = 0.94 nM).

To identify responsible amino acids for the improved affinity, combinatory mutation variants were generated by site directed mutagenesis and affinities of resulting *E. coli* expressed soluble Fab-fragments were evaluated by BLI using anti-Fab-antibody fragment biosensors. The data indicated that two mutations were sufficient for increased affinity and the corresponding variant was denoted as Fab-fragment F06v2. Interestingly, only one mutation was located in the CDR-H3 (D104Y) resulting in a

patch of seven subsequent tyrosine residues. Nevertheless, the presence of multiple tyrosines did not affect the specificity of the Fab-fragment for its target, c-MET (data not shown). This specific CDR-H3 mutation was also derived in the parsimonious-sub-library approach with high prevalence (cf. Appendix, **Figure 32**). Further rational combination with an abundant mutation derived from the epPCR-sub-library approach, which was located in CDR-H1 (Y32N) (cf. Appendix, **Figure 33**), slightly further improved affinity to c-MET. The resulting anti-c-MET Fab-antibody fragment, denoted as CS06, was selected for further analysis together with B10, F06, and B10v5 as c-MET binding moiety in the bsAbs c-MET x EGFR approach. All four binders were reformatted in mammalian expression pTT5 vectors containing IgG_1-Fc sequences including the SEED-AG sequences in the CH3 region. (Muda *et al.*, 2011) After expression as monovalent anti-c-MET Fab-SEEDS by transient transfection in Expi293F™ cells, kinetic parameters including the equilibrium dissociation constant (K_D) were determined again by BLI using anti-human Fc biosensors (AHC). Calculated K_D-value of anti-c-MET monovalent antibodies B10 to B10v5 was improved by the factor 30 (K_D = 12 nM and K_D = 0.4 nM, respectively) and of F06 to CS06 by the factor 21 (K_D = 4.2 nM and K_D = 0.2 nM, respectively, **Figure 9**).

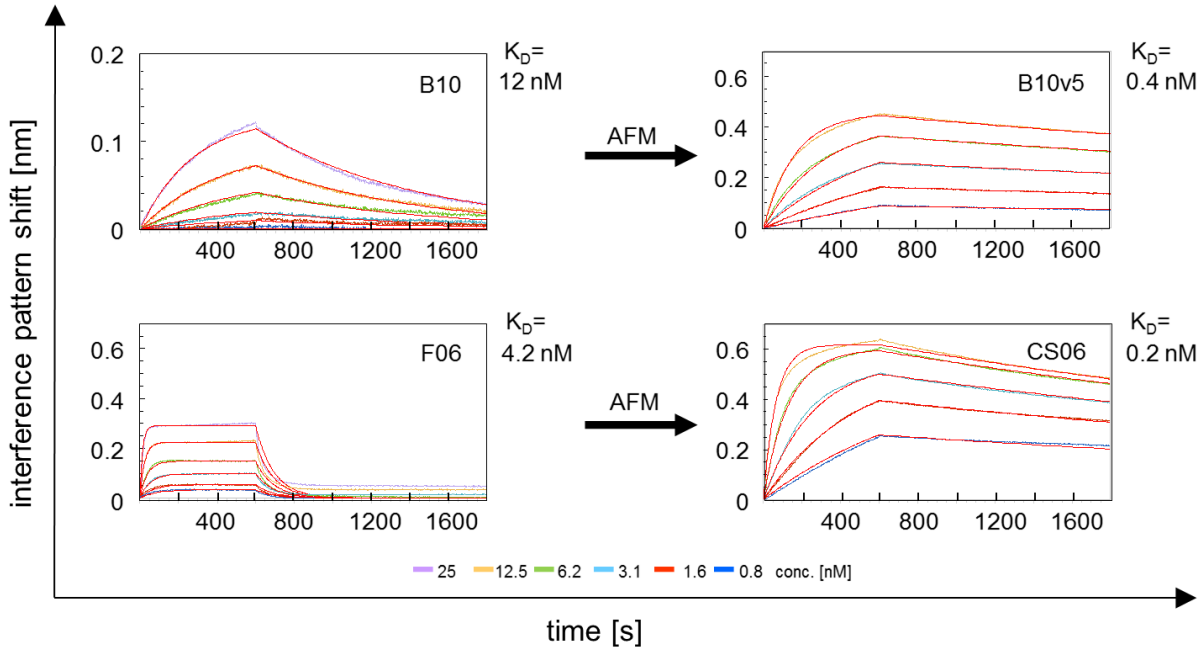

Figure 9: Comparison of parental and affinity maturated c-MET binders by kinetic analysis via BLI.

Transiently produced monovalent anti-c-MET Fab-SEED antibodies were captured on anti-human Fc (AHC) biosensor. Association and dissociation of c-MET ECD to mAbs were monitored for 600 sec and 1200 sec, respectively. Affinity maturation of Fab-antibody fragment B10 by light chain shuffling and of Fab-fragment F06 by epPCR yielded in clone B10v5 with a 30-fold improved affinity (K_D = 12 nM to K_D = 0.4 nM) and clone CS06 with improved affinity by factor 21 (K_D = 4.2 nM to K_D = 0.2 nM), respectively.

5.2.1. HGF competition by ELISA

The ability of antibodies to compete with ligand binding to respective RTKs can give a hint on the mode of action. Preliminary experiments indicated that both parental anti-c-MET binders compete with HGF binding to c-MET ECD in ELISA (communication with Merck, Darmstadt, Germany). In order to evaluate the competition of HGF binding to c-MET by anti-c-MET binders, 1 pmol/well immobilized HGF was incubated with an equimolar amount of biotinylated c-MET ECD which was pre-incubated with increasing concentrations of antibodies. c-MET binding to HGF was revealed with streptavidin-HRP conjugate and standard ELISA procedure (cf. chapter 4.3.8). Besides B10v5, CS06, B10 and F06, reproduced reference anti-c-MET antibodies LY2875358, oa5D5, and hu224G11 (all kindly provided by Merck, Darmstadt, Germany) were able to compete HGF binding to c-MET (**Figure 10**). c-MET incubated without antibody was used as positive control for 100% HGF binding and a non-related isotype control (anti-HEL SEED) was unable to compete with c-MET binding to HGF. IC_{50} values for all anti-c-MET antibodies ranged from 3 nM (hu224G11) to 10 nM (LY2875358). At high concentration (> 100 nM), all anti-c-MET binders achieved 100% blockade of HGF binding except LY2875358 which only yielded in 80% HGF displacement confirming previously presented data. (Liu *et al.*, 2014)

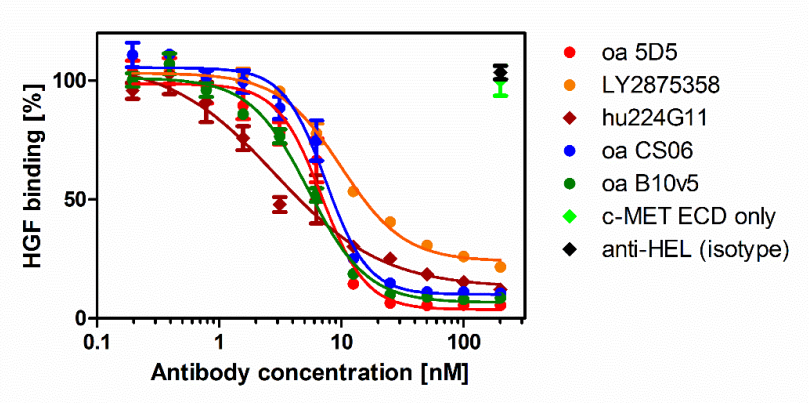

Figure 10: Anti-c-MET binders compete with HGF binding to c-MET ECD.

Serial dilutions of antibodies were pre-incubated with 1 pmol biotinylated human c-MET ECD and subjected to microtiter plates with immobilized HGF (1 pmol). Biotinylated c-MET without antibody was defined as 100% HGF binding. Anti-HEL SEED was used as a non-related isotype control. Absorbance values were calculated as % HGF binding and plotted to logarithm of antibody concentration. Sigmoid curves were fitted using four parameter fitting (4PL) with variable slope using GraphPad Prism 5.

5.2.2. Epitope binning

For the parental c-MET antibodies, it was known that the epitope of mAb B10 was located within the c-MET SEMA domain whereas anti-c-MET binder F06 in contrast demonstrated binding to the stalk domain (communication with Merck, Darmstadt, Germany). To evaluate whether the affinity matured anti-c-MET binders B10v5 and CS06 still recognize the same epitope, a binning experiment was performed employing BLI. (Estep *et al.*, 2013). Moreover, epitope bins of reproduced reference antibodies from the literature (Prat *et al.*, 2014) (LY2875358 by Eli Lilly, hu224G11 by Pierre

Fabre/AbbVie, one-armed (oa) 5D5 by Roche/Genentech, and DN30 by Comoglio and co-workers, all kindly provided by Merck, Darmstadt, Germany) were used for further characterization. Antibodies competing for the same or an overlapping epitope on the antigen's surface were classified as the same epitope bin. Briefly, the first antibody was immobilized on anti-human Fc (AHC) biosensor tips followed by quenching with an unrelated-isotype control (anti-HEL). Afterwards, c-MET and subsequently the second antibody were step-wise associated (Appendix, **Figure 34**). The assay was evaluated by alignment of the c-MET association step. Even though the biosensor tips were quenched, residual binding was observed for an anti-HEL mAb as a non-related isotype control when applied as second antibody which is exemplarily depicted in **Figure 11A**. However, residual binding could be clearly distinguished to simultaneous binding of second antibody to c-MET together with the first antibody.

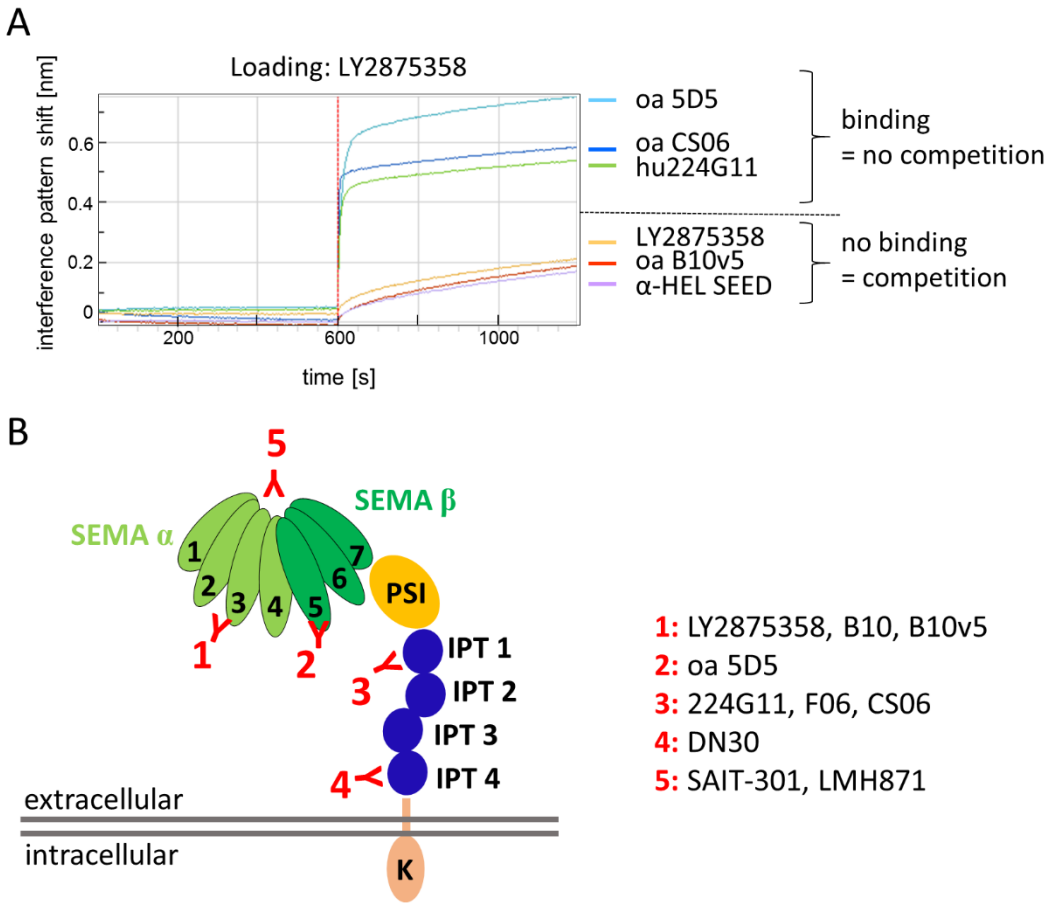

Figure 11: Schematic summary of epitope binning of anti-c-MET binders.

(A) Exemplary graph for the analysis of the epitope binning experiment by BLI. Briefly, the first antibody (here: LY2875358) was immobilized on AHC biosensors. After quenching with anti-HEL, c-MET ECD and subsequently the second antibodies were associated. For analysis, the step of the c-MET ECD association was aligned and association of the second antibody in comparison to a non-related mAb control (anti-HEL) was visually evaluated as binding/no competition or no binding/competition. In **Table 3**, a summary can be found. **(B)** Schematic representation of antibody epitope bins located in the c-MET ECD based on results of the presented epitope binning experiment and data adapted from Basilico *et al.* and Prat *et al.*. (Basilico *et al.*, 2014; Prat *et al.*, 2014) A detailed description of the c-MET structure can be found in **Figure 4**.

The results are summarized in **Table 3** and **Figure 11B**. B10, B10v5 and LY2875358 built up one epitope bin. For LY2875358 binding to SEMA blades 2 and 3 was described (Liu *et al.*, 2014). The oa 5D5 bound to a distinct epitope which is located on blade 4, 5 and 6 of the SEMA β-propeller domain demonstrated by co-crystallization by Merchant and colleagues. (Merchant *et al.*, 2013) The next epitope bin is composed of F06, CS06 and hu224G11 although there are some inconclusive results related to competitiveness with oa5D5. (Basilico *et al.*, 2014; Prat *et al.*, 2014) Since F06, CS06 and hu224G11 (patent US2012/8,329,173 B2) were not able to bind the c-MET SEMA domain, their epitope must be located within the stalk domain. Basilico and co-workers engineered MET fragment proteins lacking distinct domains. (Basilico *et al.*, 2014) The data indicated that the epitope of hu224G11 can be narrowed down to the first two IPT domains. Nevertheless, Basilico *et al.* also observed interference of hu224G11 and oa 5D5 binding to c-MET probably because of sterical hindrance due to close spatial proximity of SEMA and IPT regions. The anti-c-MET antibody DN30 is known for its different mode of action by inducing receptor ectodomain shedding. (Petrelli *et al*, 2006) In accordance with data by Basilico *et al.*, the presented results indicate that DN30 covers a distinct epitope bin which is located within the juxtamembrane region in IPT4. (Basilico *et al.*, 2008)

Table 3: Epitope binning of c-MET binders.

The epitope binning of c-MET antibodies was measured by BLI and visually analyzed. Briefly, competition of a primary antibody immobilized on AHC biosensors and associated with c-MET ECD was analyzed by association of a second antibody. Residual binding of antibodies to AHC sensors was monitored by a non-related mAb control (anti-HEL). Binding and no-binding was determined in comparison to anti-HEL binding as second antibody (cf. **Figure 11**).
Legend: + binding/no competition (green); +/- unclear results (yellow); - no binding/competition (red)

Primary antibody \ **Secondary antibody**	B10	B10v5	LY2875358	F06	CS06	hu224G11	oa 5D5	DN30
B10	-	n.d.	n.d.	+	n.d.	+	n.d.	+/-
B10v5	-	-	-	+	+	+	+	+/-
LY2875358	n.d.	-	-	n.d.	+	+	+	n.d.
F06	+	n.d.	n.d.	-	n.d.	-	n.d.	+/-
CS06	+	+	+	-	-	-	+/-	+
hu224G11	+	n.d.	n.d.	-	n.d.	-	n.d.	+
oa 5D5	+	+	+	-	-	+	-	+/-
DN30	+	n.d.	n.d.	+	n.d.	+/-	n.d.	-

5.2.3. Binding of SNP variant

The single nucleotide polymorphism (SNP) N375S within the c-MET SEMA domain was described in tumor tissues from NSCLC patients of East Asian, African-American and Caucasian ethnicities. (Krishnaswamy *et al*, 2009; Shieh *et al*, 2013) In the Taiwanese population, around 13-14% are heterozygous and 0.5 to 1.1% are homozygous for this SNP variant. (Shieh *et al.*, 2013) Even though the N375S was not associated with NSCLC occurrence or prognosis, the mutation could affect structural alterations of c-MET and result in changed HGF binding behavior ultimately influencing antibody binding. (Shieh *et al.*, 2013) To evaluate interference of this SNP variant with anti-c-MET mAbs binding, c-MET was mutated to N375S (**Figure 12A**) and expressed by transient transfection. Kinetic parameters of immobilized anti-c-MET mAbs (AHC biosensors) to c-MET wild type (wt) or c-MET SNP N375S were monitored (**Figure 12B**). Taken together, all analyzed c-MET mAbs demonstrated similar binding to c-MET wt and c-MET SNP N375S (**Table 4**) and the mutation N375S did not interfere with binding of the generated mAbs to c-MET.

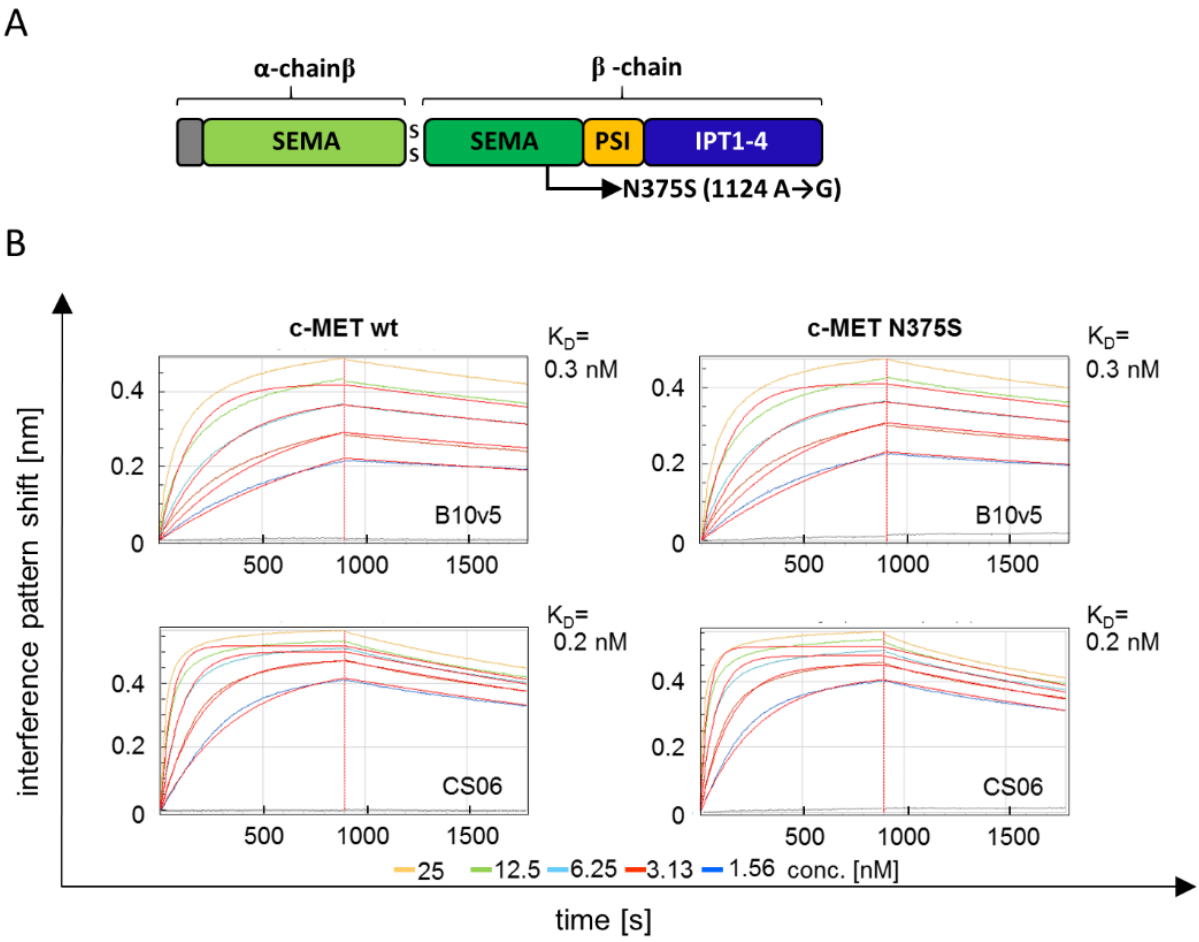

Figure 12: Schematic representation of c-MET N375S (A) and binding by anti-c-MET antibodies (B).

(A) Schematic illustration of the location of the SNP mutation N375S within the β-chain of the SEMA domain. **(B)** Kinetic analysis for binding c-MET wild type (wt) and SNP N375S (concentrations 25 to 1.56 nM) to immobilized c-MET mAbs on biosensors was conducted. No binding of 25 nM EGFR (grey) as a non-related negative control was observed. For selected concentrations, curve fitting (1:1, Langmuir; red lines) was performed.

Table 4: Binding of c-MET SNP variant (N375S) by anti-c-MET antibodies.

Kinetic analysis of anti-c-MET mAbs binding to c-MET ECD wt and N375S were performed by BLI. The mAbs were immobilized on AHC biosensors and various concentrations of respective c-MET were associated and dissociated. Affinities (equilibrium dissociation constant, K_D) as well as association and dissociation rates (k_a and k_d) were determined via Langmuir 1:1 fitting.

	c-MET			c-MET SNP variant (N375S)		
	K_D [M]	k_a [$M^{-1}s^{-1}$]	k_d [s^{-1}]	K_D [M]	k_a [$M^{-1}s^{-1}$]	k_d [s^{-1}]
oa CS06	1.7E-10	1.5E+06	2.6E-04	1.4E-10	2.1E+06	3.0E-04
oa B10v5	3.4E-10	5.1E+05	1.7E-04	3.0E-10	5.8E+05	1.8E-04
oa F06	4.2E-09	2.5E+06	1.1E-02	1.4E-09	5.4E+06	7.4E-03
oa B10	1.6E-08	7.3E+04	1.2E-03	3.2E-08	5.1E+04	1.6E-03
oa 5D5	2.7E-10	4.3E+05	1.2E-04	2.1E-10	5.3E+05	1.1E-04
LY2875358	4.0E-10	1.8E+05	7.0E-05	6.1E-10	2.1E+05	1.3E-04

5.3. Selection and characterization of EGFR binders

The inhibition of EGFR by small molecules and mAbs is associated with severe toxicities in the skin. (Lacouture, 2006; Melosky *et al.*, 2009) Thus, affinity attenuated variants of anti-EGFR antibodies in combination with the bispecific format could increase tumor selectivity and diminish adverse events in normal tissue. Affinity variants of humanized cetuximab (C225) (Muda *et al.*, 2011) were generated by *in silico* screening and kindly provided by Merck, Darmstadt, Germany. Briefly, based on the crystal structure of the C225-Fab-fragment in complex of EGFR ECD (Li *et al.*, 2005), residues in proximity to the binding interface were mutated by computational design in order to find the lowest energy rotamer via the Rosetta energy function. To this end, a triple mutant with increased affinity was found, designated as 225-H while H stands for high affinity. For attenuated variants in contrast, it was aimed for weak repulsive forces. From this approach, two clones were selected named 225-M for medium and –L for low affinity. The *in silico* mutations were then introduced into C225-Fab-fragment and the kinetic parameters of the resulting Fab-fragment clones were analyzed (kindly performed by Merck, Darmstadt, Germany). In course of this work, the mutations were transferred to vectors containing humanized C225 (hu225) scFv with the SEED-GA-chain (Muda *et al.*, 2011) for analysis in bispecific combinations together with c-MET binders. An alignment of the scFv sequences of the three variants in comparison to hu225 are illustrated in **Figure 13**. The three monovalent, one-armed anti-EGFR 225 scFv-SEEDs were expressed in Expi293F™ cells by transient transfection and kinetic parameters were analyzed by BLI with EGFR-ECD (**Figure 14A**). Additionally, humanized matuzumab (424) (Muda *et al.*, 2011) was used for expression and analysis (**Figure 14A**) since 425 occupies a distinct epitope on domain III of EGFR (**Figure 14B**). 225-H had an affinity of 0.1 nM while for C225 an affinity to EGFR-ECD in the single digit nanomolar range is described (Li *et al.*, 2005). 225-M and 225-L displayed K_D values of 4 nM and ~1 μM, respectively. For 425, an affinity of 14 nM was determined.

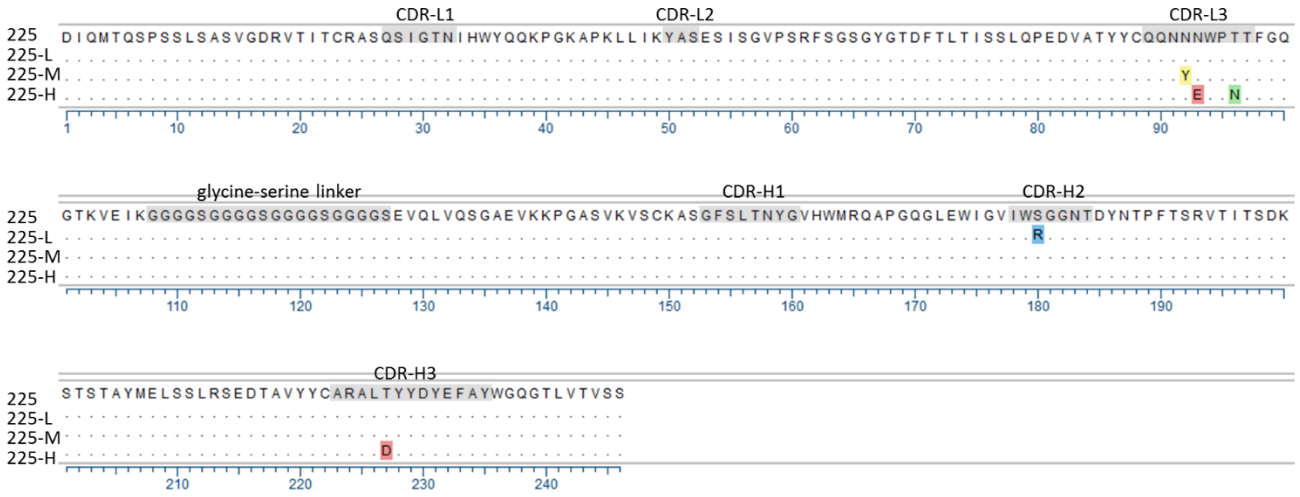

Figure 13: Multiple sequence alignment of humanized C225 scFv kinetic variants.

Both 225-L and 225-M contain a single mutation within the CDR-L-3 and CDR-H2, respectively. 225-H is composed of a combination of three individual mutations from an *in silico* screening (kindly provided by Merck, Darmstadt, Germany).

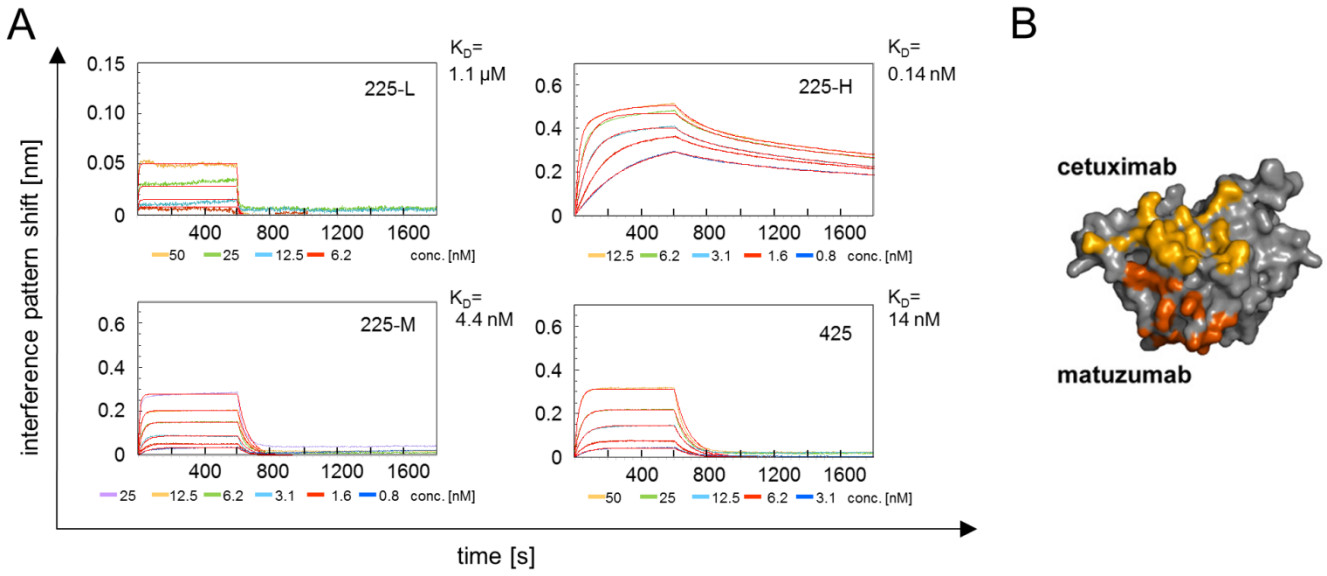

Figure 14: Kinetic analyses of EGFR binders (A) and epitopes of cetuximab and matuzumab on EGFR domain III (B).

(A) Association and dissociation of EGFR-ECD to immobilized anti-EGFR scFV-SEEDs by BLI. Fitting was performed assuming 1:1 Langmuir binding model. Equilibrium dissociation constants (K_D) are depicted next to graphs. **(B)** Binding epitopes of cetuximab (C225) and matuzumab (425) on EGFR domain III. Note that only cetuximab binding overlaps with EGF binding. This sphere structure is adapted from Schmitz and Ferguson. (Schmitz & Ferguson, 2009)

5.4. Characterization of bispecific c-MET x EGFR antibodies

5.4.1. Manufacturing and purification

The aim of the present study was to evaluate the influence of kinetic variants on the tumor selectivity of bsAbs targeting two ubiquitously expressed cancer targets, c-MET and EGFR. Based on the aforementioned broad panel of anti-c-MET and anti-EGFR binders with fast and slower off-rates targeting distinct epitopes, bispecific Fab-scFv-SEED antibodies were produced by transient transfection (**Figure 15A**). The scFv-technology was applied for correct light chain pairing. (Muda *et al.*, 2011) Briefly, VH and VL sequences have been subcloned into pTT5 mammalian expression containing cognate constant domains (CH1-CH2-SEED-AG and CL, respectively) for anti-c-MET binders (chapters 5.2 and 5.3). Kinetic hu225 variants in the scFv-CH2-SEED-GA format were generated by introduction of described mutations via site-directed mutagenesis PCR. Thereby, a glycine-serine-linker was chosen as peptide linker. As control antibodies, monovalent anti-c-MET Fab-SEEDs or monovalent anti-EGFR scFv-SEEDs were expressed (**Figure 15B** and **C**). For expression of monovalent antibodies, pTT5 vectors containing CH2-SEED-AG or CH2-SEED-GA sequences were applied.

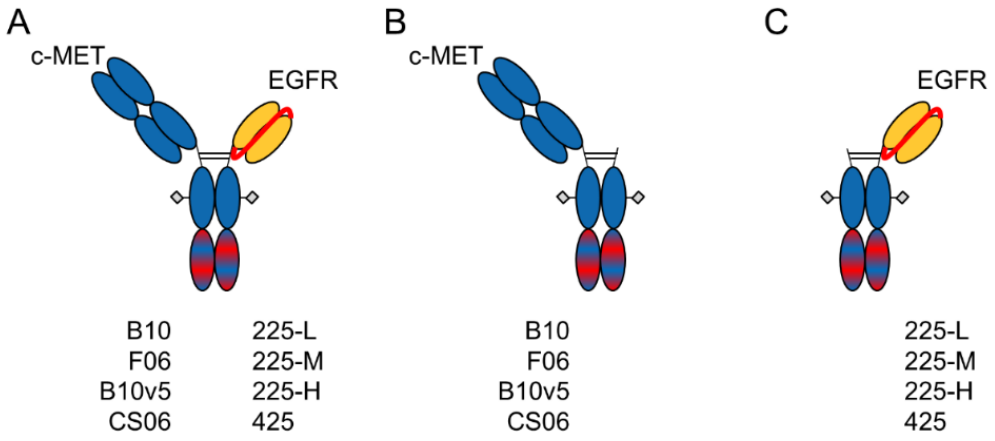

Figure 15: Schematic presentation of anti-c-MET and anti-EGFR bsAb (A) and corresponding monovalent, one-armed control SEEDs (B-C).

(A) Based on four anti-c-MET binders (B10, F06, B10v5, and CS06) and four anti-EGFR binders (225-L, 225-M, 225-H, and 425), bispecific SEED antibodies were generated, while the c-MET binding arm was composed of a Fab-fragment and the EGFR binding arm was present in a scFv format with a glycine-serine linker. B10 and F06 are the parental c-MET antibodies derived by phage display. B10v5 and CS06 represent binders from the affinity maturation. As EGFR directed antibodies, humanized cetuximab (C225) and matuzumab (425) were selected. (Muda *et al.*, 2011) **(B)** Scheme for monovalent, one-armed anti-c-MET Fab-SEED antibodies. **(C)** Presentation of monovalent, one-armed anti-EGFR scFv-SEED antibodies.

5.4.1.1 Small-scale production

The resulting sixteen different bsAbs with the corresponding eight monovalent mAbs were first expressed at small scale, then purified via protein A affinity chromatography spin columns, and analyzed by gel electrophoresis (Appendix, **Figure 35** and **Figure 36**) and size exclusion-high-performance liquid chromatography (SE-HPLC, **Table 5**). Expression yields of bsAbs ranged from 20 to 196 mg/l after purification. The bsAbs containing the 225-M variant displayed slightly poorer yields. For monovalent

control mAbs, anti-c-MET Fab-SEEDs had slightly higher yields (192-256 mg/l) with exception of Fab-F06-SEED than cetuximab based scFv-SEEDs (8-36 mg/l). Regarding monomer proportion, F06 and CS06 containing bsAbs displayed higher purity compared to B10 and B10v5 containing bsAbs. This is also true for the monovalent anti-c-MET Fab SEEDs. When comparing the influence of the anti-EGFR scFv in bsAbs on monomer percentage, 425 had a slight negative effect (for B10x425, CS06x425, and oa 425) when compared to 225 variants. However, bsAbs were only expressed one to two times at small scale for initial experiments.

Table 5: Expression yields of small scale production and monomer proportion.

Antibody yield after expression by transient transfection in Expi293F™ cells and purification via protein A affinity chromatography (calculated as mg/25ml and mg/l). Percentages of monomers were determined by analytical size exclusion high-performance liquid chromatography (SE-HPLC). n.d. = not determined.

Antibody	Yield [mg/25 ml]	Yield [mg/l]	Monomer [%]
B10x225-L	1.6	64	77
B10x225-M	1.5	60	63
B10x225-H	3.9	156	68
B10x425	2.1	84	47
F06x225-L	1.6	64	67
F06x225-M	1.1	44	74
F06x225-H	2.3	92	79
F06x425	4.9	196	80
B10v5x225-L	3.6	144	69
B10v5x225-M	0.8	32	71
B10v5x225-H	1.5	60	74
B10v5x425	2.7	108	77
CS06x225-L	1.1	44	84
CS06x225-M	0.6	24	85
CS06x225-H	1.4	56	89
CS06x425	0.5	20	81
oa 225-L	0.9	36	n.d.
oa225-M	0.2	8	63
oa 225-H	0.5	20	59
oa 425	2.2	88	45
oa F06	0.8	32	93
oa B10	4.8	192	70
oa CS06	5.9	236	84
oa B10v5	6.4	256	77

5.4.1.2 Mid-scale production

Based on initial results, the number of bsAbs was narrowed down to four constructs for mid-scale production and subsequent preparative SEC purification: B10v5x225-M, B10v5x225-H, CS06x225-M, and CS06x225-H. Corresponding monovalent control mAbs were also expressed. Final yields and monomer content before and after preparative SEC (Appendix, **Figure 37**) are summarized in **Table 6**. In general, the up-scale of the expression volume did not translate into higher yields. However, the

percentage of monomers was slightly increased when compared to small scale production. Again, mAbs containing the 225-M scFv tend to display lower yields and lower monomer percentage compared to mAbs with 225-H. Taken together, both yields and monomer contents after preparative SEC were suitable for functional characterization of bsAbs.

Table 6: Yields and purity of bsAbs and monovalent mAbs after up-scale production.

Antibody yields were photometrically (A_{280}) determined after expression of bsAbs by transient transfection in 200 ml Expi293F™ cells and purification via protein A affinity chromatography and preparative SEC (units: mg/200ml and mg/l). Percentages of monomers were calculated by analytical size exclusion high-performance liquid chromatography (SE-HPLC).

Antibody	Yield [mg/200 ml]	Yield [mg/l]	Monomer [%] before SEC	Monomer [%] after SEC
B10v5x225-M	5.1	25.5	80.9	98.0
B10v5x225-H	20.5	102.5	80.5	95.6
CS06x225-M	3.8	19.0	88.0	100.0
CS06x225-H	9.6	48.0	90.1	100.0
oa B10v5	29.6	148.0	95.6	100.0
oa CS06	10.1	50.5	87.4	98.5
oa 225-M	2.6	13.0	83.8	100.0
oa 225-H	9.4	47.0	96.5	100.0

5.4.2. Kinetic analysis of bispecific antibodies

Kinetic parameters of bsAbs and monovalent mAbs were analyzed by biolayer interferometry (BLI) to assess the influence of the reformatting in the bispecific format. Note that the detection limit of this biophysical method for kinetic measurements is considered as 100 pM. (Estep *et al.*, 2013) Briefly, mAbs were immobilized on anti-human Fc (AHC) biosensor tips and association as well as dissociation of c-MET or EGFR were monitored. Exemplary graphs of monovalent mAbs were shown in chapters 5.2 and 5.3 (cf. **Figure 9** and **Figure 14**, respectively). The kinetic parameters are summarized in **Table 7** and illustrated in iso-affinity plots (**Figure 16**). The data confirms that reformatting of anti-c-MET and anti-EGFR binders into the bispecific format did not alter kinetic profiles for functional binding of respective soluble receptor. B10v5, 225-M, and 225-H resulted in nearly identical kinetic parameters when comparing monovalent mAbs to bsAbs. For CS06, only CS06x225-H slightly differed from oa CS06 and CS06x225-M but within the instrumental error margin (factor 2).

Table 7: Kinetic parameters for bsAbs and monovalent control mAbs determined by BLI.

Affinities displayed as equilibrium dissociation constant (K_D) as well as association (k_a) and dissociation rates (k_d) were determined by BLI. The mAbs were immobilized on AHC biosensors followed by association and dissociation of c-MET or EGFR. For each measurement, six analyte concentrations were measured ranging from 50 nM to 0.8 nM. Note that C225 (cetuximab) is a bivalent, chimeric IgG and 225 variants (H and M) are based on humanized cetuximab.

Antibody	Analyte	K_D [M]	k_a [$M^{-1}s^{-1}$]	k_d [s^{-1}]
oa B10	c-MET	1.2E-08	1.0E+05	1.2E-03
oa B10v5	c-MET	3.8E-10	4.0E+05	1.6E-04
B10v5x225-M	c-MET	3.7E-10	4.0E+05	1.5E-04
B10v5x225-H	c-MET	3.6E-10	4.0E+05	1.5E-04
oa F06	c-MET	4.2E-09	2.5E+06	1.1E-02
oa CS06	c-MET	1.9E-10	1.1E+06	2.1E-04
CS06x225-M	c-MET	2.1E-10	1.1E+06	2.2E-04
CS06x225-H	c-MET	1.2E-10	3.3E+06	3.9E-04
oa 225-L	EGFR	1.1E-06	9.4E+04	1.0E-01
oa 225-M	EGFR	4.4E-09	3.7E+06	1.6E-02
B10v5x225-M	EGFR	4.7E-09	3.6E+06	1.7E-02
CS06x225-M	EGFR	3.9E-09	4.6E+06	1.8E-02
oa 225-H	EGFR	1.4E-10	3.6E+06	4.9E-04
B10v5x225-H	EGFR	1.5E-10	3.5E+06	5.3E-04
CS06x225-H	EGFR	1.2E-10	3.3E+06	3.9E-04
C225	EGFR	1.2E-09	6.1E+05	7.4E-04
oa 425	EGFR	1.4E-08	8.3E+05	1.2E-02

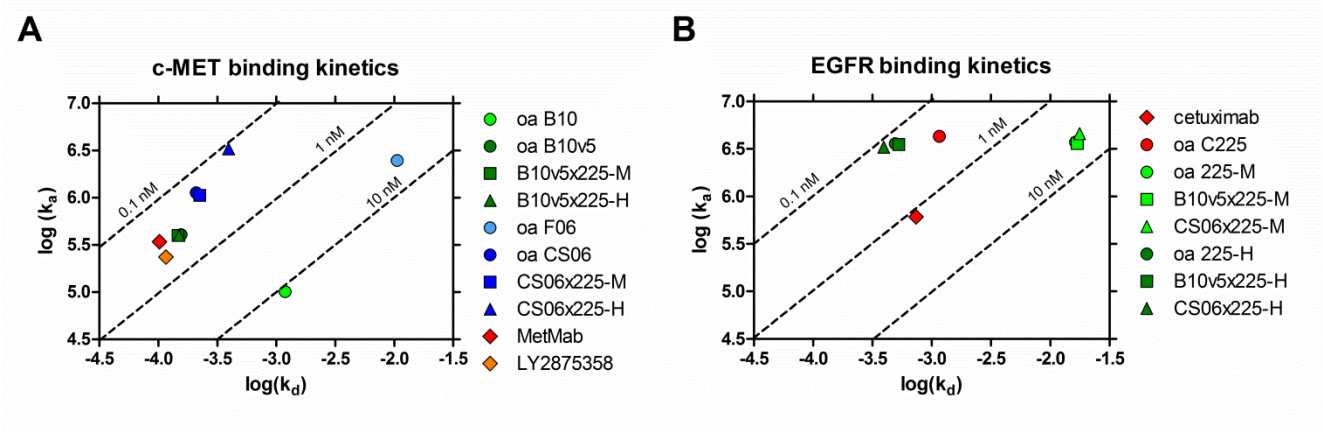

Figure 16: Iso-affinity plots of bsAbs in comparison to monovalent or bivalent reference mAbs.

Logarithm of association rate was plotted against logarithm of dissociation rate for bsAbs and mAbs to c-MET **(A)** or EGFR **(B)**. Dotted diagonals represent iso-affinities. That means that the combination of k_a and k_d values results in the same K_D. The units of k_d and k_a are s^{-1} and $M^{-1}s^{-1}$, respectively.

5.4.3. Simultaneous binding

To verify that simultaneous binding of both antigens to bsAbs is not sterically impaired, a bridging experimental setup was selected for BLI. In brief, biotinylated c-MET was captured on streptavidin biosensors which were subsequently quenched with biocytin and milk powder to prevent unspecific binding to biosensor tips. Then, bsAbs were associated followed by addition of EGFR. Exemplary graphs

for the last two association steps are depicted in **Figure 17**. Due to the smaller size of EGFR ECD (69 kDa) compared to the bispecific antibody (~125 kDa), the shift for the association of EGFR ECD is half the size of the shift for the association of bsAb: In **Figure 17A**, addition of B10v5x225-H to biosensor tips results in shift of 0.4 nm and EGFR subsequently in 0.2 nm. For CS06x225-H the shift is 0.2 nm and followed by EGFR with a shift of 0.1 nm (**Figure 17B**). That means that after association of bsAbs an equimolar amount of EGFR is associated. The second shift in interference pattern only represented EGFR association since the buffer control did not show any dissociation of bsAb. Addition of an unrelated isotype mAb (anti-HEL) and EGFR indicated no unspecific binding to streptavidin biosensors. As a consequence, the bsAbs are 100% functional and simultaneous binding of both antigens is sterically possible.

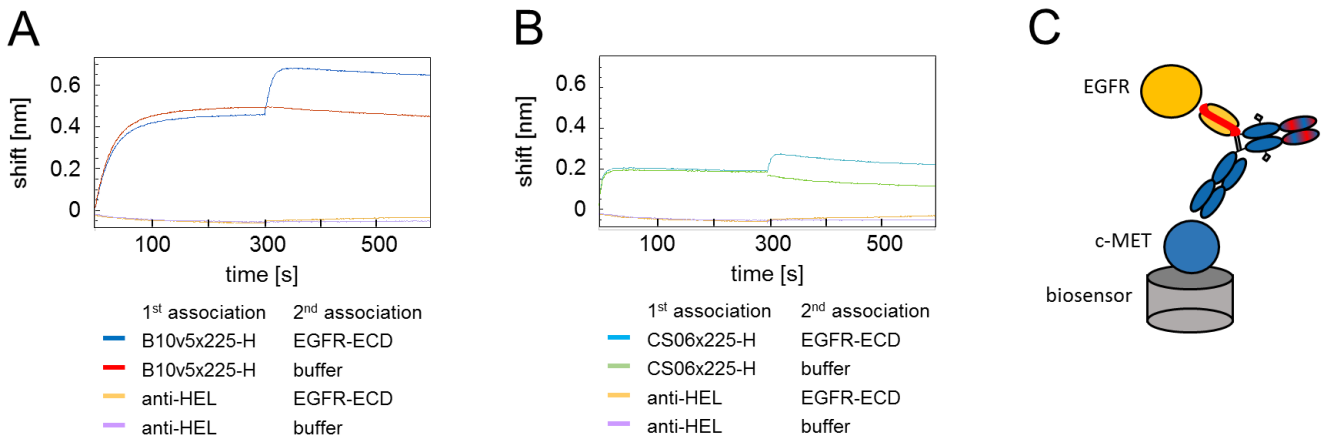

Figure 17: Simultaneous binding of c-MET and EGFR by bsAbs demonstrated via BLI.

Biotinylated c-MET was immobilized on streptavidin biosensors. Then, association of bsAbs B10v5x225-H **(A)** and CS06x225-H **(B)** followed by EGFR was monitored. For both association steps an interference pattern shift could be observed indicating simultaneous binding of both antigens by bsAbs. Controls with a non-related isotype antibody (anti-HEL) and EGFR indicated no unspecific binding to streptavidin biosensors. **(C)** Schematic representation of experimental set-up.

5.4.4. Analysis of antibody stability

5.4.4.1 Thermal shift assay

Muda *et al.* already analyzed the biophysical and biochemical properties of the SEED format and demonstrated suitability of this technology for therapeutic approaches. (Muda *et al.*, 2011) In order to evaluate the influence of binder combinations in the SEED format on bsAb stability, a differential scanning fluorimetry (DSF), which is also known as thermal shift assay (TSA), was performed. Accelerated thermal stability of proteins might also be an indicator for long-term stability during storage. During thermal denaturation of proteins, hydrophobic patches are exposed allowing attachment of a polarity-sensitive fluorescent dye, e.g. SYPRO orange. (Lo *et al.*, 2004) In summary, all evaluated mAbs had a melting temperature (T_m) above 60°C (**Table 8**) which is considered as critical T_m for therapeutic

antibodies. (King *et al*, 2011) Immunoglobulins have slightly higher stability compared to artificial SEED molecules. (Muda *et al.*, 2011) The T_m difference (ΔT_m) of cetuximab (67.3°C) and CS06x225-H (62.2°C) accounted thereby 5.1°C. The raw data is summarized in the Appendix **Figure 38**.

Table 8: Thermal stability of bsAbs in comparison to monovalent mAbs and cetuximab.

Melting temperatures (T_m) of mAbs was measured by thermal shift assay using 1 μM protein with a 20 fold excess of the fluorescent dye SYPRO orange. Raw data are summarized in **Figure 38** (Appendix). Means and standard deviations were calculated based on T_m of triplicates. oa = one-armed.

Antibody	T_m [°C]
cetuximab	67.3 ± 0.172
oa B10	65.7 ± 0.001
oa C225-Fab	65.7 ± 0.001
oa 225-M	65.2 ± 0.174
oa CS06	64.9 ± 0.001
oa F06	64.8 ± 0.172
CS06x225-M	64.8 ± 0.126
B10v5x225-M	64.5 ± 0.001
oa B10v5	64.0 ± 0.172
B10v5x225-H	62.8 ± 0.174
oa 225-H	62.7 ± 0.001
CS06x225-H	62.2 ± 0.172

5.4.4.1 Long-term stability in human and mouse serum

The bsAbs as well as cetuximab were incubated in human or mouse serum at 37°C for 24 days. Every two to three days, aliquots were immediately frozen and stored at -80°C. The concentration of bsAbs and cetuximab was normalized to 5 μg/ml. The stability of every sample to each time point was determined in triplicates by functional bridging ELISA using 100 ng immobilized EGFR and biotinylated c-MET as well as streptavidin-HRP conjugate for detection. Sera were not heat-inactivated before the experiment because no influence was shown (personal communication Merck, Darmstadt, Germany). Before the assay, mAb assay concentration were titrated in order to determine the linear range of the detection signal and to avoid signal saturation for each mAb individually. Cetuximab was detected with an anti-human Fc-HRP conjugate. ELISA signals of aliquots from time point t=0 were considered as reference value for 100% functionality for each mAb. As depicted in **Figure 18**, calculated percent decrease in bsAb or cetuximab functionality was plotted against the time. Overall, the stability of mAbs in human and mouse serum demonstrated similar tendencies. After 24 days, the functionality of cetuximab was reduced to ~95%. For bsAbs with the 225-H variant, functionality was reduced to 85% on day 10 to 14 and further dropped to 71-76% on day 24. 225-M containing bsAbs, already lost ~20% functionality on day 1 and decreased to 53-57% (for mouse serum) and 68-80% (for human serum) on day 24. Taken together, B10v5x225-M and CS06x225-M tended to be less stable in serum at 37°C compared to 225-H

bsAbs. Cetuximab IgG displayed the highest stability after 24 days again demonstrating higher stability of immunoglobulins in comparison to artificial SEED molecules. Given a standard half-life of IgGs of 20 days (Brekke & Sandlie, 2003), all four bsAbs displayed suitable thermal stability in serum.

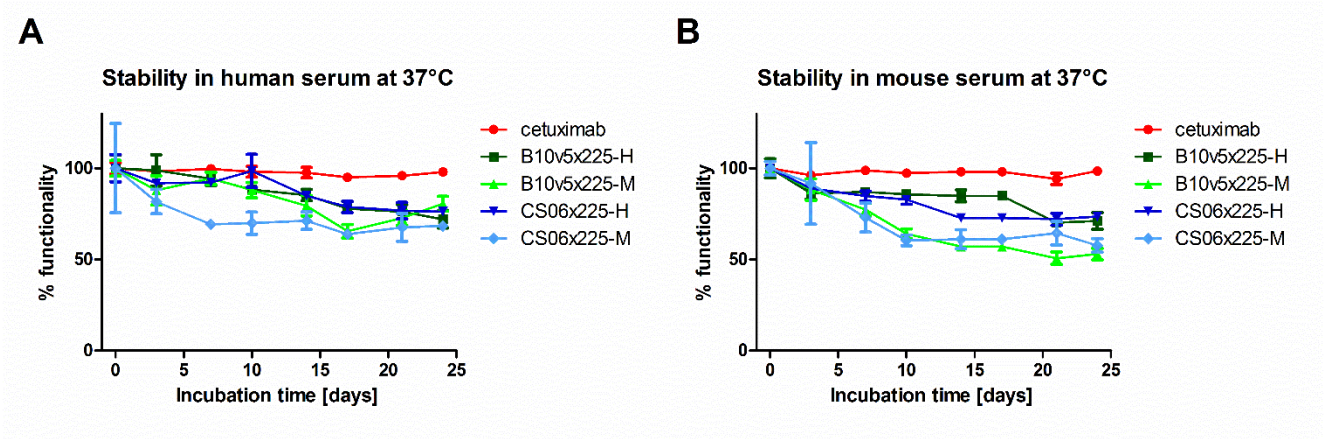

Figure 18: Long-term stability of bsAbs in comparison to cetuximab in human (A) and mouse serum (B).

100 ng EGFR were coated in microtiter plates. Cetuximab and bsAbs were incubated in human **(A)** and mouse **(B)** serum at 37°C for 0 to 24 days as triplicates. Aliquots (t=0) which were immediately frozen at -80°C after antibody dilution in serum (5 μg/ml) served as 100% reference value for functionality of each mAb and reduction in functionality of later time points were calculated based on this value. BsAbs were detected with biotinylated c-MET ECD and streptavidin-HRP conjugate. Cetuximab binding was revealed by anti-human Fc antibody-HRP conjugate using standard ELISA detection methods.

5.4.5. Cellular binding

As described before, bsAbs displayed the desired kinetic characteristics with affinities ranging from two digit nanomolar to the sub-nanomolar affinities for their cognate targets (with exception of 225-L with 1.1 μM affinity for soluble EGFR). The next step was to analyze whether binding of soluble protein can be translated into functional binding of cellular presented target protein. Therefore, binding of 100 nM bsAbs on several cancer cell lines was performed by flow cytometry (chapter 4.4.3). Cancer cell lines were chosen based on different receptor expression levels of c-MET and EGFR which were determined by receptor quantification using normalized cell numbers (chapter 5.1). An unrelated isotype control mAb (anti-HEL), unstained cells or cells only treated with secondary FITC-conjugated antibody served as controls to reveal the amount of cellular autofluorescence. Exemplary histograms for relative fluorescence intensities are depicted in **Figure 19**. BsAbs exhibited strong cellular binding to c-MET or EGFR overexpressing cell lines, e.g. c-MET amplified EBC-1 cells (**Figure 19A**) and EGFR overexpressing A431 cells (**Figure 19C**) comparable to respective monospecific reference binders oa CS06, oa B10v5 or cetuximab, respectively. For cell lines with nearly equal c-MET and EGFR expression, e.g. A549 and NCI-H441 (chapter 5.1), bsAbs tended to bind stronger compared to corresponding anti-c-MET mAbs and anti-EGFR reference binders indicating cooperative and simultaneous engagement of both antigens on the cellular surface (**Figure 19B**, **Figure 20**).

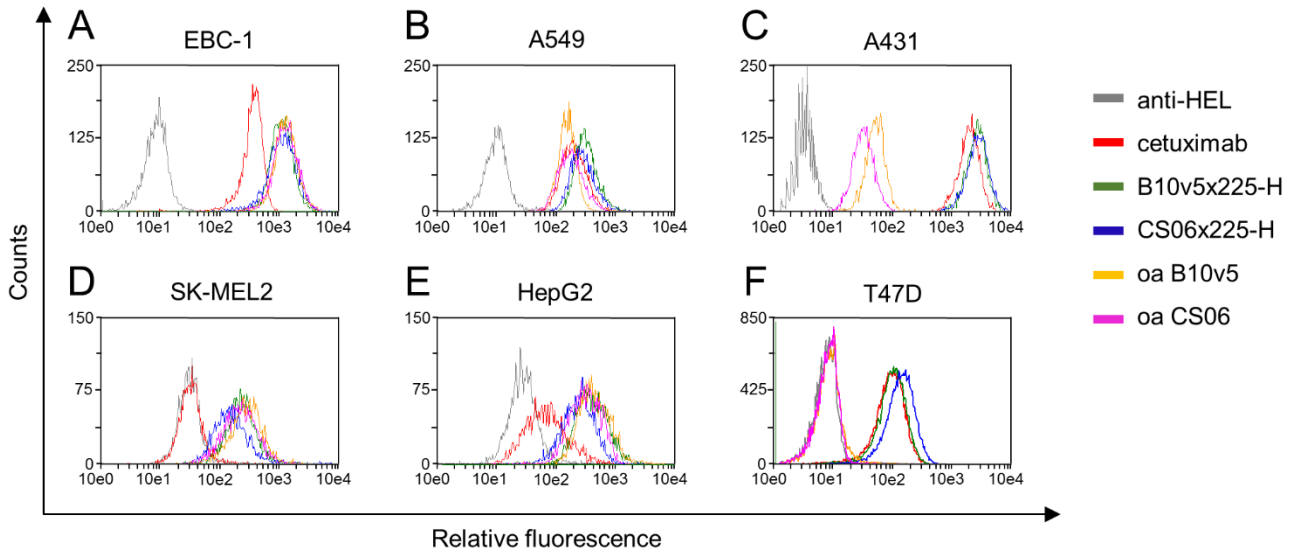

Figure 19: Cellular binding of bsAbs and reference mAbs to several cancer cell lines.

Cell lines were incubated with 100 nM mAb and binding was revealed with anti-human Fc antibody-FITC conjugate via flow cytometry (5,000 counts). **(A)** Both bsAbs and monovalent anti-c-MET antibodies displayed stronger binding to c-MET amplified EBC-1 cells with medium EGFR surface expression compared to cetuximab. **(B)** A549 cells present similar EGFR and c-MET levels on their surface and binding of bsAbs to A549 cells is slightly increased compared to monovalent anti-c-MET and anti-EGFR mAbs. **(C)** For the EGFR overexpressing cell line A431 binding of bsAbs was comparable to cetuximab. **(D)** EGFR negative cell line SK-MEL2 did not show cetuximab binding, but anti-c-MET mAb and bsAbs displayed binding. **(E)** Due to slightly higher c-MET than EGFR expression of HepG2, bsAbs and anti-c-MET mAbs demonstrated stronger binding than cetuximab. **(F)** Binding to c-MET negative T47D cells by bsAbs and cetuximab could be observed, while no binding of oa B10v5 and oa CS06 was observable. Note that for T47D only 30 nM mAbs and 20,000 counts were used.

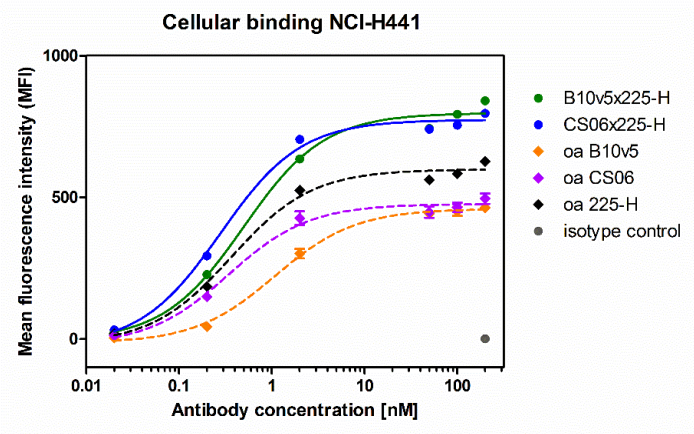

Figure 20: Cellular binding to NCI-H441 cells indicated simultaneous binding of bsAbs.

NCI-H441 cells displayed similar EGFR and c-MET receptor surface expression levels. Cells were incubated with varying concentrations of antibodies (0.02-200 nM) and binding was revealed with anti-human Fc-FITC conjugate and flow cytometry. MFI values were plotted against the logarithm of antibody concentration. Means of duplicates and standard deviations were calculated. As a result, bsAbs bound stronger to NCI-H441 cells compared to monovalent anti-c-MET mAbs, oa B10v5 and oa CS06, as well as monovalent anti-EGFR mAb oa 225-H. No unspecific binding was observed with an unrelated isotype control (anti-HEL). EC_{50} values ranged from 0.3 to 1.1 nM for cellular binding of all mAbs. The experiment was confirmed in two independent experiments.

Table 9: Cellular binding of bsAbs to tumor cell lines with different expression levels in c-MET and EGFR.

Binding of bsAbs and corresponding reference binders was analyzed via flow cytometry on several cancer cell lines. Mean fluorescence intensity (MFI) values were calculated by subtraction of fluorescence intensity of isotype control. In the table, MFI values for cells incubated with 100 nM mAb were summarized. Strong binding of bsAbs could be observed for cell lines with high c-MET and/or high EGFR expression (EBC-1, MKN45, A431). Medium to low binding was detected on A549 and HepG2 cells displaying low c-MET and EGFR surface expression levels. For A549 cells, slightly stronger binding could be observed for bsAbs in comparison to monovalent mAbs. CHO-S cells served as a non-human cell line control. Antibodies which were tested for not being cross-reactive to mouse c-MET or EGFR, e.g. cetuximab, F06, and CS06, demonstrated no unspecific binding to CHO-S cells. However, rodent-cross-reactive oa B10 and oa B10v5 as well as bsAbs containing one of those two binders demonstrated slight binding to CHO-S cells.
Color code: green = high MFI values / high binding, yellow = medium MFI values, red = low MFI values / no binding
Legend: MFI = mean fluorescence intensity, n.d. = not determined, +++ = high expression (>10^5 receptors per cell), ++ = medium expression (10^3 receptors per cell < x <10^5 receptors per cell), + = low expression (>10^3 receptors per cell), - = no expression. Quantification of receptor densities was described in chapter 5.1.

	EBC-1	MKN45	A431	A549	HepG2	CHO-S
mAb	c-MET^{+++} EGFR^{++}	c-MET^{+++} EGFR^{++}	c-MET^{+} EGFR^{+++}	c-MET^{+} EGFR^{+}	c-MET^{+} EGFR^{+}	c-MET^{-} EGFR^{-}
B10x225-L	1.1E+03	1.2E+03	9.3E+02	1.8E+02	7.2E+01	3.0E+00
B10x225-M	1.2E+03	1.8E+03	1.5E+03	5.6E+02	7.1E+01	2.3E+01
B10x225-H	1.1E+03	1.3E+03	2.0E+03	4.5E+02	8.7E+01	3.3E+01
B10x425	1.2E+03	1.3E+03	1.1E+03	2.6E+02	8.8E+01	5.0E+00
F06x225-L	9.3E+02	1.2E+03	1.2E+03	2.1E+02	8.5E+01	1.5E+01
F06x225-M	9.0E+02	1.2E+03	1.9E+03	n.d.	6.1E+01	1.0E+00
F06x225-H	8.8E+02	1.2E+03	3.2E+03	2.9E+02	7.4E+01	2.0E+00
F06x425	7.1E+02	1.2E+03	1.3E+03	2.6E+02	6.3E+01	9.0E+00
B10v5x225-L	8.4E+02	1.2E+03	8.3E+02	2.4E+02	4.3E+02	1.2E+02
B10v5x225-M	1.1E+03	1.3E+03	1.3E+03	3.7E+02	7.7E+02	2.7E+02
B10v5x225-H	1.1E+03	1.3E+03	1.7E+03	3.3E+02	3.3E+02	8.3E+01
B10v5x425	1.0E+03	1.3E+03	1.4E+03	3.2E+02	3.3E+02	9.8E+01
CS06x225-L	1.2E+03	1.5E+03	8.7E+02	2.0E+02	2.3E+02	7.0E+00
CS06x225-M	1.2E+03	1.5E+03	1.2E+03	2.6E+02	3.1E+02	3.0E+01
CS06x225-H	1.1E+03	1.5E+03	1.8E+03	2.8E+02	1.8E+02	4.0E+00
CS06x425	9.8E+02	1.4E+03	1.3E+03	2.6E+02	1.4E+02	1.0E+00
oa 225-L	1.4E+02	7.4E+01	9.9E+02	8.1E+01	1.1E+01	3.0E+00
oa225-M	2.7E+02	1.4E+02	1.1E+03	1.3E+02	2.4E+01	8.0E+00
oa 225-H	6.3E+02	1.9E+02	1.7E+03	1.7E+02	3.7E+01	1.0E+00
oa 425	2.4E+02	1.8E+02	8.6E+02	1.6E+02	4.3E+01	6.0E+00
oa F06	1.1E+03	9.1E+02	3.1E+01	8.1E+01	1.5E+01	0.0E+00
oa B10	1.3E+03	1.3E+03	9.4E+01	1.2E+02	5.6E+01	3.4E+01
oa CS06	1.3E+03	1.5E+03	1.8E+01	1.4E+02	2.7E+02	1.0E+00
oa B10v5	1.3E+03	1.5E+03	3.0E+01	1.5E+02	3.8E+02	7.7E+01

For EGFR-negative SK-MEL2 cells, bsAbs, oa CS06 and oa B10v5 displayed binding while there was no binding detectable for EGFR-specific antibody cetuximab (**Figure 19D**). *Vice versa*, cetuximab and bsAbs bound to c-MET-negative T47D cells, while oa CS06 and oa B10v5 omitted binding (**Figure 19F**). Slight EGFR expression in HepG2 cells correlated with slight binding of cetuximab (**Figure 19E**). Data also indicated affinity dependent binding (**Table 9**). Affinity matured anti-c-MET binders (CS06 and B10v5) alone or in the bsAb format demonstrated higher MFI values compared to corresponding parental binders (F06 and B10). The same tendencies could be observed for the anti-EGFR binding moieties 225-L, 225-M,

225-H and 425: The higher the affinity of the binder, the stronger the cellular binding. In general, binding behavior of bsAbs could be correlated with the higher expressed target on the surface of cells. The CHO-S cell line with non-human origin was selected as negative cell line. For cetuximab, oa F06, oa CS06 as well as F06 or CS06 containing bsAbs, no unspecific binding to CHO-S was detectable (**Table 9**). B10 and B10v5 containing monovalent mAbs and bsAbs indicated binding to CHO-S cells. This could be a result of cross-species-reactivity of B10 and B10v5 to rodent c-MET. Additionally, oa B10v5 did not bind to c-MET negative T47D cells excluding unspecific binding of the antibody. Taken together, bsAbs strongly bound to c-MET and EGFR overexpressing cell lines in an affinity dependent manner and with high specificity.

5.4.6. Pharmacodynamics

After confirming the capability of bsAbs to bind cellular bound target protein, functional analyses were conducted for bsAbs. The focus was laid on the proximal and distal receptor signaling including phosphorylation of c-MET, EGFR, AKT, and MAPK (chapter 2.3.3, **Figure 4**). For cetuximab and matuzumab, inhibition of EGFR phosphorylation were previously described by direct competition with ligand binding (Ferguson *et al.*, 2003) and prevention of conformational rearrangements for receptor activation (Schmiedel *et al.*, 2008), respectively. The presented study analyzed how kinetic variants and monovalency of the anti-EGFR and anti-c-MET binders in the bispecific format affect potency and efficacy for the inhibition of EGFR as well as c-MET signaling. For the analysis of the sixteen bsAbs produced by small scale production without further purification by preparative SEC, initial Western Blot experiments were conducted in HGF-dependent A549 cells and c-MET amplified EBC-1 cells. Briefly, cells were treated with 300 nM antibodies for 4 h before ligand stimulation and detection was carried out with antibodies directed against total and phosphorylated c-MET and EGFR as well as actin as a loading control (Appendix, **Figure 39**). BsAbs containing 225-M and 225-H efficiently inhibited EGFR phosphorylation comparable to cetuximab in A549 cells. In contrast, bsAbs with 225-L and 425 could not prevent EGFR phosphorylation completely. BsAbs with CS06 and F06 displayed highly efficient inhibition of c-MET phosphorylation in A549 cells while B10 and B10v5 containing bsAbs demonstrated medium efficiency for c-MET inactivation (Appendix, **Figure 39**). In c-MET amplified EBC-1 cells, which are not dependent on HGF stimulation, all bsAbs were not able to reduce c-MET phosphorylation. Only the reproduced anti-c-MET mAb DN-30 inducing ECD shedding resulted in a decreased total c-MET and phosphorylated MET signal. (Petrelli *et al.*, 2006) However, a slight reduction in total c-MET signal intensities was observed under treatment with B10 or B10v5 containing bsAbs indicating c-MET degradation (Appendix, **Figure 39**).

For further functional analysis, the number of evaluated bsAbs was narrowed down to four based on their ability to inhibit phosphorylation of the respective receptor: B10v5x225-M, B10v5x225-H, CS06x225-M and CS06x225-H. In order to remove aggregates and/or homodimers which could interfere with cellular assays (Joubert *et al*, 2012), preparative SEC purification was conducted. Additionally, distal signaling including phosphorylation of AKT and MAPKP as well as potential synergistic effects mediated by bsAbs in comparison to the combination of monovalent mAbs were further analyzed (**Figure 21**). Data presented in **Figure 21A** indicated that CS06x225-H inhibited c-MET phosphorylation in A549 cells with higher efficiency compared to B10v5x225-H and reproduced LY2875358.

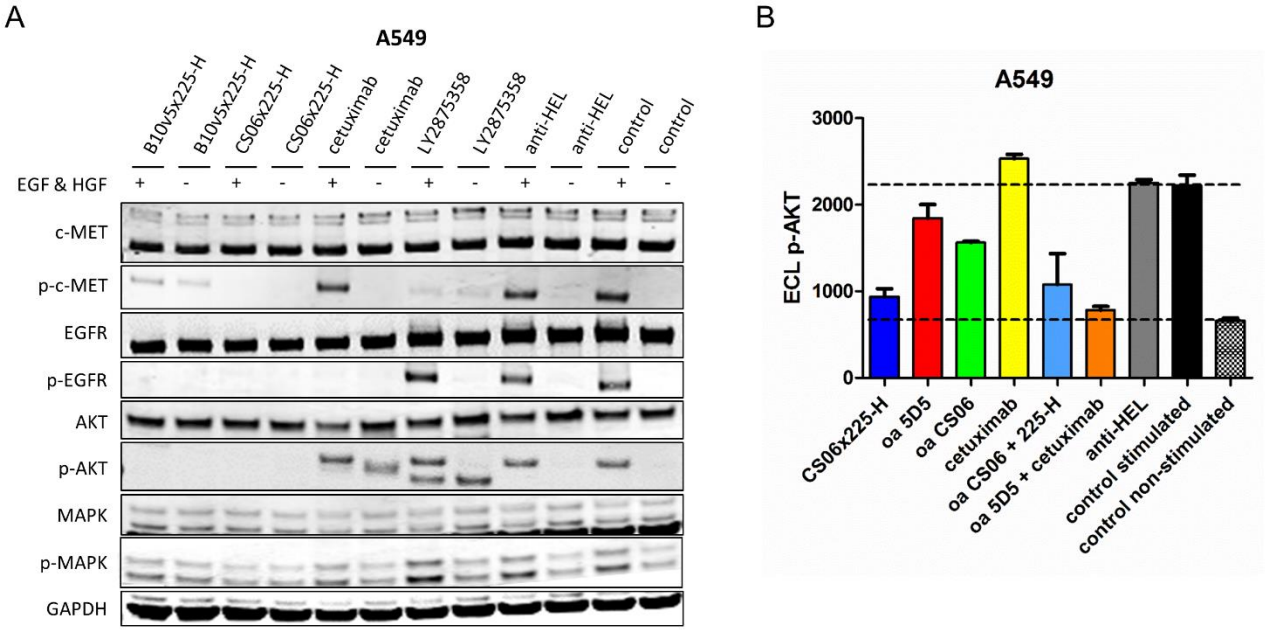

Figure 21: Simultaneous inhibition of EGFR and c-MET phosphorylation by bsAbs affected downstream signaling.

(A) After starvation, A549 cells were pre-incubated with 300 nM bsAbs and reference binders for three hours followed by stimulation with 100 ng/ml HGF and EGF and cell lysis. Cell lysates were subjected to SDS-PAGE and Western blotting. Signals were detected with antibodies directed against c-MET; phospho-c-MET (p-c-MET), EGFR, phospho-EGFR (p-EGFR), AKT, phospho-AKT (p-AKT), MAPK, phospho-MAPK (p-MAPK) and GAPDH as loading control. Treatment with bsAbs resulted in inhibition of c-MET and EGFR phosphorylation similar to respective reference antibodies (LY2875358 and cetuximab). Additionally, phosphorylation of AKT was prevented. **(B)** Serum starved A549 cells were treated with 500 nM mAbs or mAbs combinations for 1 h before stimulation with 100 ng/ml HGF and EGF. Cell lysates were subjected to MSD-assay analyzing AKT phosphorylation. p=phosphorylated

Furthermore, the two latter mAbs induced slight c-MET activation in absence of ligand stimulation potentially indicating partial agonism which was described for LY2875358. (Liu *et al.*, 2014) Cetuximab and the unrelated isotype control, anti-HEL, did not affect c-MET phosphorylation in comparison to HGF-stimulated A549 cells. No significant changes for total c-MET and total EGFR levels were observable during 3 h treatment with 300 nM mAbs. The bsAbs containing the 225-H variant reduced EGFR phosphorylation similar to cetuximab while the anti-c-MET mAb LY2875358 as well as anti-HEL did not affect phospho-EGFR levels. While no significant changes were detectable for phospho-MAPK, bsAbs efficiently reduced AKT phosphorylation in contrast to cetuximab and LY2875358 which partly induced

AKT phosphorylation under non-stimulated conditions. To note, there were no observable increase in AKT phosphorylation in untreated cells or cells incubated with anti-HEL without stimulation.

To further analyze AKT, EGFR and c-MET phosphorylation in a concentration dependent manner and to be able to compare IC_{50} values, electrochemiluminescence ELISA assays (MSD-assays) were conducted (**Figure 21B, Figure 22-23**). Treatment with 500 nM of mAbs or mAb combination revealed nearly complete reduction of AKT stimulation to levels of non-stimulated cells by CS06x225-H similar to the combination of cetuximab with reproduced oa 5D5. There is a slight increase in phospho-AKT level for the combination oa CS06 and oa 225-H. For the monovalent c-MET antibodies oa 5D5 and oa CS06, a reduction of AKT-phosphorylation of 24% and 42%, respectively, was detected when compared to stimulated A549 cells. Cetuximab in contrast slightly increased levels of phospho-AKT during stimulation with EGF and HGF similarly reported by Castoldi and colleagues. (Castoldi *et al.*, 2013)

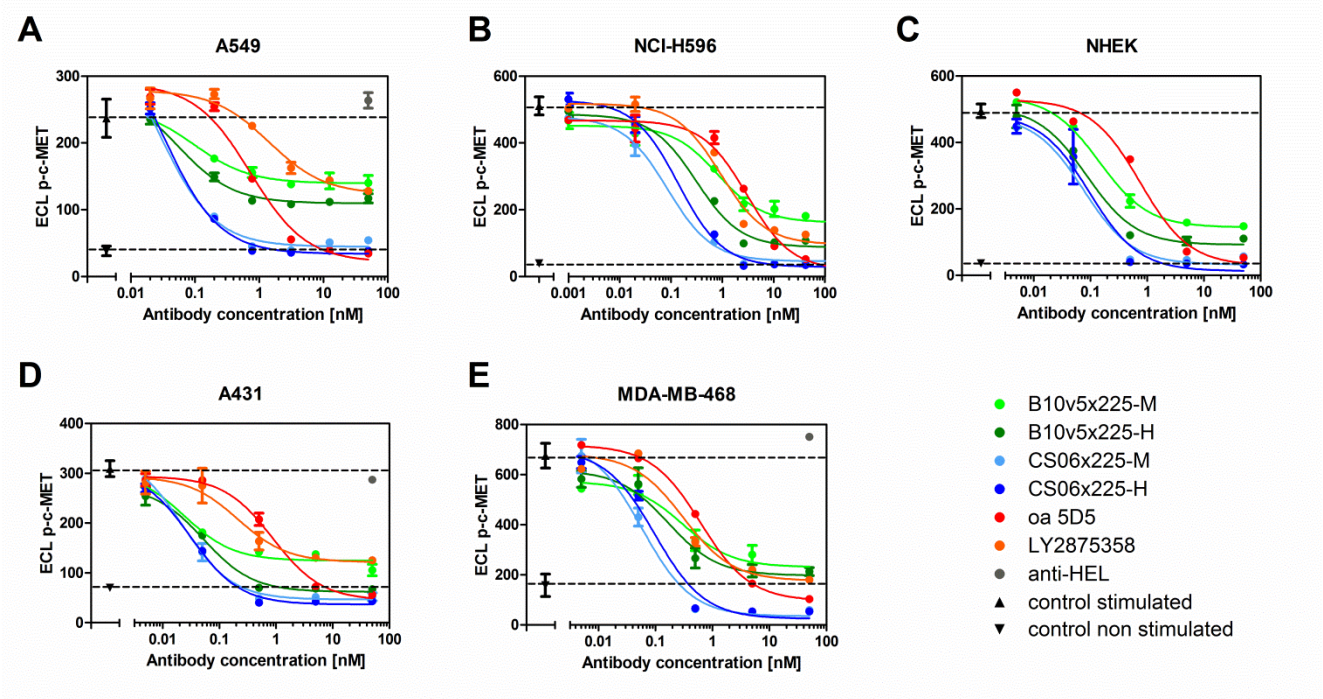

Figure 22: Inhibition of c-MET phosphorylation by bsAbs.

A549 **(A)**, NCI-H596 **(B)**, primary keratinocytes (NHEK.f-c., **C**), A431 **(D)** and MDA-MB-468 cells **(E)** were serum starved and treated with varying concentrations of bsAbs and reference anti-c-MET mAbs or anti-HEL mAb for 1 h followed by stimulation with 100 ng/ml HGF for 5 min and detection of phosphorylated c-MET by electrochemiluminescence (ECL) ELISA (MSD-assay). As controls, cells were stimulated or maintained non-stimulated without the incubation of antibodies. MSD signals were plotted against the logarithm of the antibody concentration and sigmoidal curve fitting was performed. CS06x225-M and –H inhibited c-MET phosphorylation more potently compared to oa 5D5 and LY2875358 in all five cell lines.

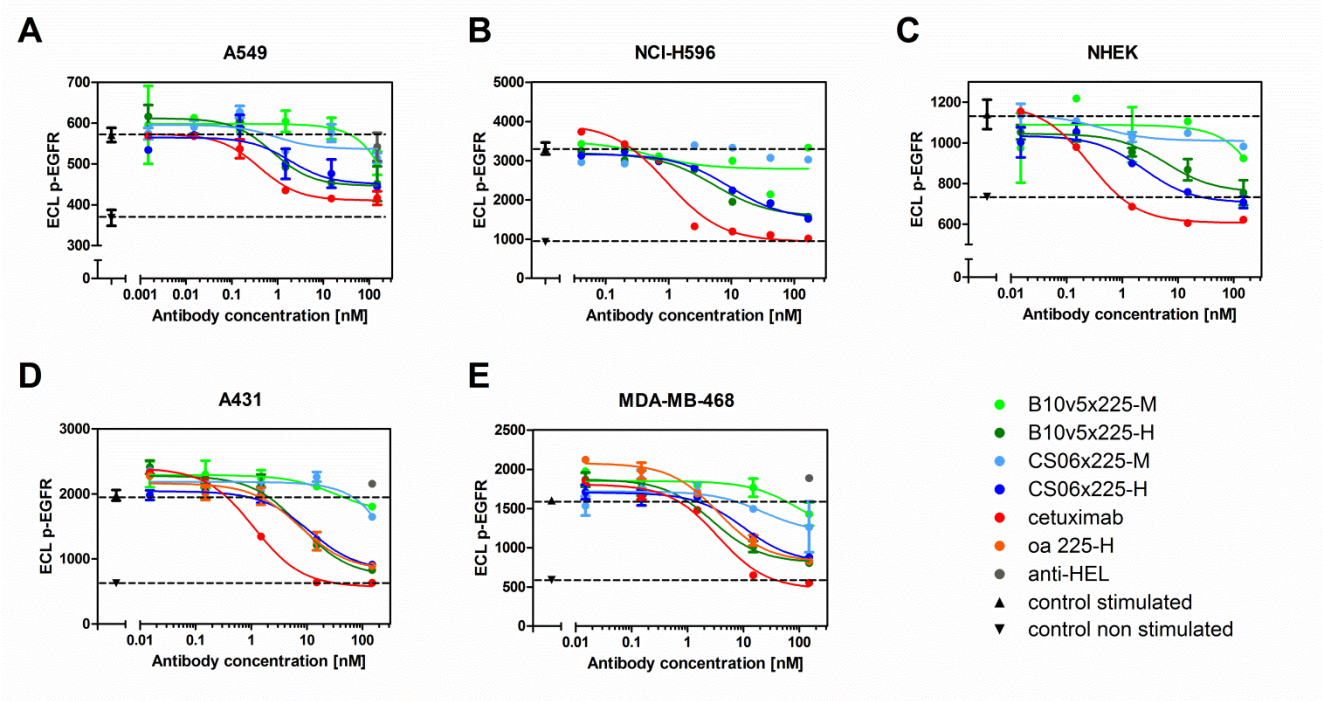

Figure 23: Inhibition of EGFR phosphorylation by bsAbs.

A549 **(A)**, NCI-H596 **(B)**, primary keratinocytes (NHEK.f-c., **C**), A431 **(D)** and MDA-MB-468 cells **(E)** were serum starved. Afterwards, serial diluted bsAbs and reference anti-EGFR mAbs (cetuximab and oa 225-H) or alternatively anti-HEL were incubated for 1 h followed by stimulation with 100 ng/ml EGF for 5 min and detection of phosphorylated EGFR by electrochemiluminescence (ECL) ELISA (MSD-assay). As controls, cells were stimulated or maintained non-stimulated without the incubation with antibodies. MSD signals were plotted against the logarithm of the antibody concentration and sigmoidal curve fitting was performed. Inhibition of EGFR phosphorylation was dependent on the valence and affinity of the EGFR binder. Cetuximab (C225) displayed a higher potency and efficacy compared to oa 225-H and oa 225-M both in monospecific and bispecific format.

Table 10: IC_{50} values for the inhibition of c-MET and EGFR phosphorylation by bsAbs.

Based on three parameter curve fitting of MSD-signals plotted against the logarithm of antibody concentration, IC_{50} values were calculated with GraphPad Prism 5. The number of independent experiments with duplicates was indicated (n). n.d. = not determined; s.d. = standard deviation.

Antibody	Receptor	A549		NHEK.f-c.	
		IC_{50} [nM] ± s.d.	*n*	IC_{50} [nM] ± s.d.	*n*
CS06x225-H	phospho-c-MET	0.3 ± 0.2	4	0.1	1
	phospho-EGFR	0.8	1	0.8	1
B10v5x225-H	phospho-c-MET	0.3 ± 0.2	2	0.2	1
	phospho-EGFR	1.1 ± 0.4	2	1.7 ± 0.3	2
oa 5D5	phospho-c-MET	0.8 ± 0.5	4	0.7	1
LY2875358	phospho-c-MET	1.0 ± 0.9	2	n.d.	-
cetuximab	phospho-EGFR	0.4 ± 0.1	3	0.3 ± 0.2	2

Regarding inhibition of c-MET phosphorylation, CS06x225-H and CS06x225-M displayed higher potency compared to oa 5D5 in primary keratinocytes, HGF-dependent A549 and NCI-H596 cells as well as in EGFR overexpressing A431 and MDA-MB-468 (**Figure 22**). B10v5x225-H and B10v5x225-M had a similar efficacy in inhibiting c-MET phosphorylation to LY2875358, but reduced efficacy compared to

CS06 bsAbs and oa 5D5 confirming the results by Western Blot. The corresponding IC_{50} values for A549 and NHEK cells are summarized in **Table 10**.

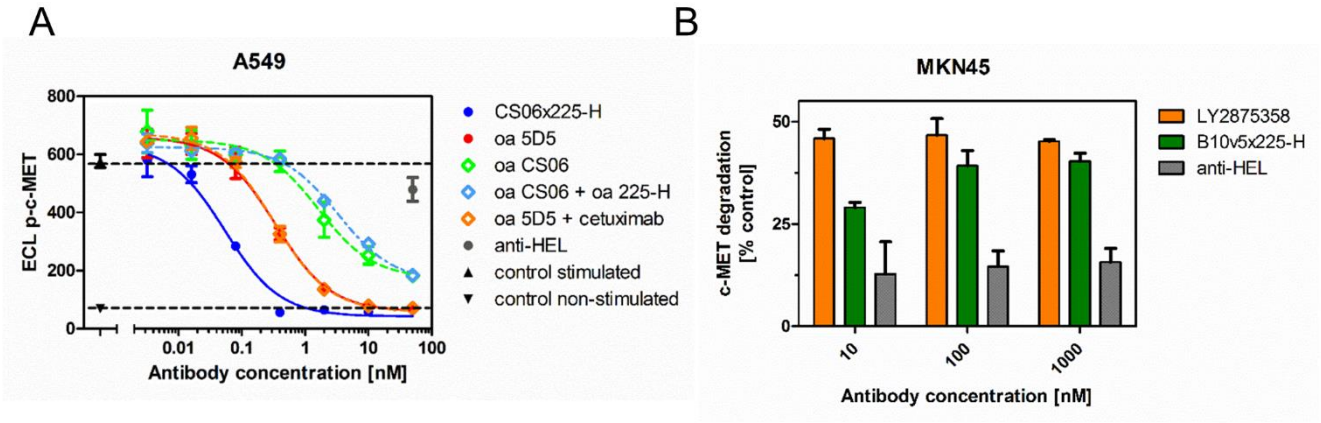

Figure 24: Potential synergistic effect of CS06x225-H (A) and B10v5x225-H induced c-MET degradation similar to LY2875358 (B).

(A) A549 cells were treated with varying concentrations of mAb or mAb combination for 1 h and subsequently stimulated with 100 ng/ml HGF. Cell lysates were subjected to MSD-assay detecting phosphorylated c-MET levels in duplicates. CS06x225-H displayed higher potency in inhibiting c-MET compared to the combination of monovalent oa CS06 and oa 225-H. Two independent experiments were performed in duplicates. **(B)** Overnight treatment of c-MET amplified MKN45 cells by 10, 100 and 1000 nM mAbs. Degradation was calculated based on untreated cells serving as 100% c-MET levels. While anti-HEL mAb resulted in detrimental degradation, both LY2875358 and B10v5x225-H yielded in nearly 50% degradation. This is a representative graph of two independent experiments with duplicates.

In the matter of c-MET inhibition, there were no significant differences between IC_{50} values for A549 and primary keratinocytes. The inhibition of EGFR phosphorylation was dependent on the affinity and the valence of the antibody (**Figure 23**). The highest potency for EGFR inhibition in A549 cells was detected for cetuximab (IC_{50} = 0.4 nM), followed by 225-H bsAbs (IC_{50} value in the range of 1 nM, **Table 10**) and 225-M bsAbs (IC_{50} > 25 nM, **Figure 23**). In summary, anti-EGFR potencies were independent of EGFR expression levels on several cell lines (chapter 5.1, **Table 2**). In contrast to c-MET, there was no synergistic effect detectable for the inhibition of EGFR phosphorylation mediated by bsAbs. For c-MET in contrast, a potential synergistic effect of c-MET and EGFR directed bsAb compared to monovalent oa CS06 or the combination of oa CS06 and oa 225-H could be observed, resulting in an increased potency by more than one log level (**Figure 24A**). Since B10v5 and the reproduced c-MET degrading antibody LY2875358 (Liu *et al.*, 2014) target an overlapping epitope on the c-MET SEMA domain, this potential mode of action was further analyzed by MSD assays. For this, the incubation time was increased from 4 h to 18 h as well as the antibody concentration was elevated up to 1 μM. To this end, B10v5x225-H resulted in similar c-MET degradation compared to LY2875358 at 100 nM and 1 μM after overnight treatment in c-MET amplified MKN45 cells up to 50%, (**Figure 24B**) in comparison to background degradation by a non-related isotype control antibody, anti-HEL, of 13%.

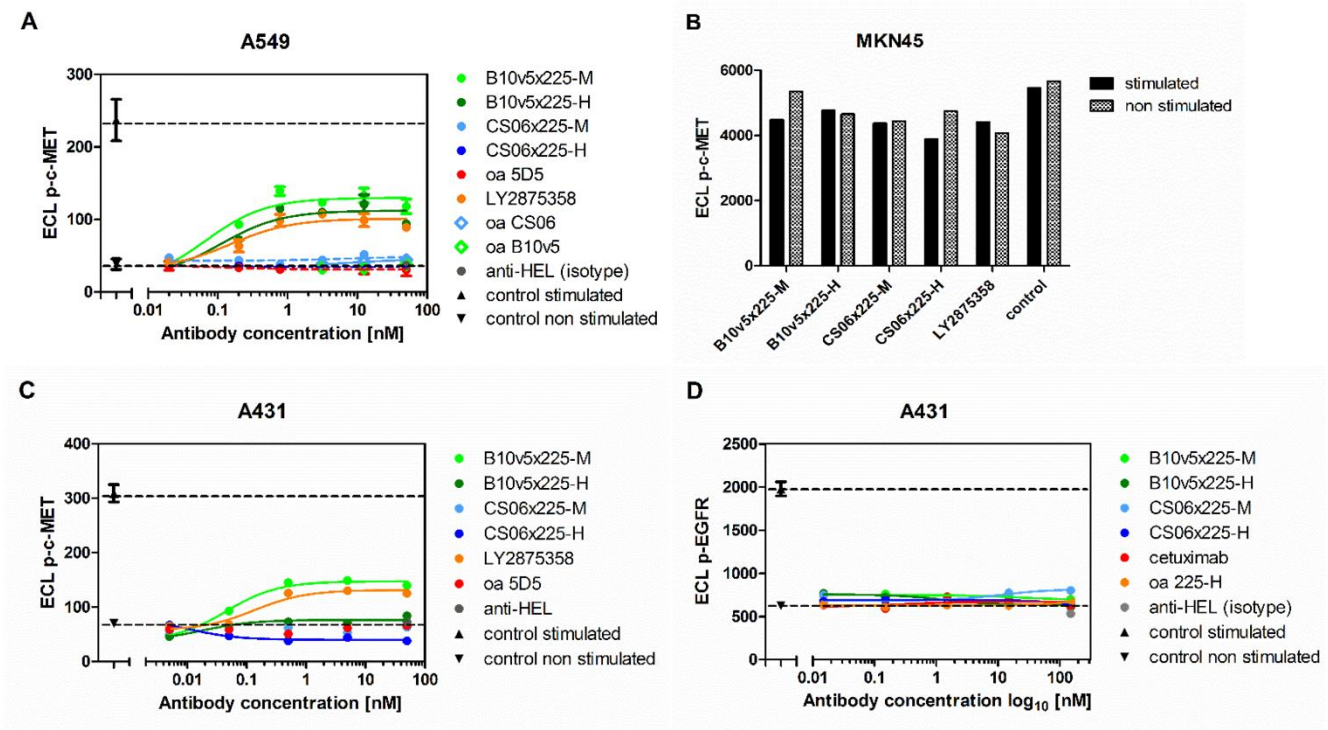

Figure 25: Analysis of potential c-MET agonism of bsAbs.

(A) A549 cells were incubated with varying concentrations of mAbs without stimulation with HGF or EGF and cell lysates were analyzed by MSD-assay for phosphorylated c-MET. B10v5 containing bsAbs displayed similar partial agonism compared to LY2875358. Non-stimulated and HGF-stimulated A549 cells served as controls. **(B)** MKN45 cells were treated with 100 nM mAbs for 1 h and were either stimulated with 100 ng/ml HGF or remained unstimulated. Cell lysates were again subjected to MSD-assay to quantify phosphorylated c-MET. There was no significant difference between stimulated or non-stimulated samples. **(C)+(D)** A431 cells were treated with varying concentrations of mAbs for 1 h and cell lysates were analyzed for phosphorylated c-MET **(C)** or phosphorylated EGFR **(D)** by MSD-assay without respective ligand stimulation.

Next, potential agonism of bsAbs was further analyzed in comparison to reproduced LY2875358 in a concentration dependent manner employing different cell lines. Due to close spatial proximity and interaction of c-MET and EGFR, which has already been demonstrated by co-immunoprecipitation (Jo *et al.*, 2000), bsAbs directed against c-MET and EGFR could theoretically induce agonistic receptor activation by heterodimerization. As depicted in **Figure 25A**, A549 cells incubated with LY2875358, B10v5x225-H and B10v5x225-M without HGF stimulation displayed an increase of c-MET phosphorylation by 35-48%. A549 cells stimulated with 100 ng/ml HGF thereby served as 100% control. In contrast, monovalent oa B10v5 did not increase c-MET phosphorylation. While no agonistic behavior was detectable in c-MET amplified MKN45 cells (**Figure 25B**), B10v5 containing bsAbs and LY2875358 displayed comparable agonistic behavior in A431 cells (**Figure 25C**) to A549 cells. However, none of the tested bsAbs activated EGFR in an agonistic manner (**Figure 25D**). Additionally, the capability of bsAbs to induce ADCC was confirmed (cf. Appendix, **Figure 40**).

5.4.7. Selectivity

Basal EGFR expression in normal tissue, in particular in keratinocytes, can give rise to off-tumor toxicities via inhibition of EGFR signaling by antagonistic mAbs, e.g. cetuximab. (Lacouture, 2006; Melosky *et al.*, 2009) This in turn can lead to severe clinical adverse events during anti-EGFR therapy and negatively influences patient's compliance. To evaluate the impact of affinity variants in the bispecific format on tumor selectivity in comparison to cetuximab, a cell mixing experiment was conducted via flow cytometry based on results presented by Robinson and co-workers (Robinson *et al.*, 2008). For this, a tumor model cell population with high c-MET and EGFR surface expression, e.g. EBC-1 cells, was stained with a green fluorescent membrane dye and mixed in a ratio 1:30 with a non-stained, normal tissue model cell population displaying basal EGFR expressing and being devoid of c-MET expression, e.g. T47D cells (chapter 5.1, **Table 2**). The membrane dye served thereby for distinction of the two cell populations during flow cytometry and the cell mixing ratio of 1:30 was selected based on data presented by Robinson and co-workers (Robinson *et al.*, 2008). Subsequently, the cell mixture was incubated with 3 or 30 nM mAbs and antibody binding was revealed with anti-human Fc PE-conjugates. For quantification, the *in vitro* selectivity was defined as the ratio of tumor to normal tissue model cellular binding, e.g. MFI of EBC-1 cells divided by MFI of T47D cells. Taken together, all bsAbs displayed higher selectivity compared to cetuximab (**Figure 26A**). Representative dot plots for green versus yellow relative fluorescence intensities are depicted in **Figure 26B**. In the upper quadrants represent mAb binding to EBC-1. While control cells only labeled with detection antibody displayed background fluorescence, there is a shift in fluorescence for cetuximab incubated EBC-1 cells. BsAbs thereby bound stronger to EBC-1 cells compared to cetuximab. The lower quadrants contain the unstained T47D cell population. Again, there is only background fluorescence for control cells. The low affinity variants B10v5x225-L and CS06x225-L displayed less binding to T47D cells compared to cetuximab and the high affinity hu225 variants in the bispecific format.

Based on the calculated selectivity as the ratio of MFIs for binding to EBC-1 versus binding to T47D cells, B10v5x225-L displayed a 23-fold and B10v5x225-M still a 5-fold increased selectivity compared to cetuximab (cf. **Figure 26A**). BsAbs with CS06 as anti-c-MET binder even further increased the tumor selectivity. Selectivity measured in this way was proportional to higher off rates or lower affinities of the EGFR binding moiety. The selectivity assay was conducted also for other cell line combinations (cf. Appendix, **Table 13**). Similar results were obtained for MKN45 and A431 cells when mixed with T47D cells. When HepG2 with low EGFR expression and slightly higher c-MET expression were used as normal tissue model cell line, bsAbs displayed still 2-fold higher selectivity to EBC-1 cells. However, the cell combination consisting of the EGFR overexpressing cell line A431 and HepG2 cells, cetuximab displayed higher selectivity compared to bsAbs due to the slightly higher c-MET expression in HepG2 cells.

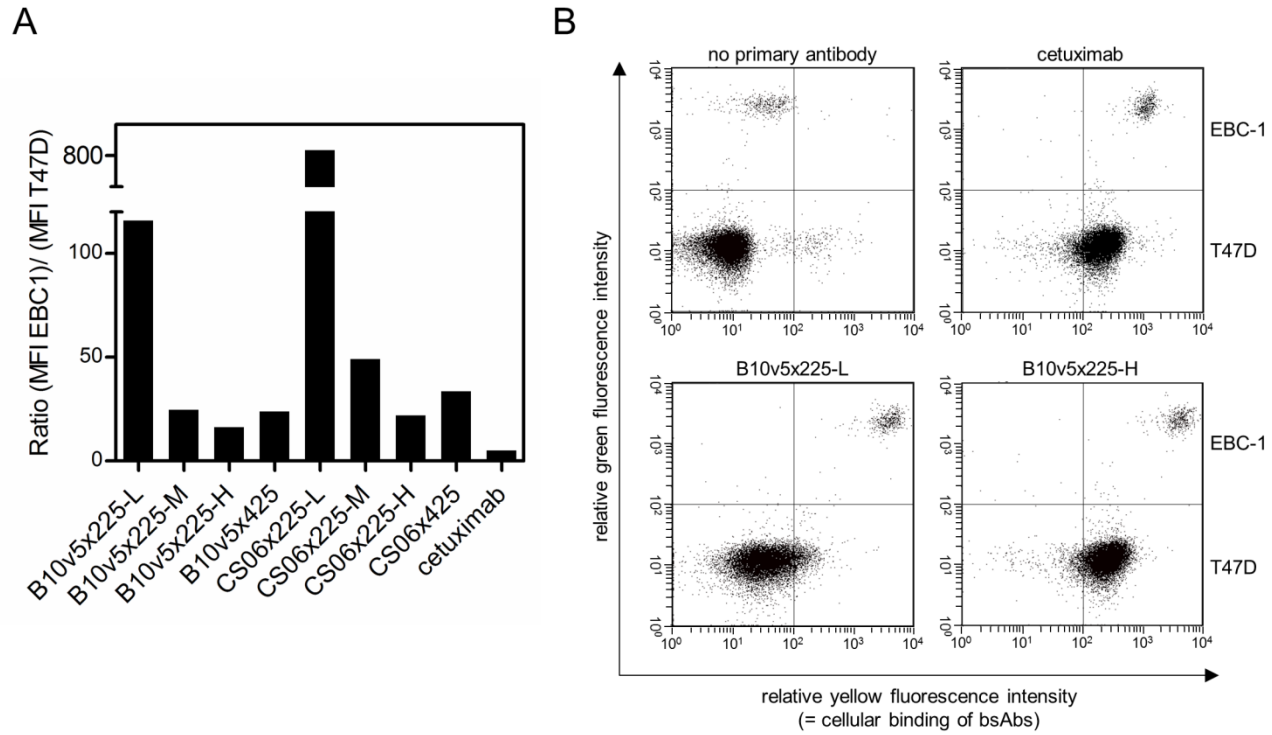

Figure 26: *In vitro* selectivity of bsAbs in comparison to cetuximab.
EBC-1 cells served as tumor model cell line with high to moderate expression in c-MET and EGFR while T47D cells were used as normal tissue model mimicking basal EGFR expression and no c-MET expression in normal tissue. In order to distinguish both cell populations during the mixing experiment, EBC-1 cells were stained with a green fluorescent membrane dye, while T47D cells remained unstained. Cells were mixed in a ratio of 1:30 for tumor to normal model cells and subsequently incubated with 30 nM mAbs. Antibody binding was revealed with anti-human Fc PE-conjugates and detection was carried out via flow cytometry. For each cell population, MFIs were calculated and the ratio of the MFI of EBC-1 cells and the one of T47D was defined as *in vitro* selectivity **(A)**. As a result, the lower the affinity of the EGFR binder, the higher the selectivity towards the tumor model cell line. Representative dot plots with green vs. yellow relative fluorescence intensity are depicted in **(B)**.

In summary, c-MET x EGFR bsAbs displayed higher selectivity towards tumor model cells in comparison to cetuximab when the normal model cell line displays basal EGFR expression and is negative for c-MET expression. The selectivity was thereby dependent on the affinity of the EGFR binding moiety.

5.4.8. Internalization

Cetuximab is known to induce EGFR internalization either by clathrin-dependent or independent mechanisms. (Gostring *et al.*, 2010; Prewett *et al*, 1996) In general, ligand binding to EGFR, e.g. by EGF, induces vesicle budding from the surface and transport to endosomes from where the receptor becomes recycled back to the surface or alternatively becomes processed in late endosomes or multivesicular bodies and finally degraded in lysosomes. (Gostring *et al.*, 2010) For the c-MET targeting antibody LY2875358, receptor degradation is described via internalization. (Liu *et al.*, 2014)

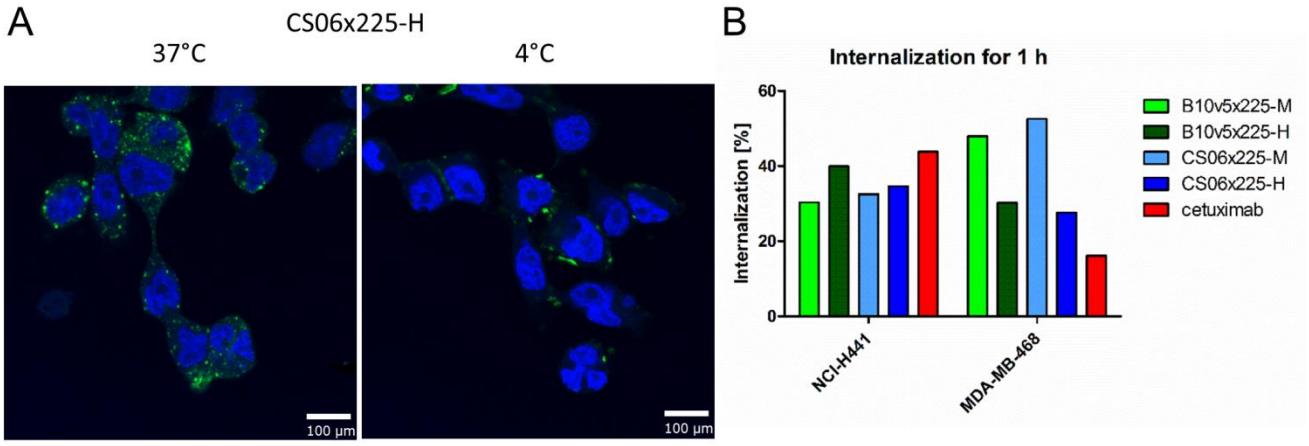

Figure 27: Internalization of bsAbs measured by confocal microscopy (A) and flow cytometry (B).

(A) For confocal microscopy, EBC-1 cells were plated on cover slides and incubated with 100 nM CS06x225-H and subsequently with anti-human Fc-AlexaFluor488 conjugate (green). This was followed by 1 h in cell specific medium at 37°C allowing internalization or at 4°C preventing internalization. Residual surface staining was removed by acidic washing. Detection was carried out by confocal microscopy. Cell nuclei were stained with DAPI (blue). Cells incubated at 37°C clearly indicated internalized antibody in vesicles. Scale bar = 100 μm. **(B)** Flow cytometric analysis of internalization was carried out by incubation of cells (NCI-H441 and MDA-MB-468) with 100 nM antibodies followed by addition of secondary antibody fragment anti-human Fc AlexaFluor488 conjugate. Afterwards, cells were either incubation for 1 h at 37°C allowing internalization or at 4°C preventing internalization. Residual surface binding was quenched with an antibody directed against AlexaFluor488. Internalization in percent was calculated as described in chapter 4.4.3 by comparing MFI of cells incubated at 37°C and those at 4°C. Non-quenched cells served thereby as control for total fluorescence. For instance, bsAbs displayed similar internalization as cetuximab (red).

A qualitative proof of internalization was evaluated for all bsAbs. Employing confocal microscopy and pH stripping of cell surface bound bsAbs, internalization of fluorescently labelled CS06x225-H as a representative could be detected in EBC-1 cells at 37°C whereas no internalization was observable at 4°C (**Figure 27A**). As an alternative, a flow cytometric assay was conducted applying an anti-Alexa 488 quenching antibody for elimination of residual surface staining of non-internalized antibodies. (Gostring *et al.*, 2010) Representative data for bsAbs incubated at either 4°C or 37°C with and without quenching antibody on NCI-H441 cells were depicted in the Appendix (**Figure 41**). The percent internalization was calculated by the difference of quenched samples at 37°C and 4°C and normalized by unquenched samples as indicated by the formula listed in chapter 4.4.3. The results for NCI-H441 and MDA-MB-468 are presented in **Figure 27B** and qualitatively confirmed the bsAbs' ability to induce internalization.

5.5. Characterization of bispecific antibody-drug conjugates (ADCs)

Given the confirmed improved tumor selectivity by affinity attenuated variants in the bispecific format and the capability to induce strong internalization, the herein presented bsAbs fulfill the prerequisites for the potential application as ADCs targeting two ubiquitously expressed cancer targets. Via conjugation of a highly cytotoxic agent, the potency of the bispecific targeting could be increased while potentially retaining the tumor selectivity.

5.5.1. ADC generation

For the generation of ADCs, monomethyl auristatin E (MMAE, cf. chapter 2.2.4, **Figure 3C**) was conjugated to a genetically C-terminally introduced recognition sequence LPETGS to both SEED heavy chains (AG and GA) via the sortase A reaction (cf. chapter 3.7) (Dickgiesser *et al.*, 2015) resulting in a drug-to-antibody-ratio (DAR) of 2. An exemplary reaction scheme was depicted in the introduction (cf. chapter 2.2.4, **Figure 3B**). The tubulin polymerization inhibitor MMAE, which is currently evaluated in various clinical studies as ADC payload (Leal *et al*, 2014; Mullard, 2013), has been selected due to its selectivity for fast dividing cells. Thus, a second layer of selectivity was added via the choice of the toxin. The vc-linker can be cleaved by lysosomal proteases (Ritchie *et al.*, 2013) restricting the toxin release to the intracellular compartment. As reference constructs, cetuximab and anti-HEL-IgG were analogously conjugated with GGG-vc-MMAE via sortase A mediated conjugation (cf. chapter 2.2.4 **Figure 3**B; generated ADCs were kindly provided by Merck, Darmstadt, Germany). After conjugation and purification of ADCs, DAR=2 could be confirmed by MALDI-TOF-MS (Matrix-assisted laser desorption/ionization time-of-flight mass spectrometry, kindly provided by Merck, Darmstadt, Germany) of bispecific ADCs in comparison to respective unconjugated bsAb carrying the sortase A recognition site (cf. Appendix, **Figure 42**). The theoretical increase of molecular weight for the linker-toxin conjugation amounts 1133 Da per chain. For both CS06x225-H and B10v5x225-H the molecular weight shift was slightly smaller with 1063 and 922 Da per chain, respectively, confirming the DAR of 2. Furthermore, kinetic characteristics and cellular binding did not alter after C-terminal MMAE-conjugation (data not shown).

5.5.2. Cytotoxicity of bispecific ADCs

In order to functionally evaluate the generated bispecific ADCs, varying concentrations of ADCs were incubated for 72 h on cancer cells with mutual c-MET and EGFR expression, on a hepatocellular carcinoma cell line (HepG2) as liver model as well as on primary keratinocytes (NHEK.f-c., normal human epidermal keratinocytes, chapter 3.1) as a normal skin model cell. This was followed by the determination of cell viability using the ATP-based luminescent assay CellTiter-Glo® (cf. chapter 4.4.6).

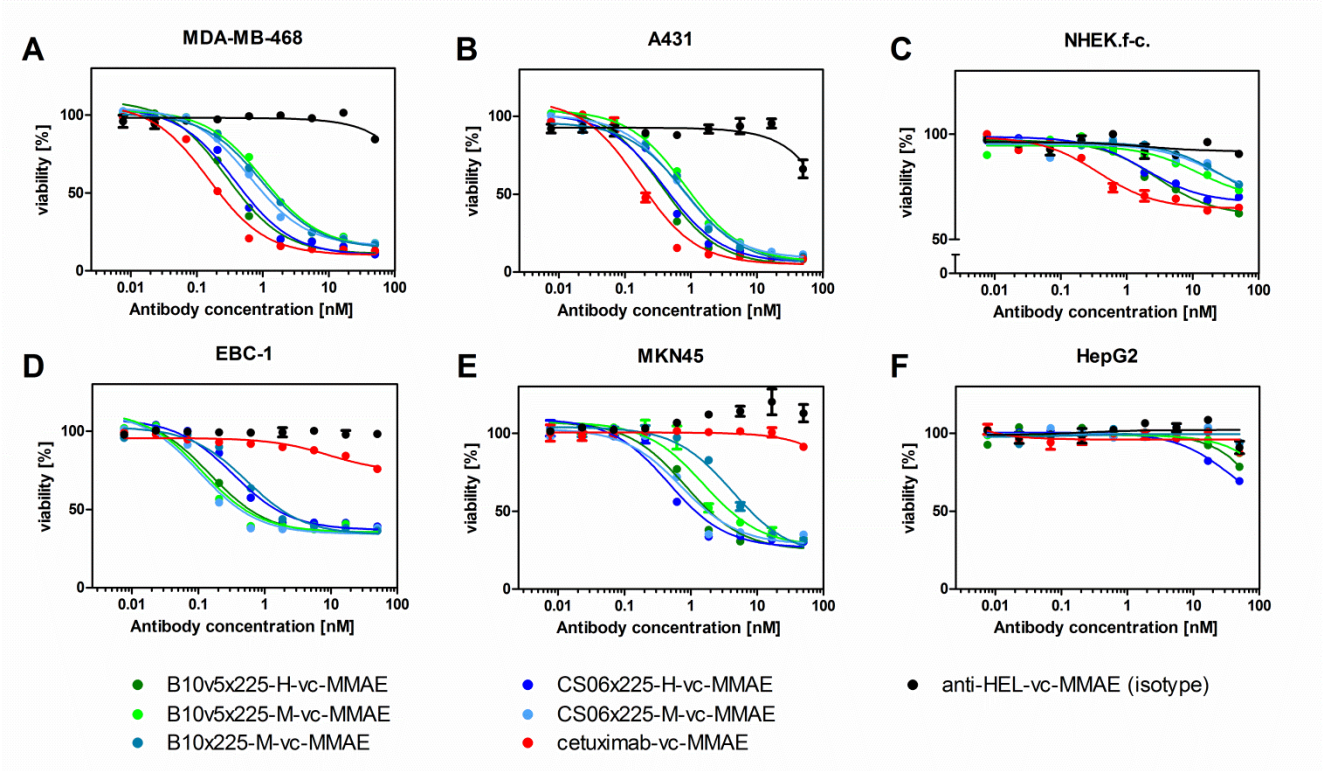

Figure 28: Cytotoxicity of bispecific ADCs on cancer cell lines, liver cells and primary keratinocytes.

Bispecific ADCs generated by enzyme-mediated, site-directed conjugation of vc-MMAE to both heavy chains were incubated on EGFR overexpressing MDA-MB-468 **(A)** and A431 cells **(B)**, on c-MET amplified EBC-1 **(D)** and MKN45 **(E)** cells, primary keratinocytes (NHEK, **C**) as epithelial cell model as well as the hepatocellular carcinoma cell line HepG2 **(F)** as liver cell model for 72 h. Viability of cells was detected with the CellTiter-Glo assay. While on either EGFR or c-MET overexpressing cells, high cytotoxicity could be detected for bispecific ADCs (IC_{50} values in the nanomolar to subnanomolar range), reduced toxicity could be observed in primary keratinocytes. In HepG2 cells, only slight reduced viability could be measured at high ADC concentrations and no IC_{50} values could be calculated. Shown are exemplary graphs from at least three independent experiments.

In EGFR overexpressing MDA-MB-468 and A431 cells (**Figure 28A** and **B**, respectively), bispecific ADCs reduced viability about 80-90% with IC_{50} values in the nanomolar to subnanomolar range comparable to cetuximab-vc-MMAE. In keratinocytes in contrast, cytotoxicity was dependent on the affinity and valence of the anti-EGFR binder with bivalent cetuximab-vc-MMAE having the lowest IC_{50} value followed by B10v5/CS06x225-H-vc-MMAE and then by bispecific ADCs containing the binding moiety 225-M (**Figure 28C**). At the highest ADC concentration, a reduction of cell viability by 30-40% could be observed. In c-MET amplified EBC-1 and MKN45 cells (**Figure 28D** and **E**, respectively), bispecific ADCs demonstrated ~ 60% efficacy, whereas cetuximab-vc-MMAE only slightly reduced cell viability despite confirmed medium EGFR expression in both cell lines (cf. **Table 2**). The low affinity anti-c-MET binder B10 in the bispecific ADC format showed reduced potencies compared to the affinity maturated variants CS06 and B10v5. In another c-MET amplified cell line, HCC-827, however cetuximab-vc-MMAE and bispecific ADCs comparably reduced cell viability (Appendix, **Figure 43C**). In HepG2 cells, no or only low cytotoxic effects could be observed in the evaluated concentration range up to 50 nM ADC (**Figure 28F**). In all tested cell lines, a non-related isotype control ADC, anti-HEL-vc-MMAE, did not indicate a

significant reduction in cell viability. For cells with low to medium c-MET and EGFR expression, e.g. A549, NCI-H1975, NCI-H596 and KP-4 cells (cf. **Table 2**), potency and efficacy in cell killing were similar and both deteriorated in comparison to EGFR and c-MET overexpressing cell lines (cf. Appendix, **Figure 43**). In contrast, bispecific ADCs and cetuximab as ADC did not induce cytotoxicity in NCI-H441 cells (cf. Appendix, **Figure 43F**).

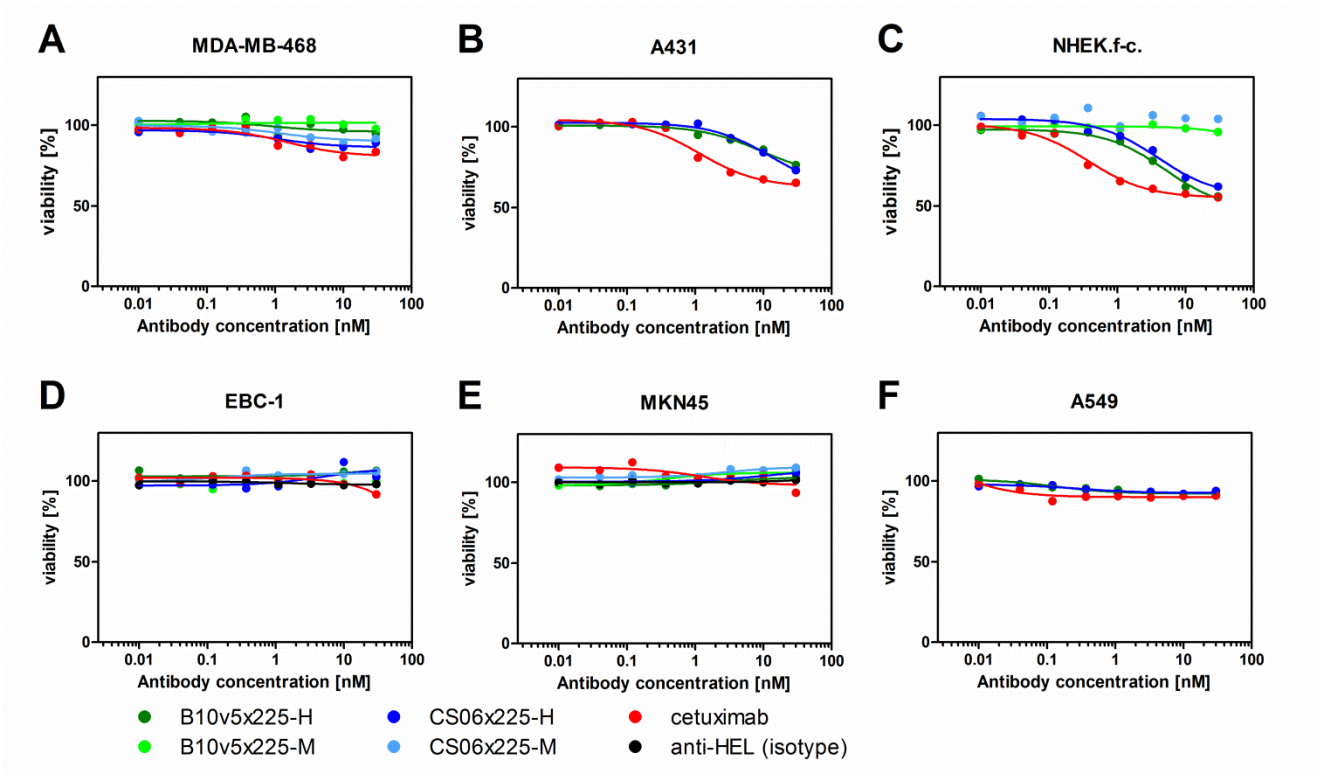

Figure 29: Cytotoxicity of bsAbs and cetuximab on cancer cell lines, liver cells and primary keratinocytes.

BsAbs without conjugated toxin were incubated in varying concentrations on cancer cell lines as well as normal tissue models for 72 h and cell viability was determined with the CellTiter-Glo® assay. Affinity and valence dependent reduction of cell viability could be observed in parts in MDA-MB-468 cells **(A)**, A431 **(B)**, and primary keratinocytes **(C)**. No cytotoxic effects could be detected for c-MET amplified EBC-1 **(D)**, MKN45 **(E)** and A549 cells **(F)**.

To evaluate the influence of the inhibition mode targeting EGFR and c-MET on cell viability, cytotoxicity assays were conducted with unconjugated bsAbs analogously (**Figure 29**). Expression levels of the higher prevalent target, EGFR or c-MET, could thereby be correlated to responsiveness of bispecific ADCs. While viability of high c-MET/EGFR expressing cell lines were potently reduced, lower expression levels led to weaker responses (**Figure 29A**, **B**, and **F**). Potency and efficacy in cell killing of cetuximab and bsAbs were similar in primary keratinocytes when compared to the corresponding ADCs (**Figure 29C** and **28C**). Since the cultured primary keratinocytes displayed slower cell division rates in comparison to the other analyzed cancer cell lines, the incubation time was elongated from 72 h to 6 days. The efficacy in reducing cell viability was thereby increased from 30% to 90% (**Figure 30**), whereas potencies did not significantly alter and were again comparable for ADCs and respective mAbs without

toxin. Once more, efficacies were dependent on the valence and the affinity of the EGFR binder (cetuximab < 225-H < 225-M).

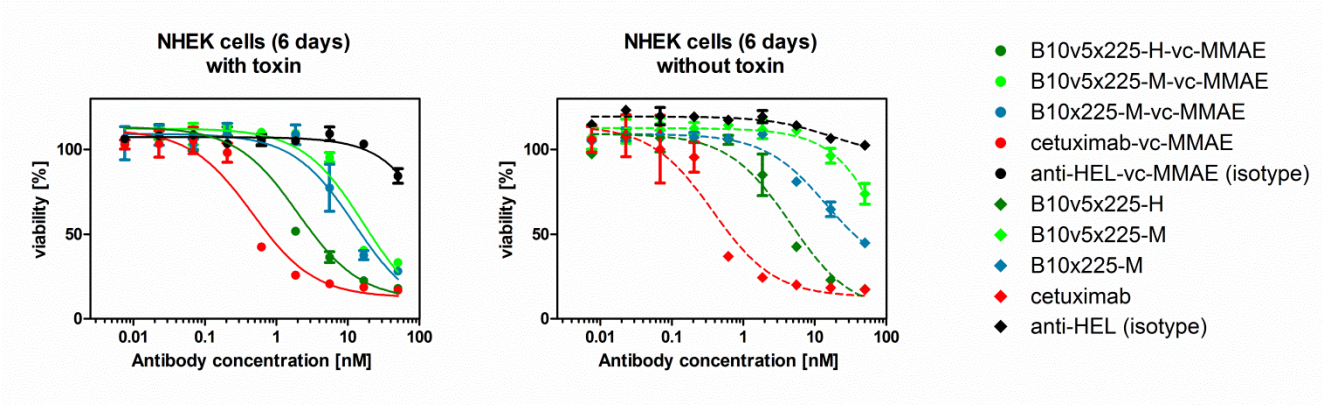

Figure 30: Cytotoxicity of bispecific ADCs and bsAbs without toxin on primary keratinocytes.

Due to the slower cell division rate of primary keratinocytes in comparison to other herein evaluated cancer cell lines, the incubation time of bispecific ADCs (left) or bsAbs (right) was increased to six days before determining the cell viability. As a result, the efficacy for cell killing was increased in comparison to 72 h incubation, whereas the potency did not change significantly. IC_{50} values were dependent on the valence and affinity of the anti-EGFR binding moiety.

Taken together, bispecific c-MET x EGFR ADCs displayed comparable efficacies in EGFR overexpressing cell lines, superior potencies in c-MET amplified cell lines and reduced cytotoxicity in primary keratinocytes as normal tissue model in comparison to cetuximab-vc-MMAE while no strong cytotoxic effects were observable in the hepatocellular carcinoma cell line HepG2 cells as a liver cell model.

5.5.3. *In vitro* therapeutic index

ADCs in general hold the potential to broaden the therapeutic window due to selective delivery of the cytotoxic compound to the tumor. (Muller & Milton, 2012; Panowski *et al.*, 2014) Comparison of increased or similar potency in tumor cells and reduced toxicity in keratinocytes indicated a potentially broadened translational *in vitro* therapeutic window. To visualize and quantify a translational *in vitro* therapeutic index, graphs representing the six above analyzed cell lines for each molecule (**Figure 31**), comparison of calculated EC_{50} and IC_{50} values were conducted and minimum effective doses (MED, ED_{80}) as well as maximum tolerated doses (MTD, TD_{20}) values were determined on the bases of *in vitro* results presented within this study. Visual evaluation of **Figure 31** indicated that the potency of bispecific ADCS was slightly reduced in comparison to cetuximab-vc-MMAE whereas both the potency and the efficacy were reduced by bispecific ADCs in comparison to cetuximab-ADC in primary keratinocytes. As a next step, quantification of a translational *in vitro* therapeutic index was envisioned. However, definitions and analysis of an *in vitro* therapeutic index can be rarely found in the literature because for most developed drugs *in vivo* studies have been conducted. Nevertheless, early safety assessment in the early drug development process is critical and animal experiments should be minimized due to ethical issues,

in particular when the targeting of tumor associated antigens with basal expression in normal tissue is aimed with an ADC approach. Usually either the difference or the ratio in dose-response curves was accounted for the calculation of the therapeutic window. (Muller & Milton, 2012; Panowski *et al.*, 2014) Within this, either the half maximal inhibitory/effective concentrations in keratinocytes/cancer cells were applied or the maximal toxic dose (MTD) with the minimal effective dose (MED). For the latter we used TD_{20} and ED_{80} instead of the usually found TD_{10} and ED_{90} in literature because ADCs maximal resulted in around 90% cell killing in A431 and around 30-40% in keratinocytes (**Table 11**).

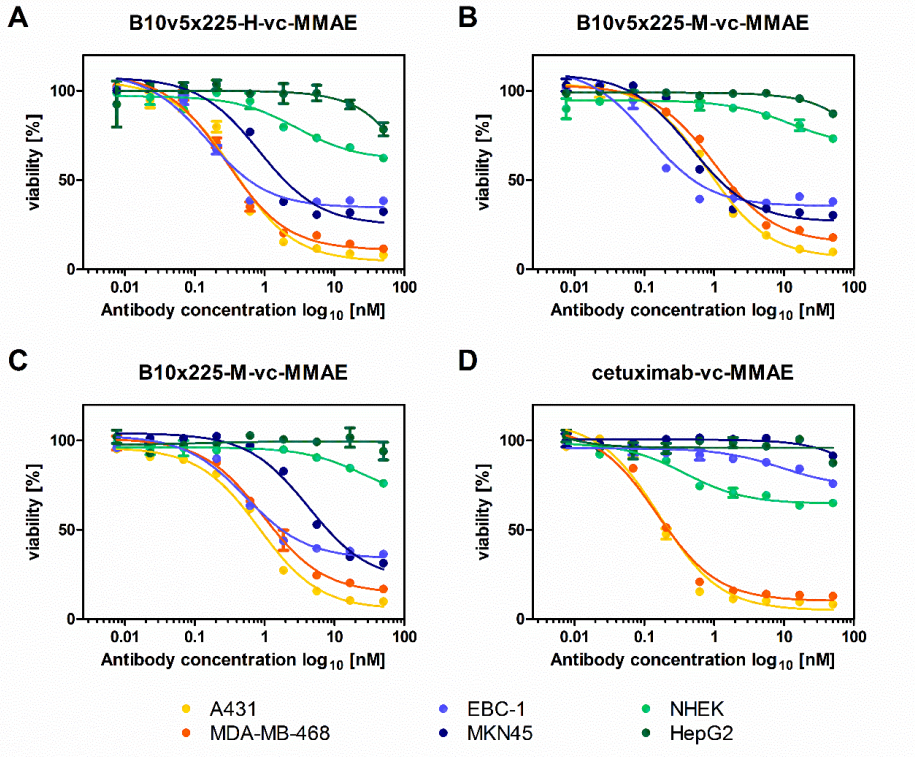

Figure 31: Cytotoxicities grouped by ADC.

Based on data presented in **Figure 28**, cell viability of the four ADCs based on the bsAbs B10v5x225-H **(A)**, B10v5x225-M **(B)** and B10x225-M **(C)** as well as the mAb cetuximab **(D)** was plotted against the logarithm of ADC concentration for two EGFR overexpressing cell lines (A431, MDA-MB-468), two c-MET amplified cell lines (EBC-1, MKN45) and two normal tissue model cell lines (NHEK, HepG2). While in EGFR-overexpressing cells bispecific ADCs displayed similar potency when compared to cetuximab-vc-MMAE, bispecific ADCs had reduced toxicity in primary keratinocytes (NHEK.f-c.) dependent on the affinity of the EGFR binding moiety.

In summary, the following two equations were used to calculate the therapeutic index (**Equation 1** and **2**) and results were summarized in **Table 11**. Since for keratinocytes (NHEK.f-c.), the bispecific ADCs B10v5x225-M-vc-MMAE and B10x225-M-vc-MMAE (with medium affinity 225-M variant) did not reach a plateau at high ADC concentrations, the IC_{50} calculations for those two molecules were assumed to be a raw estimate only. Note, that **equation 1** resulted in a stricter therapeutic window in comparison to **equation 2**.

Equation 1:

$$therapeutic\ index\ (1) = \frac{TD_{20}}{ED_{80}}$$

TD_{20}: toxic dose in keratinocytes (NHEK.f-c.) resulting in 20% reduced viability

ED_{80}: effective dose in cancer cells, e.g. A431, resulting in 80% reduced viability

Equation 2:

$$therapeutic\ index\ (2) = IC_{50} - EC_{50}$$

IC_{50}: half maximal inhibitory concentration in keratinocytes (NHEK.f-c.)

EC_{50}: half maximal effective concentration in cancer cells, e.g. A431

Table 11: Calculation of *in vitro* therapeutic window.

Based on data presented in **Figure 28**, the effective dose resulting 80% cell killing (ED_{80}) and the half maximal effective concentration (EC_{50}) were calculated for the cancer cell line A431. For normal tissue model, the primary keratinocytes (NHEK.f-c.), the toxic dose resulting in 20% cell killing (TD_{20}) and the half maximal inhibitory concentration (IC_{50}) were determined. Additionally, for both cell lines the percent cell killing at 50 nM ADC were listed. The number of independent experiments with duplicates was also indicated (*n*). Based on the **equations 1** and **2**, two translational *in vitro* therapeutic indices were calculated. As a result, the therapeutic window was increased by B10v5x225-M-vc-MMAE in comparison to cetuximab-vc-MMAE by the factor 5-6 or alternatively by 18-28, respectively. Asterisks (*) indicated estimated values as sigmoidal curves did not reached a plateau at high concentrations.

Antibody	A431				NHEK.f-c.				Therapeutic window	
	ED_{80} [nM]	EC_{50} [nM]	% cell killing at 50 nM	*n*	TD_{20} [nM]	IC_{50} [nM]	% cell killing at 50 nM	*n*	TD_{20}/ ED_{80}	IC_{50}-EC_{50} [nM]
B10v5x225-H-vc-MMAE	2.1 ± 0.7	0.4 ± 0.1	93 ± 1.3	5	3.7 ± 1.1	5.9 ± 2.9	37 ± 12	5	2	5.6
B10v5x225-M-vc-MMAE	4.4 ± 1.0	1.0 ± 0.3	91 ± 0.4	3	25 ± 8	>19*	30 ± 9	3	6	>28*
B10x225-M-vc-MMAE	3.6 ± 0.9	0.7 ± 0.2	90 ± 0.5	3	19 ± 8	>20*	27 ± 11	3	5	>19*
cetuximab-vc-MMAE	0.7 ± 0.3	0.1 ± 0.04	92 ± 1.4	5	0.8 ± 0.5	1.0 ± 0.5	34 ± 10	5	1	0.9

Taken together, bispecificity and in consequence monovalency of the EGFR binding moiety in B10v5x225-H-vc-MMAE resulted in a two-fold increased therapeutic index in comparison to cetuximab-vc-MMAE based on **equation 1** or an at least six-fold increase from 0.9 nM to 5.6 nM according to **equation 2**. For bispecific ADCs composed of the medium affinity 255-M variant, only **equation 2** yielded in reliable results since sigmoidal response curves for NHEKs did not reach a plateau at higher concentrations and in consequence the calculation of IC_{50} values was inaccurate. Both B10v5x225-M and B10x225-M as an ADC conjugated with vc-MMAE increased the translational *in vitro* therapeutic window by the factor five to six.

6. Discussion

6.1. EGFR and c-MET as cancer targets

The involvement of EGFR and c-MET in the development and progression of cancer has been independently identified in the 1980s (Cooper *et al.*, 1984; Downward *et al.*, 1984) and both are associated with tumor aggressiveness and unfavorable survival outcomes. (Nicholson *et al.*, 2001; Sierra & Tsao, 2011) (Nicholson *et al.*, 2001; Sierra & Tsao, 2011) In the present study, the mutual overexpression of both RTKs has been confirmed in several cancer cell lines derived from different indications via quantification of cellular receptor surface levels (cf. **Table 2**). This included confirmation of high EGFR expression in A431 and MDA-MB-468 cells as well as elevated c-MET surface expression levels in c-MET amplified MKN45 and EBC-1 cells. Dual expression and redundant signaling of c-MET and EGFR via MAPK and AKT pathways have been described (Guo *et al.*, 2008) leading to the propagation of pro-survival signals. Despite initial clinical successes, receptor interaction and crosstalk (Engelman *et al.*, 2007; Jo *et al.*, 2000) led therefore to the emergence of acquired resistance rendering monotherapies ineffective. One major resistance mechanism during EGFR inhibition by gefitinib involves the amplification of c-MET via activation of ErbB3 signaling. (Bean *et al.*, 2007; Engelman *et al.*, 2007) As a consequence, several combinatory treatment approaches are currently under clinical investigation including the dual application of anti-c-MET and anti-EGFR small molecule inhibitors and/or antibodies. (Prat *et al.*, 2014; Sharma & Adjei, 2011; Sierra & Tsao, 2011; Yewale *et al.*, 2013) Another factor influencing the efficacy of anti-c-MET antibodies are high HGF levels in the tumor microenvironment which can also counteract the efficacy of EGFR inhibition. (Straussman *et al.*, 2012; Wang *et al.*, 2009) Considering the interaction of both receptors, bispecific targeting of c-MET and EGFR could lead to synergistic effects and counteract c-MET mediated resistance mechanisms. Several pharmaceutical companies invested in the development of bsAbs directed against c-MET and EGFR and in parts entered clinical investigation. (Castoldi *et al.*, 2012; Castoldi *et al.*, 2013; Garber, 2014; Jarantow *et al.*, 2015; Lee *et al.*, 2016a; Lee *et al.*, 2016b; Lewis *et al.*, 2014; Spiess *et al.*, 2013) However, clinical findings underscore the importance of tumor-selective targeting as inhibition of basally expressed EGFR in normal tissue can lead to severe skin toxicities negatively influencing patient compliance. (Lacouture, 2006; Melosky *et al.*, 2009) Especially in combinatory treatment approaches, there is the risk of additive side effects for the combination of multiple single agents. Consequently, the right balance between high anti-tumor efficacy and high tumor selectivity plays a pivotal role for a cancer drug's safety profile. The combination of bsAbs with affinity-optimized binding moieties hold the potential to increase the selectivity to mutual overexpressing tumor cells via avidity while concurrently reducing binding to normal tissue. (Mazor *et al.*, 2015b; Robinson *et al.*, 2008) Thus, bsAbs with engineered affinities could

demonstrate high therapeutic benefit via dual inhibition of both RTKs on tumor cells which could also play a pivotal role in counteracting c-MET driven resistance mechanisms during anti-EGFR monotherapy.

6.2. Characterization of single antibody binding moieties

One part of this study comprised the generation of a broad panel of anti-c-MET variants with different affinities to their target by Fab-phage display and comprehensive functional characterization before the evaluation in the bispecific format. Randomization of the variable domain of the heavy chain resulted in increased affinity to soluble c-MET ECD with K_D-values in the subnanomolar range in comparison to double digit affinity of the parental binder (cf. **Figure 8** and **9**). Epitope binning experiments revealed that affinity maturation of parental anti-c-MET binder F06 and B10 to CS06 and B10v5, respectively, did not alter the epitope or target specificity (cf. **Figure 11** and **Table 3**). This experiment also indicated overlapping epitopes of B10/B10v5 with LY2875358 (Liu *et al.*, 2014) on SEMA blade 2/3 and of F06/CS06 with h224G11 (Goetsch *et al.*, 2010; Wang *et al*, 2016) within the IPT1 domain of the c-MET stalk. (Basilico *et al.*, 2014; Prat *et al.*, 2014) As assumed, the presence of the SNP N375S within the SEMA-β-chain did not influence binding of anti-c-MET antibodies to soluble mutated c-MET (cf. **Figure 12**). Thus, this SNP variant did not constrain possible patient stratification strategy. Moreover, all evaluated anti-c-MET binders displayed competition with HGF binding to c-MET ECD (cf. **Figure 10**). Whether the displacement of HGF is based on direct competition of the HGF binding sites or mediated by sterical hindrance needs further analysis of their molecular features. Based on the literature, the low affinity binding site of HGF is located within the SEMA domain. The location of the high affinity binding epitope is controversially discussed: Basilico and colleagues hypothesizes binding to the IPT region (Basilico *et al.*, 2008), while others assumed binding within the SEMA domain (Gherardi *et al.*, 2003; Stamos *et al.*, 2004). As a consequence, F06/CS06 either directly or sterically impair binding of HGF to c-MET ECD.

It could be hypothesized that similar epitopes could correlate with comparable functionality and mode of action highlighting the importance of epitope binning studies. Pharmaceutical relevant characteristics of anti-c-MET binders include the ability to compete with HGF binding, murine cross-reactivity, agonism in the bivalent format as well as the mediation of receptor degradation. Both B10 and LY2875358 displayed cross-reactivity to murine c-MET (Liu *et al.*, 2014) whereas both F06 and h224G11 did not (Goetsch *et al.*, 2010; Wang *et al.*, 2016) (personal communication Merck, Darmstadt, Germany). Furthermore, B10v5 demonstrated partial agonistic activation of c-MET in the bispecific format in absecence of ligand stimulation comparable to LY2875358 (cf. **Figure 25**) in contrast to CS06 as bsAb and bivalent h224G11 (Goetsch *et al.*, 2010; Wang *et al.*, 2016). These results corroborate the notion that B10v5 and LY2875358 might have the same mode of action via the induction of receptor

degradation. Indeed, B10v5x225-H demonstrated c-MET degradation similarily to LY2875358 in the c-MET amplified cell line MKN45 (cf. **Figure 24B**). For c-MET monotherapy approaches, biparatopic approaches combining binders targeting distinct epitopes on the same target could also be considered in order to improve the efficacy of c-MET inhibition. This was elegantly evaluated by Basilico and co-workers for combination of anti-SEMA binders with anti-IPT binders. (Basilico *et al.*, 2014) However, the presented study focused on the evaluation and characterization of bsAbs directed against c-MET and EGFR. Thus, further analysis of monospecific and biparatopic anti-c-MET targeting approaches was not in the scope of this work.

6.3. Manufacturability of bispecific c-MET x EGFR antibodies

All evaluated bsAbs displayed suitable manufacturability (cf. **Table 5** and **6**) comparable to results presented by Muda *et al*. and Davis *et al.* fulfilling the requirements for therapeutic application. (Davis *et al.*, 2010; Muda *et al.*, 2011) Over >95% purity of correctly assembled bispecific heterodimer was achieved after preparative SEC purification for all four final bispecific constructs chosen for further evaluation (B10v5x225-M and -H as well as CS06x225-M and –H, cf. **Table 6**). In order to ensure cognate light chain pairing, the anti-EGFR binder was designed as scFv fragment. Some technologies for correct light chain pairing, e.g. common light or heavy chain (Fischer *et al.*, 2015), Fab-interface engineering (Lewis *et al.*, 2014), and the CrossMab technology (Schaefer *et al.*, 2011b) may not be generically applicable to already existing binders or might be associated with extensive engineering efforts. Given the link of structure-function knowledge of c-MET and EGFR interaction and the complexity of this signaling system, an empirical approach combining several epitopes and off-rates was chosen over *in silico* predictions to develop an optimized c-MET x EGFR targeting bsAb. For this, the use of the herein presented modular toolbox approach employing scFv technology together with the SEED-technology enabled facile screening of multiple binder combination expressed in the bispecific format. However, the use of scFv fragments can be associated with instability in comparison to Fab antibody fragments (Kramer *et al*, 2002) and may also require additional stability enhancing engineering (Lee *et al.*, 2016b). The presented data indicated that kinetic features of binding moieties did not alter for mono- to bispecific formats as illustrated in **Figure 16**. High thermal stabilities, with melting temperatures of 62-68°C and long-term stability at elevated temperatures in human and mouse serum (cf. **Table 8** and **Figure 18**) assessed via dual target engagement ELISA, indicated suitable physicochemical properties for the developability of the presented bsAbs.

One essential feature of bsAbs is the ability to simultaneously engage two antigens. Using BLI, association of all evaluated bsAbs to immobilized c-MET and subsequent binding of EGFR could be observed indicating that cooperative binding of both soluble antigens is sterically feasible. The reach of antibody

binding arms to membrane anchored target is geometrically restricted with ~9 nm (Sengers *et al*, 2016) and thus constrained on close proximity and lateral diffusion of antigens within the membrane. As described earlier, interaction of c-MET and EGFR on the cellular surface has been proposed so that the antibody binding arm range should be sufficient for those two target antigens. Next, binding of bsAbs was evaluated to cell lines with different receptor surface expression levels of c-MET and EGFR (cf. **Figure 19** and **Table 9**). As a result, binding strength correlated with expression levels of the more abundant target as recently reported. (Jarantow *et al.*, 2015) For monovalent reference binders, binding strength was proportional to the affinity. Furthermore, no unspecific binding was observed for monospecific control binders for either EGFR negative or c-MET negative cell lines, e.g. SK-MEL2 and T47D, respectively, proposing target-specific antigen recognition on cells. Binding of B10/v5 to rodent CHO cells could be ascribed to cross-reactivity to murine c-MET (personal communication, Merck, Darmstadt, Germany). In case of similar c-MET and EGFR surface expression levels, e.g. NCI-H441 cells (cf. **Figure 20**), increased binding of bsAbs could be detected in comparison to monospecific one-armed mAbs presumably indicating simultaneous engagement of both antigens on cellular surface.

Thus, a proof of concept was demonstrated for the concept of highly specific and simultaneous target binding dependent on affinities and cellular receptor levels of c-MET and EGFR as envisioned by the introduced design. Differential binding pattern of bsAbs on double overexpressing cell lines in comparison to monovalent mAbs or low expressing cells thereby proposed potential for improved tumor specificity by bsAbs carrying affinity-optimized binding moieties.

6.4. Bispecific c-MET x EGFR mAbs with increased tumor selectivity and high efficacy

After confirming the affinity and receptor density dependent cellular binding of bsAbs, functional behavior was comprehensively analyzed. While anti-EGFR mAbs mainly act via ligand competition, the mode of action of anti c-MET mAbs can be either described by direct or indirect HGF competition or by the induction of receptor degradation. While onartuzumab (oa 5D5) and hu224G11 act via competition of HGF (Merchant *et al.*, 2013; Wang *et al.*, 2016), others, e.g. LY2875358 (emibetuzumab), SAIT301 and DN30 (Liu *et al.*, 2014; Oh *et al.*, 2012; Pacchiana *et al.*, 2010), induce c-MET degradation. Interestingly, receptor degradation can be achieved by different mechanisms: DN30 binds the juxtamembrane domain and induces receptor shedding via the metalloprotease ADAM. (Pacchiana *et al.*, 2010) SAIT301 in contrast mediates c-MET degradation via LRR and immunoglobulin-like domain-containing protein 1 (LRIG1). (Lee *et al.*, 2014) LY2875358 in turn inhibits both HGF binding and concurrently induces receptor internalization and degradation by an unknown molecular mechanism. (Liu *et al.*, 2014)

Initial Western blot studies presented herein demonstrated inhibition of c-MET phosphorylation by bsAbs carrying high affinity c-MET binding moieties with slightly higher efficiency in HGF dependent cells compared to parental monovalent one-armed SEEDs (cf. **Figure 39**). However, all four herein presented c-MET binders were not able to significantly reduce c-MET phosphorylation levels in constitutively activated, c-MET amplified cell lines in contrast to DN30. Due to distinct epitopes of F06/CS06 and B10/B10v5 and slightly higher efficacy of CS06 and B10v5, only the affinity matured c-MET binders were chosen for further development in the bispecific format. As for blockade of EGFR phosphorylation, 225-H and 225-M displayed superiority over 225-L and 425 (cf. **Figure 39**). Hence, functional analysis was focused on 225-M and 225-H in combination with CS06 and B10v5 as bsAbs to balance anti-tumor efficacy and tumor selectivity.

For quantitative analysis of receptor inhibition during ligand stimulation, ELISA-like MSD assays were conducted. As a result, both B10v5 and CS06 containing bsAb inhibited c-MET phosphorylation with higher potency compared to patent-based reproduced reference antibodies oa 5D5 and LY2875358, with IC_{50} values in the subnanomolar range (cf. **Figure 22**). Moreover, bsAb prevented c-MET activation with higher potency than respective monovalent one-armed anti-c-MET binders indicating a synergistic mode of action regarding c-MET inhibition in the bispecific format (cf. **Figure 24A**). Due to an overlapping epitope of B10v5 with LY2875358 (cf. **Figure 11**), bsAbs were analyzed for potential c-MET degradation during overnight treatment. Interestingly, B10v5x225-H induced c-MET degradation in c-MET amplified cell lines comparable to LY2875358 (cf. **Figure 24B**). Inhibition of EGFR phosphorylation by bsAbs was dependent on the affinity and valence of the EGFR binder (cf. **Figure 23**). Monovalency of the EGFR binding moiety due to the chosen bispecific design resulted in decreased potency of EGFR inactivation in comparison to bivalent cetuximab. However, the evaluated bsAbs also demonstrated increased inhibition of AKT downstream signaling, but not of MAPK phosphorylation, when compared to the combination of monospecific control mAbs (cf. **Figure 21**). Similarly to cetuximab, small molecule inhibitors, e.g. gefitinib, fail to prevent AKT phosphorylation in NSCLC cells. (Guo *et al.*, 2008) This supports the hypothesis that double inhibition of both EGFR and c-MET signaling pathways by bsAbs can lead to efficient inhibition of downstream signaling, at least for AKT. In summary, bsAbs displayed superiority in inhibiting c-MET and AKT phosphorylation, but reduced potency for inhibition of EGFR phosphorylation in comparison to bivalent cetuximab. Potencies for inhibition of receptor phosphorylation thereby did not correlate with target cell densities as it had been reported by Jarantow and co-workers. (Jarantow *et al.*, 2015) Thus, for efficient inhibition of EGFR phosphorylation, bivalent anti-EGFR mAbs might be required.

Some anti-c-MET mAbs are prone to mediate full or partial agonism, probably influenced by the antibody's epitope. (Liu *et al.*, 2014; Merchant *et al.*, 2013) Due to the interaction of c-MET and EGFR (Jo *et al.*, 2000), bsAbs could potentially induce agonism via receptor heterodimerization as well. The presented data indicated that B10v5 containing bsAbs partially activated c-MET phosphorylation in absence of ligand stimulation comparable to reproduced LY2875358 in contrast to monovalent B10v5 or CS06 bsAbs or mAbs (cf. **Figure 25**). Due to the mode of action via c-MET internalization and degradation, LY2875358's functionality presumably outweighs partial agonism, since this molecule is currently evaluated in clinical phase 2. (Liu *et al.*, 2014) The same could be account for B10v5 containing bsAbs. Furthermore, a degradation mode of action is potentially independent of HGF dependence of the cell line and therefore also c-MET amplified cell lines could be targeted. The need for bivalency of the bispecific molecule for improved inhibition of c-MET phosphorylation and the partial agonism by B10v5x225-H indicated receptor interaction and simultaneous engagement of both targets.

After characterizing the cellular functionality of bsAbs, the tumor selective binding was evaluated using a cell mixing experiment composed of a tumor model and an epithelial model cell line via flow cytometry. Skin related adverse events of EGFR inhibitors are probably mediated by EGFR inhibition in keratinocytes and are the main reason for treatment disruption by patients during EGFR therapy. (Lacouture, 2006) All bsAbs demonstrated increased binding to c-MET and EGFR overexpressing tumor model cell line while binding to an epithelial model cell line with basal EGFR expression was equal or even reduced compared to cetuximab. Thus, the selectivity defined as the ratio of tumor to epithelial model cell binding was improved by bispecificity as reported for other target combinations. (Mazor *et al.*, 2015b; Robinson *et al.*, 2008) In the presented study, the use of affinity attenuated EGFR binding moieties greatly improved tumor cell selectivity *in vitro* which could also result in decreased toxicities. Similar concepts have been recently experimentally evaluated for affinity-optimized CD4xCD70 bsAbs by Mazor *et al.* and subsequently mathematically modeled by Sengers *et al.*. (Mazor *et al.*, 2015a; Sengers *et al.*, 2016) In summary, increased tumor selectivity mediated by the application of affinity attenuated anti-EGFR binders can only be achieved at the cost of reduced efficacy for inhibiting EGFR phosphorylation. However, further experiments will be needed to evaluate if monovalency of the EGFR binding moiety in the bispecific format can reduce on-target off-tumor toxicity. Although no correlation between EGFR receptor density and potency of EGFR inhibition could be observed. Surface expression of c-MET and EGFR in normal tissue can be critical for a potential clinical development of such bsAbs since reduced EGFR-mediated toxicity could improve patient compliance. When compared the herein presented design to other bsAbs in clinical development targeting c-MET and EGFR, some approaches exploit tetravalent molecules carrying two EGFR binding moieties which could negatively influence the tumor selectivity in contrast to the presented heterodimeric bsAbs with monovalent EGFR targeting.

Further characterization of bsAbs included the confirmation of internalization and ADCC since both modes of action have been described for cetuximab (Kimura *et al.*, 2007; Mendelsohn & Baselga, 2003) as depicted in **Figure 27** and **Figure 40**. When aiming for applications without toxin conjugation, the induction of ADCC could be beneficial. With improved tumor selectivity and the capability to induce internalization, bsAbs fulfill the pre-requisites for the application as ADC.

6.5. Bispecific c-MET x EGFR ADCs to broaden the therapeutic window

When arming antibodies with cytotoxic agents, a careful *in vitro* evaluation of the molecule's safety profile is required early in the development process. As aforementioned, skin related adverse events are described for EGFR inhibitors due to basal expression in normal tissue. (Lacouture, 2006) As a consequence, more severe toxicities could be expected for EGFR targeting ADCs. The c-MET/HGF axis is involved among others in development and regeneration of the liver. (Birchmeier *et al.*, 2003) Hence, primary keratinocytes and a hepatocellular carcinoma cell line were chosen as a model for *in vitro* safety assessment studies.

In order to circumvent adverse events in normal tissue for their EGFR targeting ADC approach, Phillips and colleagues for example selected an antibody, ABT-806, which recognizes a tumor-specific, misfolded EGFR epitope. (Phillips *et al*, 2016; Reilly *et al*, 2015) The corresponding ADC, ABT-414, displayed high cellular binding to the glioblastoma cell line U87MGde2-7 while binding to wild-type EGFR expressing A431 cells was reduced when compared to cetuximab. (Phillips *et al.*, 2016) This translated into highly potent cytotoxicity in U87MGde2-7 cells whereas IC_{50} values for the reduction of cell viability of wild-type EGFR expressing cells was reduced dependent on receptor surface densities. (Phillips *et al.*, 2016) In the present study, bsAbs targeting c-MET and EGFR displayed greatly increased tumor selectivity when employing affinity attenuated EGFR binding moieties (cf. **Figure 26** and **Figure 28**). In order to achieve a second layer of selectivity for the ADC, the tubulin inhibitor MMAE was selected as payload for specific targeting of fast proliferating cells. Considering ADCs currently in clinical development, auristatins are the most validated payload class. (Leal *et al.*, 2014) Intracellular release of the cytotoxic agents was ensured by the use of the cleavable vc-linker which is processed by cathepsin and plasmin in the lysosome. (Ritchie *et al.*, 2013) Site-specific conjugation of MMAE C-terminally to both heavy chains of the bsAbs was mediated by sortase A. As a result, a homogenous ADC with specific toxin conjugation sites and a DAR of 2 was obtained as confirmed by mass spectrometry (cf. **Figure 42**). While unarmed bsAbs displayed no or only detrimental effects on the cell viability of c-MET or EGFR overexpressing cell lines, the generated bispecific ADCs demonstrated efficient cytotoxicity in the subnanomolar to single digit nanomolar range (cf. **Figure 28** and **31**). As control construct, cetuximab-ADC and an isotype-ADC (anti-HEL) were generated comparably to bispecific ADCs. While the potency for killing EGFR

overexpressing cells was slightly reduced for bispecific c-MET x EGFR ADCS in comparison to cetuximab-ADC, bispecific ADCs demonstrated superiority in c-MET amplified cell lines. Concurrently, bsAbs ADCs demonstrated decreased toxicity in primary keratinocytes dependent on the affinity of the EGFR binding moiety whereas no significant toxicity could be detected in hepatocellular cancer cells within the evaluated concentration range. Interestingly, treatment of keratinocytes with unarmed antibodies revealed similar cytotoxicity compared to respective bispecific ADCs. This suggests that reduction in keratinocytes viability was caused by inherent EGFR inhibition rather than ADC mediated toxin delivery. Since lower replication rates of keratinocytes could lead to less efficacy of the tubulin inhibitor MMAE, the treatment time was increased from initially three days to six days. As a result, the efficacy of cell killing increased from 50% to 80% whereas the potency did not significantly alter (cf. **Figure 30**). Nevertheless, bispecific ADCs and corresponding unarmed bsAbs displayed similar efficacy and potency regarding cytotoxicity in keratinocytes supporting the hypothesis of an antagonistic antibody mode of action rather than ADC mediated cell killing (cf. **Figure 30**). Keratinocyte proliferation is regulated by EGFR signaling and antibody-mediated receptor internalization has been shown to severe inhibition of the EGFR pathway. (Lacouture, 2006; Mendelsohn & Baselga, 2003) Although the definition of therapeutic index is usually based on *in vivo* data (Muller & Milton, 2012; Panowski *et al.*, 2014), the presented *in vitro* cytotoxicity results in EGFR overexpressing cells and primary keratinocytes were used for the calculation of a translational *in vitro* therapeutic index. The data provides the rationale that B10v5x225-M-vc-MMAE and B10x225-M-vc-MMAE broadened the *in vitro* therapeutic window by the factor five to six in comparison to EGFR targeting, bivalent cetuximab-vc-MMAE in cellular cytotoxicity experiments. Further evaluation is needed in order to correlate EGFR and c-MET receptor densities with potency of bispecific ADCs employing the cytotoxic agent MMAE.

The presented study demonstrates that the use of affinity-optimized binders with either desired higher or attenuated affinities in the bispecific format targeting the prominent tumor-associated antigens c-MET and EGFR can improve *in vitro* tumor selectivity while concurrently retaining high efficacy with potential superiority to monospecific ADC approaches. Thus, balancing high selectivity with suitable efficacy could potentially improve the therapeutic index and consequently the safety profile. In particular the reduction of on-target off-tumor toxicities will be a challenge to face since expression of most cancer targets is not restricted to the tumor site and prevention of side effects will positively influence patient compliance and consequently treatment success.

6.6. Outlook

Further studies are needed to confirm that improved *in vitro* selectivity and retained high efficacy can be translated in the highly complex *in vivo* environment both for unarmed bsAbs and bispecific ADCs targeting c-MET and EGFR. Besides the evaluation in selected rodent xenograft models to characterize selectivity and efficacy, also *in silico* modeling approaches could be envisioned. Zheng *et al.* and Sengers *et al.* recently simulated both the cross-arm binding efficiency and the selectivity of bispecific molecules, respectively, based on affinities of the binding moieties. (Sengers *et al.*, 2016; Zheng *et al.*, 2016) However, modeling the efficacy of ADCs becomes even more complex considering affinity dependent binding of ADCs, internalization rates dependent on the target, the antibody's affinity and receptor surface densities as well as intracellular and extracellular toxin release among other factors. Additionally, binder epitopes could potentially influence intracellular trafficking routes. For example binding of the anti-c-MET antibody SAIT301 seems to activate an alternative internalization pathway in comparison to other anti-c-MET antibodies. (Lee *et al.*, 2014)

Considering the multifactorial nature of cancer and the development of intrinsic and acquired resistance, combinatory treatments and targeting of multiple cancer relevant regulators seem to be a viable route for future drug design approaches. Bispecific ADCs could potentially counteract EGFR inhibitor related resistance mechanisms including c-MET amplification (Engelman *et al.*, 2007), ligand upregulation (Straussman *et al.*, 2012; Troiani *et al*, 2013), the presence of EGFR activating mutations in the kinase domain (Martin *et al*, 2016; Tang *et al*, 2008) and the mutation of downstream mediators, e.g. KRAS (Pao *et al*). The work described herein represents an illustrative case study for the design and characterization of bispecific mAbs and ADCs employing affinity-optimized binding moieties for two mutual overexpressed tumor-associated targets for high selectivity as well as high anti-tumor efficacy.

7. References

Anderson, D. R., Grillo-Lopez, A., Varns, C., Chambers, K. S. & Hanna, N. (1997). Targeted anti-cancer therapy using rituximab, a chimaeric anti-CD20 antibody (IDEC-C2B8) in the treatment of non-Hodgkin's B-cell lymphoma. *Biochem.Soc.Trans.* **25**, 705-708.

Balint, R. F. & Larrick, J. W. (1993). Antibody engineering by parsimonious mutagenesis. *Gene* **137**, 109-118.

Banerjee, S., Wang, Z., Mohammad, M., Sarkar, F. H. & Mohammad, R. M. (2008). Efficacy of selected natural products as therapeutic agents against cancer. *J.Nat.Prod.* **71**, 492-496.

Barderas, R., Desmet, J., Timmerman, P., Meloen, R. & Casal, J. I. (2008). Affinity maturation of antibodies assisted by in silico modeling. *Proc.Natl.Acad.Sci.U.S.A* **105**, 9029-9034.

Basilico, C., Arnesano, A., Galluzzo, M., Comoglio, P. M. & Michieli, P. (2008). A high affinity hepatocyte growth factor-binding site in the immunoglobulin-like region of Met. *J.Biol.Chem.* **283**, 21267-21277.

Basilico, C., Hultberg, A., Blanchetot, C., De, J. N., Festjens, E., Hanssens, V., Osepa, S. I., De, B. G., Mira, A., Cazzanti, M., Morello, V., Dreier, T., Saunders, M., de, H. H. & Michieli, P. (2014). Four individually druggable MET hotspots mediate HGF-driven tumor progression. *J.Clin.Invest* **124**, 3172-3186.

Bean, J., Brennan, C., Shih, J. Y., Riely, G., Viale, A., Wang, L., Chitale, D., Motoi, N., Szoke, J., Broderick, S., Balak, M., Chang, W. C., Yu, C. J., Gazdar, A., Pass, H., Rusch, V., Gerald, W., Huang, S. F., Yang, P. C., Miller, V., Ladanyi, M., Yang, C. H. & Pao, W. (2007). MET amplification occurs with or without T790M mutations in EGFR mutant lung tumors with acquired resistance to gefitinib or erlotinib. *Proc.Natl.Acad.Sci.U.S.A* **104**, 20932-20937.

Benatuil, L., Perez, J. M., Belk, J. & Hsieh, C. M. (2010). An improved yeast transformation method for the generation of very large human antibody libraries. *Protein Eng.Des.Sel.* **23**, 155-159.

Birchmeier, C., Birchmeier, W., Gherardi, E. & Vande Woude, G. F. (2003). Met, metastasis, motility and more. *Nat.Rev.Mol.Cell Biol.* **4**, 915-925.

Boder, E. T. & Wittrup, K. D. (1997). Yeast surface display for screening combinatorial polypeptide libraries. *Nat.Biotechnol.* **15**, 553-557.

Bradford, M. M. (1976). A rapid and sensitive method for the quantitation of microgram quantities of protein utilizing the principle of protein-dye binding. *Anal.Biochem.* **72**, 248-254.

Brekke, O. H. & Sandlie, I. (2003). Therapeutic antibodies for human diseases at the dawn of the twenty-first century. *Nat.Rev.Drug Discov.* **2**, 52-62.

Brennan, M., Davison, P. F. & Paulus, H. (1985). Preparation of bispecific antibodies by chemical recombination of monoclonal immunoglobulin G1 fragments. *Science* **229**, 81-83.

Castoldi, R., Ecker, V., Wiehle, L., Majety, M., Busl-Schuller, R., Asmussen, M., Nopora, A., Jucknischke, U., Osl, F., Kobold, S., Scheuer, W., Venturi, M., Klein, C., Niederfellner, G. & Sustmann, C. (2013). A novel bispecific EGFR/Met antibody blocks tumor-promoting phenotypic effects induced by resistance to EGFR inhibition and has potent antitumor activity. *Oncogene* **32**, 5593-5601.

Castoldi, R., Jucknischke, U., Pradel, L. P., Arnold, E., Klein, C., Scheiblich, S., Niederfellner, G. & Sustmann, C. (2012). Molecular characterization of novel trispecific ErbB-cMet-IGF1R antibodies and their antigen-binding properties. *Protein Eng.Des.Sel.* **25**, 551-559.

Chen, I., Dorr, B. M. & Liu, D. R. (2011). A general strategy for the evolution of bond-forming enzymes using yeast display. *Proc.Natl.Acad.Sci.U.S.A* **108**, 11399-11404.

Chen, K. Q., Robinson, A. C., Van Dam, M. E., Martinez, P., Economou, C. & Arnold, F. H. (1991). Enzyme engineering for nonaqueous solvents. II. Additive effects of mutations on the stability and activity of subtilisin E in polar organic media. *Biotechnol.Prog.* **7**, 125-129.

Cipriani, N. A., Abidoye, O. O., Vokes, E. & Salgia, R. (2009). MET as a target for treatment of chest tumors. *Lung Cancer* **63**, 169-179.

Cooper, C. S., Park, M., Blair, D. G., Tainsky, M. A., Huebner, K., Croce, C. M. & Vande Woude, G. F. (1984). Molecular cloning of a new transforming gene from a chemically transformed human cell line. *Nature* **311**, 29-33.

Cunningham, D., Humblet, Y., Siena, S., Khayat, D., Bleiberg, H., Santoro, A., Bets, D., Mueser, M., Harstrick, A., Verslype, C., Chau, I. & Van, C. E. (2004). Cetuximab monotherapy and cetuximab plus irinotecan in irinotecan-refractory metastatic colorectal cancer. *N.Engl.J.Med.* **351**, 337-345.

Davis, J. H., Aperlo, C., Li, Y., Kurosawa, E., Lan, Y., Lo, K. M. & Huston, J. S. (2010). SEEDbodies: fusion proteins based on strand-exchange engineered domain (SEED) CH3 heterodimers in an Fc analogue platform for asymmetric binders or immunofusions and bispecific antibodies. *Protein Eng.Des.Sel.* **23**, 195-202.

Diamantis, N. & Banerji, U. (2016). Antibody-drug conjugates-an emerging class of cancer treatment. *Br.J.Cancer* **114**, 362-367.

Dickgiesser, S., Rasche, N., Nasu, D., Middel, S., Horner, S., Avrutina, O., Diederichsen, U. & Kolmar, H. (2015). Self-assembled hybrid aptamer-Fc conjugates for targeted delivery: A modular chemoenzymatic approach. *ACS Chem.Biol.* **10**, 2158-2165.

Doerner, A., Rhiel, L., Zielonka, S. & Kolmar, H. (2014). Therapeutic antibody engineering by high efficiency cell screening. *FEBS Lett.* **588**, 278-287.

Downward, J., Yarden, Y., Mayes, E., Scrace, G., Totty, N., Stockwell, P., Ullrich, A., Schlessinger, J. & Waterfield, M. D. (1984). Close similarity of epidermal growth factor receptor and v-erb-B oncogene protein sequences. *Nature* **307**, 521-527.

Du, P. L. (1993). Phylogeny of B-cell development. *Curr.Opin.Immunol.* **5**, 185-193.

Dübel, S. (2007). *Handbook of therapeutic antibodies,* Weinheim: WILEY-VCH.

Ecker, D. M., Jones, S. D. & Levine, H. L. (2015). The therapeutic monoclonal antibody market. *MAbs.* **7**, 9-14.

Emmons, C. & Hunsicker, L. G. (1987). Muromonab-CD3 (Orthoclone OKT3): the first monoclonal antibody approved for therapeutic use. *Iowa Med.* **77**, 78-82.

Engelman, J. A., Zejnullahu, K., Mitsudomi, T., Song, Y., Hyland, C., Park, J. O., Lindeman, N., Gale, C. M., Zhao, X., Christensen, J., Kosaka, T., Holmes, A. J., Rogers, A. M., Cappuzzo, F., Mok, T.,

Lee, C., Johnson, B. E., Cantley, L. C. & Janne, P. A. (2007). MET amplification leads to gefitinib resistance in lung cancer by activating ERBB3 signaling. *Science* **316**, 1039-1043.

Engvall, E., Jonsson, K. & Perlmann, P. (1971). Enzyme-linked immunosorbent assay. II. Quantitative assay of protein antigen, immunoglobulin G, by means of enzyme-labelled antigen and antibody-coated tubes. *Biochim.Biophys.Acta* **251**, 427-434.

Estep, P., Reid, F., Nauman, C., Liu, Y., Sun, T., Sun, J. & Xu, Y. (2013). High throughput solution-based measurement of antibody-antigen affinity and epitope binning. *MAbs.* **5**, 270-278.

Ferguson, K. M., Berger, M. B., Mendrola, J. M., Cho, H. S., Leahy, D. J. & Lemmon, M. A. (2003). EGF activates its receptor by removing interactions that autoinhibit ectodomain dimerization. *Mol.Cell* **11**, 507-517.

Ferrara, C., Grau, S., Jager, C., Sondermann, P., Brunker, P., Waldhauer, I., Hennig, M., Ruf, A., Rufer, A. C., Stihle, M., Umana, P. & Benz, J. (2011). Unique carbohydrate-carbohydrate interactions are required for high affinity binding between FcgammaRIII and antibodies lacking core fucose. *Proc.Natl.Acad.Sci.U.S.A* **108**, 12669-12674.

Fischer, N., Elson, G., Magistrelli, G., Dheilly, E., Fouque, N., Laurendon, A., Gueneau, F., Ravn, U., Depoisier, J. F., Moine, V., Raimondi, S., Malinge, P., Di, G. L., Rousseau, F., Poitevin, Y., Calloud, S., Cayatte, P. A., Alcoz, M., Pontini, G., Fagete, S., Broyer, L., Corbier, M., Schrag, D., Didelot, G., Bosson, N., Costes, N., Cons, L., Buatois, V., Johnson, Z., Ferlin, W., Masternak, K. & Kosco-Vilbois, M. (2015). Exploiting light chains for the scalable generation and platform purification of native human bispecific IgG. *Nat.Commun.* **6**, 6113.

Garber, K. (2014). Bispecific antibodies rise again. *Nat.Rev.Drug Discov.* **13**, 799-801.

Gherardi, E., Youles, M. E., Miguel, R. N., Blundell, T. L., Iamele, L., Gough, J., Bandyopadhyay, A., Hartmann, G. & Butler, P. J. (2003). Functional map and domain structure of MET, the product of the c-met protooncogene and receptor for hepatocyte growth factor/scatter factor. *Proc.Natl.Acad.Sci.U.S.A* **100**, 12039-12044.

Giusti, R. M., Shastri, K. A., Cohen, M. H., Keegan, P. & Pazdur, R. (2007). FDA drug approval summary: panitumumab (Vectibix). *Oncologist.* **12**, 577-583.

Goetsch, L., Broussas, M., Fabre-Lafay, S., Robert, A., Lepecquet, A.-M., Gonzalez, A., Wurch, T., Bailly, C. & Crovaia, N. (2010). h224G11, a humanized whole antibody targeting the c-Met receptor, induces c-Met down-regulation and triggers ADCC functions.

Goldoni, S., Humphries, A., Nystrom, A., Sattar, S., Owens, R. T., McQuillan, D. J., Ireton, K. & Iozzo, R. V. (2009). Decorin is a novel antagonistic ligand of the Met receptor. *J.Cell Biol.* **185**, 743-754.

Gostring, L., Chew, M. T., Orlova, A., Hoiden-Guthenberg, I., Wennborg, A., Carlsson, J. & Frejd, F. Y. (2010). Quantification of internalization of EGFR-binding Affibody molecules: Methodological aspects. *Int.J.Oncol.* **36**, 757-763.

Greenall, S. A., Gherardi, E., Liu, Z., Donoghue, J. F., Vitali, A. A., Li, Q., Murphy, R., Iamele, L., Scott, A. M. & Johns, T. G. (2012). Non-agonistic bivalent antibodies that promote c-MET degradation and inhibit tumor growth and others specific for tumor related c-MET. *PLoS.One.* **7**, e34658.

Gunasekaran, K., Pentony, M., Shen, M., Garrett, L., Forte, C., Woodward, A., Ng, S. B., Born, T., Retter, M., Manchulenko, K., Sweet, H., Foltz, I. N., Wittekind, M. & Yan, W. (2010). Enhancing antibody

Fc heterodimer formation through electrostatic steering effects: applications to bispecific molecules and monovalent IgG. *J.Biol.Chem.* **285**, 19637-19646.

Guo, A., Villen, J., Kornhauser, J., Lee, K. A., Stokes, M. P., Rikova, K., Possemato, A., Nardone, J., Innocenti, G., Wetzel, R., Wang, Y., MacNeill, J., Mitchell, J., Gygi, S. P., Rush, J., Polakiewicz, R. D. & Comb, M. J. (2008). Signaling networks assembled by oncogenic EGFR and c-Met. *Proc.Natl.Acad.Sci.U.S.A* **105**, 692-697.

Gussow, D. & Seemann, G. (1991). Humanization of monoclonal antibodies. *Methods Enzymol.* **203**, 99-121.

Ho, M. & Pastan, I. (2009). Mammalian cell display for antibody engineering. *Methods Mol.Biol.* **525**, 337-52, xiv.

Holmes, D. (2011). Buy buy bispecific antibodies. *Nat.Rev.Drug Discov.* **10**, 798-800.

Hultberg, A., Morello, V., Huyghe, L., De, J. N., Blanchetot, C., Hanssens, V., De, B. G., Silence, K., Festjens, E., Heukers, R., Roux, B., Lamballe, F., Ginestier, C., Charafe-Jauffret, E., Maina, F., Brouckaert, P., Saunders, M., Thibault, A., Dreier, T., de, H. H. & Michieli, P. (2015). Depleting MET-expressing tumor cells by ADCC provides a therapeutic advantage over inhibiting HGF/MET signaling. *Cancer Res.* **75**, 3373-3383.

Hust, M., Dubel, S. & Schirrmann, T. (2007). Selection of recombinant antibodies from antibody gene libraries. *Methods Mol.Biol.* **408**, 243-255.

Hust, M., Meyer, T., Voedisch, B., Rulker, T., Thie, H., El-Ghezal, A., Kirsch, M. I., Schutte, M., Helmsing, S., Meier, D., Schirrmann, T. & Dubel, S. (2011). A human scFv antibody generation pipeline for proteome research. *J.Biotechnol.* **152**, 159-170.

Hyatt, D. C. & Ceresa, B. P. (2008). Cellular localization of the activated EGFR determines its effect on cell growth in MDA-MB-468 cells. *Exp.Cell Res.* **314**, 3415-3425.

Irving, R. A., Kortt, A. A. & Hudson, P. J. (1996). Affinity maturation of recombinant antibodies using E. coli mutator cells. *Immunotechnology.* **2**, 127-143.

Jackman, J., Chen, Y., Huang, A., Moffat, B., Scheer, J. M., Leong, S. R., Lee, W. P., Zhang, J., Sharma, N., Lu, Y., Iyer, S., Shields, R. L., Chiang, N., Bauer, M. C., Wadley, D., Roose-Girma, M., Vandlen, R., Yansura, D. G., Wu, Y. & Wu, L. C. (2010). Development of a two-part strategy to identify a therapeutic human bispecific antibody that inhibits IgE receptor signaling. *J.Biol.Chem.* **285**, 20850-20859.

Jakobovits, A. (1995). Production of fully human antibodies by transgenic mice. *Curr.Opin.Biotechnol.* **6**, 561-566.

Janeway, C. A., Travers, P., Walport, M. & Slomchik, M. (2001). The humoral immune response. In *Immunobiology: The Immune System in Health and Disease* . New York: Garland Science.

Jarantow, S. W., Bushey, B. S., Pardinas, J. R., Boakye, K., Lacy, E. R., Sanders, R., Sepulveda, M. A., Moores, S. L. & Chiu, M. L. (2015). Impact of cell-surface antigen expression on target engagement and function of an epidermal growth factor receptor x c-MET bispecific antibody. *J.Biol.Chem.* **290**, 24689-24704.

Jo, M., Stolz, D. B., Esplen, J. E., Dorko, K., Michalopoulos, G. K. & Strom, S. C. (2000). Cross-talk between epidermal growth factor receptor and c-Met signal pathways in transformed cells. *J.Biol.Chem.* **275**, 8806-8811.

Joubert, M. K., Hokom, M., Eakin, C., Zhou, L., Deshpande, M., Baker, M. P., Goletz, T. J., Kerwin, B. A., Chirmule, N., Narhi, L. O. & Jawa, V. (2012). Highly aggregated antibody therapeutics can enhance the in vitro innate and late-stage T-cell immune responses. *J.Biol.Chem.* **287**, 25266-25279.

Kammula, U. S., Kuntz, E. J., Francone, T. D., Zeng, Z., Shia, J., Landmann, R. G., Paty, P. B. & Weiser, M. R. (2007). Molecular co-expression of the c-Met oncogene and hepatocyte growth factor in primary colon cancer predicts tumor stage and clinical outcome. *Cancer Lett.* **248**, 219-228.

Kang, A. S., Jones, T. M. & Burton, D. R. (1991). Antibody redesign by chain shuffling from random combinatorial immunoglobulin libraries. *Proc.Natl.Acad.Sci.U.S.A* **88**, 11120-11123.

Kettleborough, C. A., Saldanha, J., Heath, V. J., Morrison, C. J. & Bendig, M. M. (1991). Humanization of a mouse monoclonal antibody by CDR-grafting: the importance of framework residues on loop conformation. *Protein Eng* **4**, 773-783.

Khazaeli, M. B., Conry, R. M. & LoBuglio, A. F. (1994). Human immune response to monoclonal antibodies. *J.Immunother.Emphasis.Tumor Immunol.* **15**, 42-52.

Kimura, H., Sakai, K., Arao, T., Shimoyama, T., Tamura, T. & Nishio, K. (2007). Antibody-dependent cellular cytotoxicity of cetuximab against tumor cells with wild-type or mutant epidermal growth factor receptor. *Cancer Sci.* **98**, 1275-1280.

King, A. C., Woods, M., Liu, W., Lu, Z., Gill, D. & Krebs, M. R. (2011). High-throughput measurement, correlation analysis, and machine-learning predictions for pH and thermal stabilities of Pfizer-generated antibodies. *Protein Sci.* **20**, 1546-1557.

Knickelbein, K. & Zhang, L. (2015). Mutant KRAS as a critical determinant of the therapeutic response of colorectal cancer. *Genes Dis.* **2**, 4-12.

Kohler, G. & Milstein, C. (1992). Continuous cultures of fused cells secreting antibody of predefined specificity. 1975. *Biotechnology* **24**, 524-526.

Kontermann, R. E. & Brinkmann, U. (2015). Bispecific antibodies. *Drug Discov.Today* **20**, 838-847.

Kramer, K., Fiedler, M., Skerra, A. & Hock, B. (2002). A generic strategy for subcloning antibody variable regions from the scFv phage display vector pCANTAB 5 E into pASK85 permits the economical production of F(ab) fragments and leads to improved recombinant immunoglobulin stability. *Biosens.Bioelectron.* **17**, 305-313.

Krishnaswamy, S., Kanteti, R., Duke-Cohan, J. S., Loganathan, S., Liu, W., Ma, P. C., Sattler, M., Singleton, P. A., Ramnath, N., Innocenti, F., Nicolae, D. L., Ouyang, Z., Liang, J., Minna, J., Kozloff, M. F., Ferguson, M. K., Natarajan, V., Wang, Y. C., Garcia, J. G., Vokes, E. E. & Salgia, R. (2009). Ethnic differences and functional analysis of MET mutations in lung cancer. *Clin.Cancer Res.* **15**, 5714-5723.

Labrijn, A. F., Meesters, J. I., de Goeij, B. E., van den Bremer, E. T., Neijssen, J., van Kampen, M. D., Strumane, K., Verploegen, S., Kundu, A., Gramer, M. J., van Berkel, P. H., van de Winkel, J. G., Schuurman, J. & Parren, P. W. (2013). Efficient generation of stable bispecific IgG1 by controlled Fab-arm exchange. *Proc.Natl.Acad.Sci.U.S.A* **110**, 5145-5150.

Labrijn, A. F., Rispens, T., Meesters, J., Rose, R. J., den Bleker, T. H., Loverix, S., van den Bremer, E. T., Neijssen, J., Vink, T., Lasters, I., Aalberse, R. C., Heck, A. J., van de Winkel, J. G., Schuurman, J. & Parren, P. W. (2011). Species-specific determinants in the IgG CH3 domain enable Fab-arm exchange by affecting the noncovalent CH3-CH3 interaction strength. *J.Immunol.* **187**, 3238-3246.

Lacouture, M. E. (2006). Mechanisms of cutaneous toxicities to EGFR inhibitors. *Nat.Rev.Cancer* **6**, 803-812.

Laemmli, U. K. (1970). Cleavage of structural proteins during the assembly of the head of bacteriophage T4. *Nature* **227**, 680-685.

Leal, M., Sapra, P., Hurvitz, S. A., Senter, P., Wahl, A., Schutten, M., Shah, D. K., Haddish-Berhane, N. & Kabbarah, O. (2014). Antibody-drug conjugates: an emerging modality for the treatment of cancer. *Ann.N.Y.Acad.Sci.* **1321**, 41-54.

Lee, B. S., Kim, H. J., Hwang, J. W., Cheong, K. H., Kim, K. A., Cha, H. Y., Lee, J. M. & Kim, C. H. (2016a). The dual inhibition of Met and EGFR by ME22S, a novel Met/EGFR bispecific monoclonal antibody, suppresses the proliferation and invasion of laryngeal cancer. *Ann.Surg.Oncol.* **23**, 2046-2053.

Lee, J. M., Kim, B., Lee, S. B., Jeong, Y., Oh, Y. M., Song, Y. J., Jung, S., Choi, J., Lee, S., Cheong, K. H., Kim, D. U., Park, H. W., Han, Y. K., Kim, G. W., Choi, H., Song, P. H. & Kim, K. A. (2014). Cbl-independent degradation of Met: ways to avoid agonism of bivalent Met-targeting antibody. *Oncogene* **33**, 34-43.

Lee, J. M., Lee, S. H., Hwang, J. W., Oh, S. J., Kim, B., Jung, S., Shim, S. H., Lin, P. W., Lee, S. B., Cho, M. Y., Koh, Y. J., Kim, S. Y., Ahn, S., Lee, J., Kim, K. M., Cheong, K. H., Choi, J. & Kim, K. A. (2016b). Novel strategy for a bispecific antibody: induction of dual target internalization and degradation. *Oncogene* **35**, 4437-4446.

Lei, S. P., Lin, H. C., Wang, S. S., Callaway, J. & Wilcox, G. (1987). Characterization of the Erwinia carotovora pelB gene and its product pectate lyase. *J.Bacteriol.* **169**, 4379-4383.

Lewis, S. M., Wu, X., Pustilnik, A., Sereno, A., Huang, F., Rick, H. L., Guntas, G., Leaver-Fay, A., Smith, E. M., Ho, C., Hansen-Estruch, C., Chamberlain, A. K., Truhlar, S. M., Conner, E. M., Atwell, S., Kuhlman, B. & Demarest, S. J. (2014). Generation of bispecific IgG antibodies by structure-based design of an orthogonal Fab interface. *Nat.Biotechnol.* **32**, 191-198.

Li, S., Schmitz, K. R., Jeffrey, P. D., Wiltzius, J. J., Kussie, P. & Ferguson, K. M. (2005). Structural basis for inhibition of the epidermal growth factor receptor by cetuximab. *Cancer Cell* **7**, 301-311.

Lin, C. H. & Patel, D. J. (1995). Solution structure of the covalent duocarmycin A-DNA duplex complex. *J.Mol.Biol.* **248**, 162-179.

Liska, D., Chen, C. T., Bachleitner-Hofmann, T., Christensen, J. G. & Weiser, M. R. (2011). HGF rescues colorectal cancer cells from EGFR inhibition via MET activation. *Clin.Cancer Res.* **17**, 472-482.

Liu, H., Gaza-Bulseco, G., Chumsae, C. & Newby-Kew, A. (2007). Characterization of lower molecular weight artifact bands of recombinant monoclonal IgG1 antibodies on non-reducing SDS-PAGE. *Biotechnol.Lett.* **29**, 1611-1622.

Liu, L., Zeng, W., Wortinger, M. A., Yan, S. B., Cornwell, P., Peek, V. L., Stephens, J. R., Tetreault, J. W., Xia, J., Manro, J. R., Credille, K. M., Ballard, D. W., Brown-Augsburger, P., Wacheck, V., Chow,

C. K., Huang, L., Wang, Y., Denning, I., Davies, J., Tang, Y., Vaillancourt, P. & Lu, J. (2014). LY2875358, a neutralizing and internalizing anti-MET bivalent antibody, inhibits HGF-dependent and HGF-independent MET activation and tumor growth. *Clin.Cancer Res.* **20**, 6059-6070.

Lo, M. C., Aulabaugh, A., Jin, G., Cowling, R., Bard, J., Malamas, M. & Ellestad, G. (2004). Evaluation of fluorescence-based thermal shift assays for hit identification in drug discovery. *Anal.Biochem.* **332**, 153-159.

Lokker, N. A., Mark, M. R., Luis, E. A., Bennett, G. L., Robbins, K. A., Baker, J. B. & Godowski, P. J. (1992). Structure-function analysis of hepatocyte growth factor: identification of variants that lack mitogenic activity yet retain high affinity receptor binding. *EMBO J.* **11**, 2503-2510.

Martin, A. & Scharff, M. D. (2002). Somatic hypermutation of the AID transgene in B and non-B cells. *Proc.Natl.Acad.Sci.U.S.A* **99**, 12304-12308.

Martin, P., Stewart, E., Pham, N. A., Mascaux, C., Panchal, D., Li, M., Kim, L., Sakashita, S., Wang, D., Sykes, J., Friess, T., Shepherd, F. A., Liu, G. & Tsao, M. S. (2016). Cetuximab inhibits T790M-mediated resistance to epidermal growth factor receptor tyrosine kinase inhibitor in a lung adenocarcinoma patient-derived xenograft mouse model. *Clin.Lung Cancer*, doi: 10.1016/j.cllc.2016.01.002 [Epub ahead of print].

Mazor, Y., Hansen, A., Yang, C., Chowdhury, P. S., Wang, J., Stephens, G., Wu, H. & Dall'Acqua, W. F. (2015a). Insights into the molecular basis of a bispecific antibody's target selectivity. *MAbs.* **7**, 461-469.

Mazor, Y., Oganesyan, V., Yang, C., Hansen, A., Wang, J., Liu, H., Sachsenmeier, K., Carlson, M., Gadre, D. V., Borrok, M. J., Yu, X. Q., Dall'Acqua, W., Wu, H. & Chowdhury, P. S. (2015b). Improving target cell specificity using a novel monovalent bispecific IgG design. *MAbs.* **7**, 377-389.

McCafferty, J., Griffiths, A. D., Winter, G. & Chiswell, D. J. (1990). Phage antibodies: filamentous phage displaying antibody variable domains. *Nature* **348**, 552-554.

McDonagh, C. F., Kim, K. M., Turcott, E., Brown, L. L., Westendorf, L., Feist, T., Sussman, D., Stone, I., Anderson, M., Miyamoto, J., Lyon, R., Alley, S. C., Gerber, H. P. & Carter, P. J. (2008). Engineered anti-CD70 antibody-drug conjugate with increased therapeutic index. *Mol.Cancer Ther.* **7**, 2913-2923.

Medzhitov, R., Preston-Hurlburt, P. & Janeway, C. A., Jr. (1997). A human homologue of the Drosophila Toll protein signals activation of adaptive immunity. *Nature* **388**, 394-397.

Melosky, B., Burkes, R., Rayson, D., Alcindor, T., Shear, N. & Lacouture, M. (2009). Management of skin rash during EGFR-targeted monoclonal antibody treatment for gastrointestinal malignancies: Canadian recommendations. *Curr.Oncol.* **16**, 16-26.

Mendelsohn, J. & Baselga, J. (2003). Status of epidermal growth factor receptor antagonists in the biology and treatment of cancer. *J.Clin.Oncol.* **21**, 2787-2799.

Merchant, M., Ma, X., Maun, H. R., Zheng, Z., Peng, J., Romero, M., Huang, A., Yang, N. Y., Nishimura, M., Greve, J., Santell, L., Zhang, Y. W., Su, Y., Kaufman, D. W., Billeci, K. L., Mai, E., Moffat, B., Lim, A., Duenas, E. T., Phillips, H. S., Xiang, H., Young, J. C., Vande Woude, G. F., Dennis, M. S., Reilly, D. E., Schwall, R. H., Starovasnik, M. A., Lazarus, R. A. & Yansura, D. G. (2013). Monovalent antibody design and mechanism of action of onartuzumab, a MET antagonist with anti-tumor activity as a therapeutic agent. *Proc.Natl.Acad.Sci.U.S.A* **110**, E2987-E2996.

Milstein, C. & Cuello, A. C. (1983). Hybrid hybridomas and their use in immunohistochemistry. *Nature* **305**, 537-540.

Morley, R., Cardenas, A., Hawkins, P., Suzuki, Y., Paton, V., Phan, S. C., Merchant, M., Hsu, J., Yu, W., Xia, Q., Koralek, D., Luhn, P. & Aldairy, W. (2015). Safety of onartuzumab in patients with solid tumors: Experience to date from the onartuzumab clinical trial program. *PLoS.One.* **10**, e0139679.

Muda, M., Gross, A. W., Dawson, J. P., He, C., Kurosawa, E., Schweickhardt, R., Dugas, M., Soloviev, M., Bernhardt, A., Fischer, D., Wesolowski, J. S., Kelton, C., Neuteboom, B. & Hock, B. (2011). Therapeutic assessment of SEED: a new engineered antibody platform designed to generate mono- and bispecific antibodies. *Protein Eng.Des.Sel.* **24**, 447-454.

Mullard, A. (2013). Maturing antibody-drug conjugate pipeline hits 30. *Nat.Rev.Drug Discov.* **12**, 329-332.

Muller, P. Y. & Milton, M. N. (2012). The determination and interpretation of the therapeutic index in drug development. *Nat.Rev.Drug Discov.* **11**, 751-761.

Mullis, K., Faloona, F., Scharf, S., Saiki, R., Horn, G. & Erlich, H. (1986). Specific enzymatic amplification of DNA in vitro: the polymerase chain reaction. *Cold Spring Harb.Symp.Quant.Biol.* **51 Pt 1**, 263-273.

Murthy, U., Basu, A., Rodeck, U., Herlyn, M., Ross, A. H. & Das, M. (1987). Binding of an antagonistic monoclonal antibody to an intact and fragmented EGF-receptor polypeptide. *Arch.Biochem.Biophys.* **252**, 549-560.

Nicholson, R. I., Gee, J. M. & Harper, M. E. (2001). EGFR and cancer prognosis. *Eur.J.Cancer* **37 Suppl 4**, S9-15.

Niemann, H. H. (2013). Structural basis of MET receptor dimerization by the bacterial invasion protein InlB and the HGF/SF splice variant NK1. *Biochim.Biophys.Acta* **1834**, 2195-2204.

Nimmerjahn, F. & Ravetch, J. V. (2010). Antibody-mediated modulation of immune responses. *Immunol.Rev.* **236**, 265-275.

Oh, Y. M., Song, Y. J., Lee, S. B., Jeong, Y., Kim, B., Kim, G. W., Kim, K. E., Lee, J. M., Cho, M. Y., Choi, J., Nam, D. H., Song, P. H., Cheong, K. H. & Kim, K. A. (2012). A new anti-c-Met antibody selected by a mechanism-based dual-screening method: therapeutic potential in cancer. *Mol.Cells* **34**, 523-529.

Pacchiana, G., Chiriaco, C., Stella, M. C., Petronzelli, F., De, S. R., Galluzzo, M., Carminati, P., Comoglio, P. M., Michieli, P. & Vigna, E. (2010). Monovalency unleashes the full therapeutic potential of the DN-30 anti-Met antibody. *J.Biol.Chem.* **285**, 36149-36157.

Panke, C., Weininger, D., Haas, A., Schelter, F., Schlothauer, T., Bader, S., Sircar, R., Josel, H. P., Baer, U., Burtscher, H., Mundigl, O., Grote, M., Brinkmann, U. & Sustmann, C. (2013). Quantification of cell surface proteins with bispecific antibodies. *Protein Eng.Des.Sel.* **26**, 645-654.

Panowski, S., Bhakta, S., Raab, H., Polakis, P. & Junutula, J. R. (2014). Site-specific antibody drug conjugates for cancer therapy. *MAbs.* **6**, 34-45.

Pao, W., Miller, V. A., Politi, K. A., Riely, G. J., Somwar, R., Zakowski, M. F., Kris, M. G. & Varmus, H. (2005). Acquired resistance of lung adenocarcinomas to gefitinib or erlotinib is associated with a second mutation in the EGFR kinase domain. *PLoS.Med.* **2**, e73.

Perez, H. L., Cardarelli, P. M., Deshpande, S., Gangwar, S., Schroeder, G. M., Vite, G. D. & Borzilleri, R. M. (2014). Antibody-drug conjugates: current status and future directions. *Drug Discov.Today* **19**, 869-881.

Petrelli, A., Circosta, P., Granziero, L., Mazzone, M., Pisacane, A., Fenoglio, S., Comoglio, P. M. & Giordano, S. (2006). Ab-induced ectodomain shedding mediates hepatocyte growth factor receptor down-regulation and hampers biological activity. *Proc.Natl.Acad.Sci.U.S.A* **103**, 5090-5095.

Phillips, A. C., Boghaert, E. R., Vaidya, K. S., Mitten, M. J., Norvell, S., Falls, H. D., DeVries, P. J., Cheng, D., Meulbroek, J. A., Buchanan, F. G., McKay, L. M., Goodwin, N. C. & Reilly, E. B. (2016). ABT-414, an antibody-drug conjugate targeting a tumor-selective EGFR epitope. *Mol.Cancer Ther.* **15**, 661-669.

Polakis, P. (2016). Antibody drug conjugates for cancer therapy. *Pharmacol.Rev.* **68**, 3-19.

Prat, M., Oltolina, F. & Basilico, C. (2014). Monoclonal antibodies against the MET/HGF receptor and its ligand: Multitask tools with applications from basic research to therapy. *Biomedicines* **2**, 359-383.

Prewett, M., Rockwell, P., Rockwell, R. F., Giorgio, N. A., Mendelsohn, J., Scher, H. I. & Goldstein, N. I. (1996). The biologic effects of C225, a chimeric monoclonal antibody to the EGFR, on human prostate carcinoma. *J.Immunother.Emphasis.Tumor Immunol.* **19**, 419-427.

Rakestraw, J. A., Sazinsky, S. L., Piatesi, A., Antipov, E. & Wittrup, K. D. (2009). Directed evolution of a secretory leader for the improved expression of heterologous proteins and full-length antibodies in Saccharomyces cerevisiae. *Biotechnol.Bioeng.* **103**, 1192-1201.

Ramakrishnan, M. S., Eswaraiah, A., Crombet, T., Piedra, P., Saurez, G., Iyer, H. & Arvind, A. S. (2009). Nimotuzumab, a promising therapeutic monoclonal for treatment of tumors of epithelial origin. *MAbs.* **1**, 41-48.

Reilly, E. B., Phillips, A. C., Buchanan, F. G., Kingsbury, G., Zhang, Y., Meulbroek, J. A., Cole, T. B., DeVries, P. J., Falls, H. D., Beam, C., Gu, J., Digiammarino, E. L., Palma, J. P., Donawho, C. K., Goodwin, N. C. & Scott, A. M. (2015). Characterization of ABT-806, a humanized tumor-specific anti-EGFR monoclonal antibody. *Mol.Cancer Ther.* **14**, 1141-1151.

Ribatti, D. (2015). Edelman's view on the discovery of antibodies. *Immunol.Lett.* **164**, 72-75.

Rich, R. L. & Myszka, D. G. (2007). Higher-throughput, label-free, real-time molecular interaction analysis. *Anal.Biochem.* **361**, 1-6.

Ridgway, J. B., Presta, L. G. & Carter, P. (1996). 'Knobs-into-holes' engineering of antibody CH3 domains for heavy chain heterodimerization. *Protein Eng.* **9**, 617-621.

Ritchie, M., Tchistiakova, L. & Scott, N. (2013). Implications of receptor-mediated endocytosis and intracellular trafficking dynamics in the development of antibody drug conjugates. *MAbs.* **5**, 13-21.

Robinson, M. K., Hodge, K. M., Horak, E., Sundberg, A. L., Russeva, M., Shaller, C. C., von, M. M., Shchaveleva, I., Simmons, H. H., Marks, J. D. & Adams, G. P. (2008). Targeting ErbB2 and ErbB3 with a bispecific single-chain Fv enhances targeting selectivity and induces a therapeutic effect in vitro. *Br.J.Cancer* **99**, 1415-1425.

Roopenian, D. C. & Akilesh, S. (2007). FcRn: the neonatal Fc receptor comes of age. *Nat.Rev.Immunol.* **7**, 715-725.

Rossin, R., van Duijnhoven, S. M., Ten, H. W., Janssen, H. M., Hoeben, F. J., Versteegen, R. M. & Robillard, M. S. (2016). Triggered drug release from an antibody-drug conjugate using fast "click-to-release" chemistry in mice. *Bioconjug.Chem.* **27**, 1697-1706.

Schaefer, G., Haber, L., Crocker, L. M., Shia, S., Shao, L., Dowbenko, D., Totpal, K., Wong, A., Lee, C. V., Stawicki, S., Clark, R., Fields, C., Lewis Phillips, G. D., Prell, R. A., Danilenko, D. M., Franke, Y., Stephan, J. P., Hwang, J., Wu, Y., Bostrom, J., Sliwkowski, M. X., Fuh, G. & Eigenbrot, C. (2011a). A two-in-one antibody against HER3 and EGFR has superior inhibitory activity compared with monospecific antibodies. *Cancer Cell* **20**, 472-486.

Schaefer, W., Regula, J. T., Bahner, M., Schanzer, J., Croasdale, R., Durr, H., Gassner, C., Georges, G., Kettenberger, H., Imhof-Jung, S., Schwaiger, M., Stubenrauch, K. G., Sustmann, C., Thomas, M., Scheuer, W. & Klein, C. (2011b). Immunoglobulin domain crossover as a generic approach for the production of bispecific IgG antibodies. *Proc.Natl.Acad.Sci.U.S.A* **108**, 11187-11192.

Schmiedel, J., Blaukat, A., Li, S., Knochel, T. & Ferguson, K. M. (2008). Matuzumab binding to EGFR prevents the conformational rearrangement required for dimerization. *Cancer Cell* **13**, 365-373.

Schmitz, K. R. & Ferguson, K. M. (2009). Interaction of antibodies with ErbB receptor extracellular regions. *Exp.Cell Res.* **315**, 659-670.

Sengers, B. G., McGinty, S., Nouri, F. Z., Argungu, M., Hawkins, E., Hadji, A., Weber, A., Taylor, A. & Sepp, A. (2016). Modelling bispecific monoclonal antibody interaction with two cell membrane targets indicates the importance of surface diffusion. *MAbs.* **8**, 905-915.

Sharma, N. & Adjei, A. A. (2011). In the clinic: ongoing clinical trials evaluating c-MET-inhibiting drugs. *Ther.Adv.Med.Oncol.* **3**, S37-S50.

Shieh, J. M., Tang, Y. A., Yang, T. H., Chen, C. Y., Hsu, H. S., Tan, Y. H., Salgia, R. & Wang, Y. C. (2013). Lack of association of C-Met-N375S sequence variant with lung cancer susceptibility and prognosis. *Int.J.Med.Sci.* **10**, 988-994.

Shields, R. L., Lai, J., Keck, R., O'Connell, L. Y., Hong, K., Meng, Y. G., Weikert, S. H. & Presta, L. G. (2002). Lack of fucose on human IgG1 N-linked oligosaccharide improves binding to human Fcgamma RIII and antibody-dependent cellular toxicity. *J.Biol.Chem.* **277**, 26733-26740.

Sierra, J. R. & Tsao, M. S. (2011). c-MET as a potential therapeutic target and biomarker in cancer. *Ther.Adv.Med.Oncol.* **3**, S21-S35.

Smith, G. P. (1985). Filamentous fusion phage: novel expression vectors that display cloned antigens on the virion surface. *Science* **228**, 1315-1317.

Smith, G. P. & Petrenko, V. A. (1997). Phage display. *Chem.Rev.* **97**, 391-410.

Spiess, C., Merchant, M., Huang, A., Zheng, Z., Yang, N. Y., Peng, J., Ellerman, D., Shatz, W., Reilly, D., Yansura, D. G. & Scheer, J. M. (2013). Bispecific antibodies with natural architecture produced by co-culture of bacteria expressing two distinct half-antibodies. *Nat.Biotechnol.* **31**, 753-758.

Spiess, C., Zhai, Q. & Carter, P. J. (2015). Alternative molecular formats and therapeutic applications for bispecific antibodies. *Mol.Immunol.* **67**, 95-106.

Stamos, J., Lazarus, R. A., Yao, X., Kirchhofer, D. & Wiesmann, C. (2004). Crystal structure of the HGF beta-chain in complex with the Sema domain of the Met receptor. *EMBO J.* **23**, 2325-2335.

Stavnezer, J., Guikema, J. E. & Schrader, C. E. (2008). Mechanism and regulation of class switch recombination. *Annu.Rev.Immunol.* **26**, 261-292.

Stemmer, W. P. (1994). DNA shuffling by random fragmentation and reassembly: in vitro recombination for molecular evolution. *Proc.Natl.Acad.Sci.U.S.A* **91**, 10747-10751.

Straussman, R., Morikawa, T., Shee, K., Barzily-Rokni, M., Qian, Z. R., Du, J., Davis, A., Mongare, M. M., Gould, J., Frederick, D. T., Cooper, Z. A., Chapman, P. B., Solit, D. B., Ribas, A., Lo, R. S., Flaherty, K. T., Ogino, S., Wargo, J. A. & Golub, T. R. (2012). Tumour micro-environment elicits innate resistance to RAF inhibitors through HGF secretion. *Nature* **487**, 500-504.

Tang, Z., Du, R., Jiang, S., Wu, C., Barkauskas, D. S., Richey, J., Molter, J., Lam, M., Flask, C., Gerson, S., Dowlati, A., Liu, L., Lee, Z., Halmos, B., Wang, Y., Kern, J. A. & Ma, P. C. (2008). Dual MET-EGFR combinatorial inhibition against T790M-EGFR-mediated erlotinib-resistant lung cancer. *Br.J.Cancer* **99**, 911-922.

Troiani, T., Martinelli, E., Napolitano, S., Vitagliano, D., Ciuffreda, L. P., Costantino, S., Morgillo, F., Capasso, A., Sforza, V., Nappi, A., De, P. R., D'Aiuto, E., Berrino, L., Bianco, R. & Ciardiello, F. (2013). Increased TGF-alpha as a mechanism of acquired resistance to the anti-EGFR inhibitor cetuximab through EGFR-MET interaction and activation of MET signaling in colon cancer cells. *Clin.Cancer Res.* **19**, 6751-6765.

Tundidor, Y., Garcia-Hernandez, C. P., Pupo, A., Cabrera, I. Y. & Rojas, G. (2014). Delineating the functional map of the interaction between nimotuzumab and the epidermal growth factor receptor. *MAbs.* **6**, 1013-1025.

Uppal, H., Doudement, E., Mahapatra, K., Darbonne, W. C., Bumbaca, D., Shen, B. Q., Du, X., Saad, O., Bowles, K., Olsen, S., Lewis Phillips, G. D., Hartley, D., Sliwkowski, M. X., Girish, S., Dambach, D. & Ramakrishnan, V. (2015). Potential mechanisms for thrombocytopenia development with trastuzumab emtansine (T-DM1). *Clin.Cancer Res.* **21**, 123-133.

van der Neut, K. M., Schuurman, J., Losen, M., Bleeker, W. K., Martinez-Martinez, P., Vermeulen, E., den Bleker, T. H., Wiegman, L., Vink, T., Aarden, L. A., De Baets, M. H., van de Winkel, J. G., Aalberse, R. C. & Parren, P. W. (2007). Anti-inflammatory activity of human IgG4 antibodies by dynamic Fab arm exchange. *Science* **317**, 1554-1557.

van der Zee, J. S., van, S. P. & Aalberse, R. C. (1986). Serologic aspects of IgG4 antibodies. II. IgG4 antibodies form small, nonprecipitating immune complexes due to functional monovalency. *J.Immunol.* **137**, 3566-3571.

Vidarsson, G., Dekkers, G. & Rispens, T. (2014). IgG subclasses and allotypes: from structure to effector functions. *Front Immunol.* **5**, 520.

Vigna, E., Chiriaco, C., Cignetto, S., Fontani, L., Basilico, C., Petronzelli, F. & Comoglio, P. M. (2015). Inhibition of ligand-independent constitutive activation of the Met oncogenic receptor by the engineered chemically-modified antibody DN30. *Mol.Oncol.* **9**, 1760-1772.

Voigt, M., Braig, F., Gothel, M., Schulte, A., Lamszus, K., Bokemeyer, C. & Binder, M. (2012). Functional dissection of the epidermal growth factor receptor epitopes targeted by panitumumab and cetuximab. *Neoplasia.* **14**, 1023-1031.

Wang, J., Goetsch, L., Tucker, L., Zhang, Q., Gonzalez, A., Vaidya, K. S., Oleksijew, A., Boghaert, E., Song, M., Sokolova, I., Pestova, E., Anderson, M., Pappano, W. N., Ansell, P., Bhathena, A., Naumovski, L., Corvaia, N. & Reilly, E. B. (2016). Anti-c-Met monoclonal antibody ABT-700 breaks oncogene addiction in tumors with MET amplification. *BMC.Cancer* **16**, 105.

Wang, W., Li, Q., Yamada, T., Matsumoto, K., Matsumoto, I., Oda, M., Watanabe, G., Kayano, Y., Nishioka, Y., Sone, S. & Yano, S. (2009). Crosstalk to stromal fibroblasts induces resistance of lung cancer to epidermal growth factor receptor tyrosine kinase inhibitors. *Clin.Cancer Res.* **15**, 6630-6638.

Wolf, E., Hofmeister, R., Kufer, P., Schlereth, B. & Baeuerle, P. A. (2005). BiTEs: bispecific antibody constructs with unique anti-tumor activity. *Drug Discov.Today* **10**, 1237-1244.

Wozniak-Knopp, G., Bartl, S., Bauer, A., Mostageer, M., Woisetschlager, M., Antes, B., Ettl, K., Kainer, M., Weberhofer, G., Wiederkum, S., Himmler, G., Mudde, G. C. & Ruker, F. (2010). Introducing antigen-binding sites in structural loops of immunoglobulin constant domains: Fc fragments with engineered HER2/neu-binding sites and antibody properties. *Protein Eng.Des.Sel.* **23**, 289-297.

Yang, X. D., Jia, X. C., Corvalan, J. R., Wang, P. & Davis, C. G. (2001). Development of ABX-EGF, a fully human anti-EGF receptor monoclonal antibody, for cancer therapy. *Crit.Rev.Oncol.Hematol.* **38**, 17-23.

Yarden, Y. & Sliwkowski, M. X. (2001). Untangling the ErbB signalling network. *Nat.Rev.Mol.Cell Biol.* **2**, 127-137.

Yewale, C., Baradia, D., Vhora, I., Patil, S. & Misra, A. (2013). Epidermal growth factor receptor targeting in cancer: a review of trends and strategies. *Biomaterials* **34**, 8690-8707.

Youles, M., Holmes, O., Petoukhov, M. V., Nessen, M. A., Stivala, S., Svergun, D. I. & Gherardi, E. (2008). Engineering the NK1 fragment of hepatocyte growth factor/scatter factor as a MET receptor antagonist. *J.Mol.Biol.* **377**, 616-622.

Zeidler, R., Reisbach, G., Wollenberg, B., Lang, S., Chaubal, S., Schmitt, B. & Lindhofer, H. (1999). Simultaneous activation of T cells and accessory cells by a new class of intact bispecific antibody results in efficient tumor cell killing. *J.Immunol.* **163**, 1246-1252.

Zhang, J., Liu, X., Bell, A., To, R., Baral, T. N., Azizi, A., Li, J., Cass, B. & Durocher, Y. (2009). Transient expression and purification of chimeric heavy chain antibodies. *Protein Expr.Purif.* **65**, 77-82.

Zheng, S., Moores, S., Jarantow, S., Pardinas, J., Chiu, M., Zhou, H. & Wang, W. (2016). Cross-arm binding efficiency of an EGFR x c-Met bispecific antibody. *MAbs.* **8**, 551-561.

8. Appendix

8.1. Supporting Information

For the affinity maturation of the parental anti-c-MET binder F06, the sequence analysis results for the parsimonious mutagenesis approach and the error prone PCR approach are depicted in **Table 12**, **Figure 32** and **Figure 33**.

Table 12: Sequence analysis of affinity matured Fab-F06 by phage display sub-libraries

For the affinity maturation of the parental anti-c-MET binder F06, the sequence analysis of two sub-library approaches, parsimonious mutagenesis and error prone PCR (epPCR), are depicted. The number of analyzable sequences of 96 sequenced clones (evaluable sequences) are listed as well as the number of complete, functional Fab-antibody fragments and the theoretical diversity.

F06 sub-library	Evaluable sequences		Complete Fab-antibody fragments		Theoretical diversity
	n	[%]	n	[%]	
Parsimonious mutagenesis of F06-CDR-H3	94	97.9	91	94.8	2.4E+06
epPCR F06-VH	74	77.1	71	74.0	4.1E+06

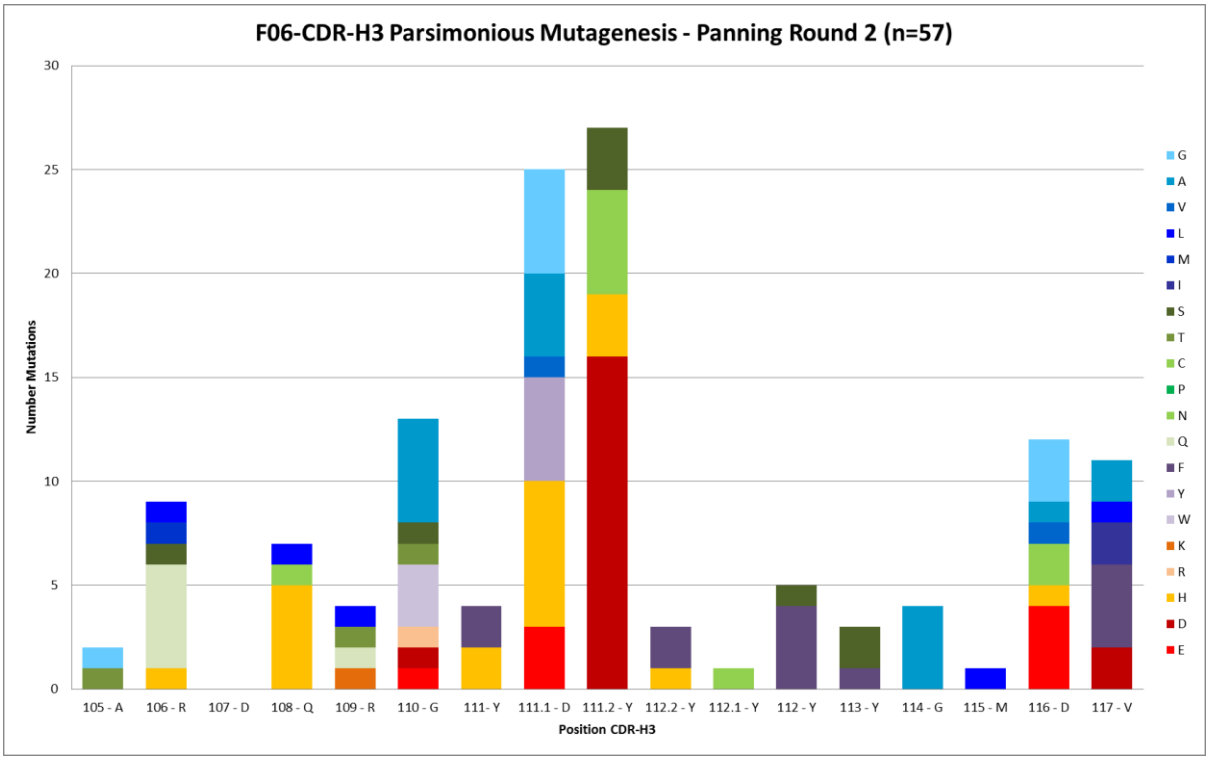

Figure 32: Sequence analysis of panning round 2 output from the F06 parsimonious sub-library.

Based on the sequence analysis, the changes of amino acids of 57 unique and functional binders based on 96 sequences of anti-c-MET binders after two rounds of panning from the Fab-F06 parsimonious mutagenesis sub-library are depicted. Each amino acid is represented by a single color as shown in the color code. Two positions 111.1 and 112.2 (after IMGT numbering) within the CDR-H3 displayed the highest abundance of mutations.

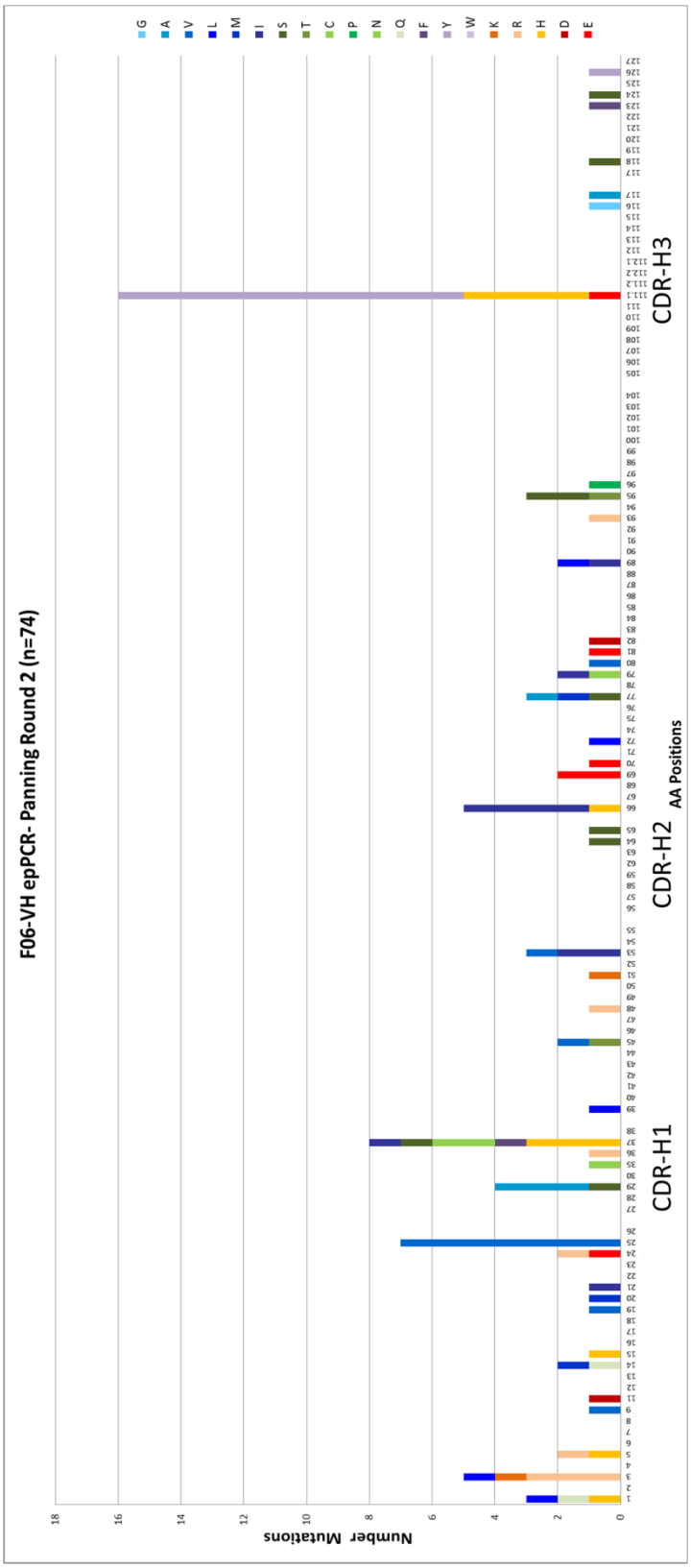

Figure 33: Sequence analysis of panning round 2 output from the F06-VH epPCR sub-library.

Based on the sequence analysis, the changes of amino acids of 74 unique and functional binders based on 96 sequences of anti-c-MET binders after two rounds of panning from the Fab-F06 error prone PCR sub-library are depicted. Each amino acid is represented by a single color as shown in the color code. Positions with high mutation rates were located in framework 1, the CDR-H1, and the CDR-H3.

For the analysis of c-MET binders, an epitope binning experiment was conducted to reveal anti-c-MET binders with overlapping (competing) epitopes. An exemplary biolayer interferogram is depicted in **Figure 34**.

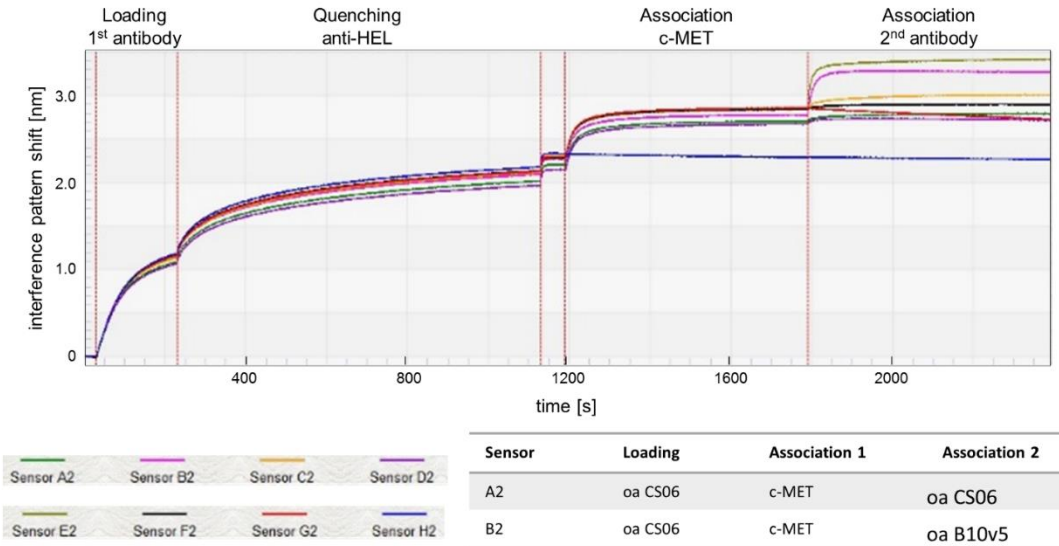

Sensor	Loading	Association 1	Association 2
A2	oa CS06	c-MET	oa CS06
B2	oa CS06	c-MET	oa B10v5
C2	oa CS06	c-MET	oa 5D5
D2	oa CS06	c-MET	224G11
E2	oa CS06	c-MET	LY2875358
F2	oa CS06	c-MET	anti-HEL
G2	oa CS06	c-MET	KB
F2	oa CS06	KB	KB

Figure 34: Exemplary raw data from the epitope binning experiment.

For the epitope binning experiment, the first antibody (e.g. oa CS06) was immobilized on anti-human Fc biosensors. This was followed by quenching with an unrelated isotype control antibody (anti-HEL) in order to saturate the biosensor surface with Fc. After a short baseline in kinetics buffer, first c-MET ECD was associated and subsequently the second antibody. Antibodies that occupy the same or an overlapping epitope, were not able to bind in the second association step (e.g. oa CS06, 224G11 and anti-HEL whereas oa B10v5 and LY2875358 could bind.

Supplemental figures including antibody characteristics, e.g. purity and thermal stability, were depicted in **Figure 35** to **Figure 38**.

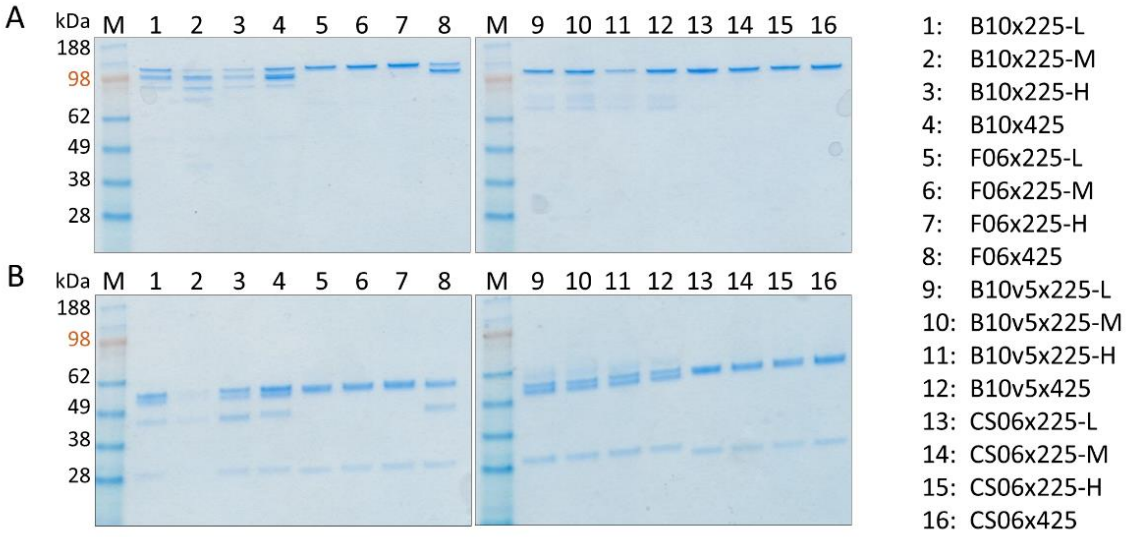

Figure 35: SDS PAGE analysis of bsAbs.

Gel electrophoresis of the 16 expressed and purified c-MET x EGFR bsAbs. Gels were stained with coomassie and samples were analyzed under non-reduced **(A)** and reduced conditions **(B)**. BsAbs have a theoretical size of 125 kDa under non-reduced conditions. Reduction of bsAbs results in three fragments: the AG-heavy chain, the c-MET light chain and the scFv-GA chain (50 kDa, 25 kDa, and 50 kDa, respectively). Some of the lower bands under non-reduced conditions could be explained by artifact bands as described by Liu *et al.* (Liu *et al*, 2007).

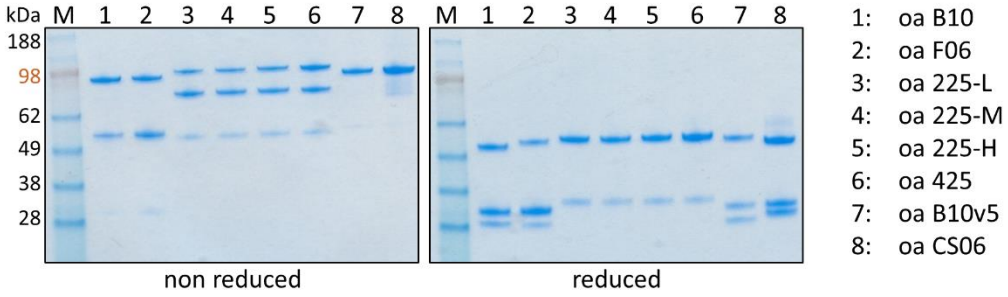

Figure 36: SDS-PAGE analysis of one-armed control SEED antibodies.

Gel electrophoresis of non-reduced and reduced monovalent control antibodies stained by coomassie. The oa Fab-SEEDs have a theoretical size of 100 kDa while monovalent scFv-SEEDs have the size of 75 kDa. As indicated by bands, GA-SEED chains formed in parts homodimers resulting in scFv-scFv-SEED with a size of 100 kDa.

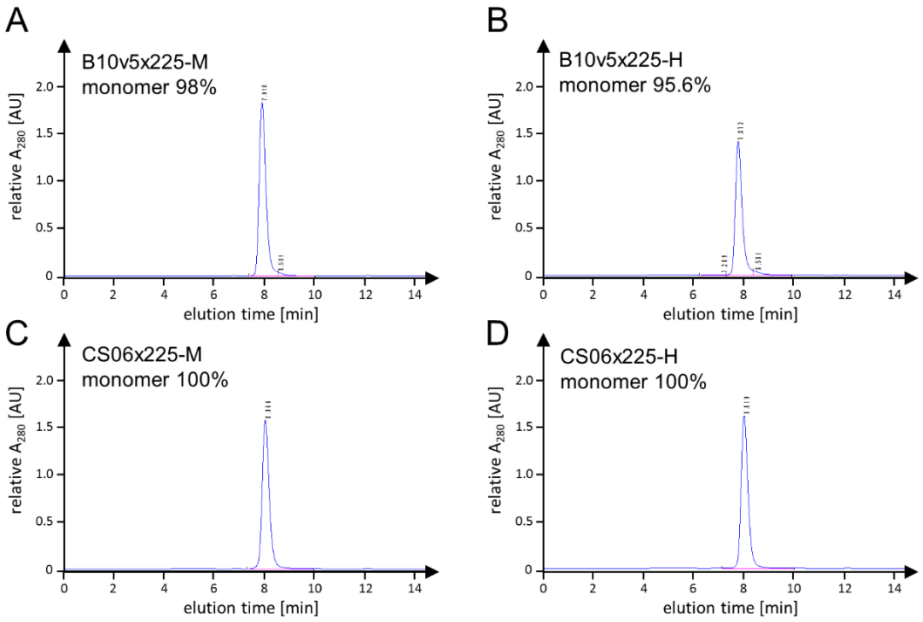

Figure 37: Size exclusion chromatography of purified bsAbs.

Analytical SEC of B10v5x225-M **(A)**, B10v5x225-H **(B)**, CS06x225-M **(C)**, and CS06x225-H **(D)** after preparative SEC are exemplarily depicted. Calculated monomer percentage [%] is indicated and ranged from 95 to 100%.

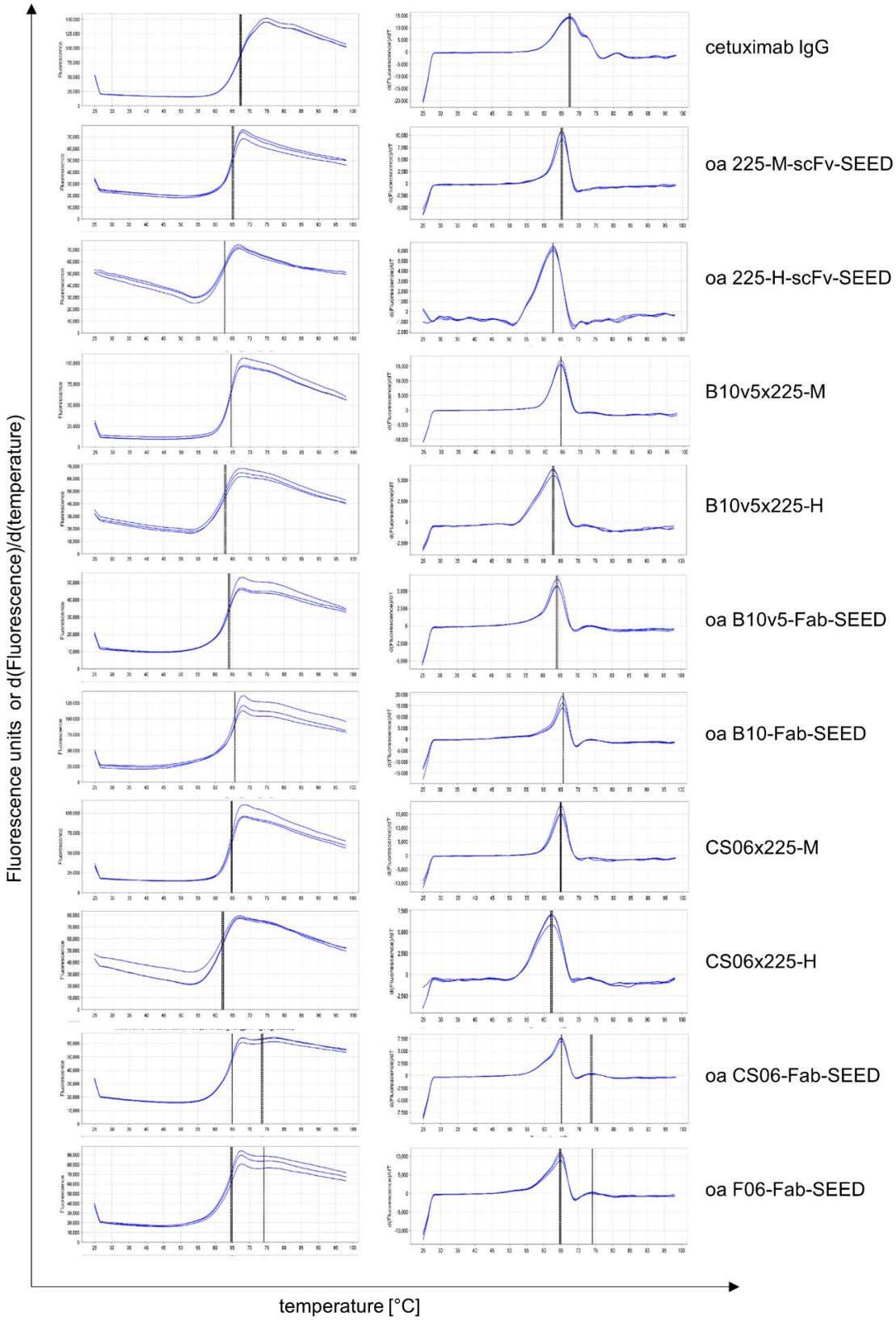

Figure 38: Summary of the thermal shift assay melting curves.

1 μM antibodies was mixed with a 20 fold excess of the fluorescent dye SYPRO orange. Protein unfolding in response of increasing temperature resulted in exposure of hydrophobic patches where the dye can attach. This in turn yielded in increase in fluorescence (left graphs). The deviation of the fluorescence (right site) indicates the melting temperature represented by maxima.

Functional analysis of bsAbs by Western blot for phosphorylated c-MET and EGFR as well as for their selectivity, the ability to induce ADCC and internalization (**Figure 39** to **Figure 41**, **Table 13**).

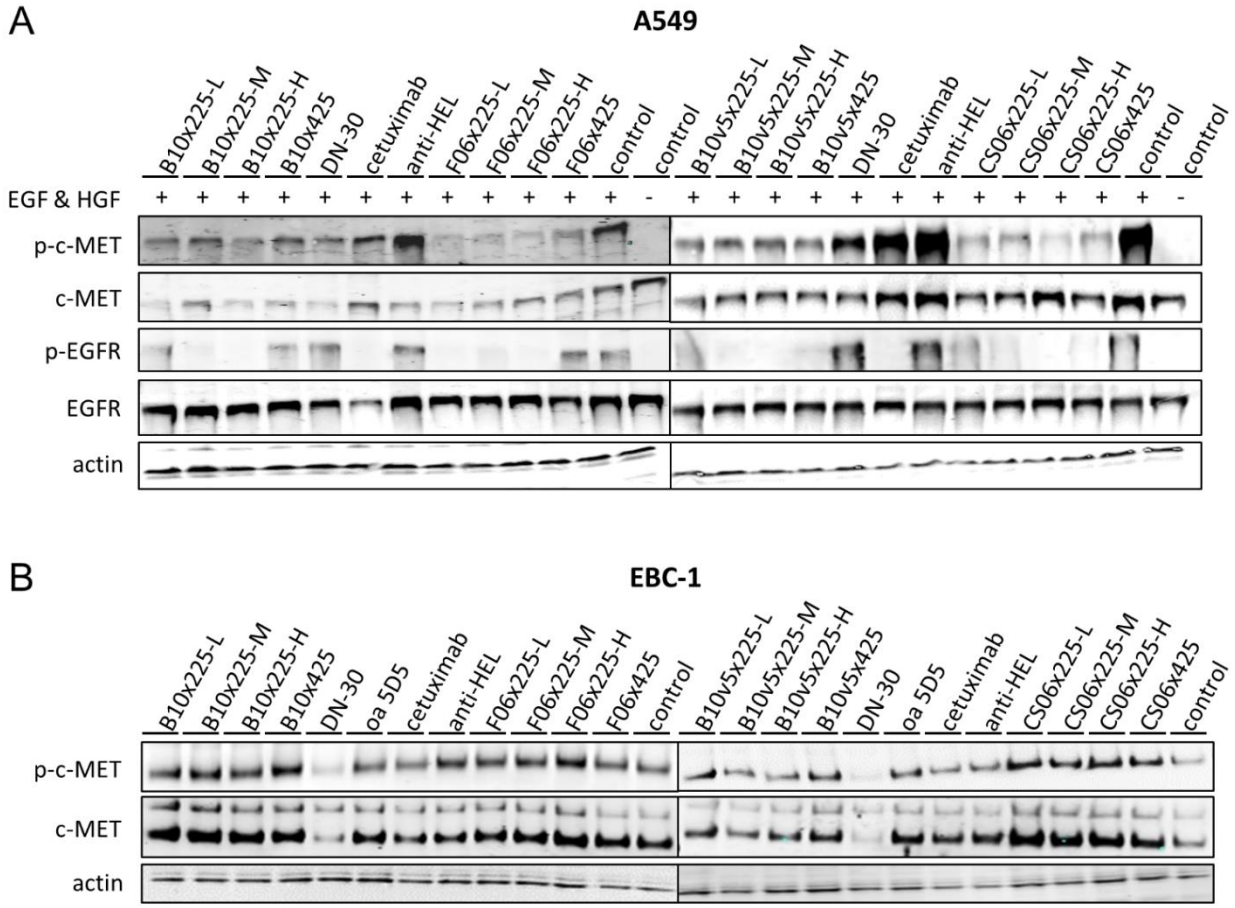

Figure 39: Phosphorylation of c-MET and EGFR in A549 (A) and EBC-1 (B) cells analyzed by Western Blot.

After serum starvation for 16 h, A549 **(A)** or EBC-1 cells **(B)** were pre-incubated with 300 nM bsAbs or reference mAbs for 4 h followed by stimulation with HGF and EGF (50 ng/ml) for A549 cells. Cell lysates were subjected to gel electrophoresis, Western blotting and bands were revealed with detection antibodies against total and phosphorylated c-MET and EGFR as well as actin. In HGF-dependent A549 cells **(A)**, bsAbs reduced c-MET and EGFR phosphorylation. For EBC-1 cells **(B)** with c-MET amplification, no effect on c-MET phosphorylation was observable. p=phosphorylated

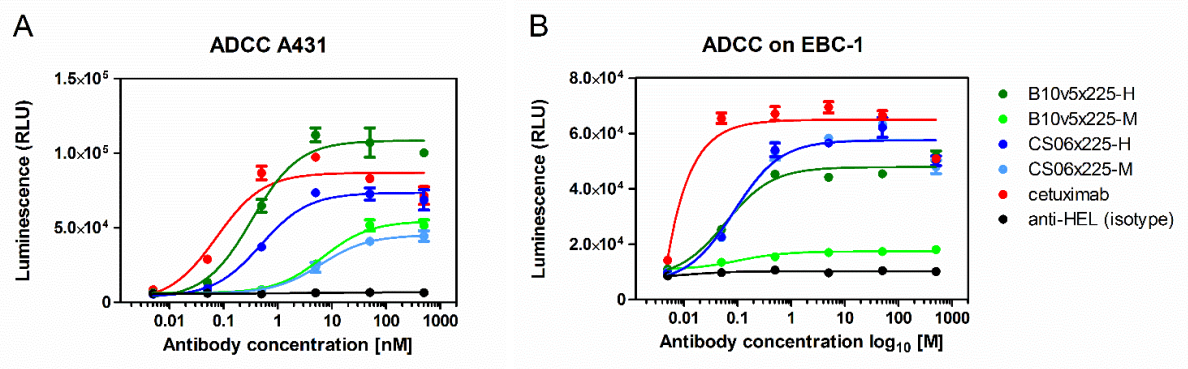

Figure 40: ADCC of bsAbs on A431 and EBC-1 cells in comparison to cetuximab.

A431 cells **(A)** and EBC-1 cells **(B)** were treated with antibodies and subsequently with recombinant Jurkat effector cells (in ratio 6:1) in which a luciferase was added in the nuclear factor of activated T-cells (NFAT) pathway. Activation of FcγRIIIa receptor by mAbs induced conversion of substrate by luciferase yielding in luminescence signal. As a result, high affinity variants in bsAb format induced ADCC comparable to cetuximab whereas isotype control did not. Shown are representative graphs of two independent experiments with triplicates. Data were plotted as relative luminescence units versus logarithm of antibody concentration.

Table 13: *In vitro* selectivity of bsAbs determined for different cell line combinations.

The tumor model cell line (EBC-1, A431 or MKN45) were stained with a green membrane dye to allow distinction of the two cell populations during the mixing experiment via flow cytometry. Tumor model cells were then mixed with a normal model cell line (HepG2 or T47D) in a ratio 1:30. HepG2 cells exhibit low EGFR surface expression and slightly more c-MET surface expression levels. T47D in contrast are devoid of c-MET and display basal EGFR expression. A431 is characterized by EGFR overexpression (+++) and low c-MET expression (+), EBC-1 and MKN45 are c-MET amplified (+++) with medium EGFR expression (++). The cell mixture was incubated with 30 nM mAbs and binding was revealed with anti-human Fc PE-conjugate via flow cytometry. The *in vitro* selectivity was defined as the ratio of tumor to normal tissue model cellular binding, e.g. MFI (EBC-1) divided by MFI (T47D). The calculated values for the cell line combinations are summarized in the table below. The color code was defined for each column with red indicating low selectivity, shades of yellow as medium selectivity and green as high selectivity. Except for A431 and HepG2 cells, for all other combinations bsAbs displayed higher selectivity in comparison to monospecific cetuximab. n.d. = not determined.

Construct name	EBC-1 vs. HepG2	A431 vs. HepG2	EBC-1 vs. T47D	A431 vs. T47D	MKN45 vs. T47D
B10x225-L	17	7	92	1911	106
B10x225-M	15	11	16	147	12
B10x225-H	14	12	10	75	6
B10x425	17	4	23	53	11
F06x225-L	16	21	n.d.	277	22
F06x225-M	19	10	23	160	13
F06x225-H	17	19	8	81	5
F06x425	19	11	16	81	7
B10v5x225-L	n.d.	n.d.	116	151	66
B10v5x225-M	n.d.	n.d.	25	39	9
B10v5x225-H	n.d.	n.d.	16	36	5
B10v5x425	n.d.	n.d.	24	33	7
CS06x225-L	n.d.	n.d.	818	1162	329
CS06x225-M	n.d.	n.d.	49	46	14
CS06x225-H	n.d.	n.d.	22	34	6
CS06x425	n.d.	n.d.	34	31	9
cetuximab	9	28	5	32	1

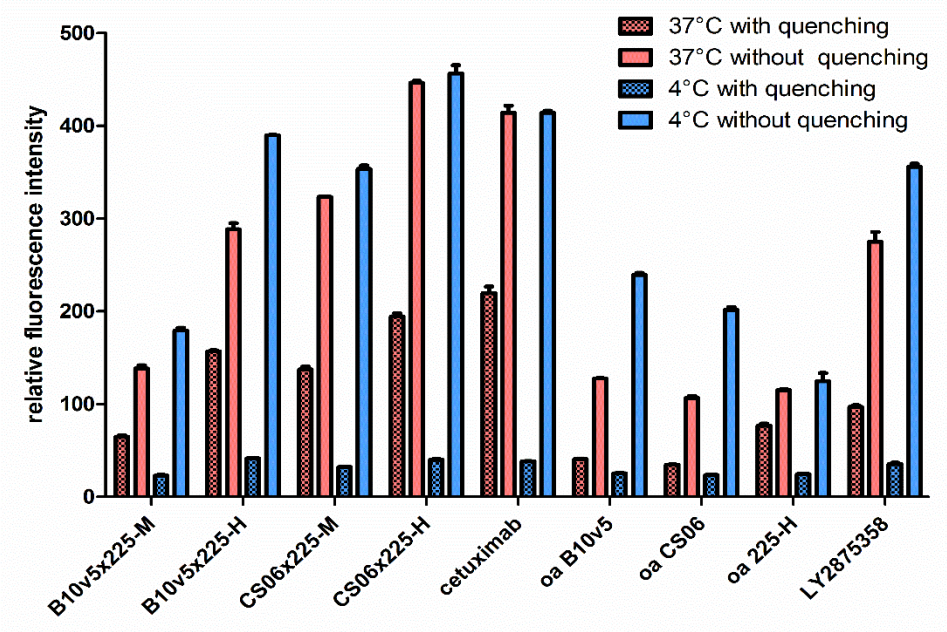

Figure 41: MFIs for internalization assay by flow cytometry with and without quenching.

Representative graph for the analysis of internalization induced by 100 nM mAbs in NCI-H441 cells at 37°C and 4°C with and without a quenching via flow cytometry. Antibodies were thereby detected with an anti-human Fc AlexaFluor488 conjugate. Relative green fluorescence intensities were calculated from duplicates and standard deviations were indicated as error bars. Residual surface binding of fluorescently labeled antibodies was quenched with an antibody directed against AlexaFluor488. As a result, non-quenched samples displayed nearly comparable MFIs at 4°C and 37°C as expected. Treated cells incubated at 4°C without quenching displayed only small MFIs indicating incomplete quenching. Difference of total fluorescence of samples without quenching to sample at 37°C with quenching indicates the portion which was internalized. During quantitative calculation of percent internalization, the minor fluorescence from the sample 4°C with quenching was also included.

Analysis of bispecific ADCs by mass spectrometry (MALDI) was depicted in **Figure 42**.

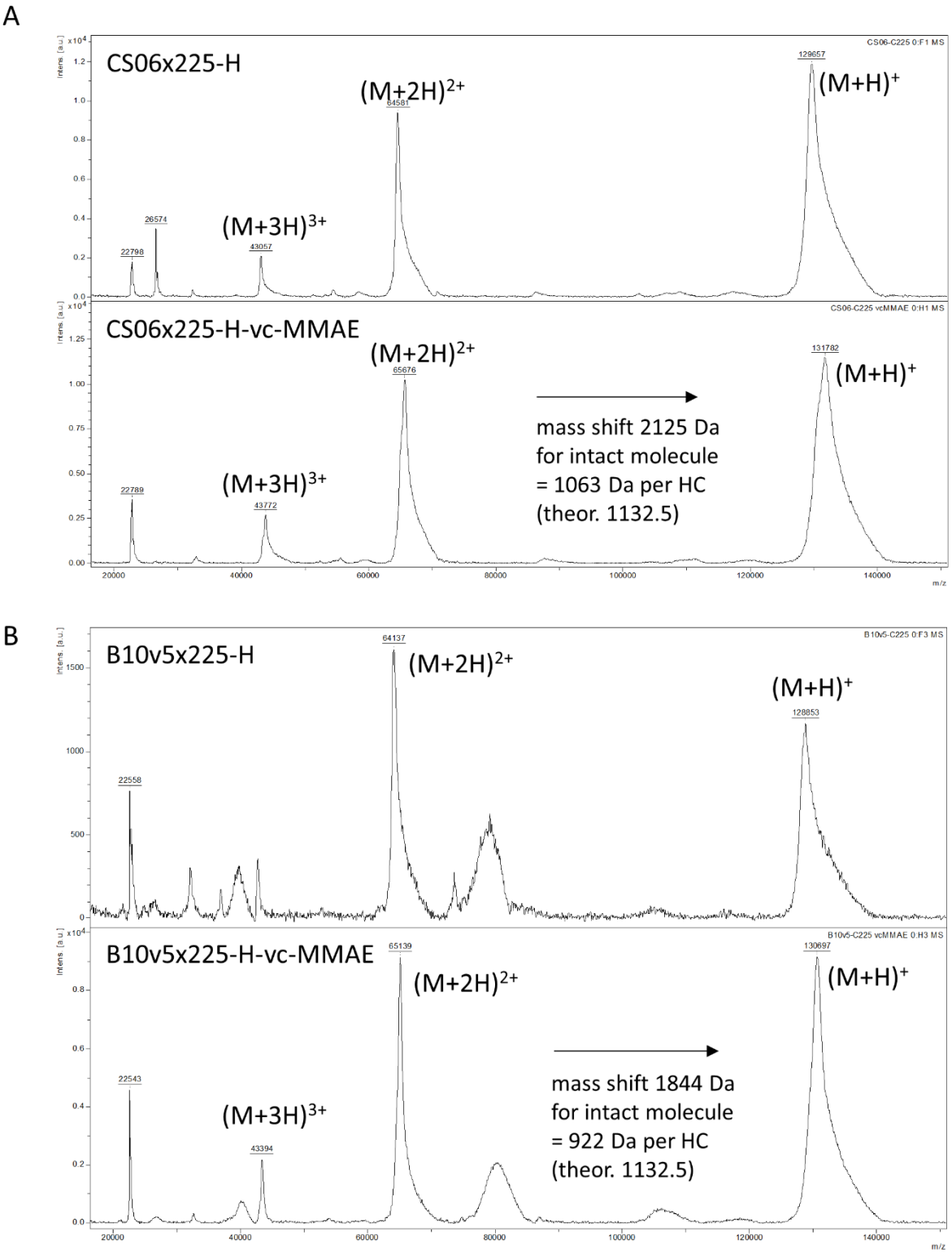

Figure 42: MALDI of bispecific ADCs.
Evaluation of native bispecific ADCs diluted 1:10 in 50 mM ammonium bicarbonate buffer by MALDI. Samples were applied on MALDI plates with C4 ZipTips. For matrix 1, plate was coated with saturated SA solution in ethanol. For matrix 2, plate was coated with saturated SA solution in 33% ACN (acetonitrile) and 0.1% TFA (trifluoroacetic acid). Measurement was carried out in LP mode and calibrated only with mass 60,000 Da. Measurements were carried out by Merck, Darmstadt, Germany. The molecular weight (MW) of GGG-vc-MMAE is 1294.58 Da.

Additional graphs for cytotoxicity assays are illustrated in **Figure 43**.

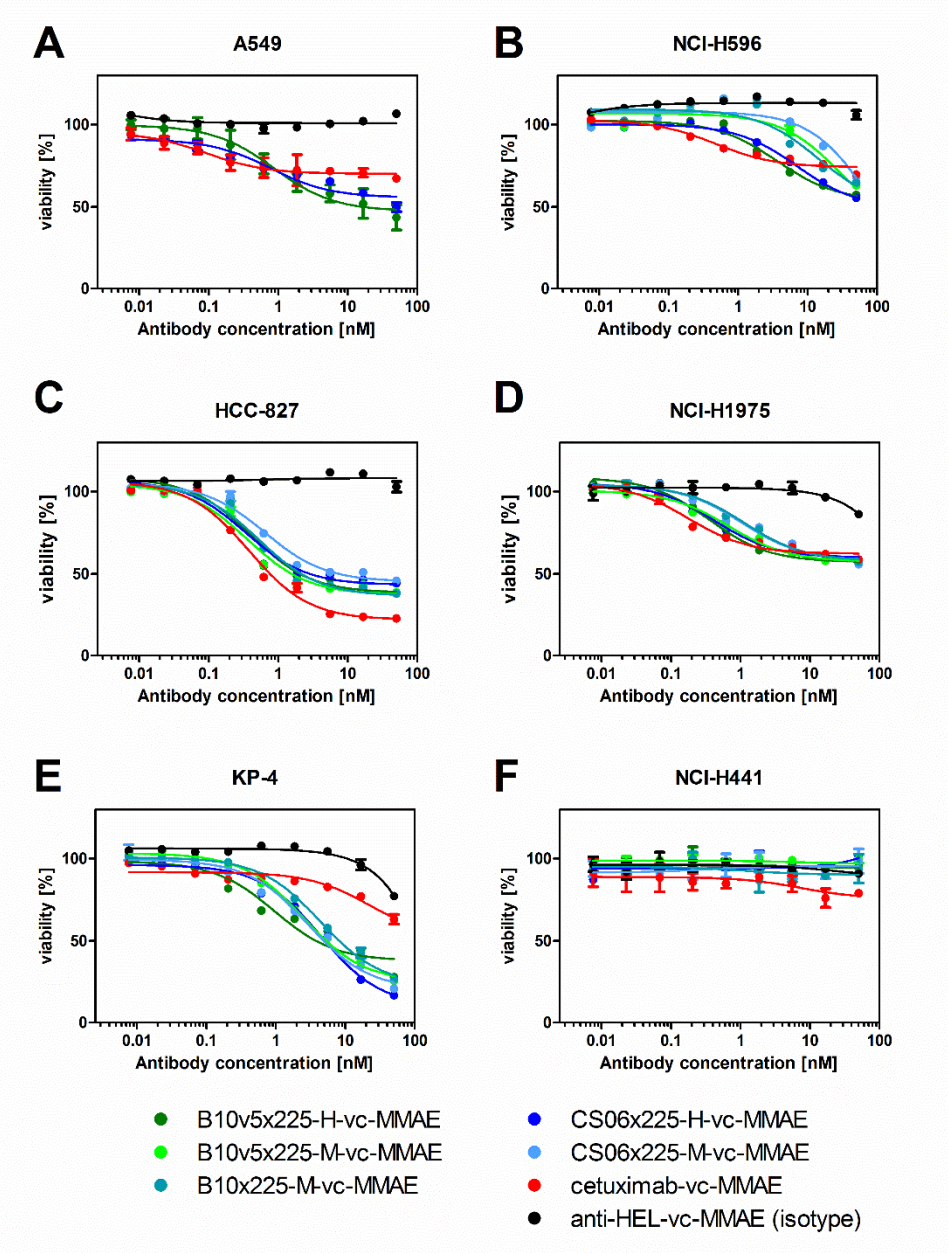

Figure 43: Cytotoxicity of bsAbs on further cancer cell lines.

Bispecific ADCs generated by site-directed conjugation of vc-MMAE to both heavy chains were incubated on cancer cell lines with low to medium c-MET and EGFR expression including A549 **(A)**, NCI-H596 **(B)**, NCI-H1975 **(D)**, KP-4 **(E)** and NCI-H441 **(F)**. ADCs were incubated for 72 h and cell viability was determined with the CellTiter-Glo® assay. Interestingly, lower c-MET and EGFR expression correlated with less potent and efficacious cell killing in comparison to c-MET or EGFR overexpressing cell lines. Only for NCI-H441 cells **(F)** carrying a KRAS mutation, nearly no cytotoxicity was detected in the evaluated concentration range. Furthermore, cytotoxicity of bispecific ADCs on another c-MET amplified cell line, HCC-827 **(C)**, was evaluated. In contrast to EBC-1 and MKN45 cells (cf. **Figure 28**), cetuximab-vc-MMAE demonstrated similar efficacy in cell killing compared to bispecific ADCs.

8.2. Abbreviations

aa	Amino acid
ADC	Antibody-drug conjugate
ADCC	Antibody dependent cellular cytotoxicity
ADCP	Antibody dependent cellular phagocytosis
AFM	Affinity maturation
AHC	Anti-human Fc biosensor
Amp	Ampicillin
APS	Aminopropylsilane
BLI	Biolayer interferometry
bp	Base pair
BSA	Bovine serum albumin
bsAb	Bispecific antibody
CD	Cluster of differentiation
CDC	Complement dependent cytotoxicity
CDR	Complementarity determining region
cfu	Colony forming unit
CH1, 2, 3	Constant domain 1, 2, 3 of the heavy chain
c-MET	Mesothelial epithelial transition, HGFR
CV	Column volume
Da	Dalton
DAR	Drug-to-antibody ratio
dH_20	Distilled water
DNA	Deoxyribonucleic acid
dNTPs	Deoxyribonucleotide triphosphate
ECD	Extracellular domain
ECL	Electrochemiluminescence
E. coli	*Escherichia coli*
EGF(R)	Epidermal growth factor (receptor)
ELISA	Enzyme-linked immunosorbent assay
epPCR	Error-prone PCR
Fab	Fragment antigen binding
FACS	Fluorescence activated cell sorting
Fc	Fragment crystallizable
FcRn	Neonatal Fc receptor

FcγR	Fcγ receptor
FCS	Fetal calf serum
FITC	Fluorescein
FR	Framework region
H	Hour
HC	Heavy chain
HER	Human epidermal growth factor receptor
HGF / SF	Hepatocyte growth factor, scatter factor
HGFR	Hepatocyte growth factor receptor, mesothelial epithelial transition; c-MET
His-tag	Histidine tag, usually composed of six histidines
HPLC	High performance liquid chromatography
HRP / POD	Horse reddish peroxidase
hu / hs	Human / *homo sapiens*
Ig	Immunoglobulin
ITAM	Immunoreceptor tyrosine-based activating motif
ITIM	Immunoreceptor tyrosine-based inhibitory motif
k_a	Association rate constant
KB	Kinetics buffer
K_D	Equilibrium dissociation constant
k_d	Dissociation rate constant
LB medium	Luria-Bertani medium
LC	Light chain
mAb / pAb	Monoclonal antibody / polyclonal antibody
MALDI-TOF MS	Matrix-assisted laser desorption/ionization time of flight mass spectrometry
MCS	Multiple cloning site
MFI	Mean fluorescence intensity
MMAE	Monomethyl auristatin E
mRNA	Messenger ribonucleic acid
MSA	Multiple sequence alignment
mu	Murine, *mus musculus*
MWCO	Molecular weight cut-off
n.d.	Not determined
NC	Nitrocellulose
NEAA	Non-essential amino acids
NK cells	Natural killer cells

NK1	N-terminal HGF fragment
oa	One-armed
OD	Optic density
PAGE	Polyacrylamide gel electrophoresis
PBMCs	Peripheral blood mononuclear cells
PBS	Phosphate buffered saline
PCR	Polymerase chain reaction
PD	Phage display
PDB	Protein Data Bank
PE	R-phycoerythrin
PEG	Polyethylene glycol
PI	Propidium iodide
PVDF	Polyvinylidene fluoride
RIPA buffer	Radioimmunoprecipitation assay buffer
rpm	Revolutions per minute
RT	Room temperature
RTK	Receptor tyrosine kinase
scFv	Single-chain variable fragment
s.d.	Standard deviation
SDS	Sodium dodecylsulfate
SEC	Size exclusion chromatography
sec	second
SEED	Strand exchange engineered domain
SHM	Somatic hypermutation
SNP	Single nucleotide polymorphism
TKI	Tyrosine kinase inhibitor
T_m	Melting temperature
Tris	Tris(hydroxymethyl)aminomethane
v/v	Volume per volume
vc	Valine-citrulline (linker)
VH	Variable domain of the heavy chain
VL	Variable domain of the light chain
w/v	Weight per volume
wt	Wild type

8.3. List of figures

8.4. List of tables

8.5. Curriculum vitae

Name:	Carolin Sellmann
Date of birth:	March 22nd, 1988
Place of birth:	Hildesheim, Germany
Nationality:	German
Address:	Pallaswiesenstraße 44, 64293 Darmstadt, Germany

Education:

08/2013 – today	Doctorate in biochemistry, Merck KGaA and Technische Universität Darmstadt, Germany, supervision Prof Dr. Harald Kolmar
09/2010 – 05/2013	Master of Science in Molecular Biotechnology, Ruprecht-Karls-Universität Heidelberg, Germany, major: Drug Research - Master thesis: "Generation of APP- and APLP-constructs for enzyme-mediated chemical labeling"
08/2011 – 05/2012	Studies abroad in Pharmaceutical Science, North Carolina Central University, Durham, NC, USA
10/2007 – 07/2010	Bachelor of Science in Molecular Biotechnology, Ruprecht-Karls-Universität Heidelberg, Germany - Bachelor thesis: "Regulation von ABC Transportern an der Blut-Hirn-Schranke unter Einwirkung von Cannabinoiden"
09/2000 – 07/2007	High school diploma Scharnhorstgymnasium Hildesheim, Germany

_____

(Carolin Sellmann)

8.6. Acknowledgments

Danksagung

Zuallererst möchte ich Prof. Dr. Harald Kolmar für die Betreuung meiner Doktorarbeit an der TU Darmstadt und die unkomplizierte Kooperation danken. Nicht nur bei den zwei Kleinwalsertal-Retreats und dem Mosbacher Kolloquium, sondern auch während meiner gesamten Promotion fühlte ich mich in die Arbeitsgruppe und die akademische Forschung integriert. Gleichermaßen gilt mein Dank Dr. Björn Hock und Dr. Lars Toleikis, die mir die Promotion in diesem interessanten und aktuellen Themengebiet bei Merck ermöglicht und mein Projekt mit vielen Anmerkungen und Anregungen immer unterstützt haben.

Prof. Dr. Heribert Warzecha möchte ich für die Übernahme des Korreferats danken. Prof. Dr. Siegfried Neumann und Prof. Dr. Beatrix Süß danke ich für die Bereitschaft, sich als Fachprüfer bereitzustellen.

Insbesondere möchte ich mich herzlich bei Dr. Mark Schütte und Dr. Achim Doerner bedanken für die Aufnahme im Labor, zahlreiche Ratschläge und Diskussionen, Unterstützung, Mitgestaltung und Betreuung des Projektes und meiner Promotion sowie die schöne Arbeitsatmosphäre. Achim, ohne dich wäre diese Doktorarbeit nicht so geworden, wie sie jetzt ist.

Des Weiteren gilt mein Dank allen Leuten aus der Abteilung, die direkt und indirekt bei meinem Projekt geholfen, die für das gute Arbeitsklima gesorgt haben und mit denen man auch gerne nach der Arbeit gerne Zeit verbracht hat (Team Building Events, Kino, Essengehen, …): Dr. Nicolas Rasche, Dr. Stefan Becker, Ralf Günther, Dr. Laura Rhiel, Dr. Birgit Piater, Dr. Christian Schröter, Marcel Rieker, Simon Krah und Dr. Stephan Dickgießer. Ein ganz großes Dankeschön möchte ich auch an meine Labor-Kollegen Daniela Pur, Angelika-Nicole Helfrich, Dominik Reitz, Konstanze Waurisch, Elke Ciesielski und Christina Bauer richten für experimentellen Input, ganz viel Lachen im Büro sowie Cocktail trinken und Essen gehen. Dem „Ecklabor“ mit Deniz Demir, Iris Willenbücher, Tanja Thole, Kerstin Hallstein, Andreas Schönemann und Jan Beck möchte ich als Initiatoren für die schönen Kaffeerunden und auch für die Hilfe bei Experimenten danken. Auch dem dritten Labor mit Nils Bahl, Sonja Dreher und Anja Lamack danke ich für ihre Hilfsbereitschaft und die schöne Arbeitsatmosphäre.

Des Weitern möchte ich auch vielen weiteren Leuten bei Merck danken für Anmerkungen, Hilfestellungen, Beantwortung all meiner Fragen und zur Bereitstellung von Materialien: Dr. Christine Knühl, Dr. Christina Esdar, Dr. Christiane Amendt, Dr. Jan Anderl, Dr. Friedhelm Bladt, Dr. Daniel Kuhn, Dr. Frank Jährling, Dr. Manja Friese-Hamim, Dr. Heike Dahmen, Dirk Müller-Pompalla, Dr. Sven Pötzsch, Dr. Frank Fischer, Jens Hannewald, Iris Mannberger, Katja Wischrop, Sabrina Duschek, Doreen

Musch, Maic Seegel, Daniel Winter, Thomas Eichhorn, Thomas Rysiok, Oliver Edler, Elvira Meissen, Ingrid Schmidt und die werksärztliche Abteilung für die Serum-Spende.

A very big thanks also to my American colleagues, especially Vanita Sood for helpful contribution and proof-reading of the publication as well as Alec Gross, Angela Lim and John Wesolowski.

Tobias Fischer möchte ich auch danken für seine freundliche Hilfsbereitschaft bei der Erstellung der Patentanmeldungen.

Einen ganz lieben Dank möchte ich auch an die „EX-Merck'ser" mit Frescilia, Simone, Daniel und Pavel richten. Besonders Simone und Frescilia haben mir einen schönen Start in die Promotion ermöglicht und waren mit verantwortlich für die Einführung gemeinsamer Kaffee- und selbstgekochten Mittagsessensrunden. Ich danke auch weiteren temporären Leuten bei Merck, insbesondere Gaby, Max, Annika, die zu einer schönen Arbeitsatmosphäre beigetragen haben und auch wissenschaftlich mein Projekt vorangetrieben haben.

Ich danke auch allen derzeitigen (und auch ehemaligen) AK Kolmar Mitgliedern für nette Gespräche und Abendgestaltung, Seminare und Konferenzbesuche: Insbesondere meinen „TU-Mädels" Doreen Könning und Vanessa Siegmund, aber auch Christian, Simon, Bernhard, Stephan, Heiko, Janine, Olga, Christina, Thomas, Julius, Jan, Sascha, Valerie, Franzi, Alex, Sebastian H., Elena, Andreas und allen, die ich vergessen habe. Ganz lieben Dank auch an Barbara Diestelmann für die tolle und immer freundliche organisatorische Hilfe.

Und zum Schluss möchte ich noch meinen Eltern danken, die mir mein Studium ermöglicht haben und mich immer uneingeschränkt unterstützt haben.

9. Affirmations

Carolin Sellmann
Pallaswiesenstraße 44
64293 Darmstadt

_____
(Datum)

Erklärung

Ich erkläre hiermit, dass ich meine Dissertation selbstständig und nur mit den angegebenen Hilfsmitteln angefertigt habe.

_____
(Carolin Sellmann)

Carolin Sellmann
Pallaswiesenstraße 44
64293 Darmstadt

_____
(Datum)

Erklärung

Ich erkläre hiermit, noch keinen Promotionsversuch unternommen zu haben.

_____
(Carolin Sellmann)